Distribution Agreement

In presenting this thesis or dissertation as a partial fulfillment of the requirements for an advanced degree from Emory University, I hereby grant to Emory University and its agents the non-exclusive license to archive, make accessible, and display my thesis or dissertation in whole or in part in all forms of media, now or hereafter known, including display on the world wide web. I understand that I may select some access restrictions as part of the online submission of this thesis or dissertation. I retain all ownership rights to the copyright of the thesis or dissertation. I also retain the right to use in future works (such as articles or books) all or part of this thesis or dissertation.

Signature:

_____	_____
Chongchao Zhao	Date

Polyoxometalates in Artificial Photosynthesis: Development of Chromophores and Water Oxidation Catalysts

By

Chongchao Zhao
Doctor of Philosophy

Chemistry

_____
Craig L. Hill
Advisor

_____
Tianquan Lian
Committee Member

_____
Cora MacBeth
Committee Member

Accepted:

_____
Lisa A. Tedesco, Ph.D.
Dean of the James T. Laney School of Graduate Studies

_____
Date

Polyoxometalates in Artificial Photosynthesis: Development of Chromophores and Water Oxidation Catalysts

By

Chongchao Zhao
B.S. Tsinghua University, China, 2006
M.S. Tsinghua University, China, 2008

Advisor: Craig L. Hill

An Abstract of
A dissertation submitted to the Faculty of the James T. Laney School of Graduate Studies of Emory University in partial fulfillment of the requirements for the degree of
Doctor of Philosophy in Chemistry

2013

ABSTRACT

Polyoxometalates in Artificial Photosynthesis: Development of Chromophores and Water Oxidation Catalysts

Polyoxometalates (POMs) have been gaining increasing interest in several research fields, especially in catalysis. The development of POM-based water-oxidation catalysts (WOCs) recently has brought unprecedented attention to POMs. The general focus of this thesis is to explore the structural features of POMs and their applications in artificial photosynthesis (AP); the specific focus is to develop POM-based chromophores and WOCs for AP.

The first part of thesis reports the synthesis, structures and reactivity of POM-supported metal carbonyl complexes. Several dimeric structures, based on $[M(CO)_3]^+$ (M = Re, Mn) and lacunary POM ligands, $[X_2W_{22}O_{74}(OH)_2]^{12-}$ (X = Sb, Bi), $[\alpha\text{-}PW_{11}O_{39}]^{7-}$ and $[\alpha_2\text{-}P_2W_{17}O_{61}]^{10-}$, have been prepared and fully characterized. They show "slipped-sandwich" and "twisted-sandwich" structures. Their electrochemical and photochemical properties have both been investigated. This work has significantly expanded the area of hybrid POMs.

The second part of the thesis focuses on the use of these hybrid POMs as chromophores for solar light conversion. A novel transition, metal-to-polyoxometalate charge-transfer (MPCT), is characterized for the first time. In the complex $[P_4W_{35}O_{124}\{Re(CO)_3\}_2]^{16-}$, the donor is an embedded Re(I) center and the acceptor is the all-inorganic d^0 POM ligand, $[\alpha_2\text{-}P_2W_{17}O_{61}]^{10-}$. The high visible-region absorptivity ($\varepsilon_{470\ nm}$ = 4000 $M^{-1}\cdot cm^{-1}$) results from a Re^I-to-POM CT transition. In complex $[P_2W_{17}O_{61}\{Re(CO)_3\}_3\{ORb(H_2O)\}(\mu_3\text{-}OH)]^{9-}$, the donor is a trinuclear Re(I) cluster, so the MPCT transition in this system can be regarded as cluster-to-cluster CT. Ultrafast spectroscopy and DFT theoretical calculations confirm instantaneous (<50 fs) MPCT processes involving electron transfer from the Re(I) center(s) to the POM ligand(s).

The third part of the thesis addresses the preparation and characterization of new cobalt(II) and tin(II) POMs. The structures and catalytic water oxidation activity of several Co(II) POMs based on $[B\text{-}SbW_9O_{33}]^{9-}$ were investigated. Multiple Sn(II) POMs based on $[B\text{-}SbW_9O_{33}]^{9-}$ and $[\alpha\text{-}XW_9O_{34}]^{10-}$ (X = Si, Ge) are the highest nuclearity Sn(II) POMs known to date. They crystallize as infinite three-dimensional all-inorganic frameworks with porous channels. These Sn(II) POMs have high absorptivity in the visible region, a feature characterized by spectroscopic techniques.

Polyoxometalates in Artificial Photosynthesis: Development of Chromophores and Water Oxidation Catalysts

By

Chongchao Zhao
B.S. Tsinghua University, China, 2006
M.S. Tsinghua University, China, 2008

Advisor: Craig L. Hill

A dissertation submitted to the Faculty of the James T. Laney School of Graduate Studies of Emory University in partial fulfillment of the requirements for the degree of Doctor of Philosophy in Chemistry

2013

Acknowledgement

I have never been alone on the road to obtaining a Ph.D. I am really fortunate to have those who guided me and paved the way for me over these years. They are such wonderful people and have always been with me. It would have been difficult for me to be where I am today without their sincere support and encouragement.

My deepest gratitude goes first and foremost to my advisor, Professor Craig L. Hill. As my advisor, Professor Hill not only discussed science, chemistry and English, but also shaped my attitude towards life. He has taught me to be brave and optimistic in the face of frustration. His everyday lifestyle has guided me to live healthy, be energetic and to thrive. When I joined his group, my writing was poor; Professor Hill consequently gave me writing homework assignments and graded them! From the start, we had many discussions about my research and overtime, I learned a lot and felt comfortable talking with him; it now feels like talking to a colleague. We spent many hours drafting manuscripts together, and I learned how to organize the text and to precisely choose words and sentences. Interestingly, I also gained a large amount of geographical knowledge, as Professor Hill loves to pop out Google Earth and show me places he has been! Some day in the future, I also want to climb those high mountains and to see these beautiful places in person.

I also wish to thank Dr. Yurii Geletii. He is a very knowledgeable, patient, and extremely careful researcher. Over these years, he has taught me step by step how to be a good researcher. From him, I am aware that I must pay adequate attention to the tiniest details of a problem in order to avoid making mistakes.

I am very thankful to all the previous and current Hill group members. I feel so lucky to have met and worked with these young people. They are smart, easy-going and hard-working. We are an efficient and effective team. The students that sat next to me in the lab, first Dr. Kevin O'Halloran and then Elliot Glass, talked a lot about one another's research and helped me improve my English. I frequently asked them some weird questions, such as how to say something in English. One Emory undergraduate, Choon Kambara, worked with me for two years and impressed me with her intelligence. Jordan Sumliner is very enthusiastic and good at organization. He helped me a lot in experimental design. Also, I want to express my gratitude to: Dr. Zhen Luo, Dr. Yu Hou, Dr. Jie Song, Jim Vickers, Dr. John Fielden, Hongjin Lv, Dr. Guibo Zhu, Weiwei Guo, Kevin Sullivan, Sarah Lauinger and others whom I have known in Hill group. I will remember all these names and the stories we shared over these days.

I am very grateful to Professor Tianquan Lian. He is another member of my research committee. He gave me important advice on my projects. He discovered the potential importance of my research, and brought it to a higher level with much interest. Without this interest, my work would have been more routine and of lesser impact within the community. I thank him and his team members, Dr. Teddy Huang, Dr. William Rodríguez-Córdoba and Ye Yang for doing laser spectroscopy experiments.

I sincerely thank Dr. Djamaladdin G. Musaev and Dr. Alexey Kaledin. They did a great deal of computational work for my projects that greatly helped my research. Dr. Musaev is very generous, kindhearted and considerate. He gave me useful research and job seeking advice.

I am particularly thankful to my committee member Dr. Cora MacBeth! She interviewed me in Beijing more than five years ago, after which I received an offer of admission from Emory University. I could say it is thanks to Dr. MacBeth that I had the opportunity to study at Emory! I took her advanced inorganic chemistry course, which helped broaden my understanding of the field. During these five years, she gave me lots of advice and encouragement with respect to my research and career development. She taught me to be a compassionate and caring person.

I really appreciate Dr. Ken Hardcastle, Dr. John Bacsa and Professor Karl Hagen. They have taught me so much about crystallography. I had a good time while working as the Service Instructor in the X-ray center and found it to be very useful experience for my career. I could not have achieved such a deep level of understanding of crystallography without their instruction.

I would also like to thank Dr. Shaoxiong Wu and Dr. Bing Wang for their help in collecting NMR data, especially on samples with uncommon heavy metals. I am thankful to Leslie Chauvin and Ann Dasher. They helped me complete important paperwork, so I could present at conferences, attend meetings and focus on my research.

Many thanks will be also to my dear friends: Ayse Öztürk, Cem Öztürk, Jung Yeon Lee, Seok-Chul Sean Kwon and Qi Shi. They are such good friends and always have been there for me through all the difficulties. I am very thankful to Professor Huizhong Kou, Professor Jinying Yuan and Professor Aili Cui, for the education I received while I was studying at Tsinghua University.

I thank my father and mother, little sister and brother. My parents are proud of their son, although they do not know what I am actually doing in the States. They did not have the opportunity to receive advanced education when they were young and do not know English or chemistry. They probably just thought their son was making soaps, toothpastes or pesticides in a country on the other side of the Pacific. However, they do worry about

me a lot. For all my life until today, my parents gave me everything they had and spent nothing on themselves. Their work is not done until they see me finally settled and safe. My little sister and brother also love me unconditionally. They did not go to graduate school, but they believed that their big brother could. I will always think of the early days when we were innocent kids. We three played together or even fought with each other. I also missed my grandpa and grandma deeply. They passed away in the five years I have been at Emory University but I was not able to either see them or attend their funeral. I wish them eternal peace in Heaven. They will always live in my memories.

Last but not the least, I always will be grateful to my beloved Yanwen Wang. We got to know each other from Emory. During these years, we have been to many places. We visited Disneyland in Orlando, saw killer whales in San Diego, climbed the Rockefeller Center in New York and explored Rocky Mountain National Park in Colorado. All of these are very valuable memories. She is smart, beautiful and confident, and has an infectious personality that almost everyone loves. She was also busily working on her Ph.D., but she spent much time on me and helped me overcome adversity. I am appreciative of her endless love, patience, wisdom and encouragement.

Life is an endless journey. In our lives, we visit many places, meet different people and have stories of both sorrow and joy. Now I have entered my 30s, although I am yet to be ready for the responsibilities of a man in his 30s. This reminds me of that oft-quoted line, "*How many roads must a man walk down, before they call him a man?*" I sometimes feel sad when I realize how quickly time flies. However, I feel so blessed and fortunate to have been where I have, and to be in the company of wonderful people travelling with me. Each person I have encountered on my way has taught me a lot and brought me unforgettable memories. They gradually strengthened me into the person I was meant to become. They are the generous gardeners who make my soul blossom. My favorite writer, Haruki Murakami, wrote in *Kafka on the Shore*: "*No matter how much time passes, no matter what takes place in the interim, there are some things we can never assign to oblivion, memories we can never rub away.*" Finally, to all those who love and once loved me, I cite an ancient Chinese poem herein to express my sincere blessings and best wishes, for the times we met and for our lifelong happiness:

But rare is perfect happiness--
The moon does wax, the moon does wane,
And so men meet and say goodbye.
I only pray our life be long,
And our souls together heavenward fly!
---- Su Shi (1037 – 1101; Song Dynasty), China

Table of Contents

List of Figures

List of Schemes

List of Tables

List of Abbreviations

Å	Angstrom
a, *b*, *c*	unit cell axial lengths
An	actinide
anal.	analysis
n-Bu	*n*-butyl
℃	degrees Celsius
calcd.	calculated
cif	crystallographic information file
cm^{-1}	reciprocal centimeter (wavenumber)
equiv	equivalent
F(000)	structure factor for the unit cell
FT-IR	Fourier transform infrared spectroscopy
g	gram(s)
h	hour(s)
Hz	Hertz
J	coupling constant in Hertz
K	Kelvin
L	ligand
m	medium (IR)
M	molarity
Me	methyl
mg	milligram(s)
MHz	megahertz
min	minute(s)
mL	milliliter(s)
mmol	millimole
mol	mole
Mr	molecular weight
nm	nanometer
NMR	nuclear magnetic resonance spectroscopy
pH	potential of hydrogen, a measure of the acidity or alkalinity
POM	polyoxometalate
ppm	part per million
R	discrepancy index for crystal structure refinement
s	strong (IR)
sh	shoulder (IR)
TBA	tetrabutylammonium
THA	tetraheptylammonium
TGA	thermal gravimetric analysis
TMA	trimethyl acetamide
UV	ultraviolet
vs	very strong (IR)
w	weak (IR)
Z	number of molecules per unit cell
α, β, γ	interaxial angles between unit cell vectors
δ	chemical shift (expressed in ppm for NMR)
ε	molar extinction (or absorption) coefficient
θ	the glancing angle of the X-ray beam to the “reflecting plane”
λ	wavelength
μ	the total linear absorption coefficient (with unit of cm^{-1})

Chapter 1

Introduction:
The Frontiers of Polyoxometalate Chemistry

1.1 General Properties of Polyoxometalates

Polyoxometalates (POMs) are early transition metal oxygen anion clusters formed through the aggregation and condensation of metal ions in aqueous environment. The metal precursors are primarily the monomeric metalate d^0 species, such as V(V), Nb(V), Ta(V), Mo(VI), W(VI) and the others.[1-3] These self-assembly processes are spontaneous and influenced by various factors, including temperature, pH, concentration, ionic strength and reaction time. The thermodynamically stable forms of the thus-formed polyanions usually crystallize with alkali metal counter cations (e.g. Na^+, K^+ and Rb^+), and hence can be isolated from the solutions. The exploration of POMs has a long history, and the first discovery of POMs by Berzelius could be dating back to 1826,[4] but this research was not dramatically facilitated until the development of advanced synthetic and analytical techniques, especially by X-ray crystallography. As new POM structures could be clearly identified by X-ray diffraction, there has been an explosion in the number of new POM compounds reported over the past decades. Consequently, research addressing synthetic methodology, the correlation between structures and reactivity, practical applications, and mechanisms, has been widely investigated since the 1980s (**Figure 1-1**). At present POM research has become a large interdisciplinary subject engaging experts from the areas of chemistry, physics and material science. POMs have contributed to the development of multiple fields including oxidation catalysis, magnetic materials, photovoltaics, microelectronics and medical diagnosis.[5,6]

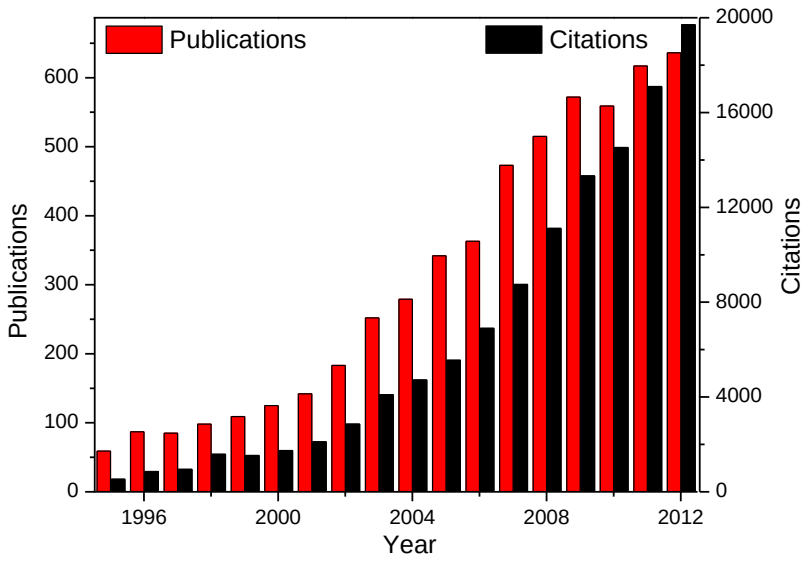

Figure 1-1 Citation report generated from Web of Knowledge under the topic of "polyoxometalate" or "polyoxometalates"

In term of elements, POM architectures assembled purely from the metal ions and oxygen atoms, such as $[W_{10}O_{32}]^{4-}$, $[Mo_7O_{24}]^{6-}$ and $[V_{10}O_{28}]^{6-}$, are designated as "isopolyanions". Most POMs contain one or more heteroatoms (typically p or d block elements) present in internal positions.[7] These "heteropolyanion" compounds appear in several different architecture types (see details below), and they are more versatile compared to isopolyanions. In term of structures, POMs are generally divided into two categories: plenary and lacunary. The structural (framework) metals in plenary POMs accommodate a complete coordination sphere which restricts access to a secondary building block (most isopolyanions are plenary in nature). Lacunary POMs derive from partial loss of one or more d^0 metal-oxo fragments from the plenary parent structures. Thus, the lacunary POMs with defect sites can react as multi-dentate chelating ligands during chemical reactions. They are widely used to generate other guest molecules and elements, and thus have much broader applications.

Scheme 1-1 shows the transformation among common POMs (we focus on polytungstates). The well-studied plenary parent Keggin-type POMs have a generic formula, $[XM_{12}O_{40}]^{n-}$ (X = P^V or Si^{IV} and M = W or Mo;[8-10] in some examples, X can be V^V, Sb^{III} and other heteroatoms[11,12]). The Keggin structure contains a tetrahedral XO_4 center. At each of its vertices, four M_3O_{13} subunits, which are linked through corner-sharing and edge-sharing contacts to other subunits, determine the isomerism of this POM subfamily. With precise control of hydrolysis conditions (e.g. pH, temperature, reaction time, etc.), several defect POMs are isolated, such as $[XW_{11}O_{39}]^{n-}$ (mono-vacant),[13,14] $[XW_{10}O_{36}]^{n-}$ (di-vacant)[15-17] and $[XW_9O_{34}]^{n-}$ (tri-vacant).[18-20] The Dawson-type parent POM, $[X_2W_{18}O_{62}]^{6-}$ (X = P^V is most common),[21] is formed by two XO_4 tetrahedral centers, two M_3O_{13} triad caps and two M_6O_{14} belts which link to each other by sharing corner oxygen atoms. Similarly, defect POMs such as the mono-vacant $[P_2W_{17}O_{61}]^{10-}$ and tri-vacant $[P_2W_{15}O_{56}]^{12-}$, can be obtained selectively from the starting solutions under different hydrolysis conditions.[19,22] The Si-, As- and V-centered Dawson POMs are less studied.[23-27] Recently, S-centered analogues have gained some attention.[28,29] For example, β-$[Mo^{VI}_{18}O_{54}(SO_3)_2]^{4-}$ shows thermochromic behavior. Although the synthetic chemistry in polytungstates is well-established, in contrast, the transformation between plenary and lacunary derivatives in polymolybdates and polyvanadates is much less well documented.

The physical and chemical properties of the above conventional POMs were well-studied.[7,30-32] In order to bring novel properties to POMs, guest molecules and metal ions can be incorporated with POMs. This chemistry is generally named as functionalizing POMs. The thus-formed derivatives, usually decorated with substituted transition metal

ions, or with covalently-bonded external organic/organometallic ligands, display distinct photochemical, electrochemical and catalytic properties. Since we can select a certain kind of metal ion (or organic derivative) or choose a particular POM host structure, an appropriate combination allows us to design many target molecules. These advantages have made POMs increasingly engaging in context with multidisciplinary research challenges.

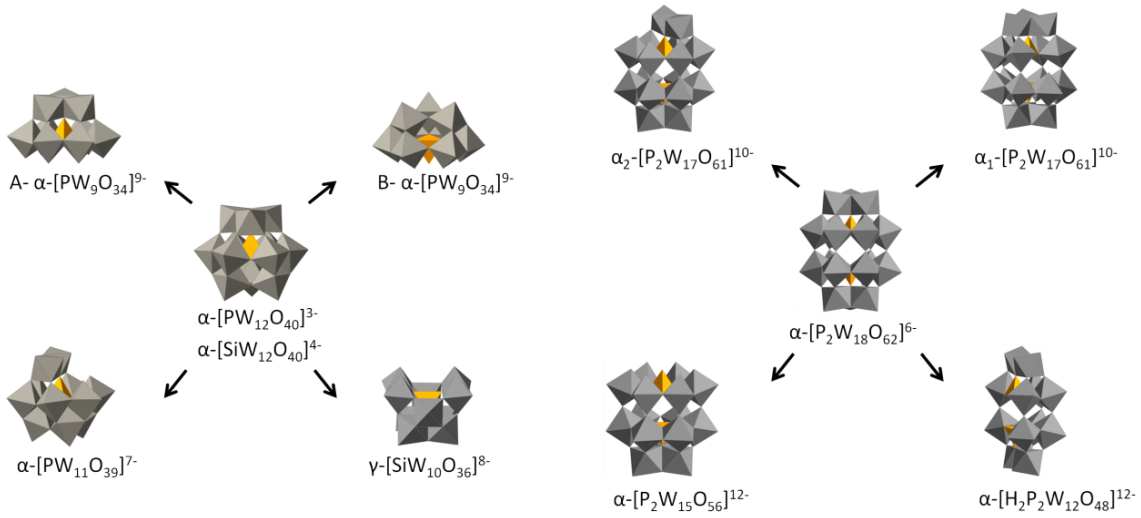

Scheme 1-1 X-ray structures of representative plenary and lacunary Keggin and Dawson POMs

1.2 Overview of POM Photochemistry

POM photochemistry has a rich record dating back to 1916.[33] Pioneers such as Yamase,[34-38] Papaconstantinou,[39-43] Hill,[44-47] and other researchers in the 1980s published several thorough reviews and high-quality articles in this topic. Generally, the photochemical activity of POMs originates from the intramolecular oxygen-to-tungsten (or molybdate) charge-transfer. A central impetus of this research is to disclose the thermodynamics and kinetics of the photo-excited energetics. The $O_{2p} \rightarrow W_{5d}$ (or Mo_{4d}) ligand-to-metal charge-transfer (LMCT) bands usually appear in the UV to near-visible regions.[47] Consequently, POMs are frequently colorless or pale-yellow. The LMCT

excited states, generated upon absorbing high-energy UV light, are derived from a promotion of an electron from a spin-paired, doubly occupied bonding orbital (HOMO) to an empty, anti-bonding orbital (LUMO).[48] The photoexcited POMs have oxo-centered radical character and react with organic substrates primarily by attracting hydrogen atoms. The quenching products of POMs, the reduced species, usually exhibit a deep blue color and are named "heteropoly blues" accordingly.[39,40,49-54] In the presence of Pt(0) as a catalyst in an anaerobic environment, hydrogen gas as a by-product is also generated.[55] The reduced POM species can be re-oxidized by dioxygen in the air. The two general classes of reactions are shown below in **Scheme 1-2(a)**:

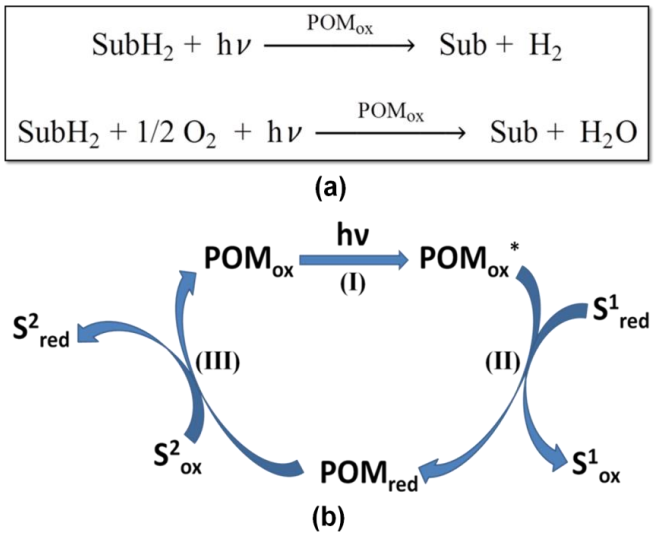

Scheme 1-2 (a) General dehydrogenation reactions catalyzed by POMs ($SubH_2$ = hydrocarbons, alcohols, alkyl halides, carboxylic acids, ketones, ethers, nitriles, thioethers). (b) Photocatalytic cycle of oxidation/dehydrogenation of substrates by POMs: (I) Photoexcitation of POMs; (II) Organic substrate, S^1, oxidized by excited POM; (III) Re-oxidation of reduced POMs and simultaneous reduction of a secondary substrate S^2. This re-oxidation can involve protons, O_2 or another organic molecule.

The overall photo-induced catalytic cycle for oxidation of organic substrates with POMs is shown in **Scheme 1-2(b)**.[47,56] A wide variety of organic compounds are readily

oxidized and a diversity of C-H functionalized products form depending on the reaction conditions. A large number of POMs have served as photocatalysts, yet the great majority of studies involve either $[W_{10}O_{32}]^{4-}$ and $[PW_{12}O_{40}]^{3-}$ (see **Table 1-1**). **Scheme 1-2(b)** does not provide the detailed mechanisms involving the radical intermediates. Actually, the mechanisms involve multiple steps and vary in some aspects from case by case. Generally, the excited state of POMs, named POM_{ox}^{*}, is generated upon absorbing high-power light. It then undergoes the processes of 1) radiationless decay, 2) emission (low quantum yield), and 3) photo-oxidation of organic substrates. The last step, which converts radiant energy into chemical energy, is frequently the slowest and thus exhibits lower quantum yields than the other two processes. The resulting initial radical pair upon photoexcitation of the POM, undergoes radical escape to produce POM_{red} and the organic radical, R·. The subsequent processes involving POM_{ox}, POM_{red} and R·, such as radical-radical reactions, and R· oxidation/reduction by POM_{ox} or POM_{red}, respectively, lead to different products accordingly. These reactions are affected by various factors such as protonation states, and ground state redox potential of the POM (see **Scheme 1-3**).[47]

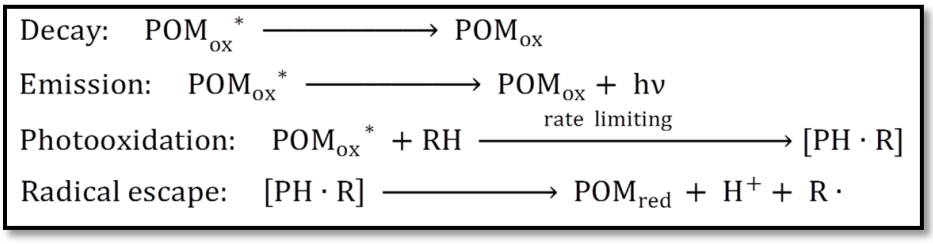

Scheme 1-3 General processes involving the POM-catalyzed photoredox transformations of organic substrates.

Table 1-1 Photocatalytic transformation of organic substrates by representative POMs ($[W_{10}O_{32}]^{4-}$, $[PW_{12}O_{40}]^{3-}$, $[PMo_{12}O_{40}]^{3-}$, $[SiW_{12}O_{40}]^{4-}$, $[P_2W_{18}O_{62}]^{6-}$ and $[PMo_{10}V_2O_{40}]^{5-}$). The POMs are converted to tetrabutylammonium salts for reactions in organic solvents.

$[W_{10}O_{32}]^{4-}$-catalyzed processes			
Substrate	**Products**	**Comments**	**References**
alkane (2,3-dimethylbutane, 2,3-dimethylpentane, isobutene cyclooctane, cyclohexane)	alkene, alkylalkane dimer, alkyl methyl ketone, alkyl hydroperoxide*	MeCN solutions of POM and alkane; room temperature; λ = 280 nm cutoff filter; Ar atmosphere (*using O_2)	57-62
phenol, *p*-cresol	pyrocatechol, hydroquinone, 4-hydroxybenzyl alcohol, CO_2	Aqueous solutions; room temperature; λ > 320 nm cutoff filter; pH =1 or 2.5	63
butanol	H_2	w/ RuO_2, IrO_2 or Pt(0); λ > 350 nm cutoff filter; CH_3CN-BuOH solution	64
olefins	olefin dimers	CH_3CN solution; λ = 310 nm irradiation; RuO_2 catalyst	65
alkane	aldehyde	CH_3CN solution; λ > 280 nm; 1 atm CO; radical carbonylation	66
chlorinated phenols	CO_2, HCl	aqueous solution; λ > 320 nm; pH = 2.5; temperature 20 ^oC	67
cis-2-decalone	*trans*-2-decalone	CH_3CN solution; λ > 360 nm; room temperature; Ar atmosphere	68
isopropyl alcohol; cyclohexanol	acetone; cyclohexanone	CH_3CN solution; 75W mercury lamp; λ > 300 nm; room temperature; excess O_2 environment	69,70
carbon tetrachloride	dehalogenation products, CCl_3 and others	different solvents were investigated: EtOH, PrOH, MeCN, DMF; 550W Hg lamp λ > 280 nm; room temperature; Ar atmosphere	71
acetoin; biacetyl	acetic acid	CH_3CN solution or CH_3CN-H_2O (1:1, pH = 2.5); λ > 300 nm; room temperature; excess O_2 environment	72
isobutane (and others)	*tert*-butyl hydroperoxide (and others)	CH_3CN solution; temperature 21 ^oC; 1000W Xe lamp λ > 280 nm; zero grade air (21% O_2)	73
thioether (tetrahydrothiophene; dimethyl sulfide)	α,α'-dimeric coupling product; (methylthio)methanol	CH_3CN solution; 550W Hg lamp for anaerobic oxidation (Ar atmosphere) or 1000W Xe lamp λ > 340 nm for aerobic reactions; temperature 25 ^oC	74,75
caged hydrocarbon, 1,8-cineole	oxygenated products	CH_3CN solution; Pt (0); temperature 15 ^oC; 550W Hg lamp λ > 280 nm; anaerobic conditions	76,77
cyclooctane, tetrahydrofuran	oxygenated products	organic solvents; Pt(0); temperature 57 ^oC; 550W Hg lamp λ > 280 nm; Ar environment	75,78
p-xylene, toluene, ethylbenzene	toluic acid, benzoic acid, acetophenone	CH_3CN solution; 125W Hg lamp λ > 320 nm; O_2 environment; temperature 25 ^oC;	79,80
nitroxide radicals	nitrosonium salts	CH_3CN solution; 900W Xe lamp λ > 280 nm; Ar environment; room temperature	81
$[PW_{12}O_{40}]^{3-}$-catalyzed processes			

Substrate	Products	Comments	References
alkane (dimethylbutane, dimethylpentane, dimethylcyclohexane, cyclooctane, cyclohexane	alkene, alkylalkane dimer,	MeCN solutions of POM and alkane; room temperature; $\lambda > 260$ nm cutoff filter; Ar atmosphere; w/wo Pt(0)	44,45,57-59,82
phenol, *p*-cresol	pyrocatechol, hydroquinone, 4-hydroxybenzyl alcohol, CO_2	Aqueous solutions; room temperature; $\lambda > 320$ nm cutoff filter; pH =1	63
alkane	aldehyde	CH_3CN solution; $\lambda > 280$ nm; 1 atm CO; radical carbonylation	66
chlorinated phenols	CO_2, HCl	aqueous solution; $\lambda > 320$ nm; pH = 1.0; temperature 20 ^oC	67
cis-2-decalone	octalones	CH_3CN solution; $\lambda > 290$ nm; room temperature; Ar atmosphere	68
isopropyl alcohol	acetone	CH_3CN solution; 75W mercury lamp; $\lambda > 300$ nm; room temperature; excess O_2 environment	69,70,83
variety of organic substrate (alcohols, ethers, etc.)	not specified	the related organic solvents; 1000W Xe lamp, $\lambda > 290$ nm; Ar environment; room temperature	44,46,60

$[PMo_{12}O_{40}]^{3-}$-catalyzed processes

Substrate	Products	Comments	References
thioether (tetrahydrothiophene; dimethyl sulfide)	α,α'-dimeric coupling product; (methylthio)methanol	CH_3CN solution; 550W Hg lamp for anaerobic oxidation (Ar atmosphere) or 1000W Xe lamp $\lambda > 340$ nm for aerobic reactions; temperature 25 ^oC	74
variety of organic substrate (alcohols, ethers, etc.)	not specified	the related organic solvents; 1000W Xe lamp, $\lambda > 290$ nm; Ar environment; room temperature	44

$[SiW_{12}O_{40}]^{4-}$-catalyzed processes

Substrate	Products	Comments	References
phenol, *p*-cresol	pyrocatechol, hydroquinone, 4-hydroxybenzyl alcohol, CO_2	Aqueous solutions; room temperature; $\lambda > 320$ nm cutoff filter; pH =3	63
chlorinated phenols	CO_2, HCl	aqueous solution; $\lambda > 320$ nm; pH = 3.0; temperature 20 ^oC	67

$[P_2W_{18}O_{62}]^{6-}$-catalyzed processes

Substrate	Products	Comments	References
alkane (2,3-dimethylbutane)	alkene	MeCN solutions of POM and alkane; room temperature; $\lambda = 280$ nm cutoff filter; Ar atmosphere	57,58
cis-2-decalone	octalones	CH_3CN solution; $\lambda > 305$ nm; room temperature; Ar atmosphere	68
Thioether (tetrahydrothiophene; dimethyl sulfide)	α,α'-dimeric coupling product; (methylthio)methanol	CH_3CN solution; 550W Hg lamp for anaerobic oxidation (Ar atmosphere) or 1000W Xe lamp $\lambda > 340$ nm for aerobic reactions; temperature 25 ^oC	74

$[PMo_{10}V_2O_{40}]^{5-}$-catalyzed processes

Substrate	Products	Comments	References

cyclic diene (9,10-dihydroanthracene, 1,4-cyclohexadiene, etc.)	aromatization products	1,2-dichloroethane solution of POM and substrates, tetraglyme, 70 ^{o}C, 1 atm O_2	84
thioether (tetrahydrothiophene; dimethyl sulfide)	α,α'-dimeric coupling product; (methylthio)methanol	CH_3CN solution; 550W Hg lamp for anaerobic oxidation (Ar atmosphere) or 1000W Xe lamp λ > 340 nm for aerobic reactions; temperature 25 ^{o}C	74

1.3 Merging Organometallics with POM Chemistry

Functionalization of POMs with an organic or organometallic unit has garnered growing consideration for a long time. Several comprehensive reviews and a many reports on this topic have been published over decades.[2,6,85-88] Initially, the motivation for this research was to use POMs as structurally well-defined metal-oxide molecular analogues.[89,90] Metal-oxide-supported catalysts are of great versatility and practical importance in academic and industrial synthetic organic transformations, but the intimate mechanisms of these heterogeneous catalysts are hard to investigate. Hence, as molecular metal-oxide analogues, the POMs, can simulate some of the properties of the above catalysts structurally and mechanistically.[91] The interfaces between POMs and the grafted organic/organometallic compounds can be characterized at an atomic level. Moreover, the non-oxidizable POM supports can stabilize the less-stable organic/organometallic compounds. The resulting hybrids sometimes display noteworthy features as multi-functional catalysis, photochromic and electrochromic materials.[92-94]

Overall the organic-inorganic hybrid POMs comprise two categories.[87] One incorporates the systems where no covalent bonds are shared between the organic and inorganic components. These hybrids are usually constructed through electrostatic interactions, hydrogen bonds and Van der Waals forces. The physical and chemical properties in this class are usually limited by diffusion so they are less interesting. The other class involves strong covalent bonds connecting the POMs and organic moieties.

We focus on the latter class in this thesis. The embedded functional groups are present as pure organic ligands or organometallic complexes. A central difficulty in this work is the development of controlled predictable syntheses of these compounds. The reactivity of POMs with attached organic or organometallic units has been rarely studied. Most of these compounds have been made from one-pot reactions. Nevertheless, quite a few of these hybrids have now been reported: one is referred to the itemized lists in previous reviews and follow-up publications.[85-87] We select several representative examples to introduce this area briefly.

The trisalkoxo ligands of the type $\{RC(CH_2O)_3\}^{3-}$ (tris; R = Me, NO_2, NH_2, CH_2OH, $CHNC(O)CH=CH_2$) have been widely used. They specifically bridge three metal centers in a triangular arrangement, or cap the triangular faces of POM frameworks. These ligands readily react with several polymolybdates and polyoxovanadates, resulting in a series of hybrid POMs with different structures, such as $[Mo_2O_4(tris)_2]^{2-}$, $[Mo_3O_6(OR)(tris)_2]^{-}$, $[Mo_4O_8(OR)_2(tris)_2]$, $[Mo_8O_{20}(OR)_4(tris)_2]^{2-}$, $[V_6O_{13}(tris)_2]^{2-}$, $[V_{10}O_{16}(tris)_4]^{4-}$, $[V_{16}O_{20}\{RC(CH_2O)_3\}_8(H_2O)_4]$, $[(RC(CH_2O)_3)P_2V_3W_{15}O_{59}]^{6-}$ and the others.[85,95-101]

It should be noted that the precursor $[V_6O_{13}(tris)_2]^{2-}$ are amenable for an additional type of reaction, a process that can be referred to as post-functionalization. For example, treating $(n\text{-}Bu_4N)_2[V_6O_{13}(tris)_2]$ with a pyrene-containing succinate ester generates novel inorganic-organic hybrids which display fluorescent properties (**Scheme 1-4**).[102] In polar solvents, these hybrid clusters show noteworthy amphiphilic properties by forming spherical vesicular structures, which suggests potential applications in artificial cells, nanoreactors, and drug/gene delivery. Another interesting example shows a self-assembly

process involving a pre-functionalized hybrid, $[V_6O_{13}\{(OCH_2)_3C(NHCH_2C_6H_4\text{-}4\text{-}CO_2)\}_2]^{4-}$, organic ligand 4,4'-bis(pyridine-*N*-oxide) and Tb(III) ions. The resulting coordination polymer shows catalytic activity for aerobic oxidation (**Scheme 1-5**).[103,104]

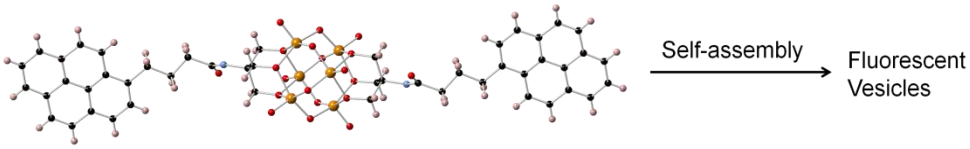

Scheme 1-4 Schematic representation for construction of a fluorescent vesicle

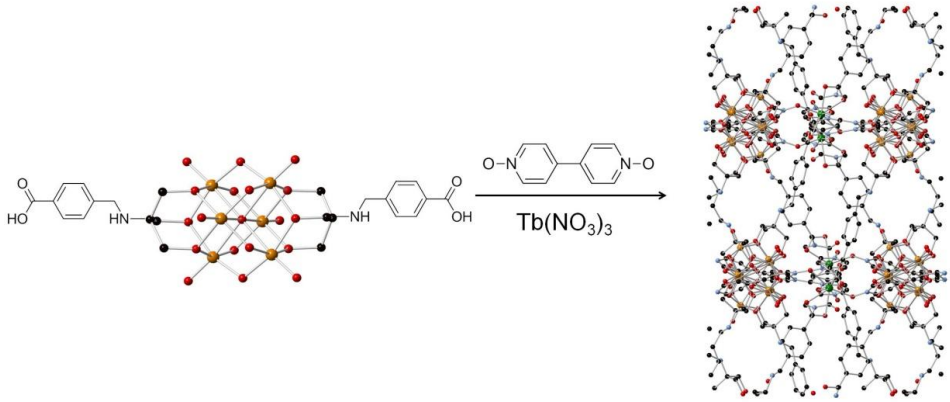

Scheme 1-5 Construction of a POM-based coordination framework from a functionalized hybrid precursor, $[V_6O_{13}\{(OCH_2)_3C(NHCH_2C_6H_4\text{-}4\text{-}CO_2)\}_2]^{4-}$.

Another well-studied family includes POMs functionalized by multiply bonded nitrogen ligands. Typically, treating the Lindqvist-type $[Mo_6O_{19}]^{2-}$ polyanions with isocyanates, phosphinimines, sufinylamines or amines in organic solvents results in a family of hybrid compounds, $(n\text{-}Bu_4N)_2[Mo_6O_{18}(NR)]$ (R = *p*-Tol, *t*-Bu, *o*-Tol, $(i\text{-}Pr)_2$-2,6-C_6H_3, Cy, Fc, Ph, (O_2N)-*p*-C_6H_4, etc.).[105-107] The itemized lists of previously reported compounds before and after 1998 can be found in reviews.[85,87] Recently, these compounds have shown interesting applications in constructing post-functionalized hybrids. By incorporating an iodo group (**Scheme 1-6**), POM-containing conjugated polymers or terpyridine-POM clusters, could be made through the palladium-catalyzed

cross-coupling reaction engaging 2,5-di(2,2-dimethylpropoxy-1,4-diethynylbenzene) or 4'-ethynyl-2,2',6',2''-terpyridine, respectively.[108-110] The later can be used to capture transition metals to form POM-photosensitizer dyads.

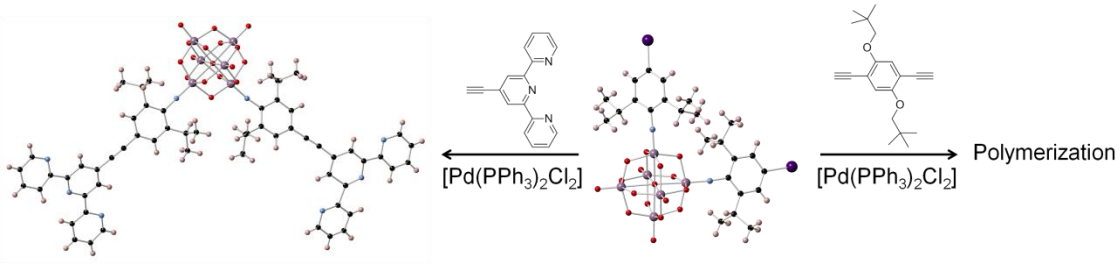

Scheme 1-6 Synthesis of conjugated hybrids through Pd-catalyzed cross-coupling reactions involving the functionalized Lindqvist-type POM, $[Mo_6O_{19}]^{2-}$

The majority of studies in this area involve complexation of organometallic cations with POM anions, a research area investigated by Knoth, Day and Klemperer, Finke, Isobe, Proust and Gouzerh.[85,90,111-113] The difference between organometallic "supported" on and "incorporated" into POMs, as emphasized by Finke, relies on the bonded oxygen atoms.[112] The supported mode means that species attach to the surface oxygen atoms of POMs, while the incorporated mode indicates that organometallic cations residue in the vacant sites of lacunary POMs. The first example of these hybrids was $[PW_{11}O_{39}(TiCp)]^{4-}$, prepared by reaction of $(n\text{-}Bu_4N)_4[H_3PW_{11}O_{39}]$ with $[CpTiCl_3]$ in 1,2-$C_2H_4Cl_2$.[114] Most of organometallic cations used are cyclopentadienyl derivatives, such as $CpTi^{3+}$, Cp^*Rh^{2+}. Some are d^6 metal derivatives such as $(\eta_6\text{-}C_6H_6)Ru^{2+}$, $(1,5\text{-COD})Ir^+$, and metal carbonyl groups ($[Re(CO)_3]^+$, $[Mn(CO)_3]^+$). A wide range of Lindqvist, Keggin and Dawson POMs have been used. In some cases, surface activation can only be achieved by replacing Mo(VI) or W(VI) centers with one or more lower-valent metals, such as V(V) or Nb(V). This gives the resulting POMs sufficient charge density at the surface oxygen

atoms. For example, β-$[SiW_9M_3O_{40}]^{7-}$ and $[P_2W_{15}M_3O_{62}]^{9-}$ (M = V and Nb) are very reactive with organometallic cations.[115,116] Several representative examples are illustrated in **Scheme 1-7**.[117-122] The full tables can be found in the two reviews in 1998 and 2010 respectively.[85,87]

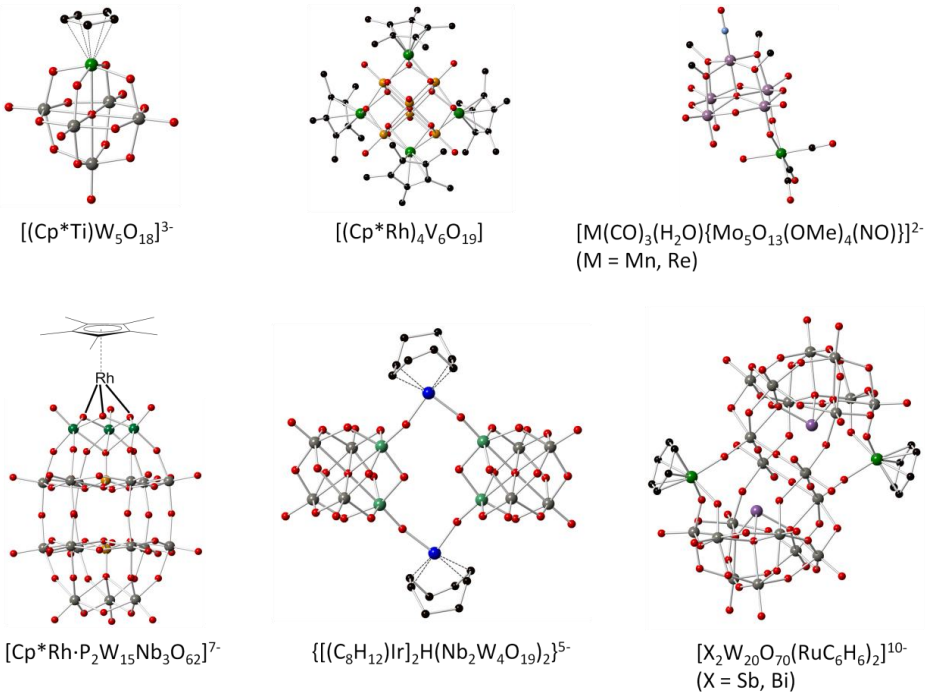

Scheme 1-7 Representative examples of POM-organometallic hybrids

POMs functionalized with organosilyl, organophosphorus, organoarsenic, and organoantimony ligands provide opportunities for post-functionalization. As seen in **Scheme 1-8**, the bis(silyl) and bis(phosphonyl) derivatives of $[P_2W_{17}O_{61}]^{10-}$ with terminal azides or alkynes are reactive with perylene and porphyrin conjugates. The resulting POM-chromophore dyads, which are obtained through Huisgen 1,3-dipolar cycloadditions, show fluorescence quenching behavior due to intramolecular electron transfer to the POM ligands.[123,124] Upon changing the azide or alkyne group to iodo, the above post-functionalization can be achieved through Sonogashira coupling reactions.

Several POM hybrids with grafted ruthenium/iridium polypyridyl complexes were recently prepared. The photophysical properties of these systems were thoroughly studied by transient absorption and spectroelectrochemical measurements. The photo-induced electron-transfer process from the chromophores to the POM acceptors has been documented. Among these compounds, the heteroleptic cyclometalated iridium(III) complex exhibits the longest lifetime in the charge-separation excited states to date. These features allow the excited states to be captured by external substrates, and thus these compounds become potentially useful for photo-driven chemical reactions.[94,125,126]

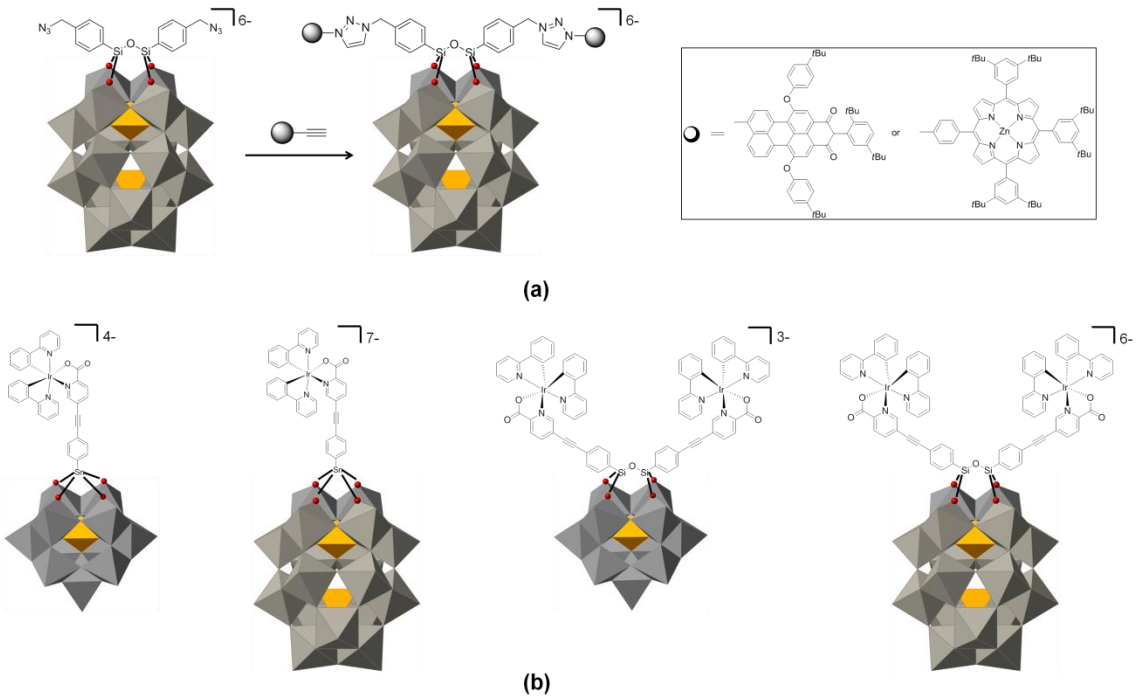

Scheme 1-8 Schematic illustrations of POM-photosensitizer dyads involving chromophores of (a) perylene/porphyrin and (b) ruthenium/iridium polypyridyl complexes

1.4 Transition-Metal-Substituted POMs with Applications in Catalytic Water Oxidation

Lacunary POMs have been widely used as rigid and multi-dentate inorganic ligands to capture transition metals. They particularly can stabilize the polynuclear metallic cores. These transition-metal-substituted POMs exhibit not only structural diversity, but also have versatile applications in catalysis, medicine and materials. A very large number of such compounds were reported previously. Several reviews, including the special issue in 1998 and some recent ones by Cronin *et al.*, have addressed the fundamentals in this area.[6,127-130] Yang and co-workers recently published a review, including a detailed list of all the transition-metal-substituted POMs to date, containing the first-row paramagnetic metals.[131]

The magnetism of first-row transition-metal-substituted POMs has been explored for a long time. Some noteworthy examples, such as $\{[SiW_9O_{34}]_2[Mn^{III}_4Mn^{II}_2O_4(H_2O)_4]\}^{12-}$,[132] $[(Fe_4W_9O_{34}(H_2O))_2(FeW_6O_{26})]^{19-}$, $[Fe_4(H_2O)_2(FeW_9O_{34})_2]^{10-}$,[133,134] as well as $[\{Co_4(OH)_3PO_4\}_4(PW_9O_{34})_4]^{28-}$,[135] and others, exhibit single-molecule-magnet (SMM) behavior. In addition, the catalytic activities of transition-metal-substituted POMs make them particularly attractive, potentially, for industrial applications.[136-139] For instance, there is a Japanese process involving palladium and POMs as co-catalysts for the direct oxidation of ethylene to acetic acid on a scale of 100,000 tons per year. The vanadate-substituted polymolybdates, such as $Cs_{2.5}H_{1.5}PVMo_{11}O_{40}$ and $H_5PV_2Mo_{10}O_{40}$ for aerobic oxidation, were investigated thoroughly by Mizuno, Neumann and co-workers.[84,140,141] $TBA_4[\gamma\text{-}HPV_2W_{10}O_{40}]$ was demonstrated as an effective homogeneous catalyst for the H_2O_2-based oxidative bromination of alkenes, alkynes and aromatic compounds.[142]

$TBA_4[\gamma\text{-}H_2SiW_{10}O_{36}Pd_2(OAc)_2]$ displays high catalytic activity for the hydration of nitriles including aromatic, aliphatic, heteroaromatic and double-bond-containing species.[143] $K_9[(Fe^{III}(OH_2)_2)_3(A\text{-}\alpha\text{-}PW_9O_{34})_2]$, when supported on silica nanoparticles, exhibits efficient catalytic activity for the aerobic oxidation of sulphides and aldehydes.[144,145]

Recently, the incorporation of POMs and metal-organic-frameworks (MOFs), named POM-MOFs, has received increasng attention. Most of these POM-MOFs were based on the plenary Keggin POMs such as $[PW_{12}O_{40}]^{3-}$ and $[PMo_{12}O_{40}]^{3-}$. Liu *et al.* prepared a series of POM-MOFs in the type of $[Cu_2(BTC)_{4/3}(H_2O)_2]_6[H_nXM_{12}O_{40}]$ (X = Si, Ge, P, As; M = W, Mo).[146] These compounds were generally obtained using a simple one-step hydrothermal reaction involving copper ions, benzentricaboxylate (BTC) and POMs. If the plenary POMs are replaced with their transition-metal-substituted analogous, the resulting POM-MOFs exhibit additional noteworthy properties. For example, Hill *et al.* used encapsulate the copper-substituted POM, $[CuPW_{11}O_{39}]^{5-}$, in MOF-199 to construct a POM-MOF which shows synergistic reactivity for detoxification of sulfides (**Scheme 1-9(a)**).[147] Dolbecq *et al.* made several structures in which the POM unit functions as a connector in the MOF framework, and not simply incorporated in the MOF pores. These "POMOFs", i.e. $[PMo^{V}_{8}Mo^{VI}_{4}O_{37}(OH)_3Zn_4][C_6H_3(COO)_3]^{3-}$, comprise molecular Zn-capped Keggin units connected by BTC linkers. These complexes are active for electrocatalytic hydrogen evolution.[148] Purely inorganic 3D frameworks based on transition-metal-substituted POMs are also reported. For example, Cronin *et al.* recently reported a giant cluster, which is built from $[P_8W_{48}O_{184}]^{40-}$ as faces and Mn(II) as linkages (**Scheme 1-9(b)**). This macrocyclic polyoxometalate structure contains 7.24 nm^3

cavities which are accessible for transition-metal ions, as demonstrated by an ionic exchange process with alkali cations.[149]

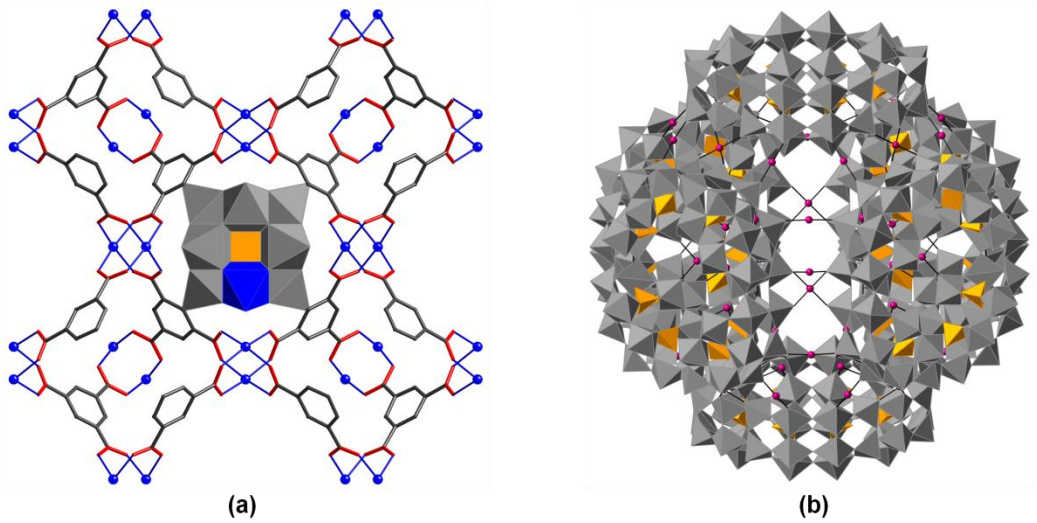

Scheme 1-9 X-ray structures of (a) a POM-MOF, $[\{Cu_3(C_9H_3O_6)_2\}_4\{CuPW_{11}O_{39}H\}]^{4-}$ and (b) a purely inorganic POM framework, $[Mn_8(H_2O)_{48}P_8W_{48}O_{184}]^{24-}$.

A breakthrough in POM catalysis involves their use as catalysts in solar fuel production. Solar is the ultimate renewable energy source because the planet is bathed in an essentially inexhaustible quantity of such energy.[150] The most evident conversion of solar light into chemical energy is green-plant photosynthesis. Artificial photosynthesis based on some photovoltaic systems has been developed rapidly in recent years.[151,152] The production of solar fuels is a field that requires achievement of several scientific and engineering goals. The reactions of great interest in conjunction with solar fuels technology are water splitting and CO_2 reduction, and a practical platform must include several operations such as light absorption, charge separation, multiple electron or hole transfer, and so on.[153] While the photosensitizers and reduction catalysts are relatively more researched and developed, water-oxidation catalysts (WOCs) were far less studied in the past but are currently undergoing intense investigation.[154,155] An ideal WOC should

be water compatible, have several oxidation states to facilitate multi-electron transfer processes such as water oxidation, $2H_2O \rightarrow O_2 + 4H^+ + 4e^-$, a four-electron process.

A range of homogeneous, heterogeneous, and inorganic-organic hybrid composite WOCs have been reported previously. They can be found in some reviews.[156-165] Compared to previous catalysts, the POM-based WOCs contain multi-nuclear redox centers, and display high solubility and stability in aqueous solutions. Consequently, they are particularly attractive for the development of robust and water-compatible WOCs. The multi-metallic cores stabilized by POMs constitute a model of sorts for the oxygen-evolution center (OEC) in green-plant photosynthesis, a cluster of Mn_4CaO_5, in photosynthetic system.[166,167] These all-inorganic WOCs have attracted considerable attention in the area of solar fuels. This sub-field was initiated by two publications, one by the Hill group and one by the Bonchio group, published the same day in 2008, that reported the synthesis of $[Ru^{IV}_4O_4(OH)_2(OH_2)_4(\gamma\text{-}SiW_{10}O_{36})_2]^{12-}$ (**Ru4**) and demonstrated its activity for catalytic water oxidation.[168-171] Subsequently, the Hill group reported two additional Ru/Ir-substituted POMs, $[(\gamma\text{-}PW_{10}O_{36})_2Ru^{IV}_4O_6(OH_2)_4]^{10-}$ and $[(IrCl_4)KP_2W_{20}O_{72}]^{14-}$, which are also fast water-oxidation catalysts.[172,173] A more significant catalyst is the more-recently reported $[Co_4(H_2O)_2(PW_9O_{34})_2]^{10-}$ (**Co4**), which is composed by only earth abundant elements and shows high efficiency in photocatalytic water-oxidation.[164,174] Thereafter several POM-based WOCs have been reported, the details of which can be found in the recent review from Hill group.[165]

Several studies have been conducted on **Ru4**. The Bonchio group studied oxygen evolution at pH ~0.6 using excess Ce(IV) as the oxidant and reported a TON of 500 with an initial TOF of 0.125 s^{-1}. Upon using $[Ru(bpy)_3]^{2+}$ as a photosensitizer and $S_2O_8^{2-}$ as a

sacrificial electron acceptor, the Hill group obtained up to 350 turnovers with an initial TOF and quantum yield ($\Phi(O_2)$) of 0.08 s^{-1} and 9%, respectively. **Co4** was synthesized many years ago but was only shown to be a WOC in 2010 by the Hill group. Initially the ability of **Co4** to catalyze water oxidation in the dark, by using $[Ru(bpy)_3]^{3+}$ as a chemical oxidant in aqueous phosphate buffer solution at pH 8.0 was reported. The TON is over 1000 in 3 min affording a TOF of 5 s^{-1}, which was the highest rate for a homogeneous WOC at that time. **Co4** also catalyzes water oxidation under visible-light-driven conditions. Under optimal conditions using $[Ru(bpy)_3]^{2+}$ as the photosentizer and $S_2O_8^{2-}$ as the sacrificial electron donor, a TON of over 220 and high quantum yield of 30% were obtained in pH 8.0 borate buffer.

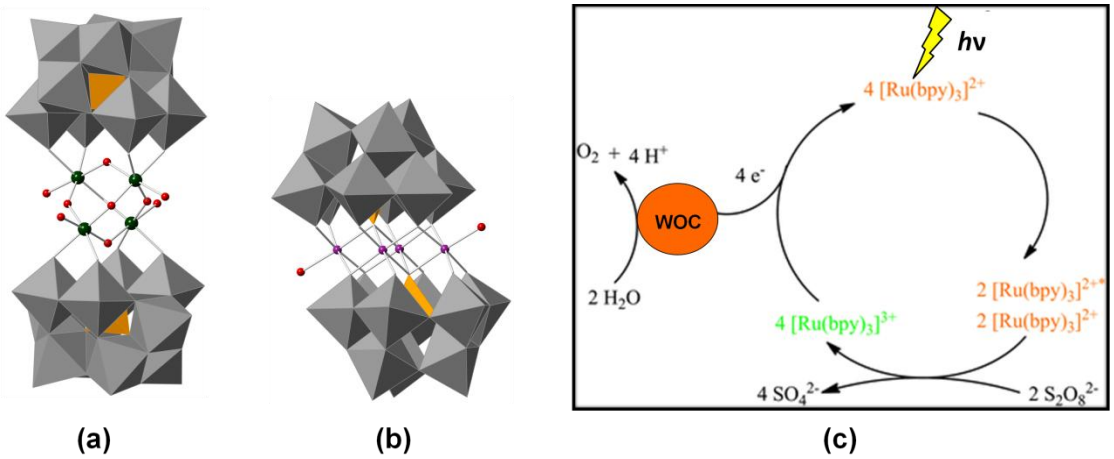

Scheme 1-10 Schematic presentations for the X-ray structures of (a) $[Ru^{IV}_4O_4(OH)_2(OH_2)_4(\gamma\text{-}SiW_{10}O_{36})_2]^{12-}$ (**Ru4**), (b) $[Co_4(H_2O)_2(PW_9O_{34})_2]^{10-}$ (**Co4**) and (c) a scheme for homogeneous light-driven water oxidation catalyzed by these POMs.

It should be noted that the above homogeneous light-driven system, containing $[Ru(bpy)_3]^{2+}$ and $S_2O_8^{2-}$, has been well-studied for a long time.[175-177] Basically, the triplet ^{3}MLCT excited state, $[Ru(bpy)_3]^{2+}$*, is quenched by $S_2O_8^{2-}$ through both bimolecular and unimolecular processes, which generates $[Ru(bpy)_3]^{3+}$ and $SO_4^{-\cdot}$. The latter radical

subsequently oxidizes a second $[Ru(bpy)_3]^{2+}$ quantitatively to $[Ru(bpy)_3]^{3+}$. Four equivalents of $[Ru(bpy)_3]^{3+}$ are accumulated for the oxidation of water.

Nanoscale structures for oxygen evolution constructed by anchoring WOCs onto robust supports is currently under the focus of much exploration, because these hybrid systems display controllable mechanical properties, high surface areas and have high thermal stability. Bonchio's group successfully attached **Ru4** and polyamidoamine electrostatically onto multi-wall carbon nanotubes (MWCNTs).[178] A modified method of directly functionalizing MWCNT surfaces with positive charge was also reported.[179] They can absorb negatively-charged **Ru4** POMs electrostatically. The electrocatalytic activities of these hybrid nanocomposites were carefully evaluated. Similarly, **Co4** was immobilized on mesoporous carbon nitride (MCN).[180] The **Co4**/MCN composite efficiently catalyzes the oxygen evolution with a Faradaic efficiency as high as 95% and a TOF of ~0.3 s^{-1}, which indicates a much higher efficiency compared to **Ru4**/MWCNTs composite.

1.5 Metal-to-Metal Charge-Transfer Chromophores

As mentioned in the previous section, to date the light-harvesting centers in photo-driven catalytic systems are mostly based on organic dyes and organometallic complexes. These compounds exhibit intense ligand-centered absorption bands in the UV region and metal-to-ligand charge-transfer (MLCT) bands in the visible region. They also show a relatively long-lived luminescence in the red spectral region, originating from the lowest ^{3}MLCT state. These features make them excellent photosensitizers.[153,175-177] Nevertheless, the oxidizable organic ligands are usually unstable under turnover conditions (in which

strong oxidants are frequently used or generated *in situ*). This limitation restricts their applications in development of robust and water-compatible photovoltaic devices. One method en route to stable and inorganic chromophores is by grafting transition metals into the frameworks of micro- or mesoporous sieves such as silicates or aluminophosphates. The resulting chromophores exhibit ligand-to-metal charge-transfer (LMCT) transitions rooted from framework oxygen to the metal center. However, these transitions usually show up in the UV region, so they are generally accessible to only a less than 5% of incident solar radiation.[181-183] Therefore, obtaining inorganic porous materials with visible-light activity remains a great challenge.

Through engaging a second metal center, the electron donor, in the above mesoporous sieves, Frei *et al.* developed several oxo-bridged metal-to-metal charge-transfer (MMCT) chromophores.[184-193] These novel bimetallic assemblies exhibit absorption bands in the visible or even near-IR regions. Since a wide variety of transition metals in different oxidation states are compatible with construction of these assemblies, some of these assemblies could potentially function as effective harverters of solar light. More significantly, some MMCT chromophores show extremely low rates of back electron-transfer. The long-lived excited states of these assemblies make them suitable for driving multi-electron-transfer catalytic reactions.[193]

For example, the bimetallic assembly Ti^{IV}-O-Mn^{II} supported on SBA-15 has a long excited-state lifetime of 2 μs.[193] Upon irradiation by visible light, the Ti^{IV}-O-Mn^{II} to Ti^{III}-O-Mn^{III} MMCT transition occurs along with structural reorganization of the silica coordination sphere. This transformation, involving a proposed temporary break of Ti^{IV}-O bonds and formation of Mn^{III}-O bonds, imposes a significant barrier to back electron

transfer. The long lifetimes of these MMCT chromophores could explain their photochemical activity. For example, the bimetallic Zr(IV)-O-Cu(I) MMCT chromophore on MCM-41 is active for the photochemical reduction of CO_2 to CO (**Scheme 1-11**). A mechanistic study indicates the dissociation of CO_2 and capture of an electron from the MMCT-excited Zr(III) center. The resulting OH· radicals then diffuse through the pores and are trapped and reduced to H_2O.

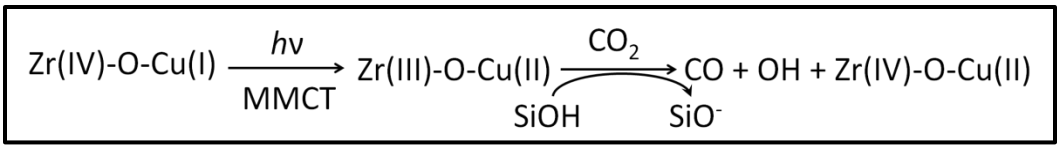

Scheme 1-11 Scheme for CO_2 splitting by a MMCT chromophore

The Cr^{VI}-centered MCM-41 silica, coupled with an Ir oxide nanoparticle WOC, shows water-oxidation activity under visible-light irradiation.[187] In this example, the absorption in the visible region is basically due to the LMCT transition concerning the Cr^{VI} centers. The resulting transient hole on oxygen bears a potential of over +3 V, which is far more than enough for water oxidation (E = 1.23 V *vs.* NHE). By replacing the CrO LMCT chromophore with a bimetallic MMCT $TiOCr^{III}$ chromophore anchored to a mesoporous silica AlMCM-41, oxygen evolution with a quantum yield of >13% was achieved (**Scheme 1-12**). The photo-driven experiments were performed by irradiation of an aqueous suspension of the Ir-oxide/$TiOCr^{III}$/AlMCM-41 powders. EXAFS studies found these MMCT chromophores have shorter Cr-O bonds in the Ti-O-Cr bridges, than in Cr-O-Si, indicating the partial charge-transfer character of the ground electronic state. EPR signals demonstrated that electron donation from Ir oxide cluster to transient Cr^{IV} successfully competes with back electron-transfer from Ti^{III}.

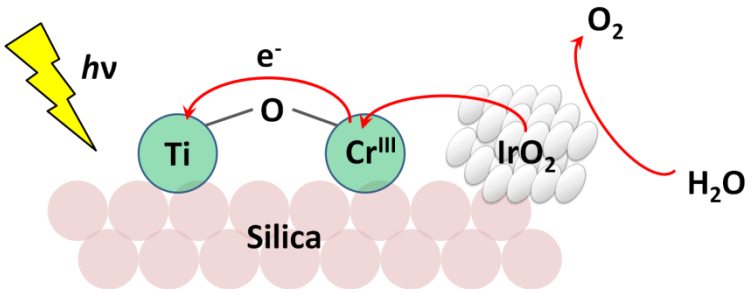

Scheme 1-12 Scheme for photo-driven water oxidation on a bimetallic MMCT chromophore coupled with an iridium oxide WOC.

Hashimoto *el al.* also investigated MMCT systems. An MMCT chromophore constructed from Ti^{IV}-O-Ce^{III} bimetallic assembly on MCM-41 results in high quantum efficiency isopropanol oxidation upon irradation with 460-nm monochromic light.[194] This is a better photocatalyst than the most active semiconductor, i.e. nitrogen-doped TiO_2. POMs were also introduced to this research area. As mentioned previously, POMs have a very rich redox chemistry. POMs are all-inorganic clusters and can easily function as multi-electron acceptors, but the coupled photochemical reactions are usually driven with UV-light irradiation. Hashimoto *el al.* made POM-containing chromophores absorb in the visible region by anchoring the POMs (electron acceptors) and Ce(III) centers (electron donors) in the pores of MCM-41.[195] The resulting complex contains oxo-bridged W^{VI}-O-Ce^{III} linkages between Ce and an immobilized $PW_{12}O_{40}$ cluster which exhibits a new kind of absorption in the visible region. This feature was assigned as a Ce^{III}-W^{VI} MMCT transition. A trimetallic charge-transfer unit was also developed upon replacing $PW_{12}O_{40}$ with a Cu-substituted Keggin POM, $Cu^{II}PW_{11}O_{39}$. The Cu center is capable of accommodating two electrons following irradiation of the Ce^{III}-W^{VI} MMCT chromophore.[196]

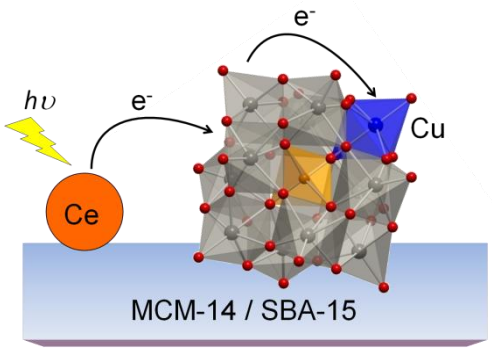

Scheme 1-13 Schematic illustrations of MMCT transitions occurring at anchored oxo-bridged Cu/W/Ce trimetallic complexes

However, all the above MMCT chromophores are heterogeneous systems. As a resut, there is no detailed molecular-level information about the interfaces between the metal oxides and anchored donors. The dynamics and kinetics of charge separation in the excited states are not clear either. As we noted above, POMs provide an excellent molecular model to study the interfaces between metal oxides and supported guest compounds. Therefore, we targeted the preparation of visible-light-active POMs to facilitate a detailed study of these MMCT transitions and possible redox chemistry induced by these excited states.

1.6 Goal of This Work and Outline

The first object of this dissertation is to investigate the coordination chemistry of POMs with organometallic complexes. We focus initially on a family of POM-supported metal carbonyl complexes. **Chapter 2** reports a facile and water-compatible procedure to make these hybrid complexes by carefully choosing suitable POM supports, the Krebs-type subvalent Sb^{III}/Bi^{III}-centered polyanions. The synthesis, characterization and photochemical properties of the resulting "slipped-sandwich" series of POMs are described in detail in **Chapter 2**. In **Chapter 3** we expand the work in an attempt to

synthesize the tungstophosphate analogues. Instead of making similar "slipped-sandwich" architectures, we obtain several "twisted-sandwich" hybrids from the mono-vacant tungstophosphates. These hybrids show interesting molecular chirality in the solid state. This work culminated in production of a new family of dimeric structures of POM-supported metal carbonyl compounds.

The second object and the central imputes of this thesis is to characterize visible-light-active POM chromophores. In **Chapter 4**, we comprehensively investigate the photochemical properties of the above functionalized POMs. A detailed study including time-resolved spectroscopy and computational work has been used to characterize the excited states of a POM-supported rhenium carbonyl complex. The results clearly indicate that a novel transition occurs from the rhenium center to the POM ligand, which we consequently define as a "metal-to-POM charge-transfer or MPCT" process. A novel hybrid structure constructed from a POM scaffold and an embedded tri-rhenium carbonyl cluster is described in **Chapter 5**. This work entails a comprehensive study involving synthesis, characterization, transient spectroscopy, spectroelectrochemistry and theoretical calculations, to interpret the excited states of this "double-cluster". The MPCT transition in this compound can thus be regarded as cluster-to-cluster charge-transfer.

Finally, in **Chapter 6**, we describe the synthesis and crystal structures of several high-nuclear cobalt(II) and tin(II) substituted POMs. The cobalt(II) derivatives have been evaluated for catalytic water oxidation activity. The tin(II) POMs are all-inorganic nanoscaled clusters which display porous channels in their crystal structures, and show high absorption in the visible region. They are potentially another class of inorganic chromophores for solar light conversion.

References

(1) Pope, M. T. *Heteropoly and Isopoly Oxometalates*; Springer-Verlag: Berlin, 1983.

(2) *Polyoxometalates: From Platonic Solids to Anti-retroviral Activity*; Pope, M. T.; Müller, A., Eds.; Kluwer Academic Publishers: Dordrecht, Netherlands, 1993.

(3) *Polyoxometalate Chemistry From Topology via Self-Assembly to Applications*; Pope, M. T.; Müller, A., Eds.; Kluwer Academic Publishers: Dordrecht, 2001.

(4) Berzelius, J. J. *Poggendorfs Ann. Phys. Chem.* **1826**, *6*, 369.

(5) Katsoulis, D. E. *Chem. Rev.* **1998**, *98*, 359.

(6) *Special Thematic Issue on Polyoxometalates*; Hill, C. L., Ed., 1998; Vol. 98, No. 1.

(7) Pope, M. T. In *Comprehensive Coordination Chemistry*; Wilkinson, G., Gillard, R. D., McCleverty, J. A., Eds.; Pergamon Press: New York, 1987; Vol. 3, p Chapter 38.

(8) Keggin, J. F. *Nature* **1933**, *131*, 908.

(9) Baker, L. C. W.; Figgis, J. S. *J. Am. Chem. Soc.* **1970**, *92*, 3794.

(10) Brown, G. M.; Noe-Spirlet, M. R.; Busing, W. R.; Levy, H. A. *Acta Crystallogr., Sect. B: Struct. Sci.* **1977**, *B33*, 1038.

(11) Naruke, H.; Yamase, T. *Acta Crystallogr., Sect. C: Cryst. Struct. Commun.* **1992**, *48*, 597.

(12) Khan, M. I.; Cevik, S.; Hayashi, R. *J. Chem. Soc., Dalton Trans.* **1999**, 1651.

(13) Brevard, C.; Schimpf, R.; Tourné, G.; Tourné, C. M. *J. Am. Chem. Soc.* **1983**, *105*, 7059.

(14) Matsumoto, K. Y.; Sasaki, Y. *Bull. Chem. Soc. Jpn.* **1976**, *49*, 156.

(15) Canny, J.; Tézé, A.; Thouvenot, R.; Hervé, G. *Inorg. Chem.* **1986**, *25*, 2114.

(16) Domaille, P. J. In *Inorg. Synth.*; Ginsberg, A. P., Ed.; John Wiley and Sons: New York, 1990; Vol. 27, p 96.

(17) Nsouli, N. H.; Bassil, B. S.; Dickman, M. H.; Kortz, U.; Keita, B.; Nadjo, L. *Inorg. Chem.* **2006**, *45*, 3858.

(18) Robert, F.; Tézé, A. *Acta Crystallogr.* **1981**, *B37*, 318.

(19) Randall, W. J.; Droege, M. W.; Mizuno, N.; Nomiya, K.; Weakley, T. J. R.; Finke, R. G. In *Inorg. Synth.*; Cowley, A. H., Ed.; John Wiley & Sons, Inc.: New York, 1997; Vol. 31, p 167.

(20) Bosing, M.; Loose, I.; Pohlmann, H.; Krebs, B. *Chem. Eur. J.* **1997**, *3*, 1232.

(21) Dawson, B. *Acta Crystallogr., Sect. B: Struct. Sci.* **1953**, *6*, 113.

(22) Randall, W. J.; Lyon, D. K.; Domaille, P. J.; Finke, R. G. In *Inorg. Synth.*; Darensbourg, M. Y., Ed.; John Wiley & Sons, Inc.: New York, 1998; Vol. 32, p 242.

(23) Contant, R.; Thouvenot, R. *Can. J. Chem. - Revue Canadienne de Chimie* **1991**, *69*, 1498.

(24) Contant, R.; Thouvenot, R. *Inorg. Chim. Acta* **1993**, *212*, 41.

(25) Laronze, N.; Marrot, J.; Hervé, G. *Chem. Commun.* **2003**, 2360.

(26) Miras, H. N.; Long, D.-L.; Kogerler, P.; Cronin, L. *Dalton Trans.* **2008**, *0*, 214.

(27) Wang, J.; Li, S.; Shen, Y.; Niu, J. *Cryst. Growth Des.* **2008**, *8*, 372.

(28) Long, D.-L.; Kögerler, P.; Cronin, L. *Angew. Chem. Int. Ed.* **2004**, *43*, 1817.

(29) Long, D.-L.; Abbas, H.; Kögerler, P.; Cronin, L. *Angew. Chem. Int. Ed.* **2005**, *44*, 3415.

(30) Cronin, L. In *Comprehensive Coordination Chemistry II: From the Molecular to the Nanoscale: Synthesis, Structure, and Properties*; McCleverty, J. A., Meyer, T. J., Eds.; Elsevier: Amsterdam, 2004; Vol. 7, p 1.

(31) Hill, C. L. In *Comprehensive Coordination Chemistry-II: From Biology to Nanotechnology*; Wedd, A. G., Ed.; Elsevier Ltd.: Oxford, UK, 2004; Vol. 4, p 679.

(32) Pope, M. T. In *Comprehensive Coordination Chemistry II: From Biology to Nanotechnology*; Wedd, A. G., Ed.; Elsevier Ltd.: Oxford, UK, 2004; Vol. 4, p 635.

(33) Rindl, M. *South African Journal of Science* **1916**, *11*, 362.

(34) Yamase, T. *Chem. Lett.* **1973**, 615.

(35) Yamase, T.; Hayashi, H.; Ikawa, T. *Chem. Lett.* **1974**, 1055.

(36) Yamase, T.; Ikawa, T. *Bull. Chem. Soc. Jpn.* **1977**, *50*, 746.

(37) Yamase, T. *J. Chem. Soc., Dalton Trans.* **1978**, 283.

(38) Yamase, T. *Chem. Rev.* **1998**, *98*, 307.

(39) Pope, M. T.; Papaconstantinou, E. *Inorg. Chem.* **1967**, *6*, 1147.

(40) Varga, G. M.; Papaconstantinou, E.; Pope, M. T. *Inorg. Chem.* **1970**, *9*, 662.

(41) Papaconstantinou, E.; Dimotikali, D.; Politou, A. *Inorg. Chim. Acta* **1980**, *43*, 155.

(42) Dimotikali, D.; Papaconstantinou, E. *Inorg. Chim. Acta* **1984**, *87*, 177.

(43) Papaconstantinou, E. *Chem. Soc. Rev.* **1989**, *18*, 1.

(44) Hill, C. L.; Bouchard, D. A. *J. Am. Chem. Soc.* **1985**, *107*, 5148.

(45) Renneke, R. F.; Hill, C. L. *J. Am. Chem. Soc.* **1986**, *108*, 3528.

(46) Hill, C. L.; Bouchard, D. A.; Kadkhodayan, M.; Williamson, M. M.; Schmidt, J. A.; Hilinski, E. F. *J. Am. Chem. Soc.* **1988**, *110*, 5471.

(47) Hill, C. L.; Prosser-McCartha, C. M. In *Photosensitization and Photocatalysis Using Inorganic and Organometallic Compounds*; Kalyanasundaram, K., Grätzel, M., Eds.; Kluwer Academic Publishers: Dordrecht, 1993; Vol. 14, p 307.

(48) Duncan, D. C.; Netzel; L., T.; Hill, C. L. *Inorg. Chem.* **1995**, *34*, 4640.

(49) Pope, M. T.; Varga, G. M. *Inorg. Chem.* **1966**, *5*, 1249.

(50) El-Shamy, H. K.; Iskander, M. F. *J. Inorg. Nucl. Chem.* **1973**, *35*, 1227.

(51) Altenau, J.; Pope, M. T.; Prados, R. A.; So, H. *Inorg. Chem.* **1975**, *14*, 417.

(52) Pope, M. T. *NATO Adv. Study Inst. Ser., Ser. C* **1980**, *58*, 365.

(53) Kozik, M.; Hammer, C. F.; Baker, L. C. W. *J. Am. Chem. Soc.* **1986**, *108*, 7627.

(54) Kozik, M.; Hammer, C. F.; Baker, L. C. W. *J. Am. Chem. Soc.* **1986**, *108*, 2748.

(55) Darwent, J. R. *J. Chem. Soc., Chem. Commun.* **1982**, *14*, 798.

(56) Streb, C. *Dalton Trans.* **2012**, *41*, 1651.

(57) Renneke, R. F.; Pasquali, M.; Hill, C. L. *J. Am. Chem. Soc.* **1990**, *112*, 6585.

(58) Renneke, R. F.; Hill, C. L. *Angew. Chem. Int. Ed.* **1988**, *27*, 1526.

(59) Renneke, R. F.; Kadkhodayan, M.; Pasquali, M.; Hill, C. L. *J. Am. Chem. Soc.* **1991**, *113*, 8357.

(60) Hill, C. L.; Renneke, R. F.; Combs, L. *Tetrahedron* **1988**, *44*, 7499.

(61) Awad, M. K.; Anderson, A. B. *J. Am. Chem. Soc.* **1990**, *112*, 1603.

(62) Folcher, G.; Paris, J.; Chauveau, F. *Can. J. Chem.* **1985**, *63*, 2703.

(63) Mylonas, A.; Papaconstantinou, E.; Roussis, V. *Polyhedron* **1996**, *15*, 3211.

(64) Yamase, T.; Takabayashi, N.; Kaji, M. *J. Chem. Soc., Dalton Trans.* **1984**, 793.

(65) Yamase, T.; Usami, T. *J. Chem. Soc., Dalton Trans.* **1988**, 183.

(66) Jaynes, B. S.; Hill, C. L. *J. Am. Chem. Soc.* **1995**, *117*, 4704.

(67) Mylonas, A.; Papaconstantinou, E. *J. Photochem. Photobiol. A* **1996**, *94*, 77.

(68) Combs-Walker, L. A.; Hill, C. L. *J. Am. Chem. Soc.* **1992**, *114*, 938.

(69) Nomiya, K.; Sugie, Y.; Miyazaki, T.; Miwa, M. *Polyhedron* **1986**, *5*, 1267.

(70) Nomiya, K.; Miyazaki, T.; Maeda, K.; Miwa, M. *Inorg. Chim. Acta* **1987**, *127*, 65.

(71) Sattari, D.; Hill, C. L. *J. Chem. Soc., Chem. Commun.* **1990**, 634.

(72) Nomiya, K.; Maeda, K.; Miyazaki, T.; Miwa, M. *J. Chem. Soc., Dalton Trans.* **1987**, *4*, 961.

(73) Chambers, R. C.; Hill, C. L. *Inorg. Chem.* **1989**, *28*, 2509.

(74) Chambers, R. C.; Hill, C. L. *Inorg. Chem.* **1991**, *30*, 2776.

(75) Chambers, R. C.; Hill, C. L. *J. Am. Chem. Soc.* **1990**, *112*, 8427.

(76) Prosser-McCartha, C. M.; Hill, C. L. *J. Am. Chem. Soc.* **1990**, *112*, 3671.

(77) Zakrzewski, J.; Giannotti, C. *J. Photochem. Photobiol. A* **1992**, *63*, 173.

(78) Hill, C. L.; Kozik, M.; Winkler, J.; Hou, Y.; Prosser-McCartha, C. M. *Adv. Chem. Ser.* **1993**, *238*, 243.

(79) Attanasio, D.; Suber, L.; Thorslund, K. *Inorg. Chem.* **1991**, *30*, 590.

(80) Attanasio, D.; Suber, L. *Inorg. Chem.* **1989**, *28*, 3779.

(81) Zakrzewski, J.; Giannotti, C. *J. Photochem. Photobiol. A* **1991**, *57*, 453.

(82) Renneke, R. F.; Hill, C. L. *J. Am. Chem. Soc.* **1988**, *110*, 5461.

(83) Papaconstantinou, E. *J. Chem. Soc., Chem. Commun.* **1982**, 12.

(84) Neumann, R.; Lissel, M. *J. Org. Chem.* **1989**, *54*, 4607.

(85) Gouzerh, P.; Proust, A. *Chem. Rev.* **1998**, *98*, 77.

(86) Proust, A.; Thouvenot, R.; Gouzerh, P. *Chem. Commun.* **2008**, 1837.

(87) Dolbecq, A.; Dumas, E.; Mayer, C. R.; Mialane, P. *Chem. Rev.* **2010**, *110*, 6009.

(88) Proust, A.; Matt, B.; Villanneau, R.; Guillemot, G.; Gouzerh, P.; Izzet, G. *Chem. Soc. Rev.* **2012**, *41*, 7605.

(89) Pope, M. T. *Heteropoly and Isopoly Oxometalates*; Nauka. Sib. Otd., Novosibirsk, USSR, 1990.

(90) Day, V. W.; Klemperer, W. G. *Science* **1985**, *228*, 533.

(91) Pohl, M.; Lyon, D. K.; Mizuno, N.; Nomiya, K.; Finke, R. *Inorg. Chem.* **1995**, *34*, 1413.

(92) Proust, A.; Gouzerh, P.; Robert, F. *Inorg. Chem.* **1993**, *32*, 5291.

(93) Uehara, K.; Nakao, H.; Kawamoto, R.; Hikichi, S.; Mizuno, N. *Inorg. Chem.* **2006**, *45*, 9448.

(94) Matt, B.; Coudret, C.; Viala, C.; Jouvenot, D.; Loiseau, F. é é; Izzet, G.; Proust, A. *Inorg. Chem.* **2011**, *50*, 7761.

(95) Chen, Q.; Liu, S.; Zubieta, J. *Inorg. Chem.* **1989**, *28*, 4433.

(96) Villanneau, R.; Delmont, R.; Proust, A.; Gouzerh, P. *Chem. Eur. J.* **2000**, *6*, 1184.

(97) Proust, A.; Villanneau, R.; Delmont, R.; Artero, V.; Gouzerh, P. In *Polyoxometalate Chemistry*; Pope, M. T., Mueller, A., Eds.; Kluwer Academic Publishers: Dordrecht, 2001, p 55.

(98) Khan, M. I.; Chen, Q.; Goshorn, D. P.; Hope, H.; Parkin, S.; Zubieta, J. *J. Am. Chem. Soc.* **1992**, *114*, 3341.

(99) Khan, M. I.; Lee, Y. S.; Oconnor, C. J.; Zubieta, J. *J. Am. Chem. Soc.* **1994**, *116*, 5001.

(100) Hou, Y.; Hill, C. L. *J. Am. Chem. Soc.* **1993**, *115*, 11823.

(101) Pradeep, C. P.; Long, D.-L.; Newton, G. N.; Song, Y.-F.; Cronin, L. *Angew. Chem. Int. Ed.* **2008**, *47*, 4388.

(102) Li, D.; Song, J.; Yin, P.; Simotwo, S.; Bassler, A. J.; Aung, Y.; Roberts, J. E.; Hardcastle, K. I.; Hill, C. L.; Liu, T. *J. Am. Chem. Soc.* **2011**, *133*, 14010.

(103) Han, J. W.; Hardcastle, K. I.; Hill, C. L. *Eur. J. Inorg. Chem.* **2006**, 2598.

(104) Han, J. W.; Hill, C. L. *J. Am. Chem. Soc.* **2007**, *129*, 15094.

(105) Nugent, W. A.; Mayer, J. M. *Metal-Ligand Multiple Bonds*; John Wiley & Sons, Inc.: New York, 1988.

(106) Kang, H.; Zubieta, J. *J. Chem. Soc., Chem. Commun.* **1988**, 1192.

(107) Strong, J. B.; Yap, G. P. A.; Ostrander, R.; Liable-Sands, L. M.; Rheingold, A. L.; Thouvenot, R.; Gouzerh, P.; Maatta, E. A. *J. Am. Chem. Soc.* **2000**, *122*, 639.

(108) Kang, J.; Xu, B.; Peng, Z.; Zhu, X.; Wei, Y.; Powell, D. R. *Angew. Chem. Int. Ed.* **2005**, *44*, 6902.

(109) Zhang, J.; Xiao, F.; Hao, J.; Wei, Y. *Dalton Trans.* **2012**, *41*, 3599.

(110) Xu, L.; Lu, M.; Xu, B.; Wei, Y.; Peng, Z.; Powell, D. R. *Angew. Chem. Int. Ed.* **2002**, *41*, 4129.

(111) Knoth, W. H. *J. Am. Chem. Soc.* **1979**, *101*, 759.

(112) Finke, R. G. In *Polyoxometalates: From Platonic Solids to Anti-retroviral Activity*; Pope, M. T., Müller, A., Eds.; Kluwer Academic Publishers: Dordrecht, 1994; Vol. 10, p 267.

(113) Isobe, K.; Yagasaki, A. *Acc. Chem. Res.* **1993**, *26*, 524.

(114) Ho, R. K. C.; Klemperer, W. G. *J. Am. Chem. Soc.* **1978**, *100*, 6772.

(115) Finke, R. G.; Nomiya, K.; Green, C. A.; Droege, M. W.; Siedle, A. R. *Inorg. Synth.* **1992**, *29*, 239.

(116) Finke, R. G.; Nomiya, K.; Green, C. A.; Droege, M. W. In *Inorg. Synth.*; Grimes, R. N., Ed.; John Wiley & Sons, Inc.: New York, 1992; Vol. 29, p 239.

(117) Che, T. M.; Day, V. W.; Francesconi, L. C.; Fredrich, M. F.; Klemperer, W. G.; Shum, W. *Inorg. Chem.* **1985**, *24*, 4055.

(118) Klemperer, W. G.; Main, D. J. *Inorg. Chem.* **1990**, *29*, 2355.

(119) Mizuno, N.; Lyon, D. K.; Finke, R. G. *J. Catal.* **1991**, *128*, 84.

(120) Villanneau, R.; Proust, A.; Robert, F.; Gouzerh, P. *Chem. Eur. J.* **2003**, *9*, 1982.

(121) Bi, L.-H.; Al-Kadamany, G.; Chubarova, E. V.; Dickman, M. H.; Chen, L.; Gopala, D. S.; Richards, R. M.; Keita, B.; Nadjo, L.; Jaensch, H.; Mathys, G.; Kortz, U. *Inorg. Chem.* **2009**, *48*, 10068.

(122) Chae, H. K.; Klemperer, W. G.; Day, V. W. *Inorg. Chem.* **1989**, *28*, 1423.

(123) Harriman, A.; Elliott, K. J.; Alamiry, M. A. H.; Pleux, L. L.; Séverac, M.; Pellegrin, Y.; Blart, E.; Fosse, C.; Cannizzo, C.; Mayer, C. R.; Odobel, F. *J. Phys. Chem. C* **2009**, *113*, 5834.

(124) Odobel, F.; Séverac, M.; Pellegrin, Y.; Blart, E.; Fosse, C.; Cannizzo, C.; Mayer, C. R.; Elliott, K. J.; Harriman, A. *Chem. Eur. J.* **2009**, *15*, 3130.

(125) Matt, B.; Xiang, X.; Kaledin, A. L.; Han, N.; Moussa, J.; Amouri, H.; Alves, S.; Hill, C. L.; Lian, T.; Musaev, D. G.; Izzet, G.; Proust, A. *Chem. Sci.* **2013**, *4*, 1737.

(126) Santoni, M.-P.; Pal, A. K.; Hanan, G. S.; Proust, A.; Hasenknopf, B. *Inorg. Chem.* **2011**, *50*, 6737.

(127) Pope, M. T.; Müller, A. *Angew. Chem. Int. Ed.* **1991**, *30*, 34.

(128) Long, D.-L.; Burkholder, E.; Cronin, L. *Chem. Soc. Rev.* **2007**, *36*, 105.

(129) Long, D.-L.; Tsunashima, R.; Cronin, L. *Angew. Chem. Int. Ed.* **2010**, *49*, 1736.

(130) Miras, H. N.; Yan, J.; Long, D.-L.; Cronin, L. *Chem. Soc. Rev.* **2012**, *41*, 7403.

(131) Zheng, S.-T.; Yang, G.-Y. *Chem. Soc. Rev.* **2012**, *41*, 7623.

(132) Ritchie, C.; Ferguson, A.; Nojiri, H.; Miras, H. N.; Song, Y.-F.; Long, D.-L.; Burkholder, E.; Murrie, M.; Kögerler, P.; Brechin, E. K.; Cronin, L. *Angew. Chem. Int. Ed.* **2008**, *47*, 5609.

(133) Giusti, A.; Charron, G.; Mazerat, S.; Compain, J.-D.; Mialane, P.; Dolbecq, A.; Rivière, E.; Wernsdorfer, W.; Ngo Biboum, R.; Keita, B.; Nadjo, L.; Filoramo, A.; Bourgoin, J.-P.; Mallah, T. *Angew. Chem. Int. Ed.* **2009**, *48*, 4949.

(134) Compain, J.-D.; Mialane, P.; Dolbecq, A.; Mbomekallé, I. M.; Marrot, J.; Sécheresse, F.; Rivière, E.; Rogez, G.; Wernsdorfer, W. *Angew. Chem. Int. Ed.* **2009**, *48*, 3077.

(135) Ibrahim, M.; Lan, Y. H.; Bassil, B. S.; Xiang, Y. X.; Suchopar, A.; Powell, A. K.; Kortz, U. *Angew. Chem. Int. Ed.* **2011**, *50*, 4708.

(136) Kozhevnikov, I. V. *Catal. Rev. Sci. Eng.* **1995**, *37*, 311.

(137) Okuhara, T.; Mizuno, N.; Misono, M. *Advances in Catalysis* **1996**, *41*, 113.

(138) Corma, A. *Chem. Rev.* **1997**, *97*, 2373.

(139) Mizuno, N.; Yamaguchi, K.; Kamata, K. *Coord. Chem. Rev.* **2005**, *249*, 1944.

(140) Mizuno, N.; Tateishi, M.; Iwamoto, M. *Appl. Catal., A* **1996**, *134*, 183.

(141) Haimov, A.; Neumann, R. *Chem. Commun.* **2002**, 876.

(142) Yonehara, K.; Kamata, K.; Yamaguchi, K.; Mizuno, N. *Chem. Commun.* **2011**, *47*, 1692.

(143) Hirano, T.; Uehara, K.; Kamata, K.; Mizuno, N. *J. Amer. Chem. Soc.* **2012**, *134*, 6425.

(144) Okun, N. M.; Anderson, T. M.; Hill, C. L. *J. Am. Chem. Soc.* **2003**, *125*, 3194.

(145) Okun, N. M.; Ritorto, M. D.; Anderson, T. M.; Apkarian, R. P.; Hill, C. L. *Chem. Mater.* **2004**, *16*, 2551.

(146) Ma, F.-J.; Liu, S.-X.; Sun, C.-Y.; Liang, D.-D.; Ren, G.-J.; Wei, F.; Chen, Y.-G.; Su, Z.-M. *J. Am. Chem. Soc.* **2011**, *133*, 4178.

(147) Song, J.; Luo, Z.; Britt, D.; Furukawa, H.; Yaghi, O. M.; Hardcastle, K. I.; Hill, C. L. *J. Am. Chem. Soc.* **2011**, *133*, 16839.

(148) Nohra, B.; El Moll, H.; Rodriguez-Albelo, L. M.; Mialane, P.; Marrot, J. é; Mellot-Draznieks, C.; O'Keeffe, M.; Ngo Biboum, R.; Lemaire, J.; Keita, B.; Nadjo, L.; Dolbecq, A. *J. Am. Chem. Soc.* **2011**, *133*, 13363.

(149) Mitchell, S. G.; Streb, C.; Miras, H. N.; Boyd, T.; Long, D.-L.; Cronin, L. *Nature Chem.* **2010**, *2*, 308.

(150) Lewis, N. S.; Nocera, D. G. *Proc. Natl. Acad. Sci.* **2006**, *103(43)*, 15729.

(151) Service, R. F. *Science* **2011**, *332*, 293.

(152) Nielsena, T. D.; Cruickshankb, C.; Fogedc, S.; Thorsenc, J.; Krebs, F. C. *Sol. Energy Mater. Sol. Cells* **2010**, *94*, 1553.

(153) Balzani, V.; Credi, A.; Venturi, M. *ChemSusChem* **2008**, *1*, 26.

(154) Bard, A. J.; Fox, M. A. *Acc. Chem. Res.* **1995**, *28*, 141.

(155) Gust, D.; Moore, T. A.; Moore, A. L. *Acc. Chem. Res.* **2009**, *42*, 1890.

(156) Kanan, M. W.; Surendranath, Y.; Nocera, D. G. *Chem. Soc. Rev.* **2009**, *38*, 109.

(157) Kanan, M. W.; Nocera, D. G. *Science* **2008**, *321*, 1072.

(158) Concepcion, J. J.; Jurss, J. W.; Brennaman, M. K.; Hoertz, P. G.; Patrocinio, A. O. T.; Iha, N. Y. M.; Templeton, J. L.; Meyer, T. J. *Acc. Chem. Res.* **2009**, *42*, 1954.

(159) Hurst, J. K. *Coord. Chem. Rev.* **2005**, *249*, 313.

(160) Sartorel, A.; Bonchio, M.; Campagna, S.; Scandola, F. *Chem. Soc. Rev.* **2013**, *42*, 2262.

(161) Puntoriero, F.; Sartorel, A.; Orlandi, M.; Ganga, G. L.; Serroni, S.; Bonchio, M.; Scandola, F.; Campagna, S. *Coord. Chem. Rev.* **2011**, *255*, 2594.

(162) McEvoy, J. P.; Brudvig, G. W. *Chem. Rev.* **2006**, *106*, 4455.

(163) Szalai, V. A.; Brudvig, G. W. *American Scientist* **1998**, *86*, 542.

(164) Yin, Q.; Tan, J. M.; Besson, C.; Geletii, Y. V.; Musaev, D. G.; Kuznetsov, A. E.; Luo, Z.; Hardcastle, K. I.; Hill, C. L. *Science* **2010**, *328*, 342.

(165) Lv, H.; Geletii, Y. V.; Zhao, C.; Vickers, J. W.; Zhu, G.; Luo, Z.; Song, J.; Lian, T.; Musaev, D. G.; Hill, C. L. *Chem. Soc. Rev.* **2012**, *41*, 7572.

(166) Barber, J. *Chem. Soc. Rev.* **2009**, *38*, 185.

(167) Ferreira, K. N.; Iverson, T. M.; Maghlaoui, K.; Barber, J.; Iwata, S. *Science* **2004**, *303*, 1831.

(168) Sartorel, A.; Carraro, M.; Scorrano, G.; Zorzi, R. D.; Geremia, S.; McDaniel, N. D.; Bernhard, S.; Bonchio, M. *J. Am. Chem. Soc.* **2008**, *130*, 5006.

(169) Sartorel, A.; Miro, P.; Salvadori, E.; Romain, S.; Carraro, M.; Scorrano, G.; Valentin, M. D.; Llobet, A.; Bo, C.; Bonchio, M. *J. Am. Chem. Soc.* **2009**, *131*, 16051.

(170) Geletii, Y. V.; Botar, B.; Kögerler, P.; Hillesheim, D. A.; Musaev, D. G.; Hill, C. L. *Angew. Chem. Int. Ed.* **2008**, *47*, 3896.

(171) Geletii, Y. V.; Besson, C.; Hou, Y.; Yin, Q.; Musaev, D. G.; Quinonero, D.; Cao, R.; Hardcastle, K. I.; Proust, A.; Kögerler, P.; Hill, C. L. *J. Am. Chem. Soc.* **2009**, *131*, 17360.

(172) Cao, R.; Ma, H.; Geletii, Y. V.; Hardcastle, K. I.; Hill, C. L. *Inorg. Chem.* **2009**, *48*, 5596.

(173) Besson, C.; Huang, Z.; Geletii, Y. V.; Lense, S.; Hardcastle, K. I.; Musaev, D. G.; Lian, T.; Proust, A.; Hill, C. L. *Chem. Commun.* **2010**, 2784.

(174) Huang, Z.; Luo, Z.; Geletii, Y. V.; Vickers, J.; Yin, Q.; Wu, D.; Hou, Y.; Ding, Y.; Song, J.; Musaev, D. G.; Hill, C. L.; Lian, T. *J. Am. Chem. Soc.* **2011**, *133*, 2068.

(175) Shafirovich, V. Y.; Khannanov, N. K.; Strelets, V. V. *Nouveau J. Chim.* **1980**, *4*, 81.

(176) Harriman, A.; Porter, G.; Walters, P. *J. Chem. Soc., Faraday Trans. 2* **1981**, *77*, 2373.

(177) White, H. S.; Becker, W. G.; Bard, A. J. *J. Phys. Chem.* **1984**, *88*, 1840.

(178) Toma, F. M.; Sartorel, A.; Iurlo, M.; Carraro, M.; Parisse, P.; Maccato, C.; Rapino, S.; Gonzalez, B. R.; Amenitsch, H.; Ros, T. D.; Casalis, L.; Goldoni, A.; Marcaccio, M.; Scorrano, G.; Scoles, G.; Paolucci, F.; Prato, M.; Bonchio, M. *Nature Chem.* **2010**, *2*, 826.

(179) Toma, F. M.; Sartorel, A.; Carraro, M.; Bonchio, M.; Prato, M. *Pure Appl. Chem.* **2011**, *83*, 1529.

(180) Steinmiller, E. M. P.; Choi, K.-S. *Proc. Natl. Acad. Sci.* **2009**, *106*, 20633.

(181) Ulagappan, N.; Frei, H. *J. Phys. Chem. A* **2000**, *104*, 7834.

(182) Matsuoka, M.; Anpo, M. *J. Photochem. Photobiol. C* **2003**, *3*, 225.

(183) Lin, W.; Han, H.; Frei, H. *J. Phys. Chem. B* **2004**, *108*, 18269.

(184) Lin, W.; Frei, H. *J. Am. Chem. Soc.* **2005**, *127*, 1610.

(185) Lin, W.; Frei, H. *J. Phys. Chem. B* **2005**, *109*, 4929.

(186) Lin, W.; Frei, H. *C. R. Chim.* **2006**, *9*, 207.

(187) Nakamura, R.; Frei, H. *J. Am. Chem. Soc.* **2006**, *128*, 10668.

(188) Han, H.; Frei, H. *Microporous Mesoporous Mater.* **2007**, *103*, 265.

(189) Han, H.; Frei, H. *J. Phys. Chem. C* **2008**, *112*, 8391.

(190) Han, H.; Frei, H. *J. Phys. Chem. C* **2008**, *112*, 16156.

(191) Jiao, F.; Frei, H. *Angew. Chem. Int. Ed.* **2009**, *48*, 1841.

(192) Wu, X.; Weare, W. W.; Frei, H. *Dalton Trans.* **2009**, 10114.

(193) Cuk, T.; Weare, W. W.; Frei, H. *J. Phys. Chem. C* **2010**, *114*, 9167.

(194) Nakamura, R.; Okamoto, A.; Osawa, H.; Irie, H.; Hashimoto, K. *J. Am. Chem. Soc.* **2007**, *129*, 9596.

(195) Takashima, T.; Nakamura, R.; Hashimoto, K. *J. Phys. Chem. C* **2009**, *113*, 17247.

(196) Takashima, T.; Yamaguchi, A.; Hashimoto, K.; Nakamura, R. *Chem. Commun.* **2012**, *48*, 2964.

Chapter 2

Metal Carbonyl Complexes Supported on Subvalent Sb^{III}/Bi^{III}-centered Polyoxoanions

(Published partially in *Inorg. Chem.*, **2013**, *52(2)*, 671–678.)

With Choon Sung Kambara, Ye Yang, Alexey L. Kaledin, Djamaladdin G. Musaev, Tianquan Lian and Craig L. Hill

2.1 Introduction

As mentioned in the first chapter, POM-supported metal carbonyl derivatives have long been studied as tractable, molecular analogues of solid-oxide-supported metal complexes and exhibit a wide range of properties.[1,2] A series of these hybrid compounds with their preparation strategies, unique structures and catalytic properties were reported previously.[3-16] Most of these compounds involve Lindqvist-type POMs.[3-7] Lacunary POMs (Keggin or Dawson), which tend to form stronger covalent bonds to the incorporated metal multi-carbonyl units, haven't been used as extensively in this context.[13] As a result, we sought to investigate multi-dentate polytungstates with appended metal multi-carbonyl donor groups such as $\{M(CO)_3\}^+$ (M = Re or Mn).

POM-supported metal carbonyl derivatives, which can be regarded as a sub-category of functionalized POMs, are best prepared by stepwise and controlled methods. In this context, the use of appropriate defect POMs as chelating ligands is important for directing the reactions towards the desired products.[17-21] Since all POM-supported metal carbonyl compounds contain a *fac*-$\{M(CO)_3\}^+$ d^6 metal carbonyl fragment, defect POMs which can act as tridentate ligands are logical synthetic precursors. Krebs and co-workers prepared and thoroughly characterized tungstoantimonates and tungstobismuthates structurally related to those in this article with the general formula $[X_2W_{20}M_2O_{70}(H_2O)_6]^{(14-2n)-}$ (X = Sb, Bi; M = Fe, Co, Zn).[22,23] In Krebs dimers, the terminal aqua *fac*-$\{M(H_2O)_3\}^{2+/3+}$ groups replace the *fac*-$\{WO(OH)_2\}^{2+}$ moieties on the parent POM scaffolds. Kortz used a similar procedure to immobilize the organo-ruthenium groups onto the Krebs POM scaffolds.[24] Appreciating that the tricarbonyl *fac*-$\{M(CO)_3\}^+$ unit is also topologically equivalent to *fac*-$\{M(H_2O)_3\}^{2+/3+}$ and *fac*-

$\{WO(OH)_2\}^{2+}$, we utilized these POM ligands as multidentate building blocks to coordinate *fac*-$\{M(CO)_3\}^+$ fragments. In this context, we have successfully obtained four Krebs-type structures each with two $\{M(CO)_3\}^+$ units per POM unit: $Na_{11}H[Sb_2W_{20}O_{70}\{Re(CO)_3\}_2]\cdot 34H_2O$ (**2.1**), $Na_{11}H[Bi_2W_{20}O_{70}\{Re(CO)_3\}_2]\cdot 33H_2O$ (**2.2**), $K_9Na_3[Sb_2W_{20}O_{70}\{Mn(CO)_3\}_2]\cdot 32H_2O$ (**2.3**) and $K_9Na_3[Bi_2W_{20}O_{70}\{Mn(CO)_3\}_2]\cdot 32H_2O$ (**2.4**).

2.2 Experimental

2.2.1. Materials and Instrumentation

All chemicals were reagent grade and used as supplied. The Sb^{III}/Bi^{III} polyoxometalate precursors $Na_{12}[Sb_2W_{22}O_{74}(OH)_2]\cdot 27H_2O$ and $Na_{12}[Bi_2W_{22}O_{74}(OH)_2]\cdot 44H_2O$ were prepared by literature methods.[22,23] Their purities were determined through FT-IR spectroscopy. The low-valent complexes, $Re(CO)_3(CH_3CN)_3(BF_4)$ and $Mn(CO)_3(CH_3CN)_3(BF_4)$, were made according to the known procedures but using $AgBF_4$. in place of $AgClO_4$. Their purities were analyzed by ^1H NMR and FT-IR.

UV-vis spectra were acquired using an Agilent 8453 spectrophotometer equipped with a diode-array detector and an Agilent 89090A cell temperature controller unit. The FT-IR spectra were measured on a Thermo Nicolet 6700 spectrometer with KBr pellets (2%). Elemental analyses (Bi, K, Mn, Na, Sb, Re, W) were performed by Galbraith Lab Inc., Knoxville, TN, 37921. Thermogravimetric analysis was acquired on a Perkin Elmer STA 6000 analyzer.

2.2.2. Synthesis

$Na_{11}H[Sb_2W_{20}O_{70}\{Re(CO)_3\}_2]\cdot 34H_2O$ (2.1). $Na_{12}[Sb_2W_{22}O_{74}(OH)_2]\cdot 27H_2O$ (0.1 mmol, 670 mg) and $Re(CO)_3(CH_3CN)_3(BF_4)$ (0.2 mmol, 98 mg) were dissolved in 20 mL H_2O. The mixture was heated at *ca.* 70 ºC for 30 minutes and the color changed to orange. NaCl (400 mg) was added to the solution and the pH was adjusted to 5 by addition of 1.0 M NaOH. The solution was cooled to room temperature and then filtered. The solution was allowed to stand out at room temperature for about a week at which point large orange block-shaped crystals were obtained. Yield: 150 mg (22 % based on Sb). FTIR (2% KBr pellet, 2500 – 400 cm^{-1}): 2016 (s), 1925 (s), 1906 (s), 955 (s), 836 (m), 808 (s), 767 (m), 657 (m), 472 (sh). Electronic spectral data (300 – 800 nm, in H_2O): ε_{400nm} *ca.* 2200 $M^{-1}\cdot cm^{-1}$. Anal. Calcd. for $C_6H_{69}O_{110}Na_{11}Re_2Sb_2W_{20}$: Na, 3.9; Re, 5.8; Sb, 3.8; W, 57.0. Found: Na, 4.0; Re, 5.3; Sb, 3.3; W, 55.4. Thermogravimetric analysis (TGA; 30 – 500 ^oC): weight loss, 12.1%.

$Na_{11}H[Bi_2W_{20}O_{70}\{Re(CO)_3\}_2]\cdot 33H_2O$ (2.2). This compound was prepared using a similar procedure to **2.1** except that $Na_{12}[Bi_2W_{22}O_{74}(OH)_2]\cdot 44H_2O$ was used as the POM ligand precursor. Orange-red crystals were obtained after several days of evaporation. Yield: 130 mg (20% based on Bi). FTIR (2% KBr pellet, 2500 – 400 cm^{-1}): 2014 (s), 1923 (s), 1900 (s), 945 (s), 837 (sh), 798 (s), 765 (m), 646 (m), 459 (sh). Electronic spectral data (300 – 800 nm, in H_2O): ε_{400nm} *ca.* 2100 $M^{-1}\cdot cm^{-1}$. Anal. Calcd. for $C_6H_{67}O_{109}Bi_2Na_{11}Re_2W_{20}$: Bi, 6.3; Na, 3.8; Re, 5.6; W, 55.7. Found: Bi, 6.5; Na, 3.8; Re, 5.3; W, 55.7. Thermogravimetric analysis (TGA; 30 – 500 ^oC): weight loss, 11.5%.

$K_9Na_3[Sb_2W_{20}O_{70}\{Mn(CO)_3\}_2]\cdot 32H_2O$ (2.3). $Na_{12}[Sb_2W_{22}O_{74}(OH)_2]\cdot 27H_2O$ (0.1 mmol, 670 mg) was dissolved in 20 ml H_2O, then excess $Mn(CO)_3(CH_3CN)_3(BF_4)$ (0.25 mmol, 88 mg) in 2 ml CH_3OH was added slowly. The reaction beaker was covered with aluminum foil. The mixture was stirred for 30 minutes in dark and the pH was adjusted to 6.0 by 0.1 M KOH. KCl (0.5 mL of a 1.0 M solution) was then added to the mixture. The solution was quickly passed through a filter paper and kept in the dark. Dark-red crystals in plate-shape were collected after 2 weeks. Yield: 120 mg (20% based on Sb). FTIR (2% KBr pellet, 2500 – 400 cm^{-1}): 2031 (s), 1936 (s), 1919 (s), 946 (s), 838 (m), 806 (m), 768 (m), 667 (w), 455 (sh). Electronic spectral data (300 – 800 nm, in H_2O): ε_{400nm} *ca.* 3500 $M^{-1}\cdot cm^{-1}$. Anal. Calcd. for $C_6H_{64}O_{108}Mn_2K_9Na_3Sb_2W_{20}$: K, 5.6; Mn, 1.7; Na, 1.1; Sb, 3.9; W, 58.2. Found: K, 6.0; Mn, 1.7; Na, 1.1; Sb, 3.5; W, 60.7. Thermogravimetric analysis (TGA; 30 – 500 ^oC): weight loss, 11.8%.

$K_9Na_3[Bi_2W_{20}O_{70}\{Mn(CO)_3\}_2]\cdot 32H_2O$ (2.4). This compound was made by a similar procedure as **2.3**. Yield: 100 mg (18% based on Bi). FTIR (2% KBr pellet, 2500 – 400 cm^{-1}): 2030 (s), 1935 (s), 1919 (s), 941 (s), 826 (m), 797 (m), 760 (m), 651 (w), 409 (sh). Electronic spectral data (300 – 800 nm, in H_2O): ε_{400nm} *ca.* 3400 $M^{-1}\cdot cm^{-1}$. Anal. Calcd. for $C_6H_{64}O_{110}K_9Na_3Mn_2Bi_2W_{20}$: Bi, 6.4; K, 5.4; Mn, 1.7; Na, 1.1; W, 56.7. Found: Bi, 6.1; K, 5.6; Mn, 1.8; Na, 1.2; W, 56.8. Thermogravimetric analysis (TGA; 30 – 500 ^oC): weight loss, 11.4%.

2.2.3. Crystallography

X-ray analysis was performed on a Bruker D8 SMART APEX CCD sealed tube diffractometer at Emory University. Diffraction intensities were measured using graphite

monochromated Mo Kα radiation (λ = 0.71073 Å) at 173(2) K. Data collection, indexing, and initial cell refinements were carried out by using SMART; frame integration and final cell refinements were done by SAINT. A multiple absorption correction including face-indexing was done by the program SADABS. The molecular structures of **2.1**, **2.2**, **2.3** and **2.4** were determined by Direct Methods and Fourier techniques and refined by full-matrix least squares. Structure solution, refinement, graphic and generation of publication materials were accomplished using SHELXTL-97 software.[25,26] The largest residual electron density for each structure was located close to the Sb, Bi and W atoms and was most likely due to imperfect absorption corrections frequently encountered in heavy-metal atom structures. Crystal data collection and refinement parameters are given in **Error! Reference source not found.**. Complete details can be found in the .cif files in the Supporting Information.

Table 2-1 Selective bond lengths (Å) and bond angles (°)

	2.1	**2.1** (calcd.)	**2.2**	**2.3**	**2.4**
X-O[a]	2.01-2.02	2.01-2.03	2.13-2.16	1.98-2.00	2.13-2.15
M-O[a]	2.13-2.16	2.16-2.18	2.12-2.15	2.08-2.12	2.06-2.08
M-C[b]	1.87-1.88	1.90	1.85-1.90	1.80-1.90	1.85-1.87
M-C-O[c]	176-179	178-179	177-179	173-177	171-175

[a] Oxygen from the POM frameworks (X = Sb or Bi; M = Re or Mn). [b] Carbon from the carbonyl groups. [c] Oxygen from the carbonyl groups.

Table 2-2 Crystal structure data for compounds **2.1**, **2.2**, **2.3** and **2.4**

	2.1	**2.2**	**2.3**	**2.4**
Empirical formula	$C_6H_{69}O_{110}Na_{11}Re_2Sb_2W_{20}$	$C_6H_{67}O_{109}Bi_2Na_{11}Re_2W_{20}$	$C_6H_{64}O_{108}Mn_2K_9Na_3Sb_2W_{20}$	$C_6H_{64}O_{110}K_9Na_3Mn_2Bi_2W_{20}$
T [K]	173(2)	173(2)	173(2)	173(2)
M_r [g mol^{-1}]	6447.16	6603.79	6315.55	6521.99
Crystal system	Triclinic	Triclinic	Triclinic	Triclinic
Space group	$P\bar{1}$	$P\bar{1}$	$P\bar{1}$	$P\bar{1}$
a [Å]	13.724(6)	13.672(3)	12.443 (1)	12.446(3)
b [Å]	14.244(6)	14.815(3)	13.095(1)	13.089(3)
c [Å]	17.610(7)	15.385(3)	15.808(1)	15.723(4)
α [°]	90.315(6)	103.492(3)	83.375 (1)	82.883(4)
β [°]	107.851(5)	106.042(3)	74.307(1)	73.810(4)
γ [°]	112.456(6)	104.397(3)	75.043(1)	74.750(3)
V [Å^3]	2999(2)	2743.9(10)	2392.8(3)	2369.7(10)
Z	1	1	1	1
ρ_{calcd} [g cm^{-3}]	3.558	3.897	4.066	4.402
μ [mm^{-1}]	21.691	26.403	25.255	28.642
Reflection collected	46970	47376	37914	34752
Independent reflections (R_{int})	13181 (0.0829)	13169 (0.0567)	10154 (0.0544)	9310 (0.0611)
Goodness-of-fit	1.038	1.037	1.065	1.032
R_1 [I>2σ(I)]	0.0575	0.0442	0.0487	0.0584
wR_2	0.1328	0.1213	0.1177	0.1521
R_1 (all data)	0.0873	0.0579	0.0651	0.0764
wR_2	0.1472	0.1307	0.1253	0.1644
Largest diff. peak and hole [e Å^3]	4.714, -2.944	3.131, -1.980	3.282, -2.620	8.043, -2.558

$R_1 = \Sigma\ ||F_0|-|F_c||/\Sigma|F_0|$; w$R_2 = \{\Sigma[w(F_0^2-F_c^2)^2/\Sigma w(F_0^2)^2]\}^{1/2}$

2.3 Results and Discussion

2.3.1 Synthesis

The natural pH of the POM ligands, $[X_2W_{22}O_{74}(OH)_2]^{12-}$ (X = Sb or Bi), is *ca.* 4.5. When the pH increases, two terminal *fac*-$\{WO(OH)_2\}^{2+}$ groups are released from the POM frameworks and the resulting vacant sites can be occupied by transition metal centers with multiple terminal aqua ligands.[22,23] This assertion is further supported in this paper. The preparation of the four new compounds above is conducted in a weakly acidic aqueous solution (pH 5-6); when pH values are lower than 3, these compounds do not form. The two general steps affording these complexes are illustrated in **Figure 2-1**.

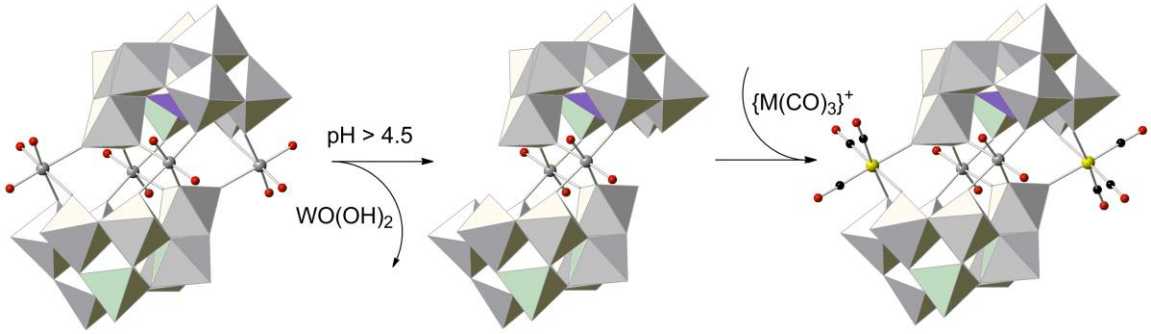

Figure 2-1 Representative synthetic steps for preparation of the indicated POMs in combined ball-and-stick and polyhedral notations. O: red; C: black; W: gray; Sb/Bi: purple; Re/Mn: yellow.

The FTIR spectra of these four compounds are shown in **Figure 2-2**. As expected, **2.1** and **2.2** share similar patterns in their FTIR spectra as do **2.3** and **2.4**, but the spectra of the former are slightly distinct from the latter. Since each $\{M(CO)_3\}^+$ moiety has local C_{3v} symmetry and the two $\{M(CO)_3\}^+$ groups are symmetrical, only two symmetric and one anti-symmetric IR-active C-O stretching modes are present in the FTIR spectra. This spectral region also reveals the purity of these compounds. As expected, **2.1** and **2.2** have lower C-O frequencies relative to those in **2.3** and **2.4**. This is due to stronger M-to-CO

dπ-π* back bonding from Re compared to Mn because Re(I) is more electron donating (and generally has a more negative potential) than Mn(I). Furthermore, the frequencies of the carbonyl bands in **2.1** and **2.2** are similar to those of $[Re(CO)_3(H_2O)\{Mo_5O_{13}(OMe)_4(NO)\}]^{2-}$ (2013, 1910, 1885 cm^{-1}), but higher than those of $\{[H_2W_8O_{30}][Re(CO)_3]_2\}^{8-}$ (2007, 1885 cm^{-1}).[12,14] In the same context, the frequencies for the manganese carbonyl species follow a similar trend: **2.3** has bands at 2031, 1936, 1919 cm^{-1} and **2.4** has bands at 2030, 1935, 1919 cm^{-1}, respectively, which are similar to those of $[Mn(CO)_3(H_2O)\{Mo_5O_{13}(OMe)_4(NO)\}]^{2-}$ (2029, 1933, 1916 cm^{-1}) but higher than those in $\{[H_2W_8O_{30}][Mn(CO)_3]_2\}^{8-}$ (2022, 1932 cm^{-1}). These results imply that both $[X_2W_{20}O_{70}]^{14-}$ and $\{Mo_5O_{13}(OMe)_4(NO)\}^{3-}$ have similar electron acceptor strengths and both are stronger acceptors than $[H_2W_8O_{30}]^{10-}$.

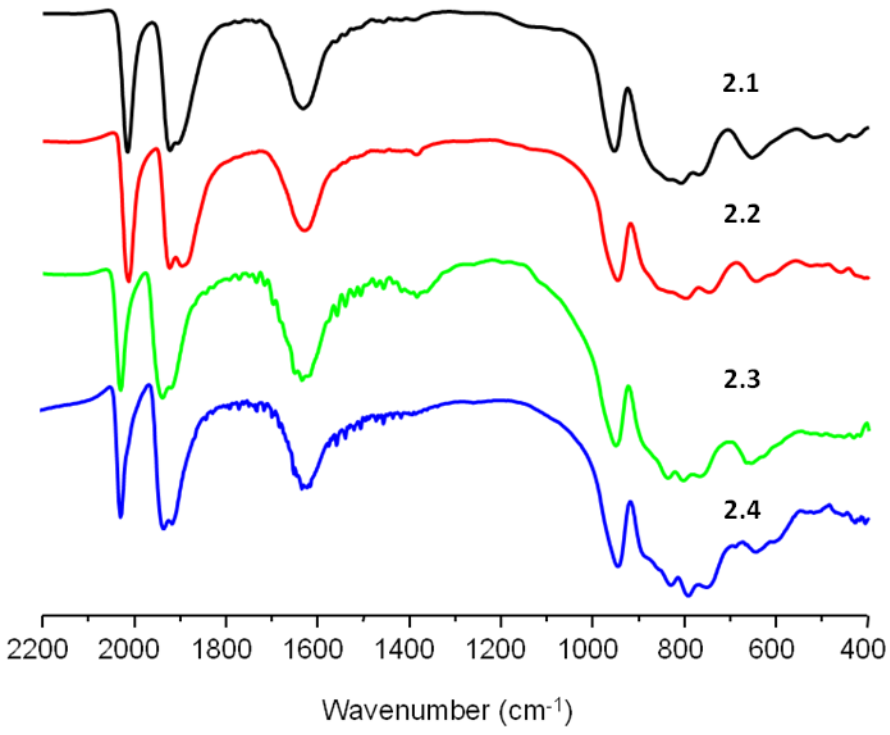

Figure 2-2 FTIR spectra (KBr pellets) of **2.1**, **2.2**, **2.3** and **2.4**

2.3.2 Structures.

All four metal-donor-POM-acceptor compounds have similar structures and contain two identical β-*B*-$[XW_9O_{33}]^{9-}$ (X = Sb or Bi) units joined by two WO_6 octahedra and two *fac*-$\{M(CO)_3\}^+$ moieties (**Figure 2-3**). The Re and Mn centers exhibit MO_3C_3 coordination octahedra but with slight differences in relative bond distances. The MnO_3C_3 moieties, as reflected in M-C distances and M-C-O angle variations, are slightly more distorted from pure octahedral symmetry than the Re derivatives. Typically, the three Re-C bond distances in **2.1** and **2.2** are almost identical and the Re-C-O angles are nearly 180° (Table 1). The M-C bond distances are 1.87 Å (Re-C) and 1.84 Å (Mn-C) on average, which are similar with those in analogous complexes reported previously.[11,12,14] Compared to **2.1** and **2.2**, the Mn-C bonds in **2.3** and **2.4** are more variable and the Mn-C-O angles are not quite linear (e.g. 171°).

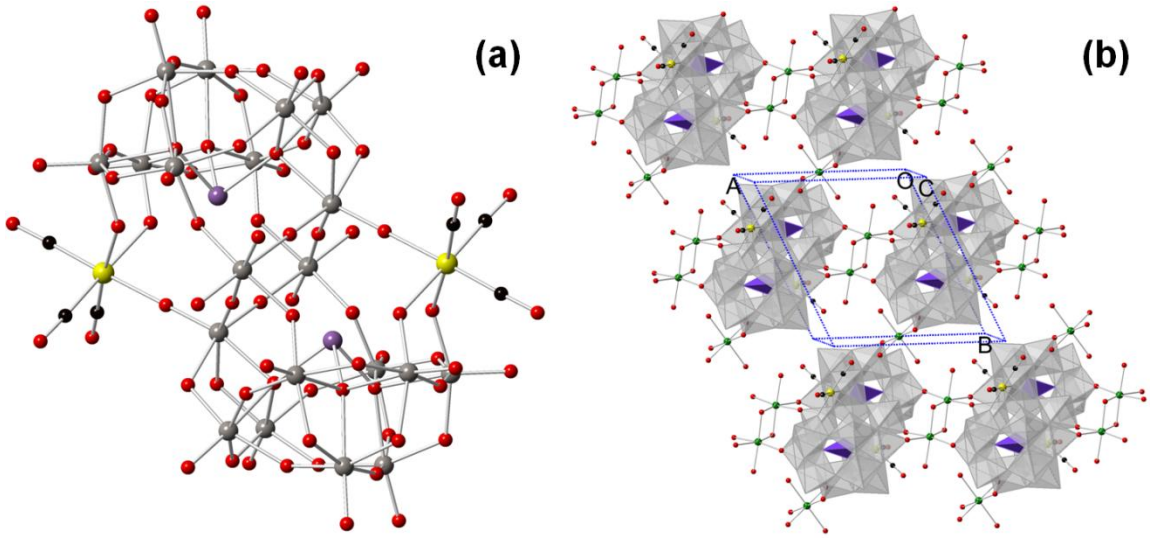

Figure 2-3 (a) Ball-and-stick representation of **2.1**, **2.2**, **2.3** and **2.4**. Cations K^+, Na^+ and solvent H_2O are omitted for clarity. O: red; C: black; W: gray; Sb/Bi: purple; Re/Mn: yellow. (b) View of the 2D sheet of **2.1** in combined ball-and-stick and polyhedral notation. Na: green; O: red; C: black; Re: yellow; WO_6: gray; SbO_3: purple.

Furthermore, the polyanions in **2.1** are linked by two symmetry-equivalent hydrated Na^+ ions to form a 2D framework. Along the *a*-axis, the polyanions are connected by dinuclear $\{Na(H_2O)_2\}_2^{2+}$ groups *via* terminal oxygen atoms on the POM units with Na-O distances of 2.32(2)-2.49(2) Å to form a 1D chain. The adjacent 1D chains are further bridged through mononuclear $\{Na(H_2O)_2\}^+$ units along the *b*-axis with Na-O (terminal) distances of 2.32(2)-2.35(2) Å to form a 2D network (**Figure 2-3**). The structure of **2.2**, like that of **2.1**, consists of a 2D framework where the polyanions are connected by the hydrated Na^+ ions. Along the *a*-axis, a dinuclear unit $\{Na(H_2O)_2\}_2^{2+}$ joins each polyanion to form a 1D chain, as in the structure of **2.1**. However, the 1D chains are linked by a dinuclear moiety $[Na_2(H_2O)_7]^{2+}$ via a terminal oxygen on tungsten and a carbonyl group on rhenium along the *b*-axis (forming a Na-O-C-Re linkage) in contrast to the connection in **2.1** (**Figure 2-4**).

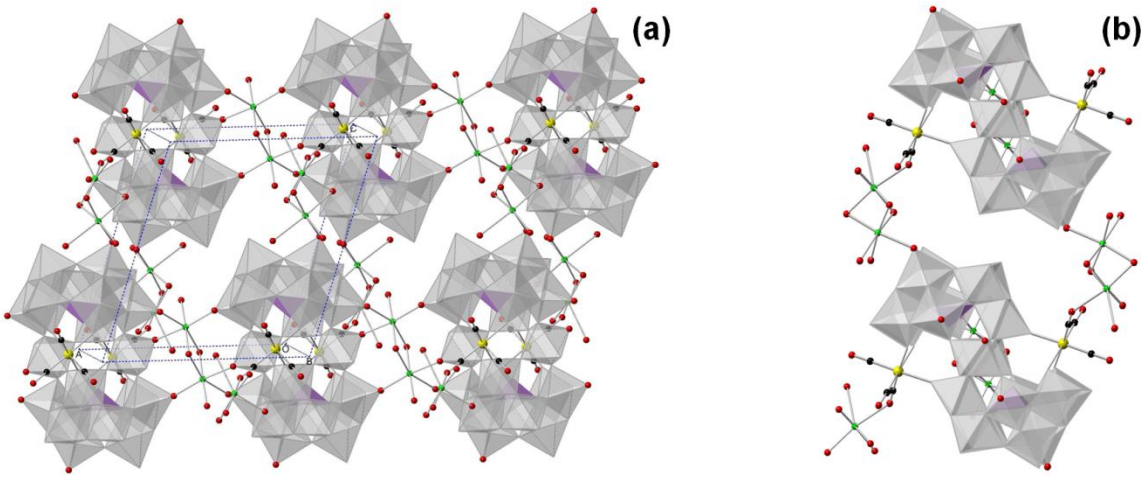

Figure 2-4 (a) View of the 2D sheet of **2.2** in the combined ball-and-stick and polyhedral notation. (b) View of **2.2** along the *a*-axis. Na: green; O: red; C: black; Re: yellow; WO_6: gray; SbO_3: purple.

2.3.3 Spectroscopic and Computational Studies

The precursors are colorless: the POM ligands $[X_2W_{22}O_{74}(OH)_2]^{12-}$ have O(*2p*) → W(*5d*) transitions, which absorb significantly only below 300 nm, and the moiety *fac*-$\{Re(CO)_3\}^+$, which has a ligand-to-metal charge-transfer (LMCT) band, only absorbs below 350 nm. In contrast, the UV-vis spectra of **2.1** and **2.2** show a broad absorption covering the entire UV and visible regions extending to *ca.* 600 nm (**Figure 2-5**) with high absorptivity (**2.1**: ε_{400nm} *ca.* 2400 $M^{-1}\cdot cm^{-1}$; **2.2**: *ca.* 2100 $M^{-1}\cdot cm^{-1}$). Furthermore, **2.1** and **2.2** are very stable in aqueous solutions. The spectra of the stored solutions do not change overnight or after several hours of visible-light (LED; λ = 455 nm) irradiation.

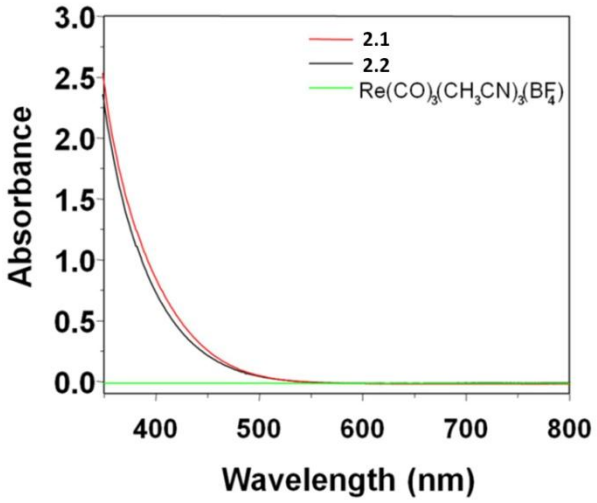

Figure 2-5 Normalized UV-vis spectra of aqueous **2.1** (red), **2.2** (black), and $[Re(CO)_3]^+$ (green).

We investigated the origin of the high visible absorptivity of **2.1** by computational modeling. Full DFT-optimized geometry parameters of **2.1,** in its ground singlet electronic state, are given in **Table 2-3**. The frontier molecular orbitals are shown in **Figure 2-6**. As seen in Table 1, the calculated important geometry parameters of **2.1** are in very good agreement with their experimental values. As seen in this figure, the two highest occupied orbitals of **2.1**, H and H_{-1}, form a near degenerate pair. Each of them has

a strong contribution from rhenium d and antimony p orbitals. There is a smaller contribution from the p orbitals of bridging oxygens. The lowest unoccupied orbitals, L and L_{+1}, also form a near degenerate pair. Their character is mainly the d orbitals of the outer W atoms with a small mixture from the p orbitals of associated O atoms. Thus, the $H/H_{-1} \rightarrow L/L_{+1}$ excitations are expected to be a $[Re(CO)_3 + Sb] \rightarrow$ POM charge transfer excitations. Based on the H-L gap, the band origin of the electronic spectrum is estimated to be *ca.* 2.5 eV. The calculated UV-vis spectrum of the singlet excitations is shown in **Figure 2-6**. As expected from the frontier orbital analysis, the first excited state S_1 is a HOMO $\rightarrow$ LUMO, i.e. $[Re(CO)_3 + Sb] \rightarrow$ POM, transition occurring at 2.51 eV (492 nm). The following several states are dark until the group of states at *ca.* 470 nm, S_8-S_{12}, which are pure Re $\rightarrow$ POM transitions. Continuing towards the shorter wavelengths, the spectrum begins to be dominated by pure Re $\rightarrow$ POM transitions, such as those at *ca.* 440, 430 and 410 nm, with a few mixed Re/Sb $\rightarrow$ POM and POM $\rightarrow$ POM bands (see labeling in **Figure 2-6**; the summary of S_0-S_n transitions is in **Table 2-4**). Thus, the entire calculated spectrum is consistent with the experimental result in the visible range (400 – 600 nm) shown in **Figure 2-5** above.

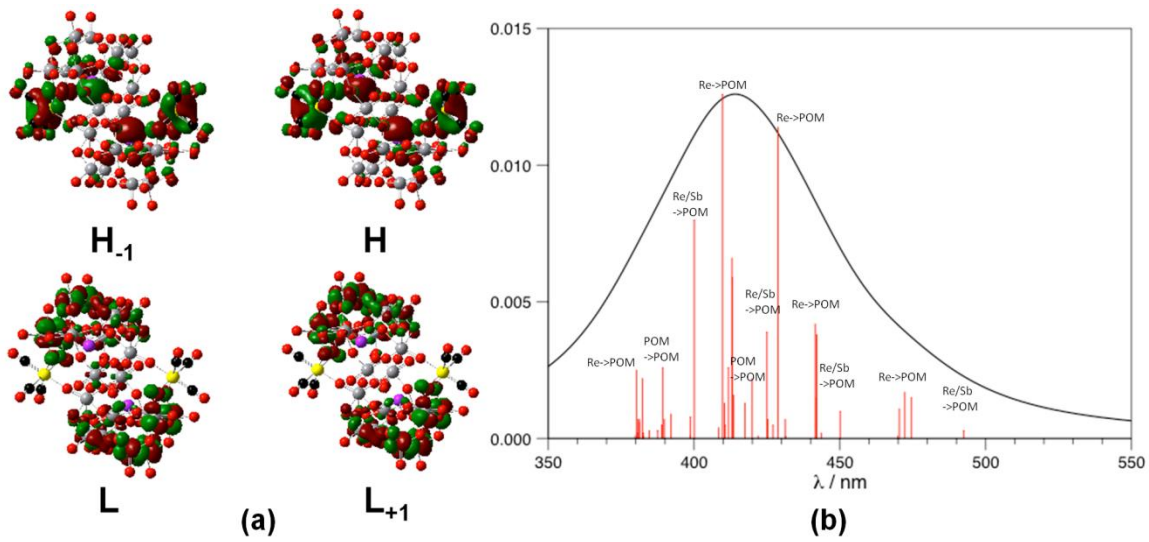

Figure 2-6 (a) Molecular orbitals and orbital energies (in ascending order -4.82, -4.79, -2.28, -2.25 eV) of S_0 $[Sb_2W_{20}O_{70}\{Re(CO)_3\}_2]^{12-}$ (the polyanion in **2.1**) in water. H = HOMO, L = LUMO. Color codes: Re, yellow; W, gray; Sb, purple; O, red; C, black. (b) Calculated UV spectrum of the same polyanion (S_0 state) in water using the first 70 excited singlet states.

Complexes **2.3** and **2.4** as solids are dark-red in color and their UV-vis spectra in aqueous solution have the characteristic peaks at *ca.* 420 nm and a broad absorption up to *ca.* 650 nm (**Figure 2-7**). However, **2.3** and **2.4** are fairly stable in the aqueous solution. The solutions slowly become greenish under indoor lighting. This green color indicates that the POM ligands have been reduced (green is a superposition of the yellow oxidized complex with small quantities of the blue reduced complex). This hydrolytic instability likely results in part from photo-generation of d^5 high spin Mn(II) centers which have little or no ligand field stabilization energy and are consequently quite labile.

In order to monitor the charge-transfer process of **2.3** in aqueous solution, a photolysis reaction was performed in a sealed cell deaerated by argon. Upon irradiation (*ca.* 20 min), the characteristic band at *ca.* 420 nm decreases, new broad absorptions with maximum at *ca.* 650 nm and 1000 nm grow and a point at *ca.* 480 nm, which is nearly

isosbestic, is observed in the UV-vis spectrum (**Figure 2-7**). These absorption features can be attributed to a bleach of the ground state absorption and the development of W(V) d-d transitions and W(V)-W(VI) IVCT transitions in the reduced Krebs-type polytungstate ligands respectively.[27-32] In addition to producing the "heteropoly blues", CO is detected in the head space gas by GC in *ca.* 80% yield. The photolysis reaction leads to the dissociation of **2.3** which generates the reduced POM ligands and the stoichiometrically oxidized products, Mn^{2+} ions and CO. In the next step, the disappearance of "heteropoly blues" by O_2-based re-oxidation is also followed by UV-vis spectra. The absorptions from *ca.* 650 nm to 1000 nm decrease and the solution becomes colorless. The absence of the starting characteristic absorption at *ca.* 420 nm indicates that the dissociation of **2.3** is nearly complete.

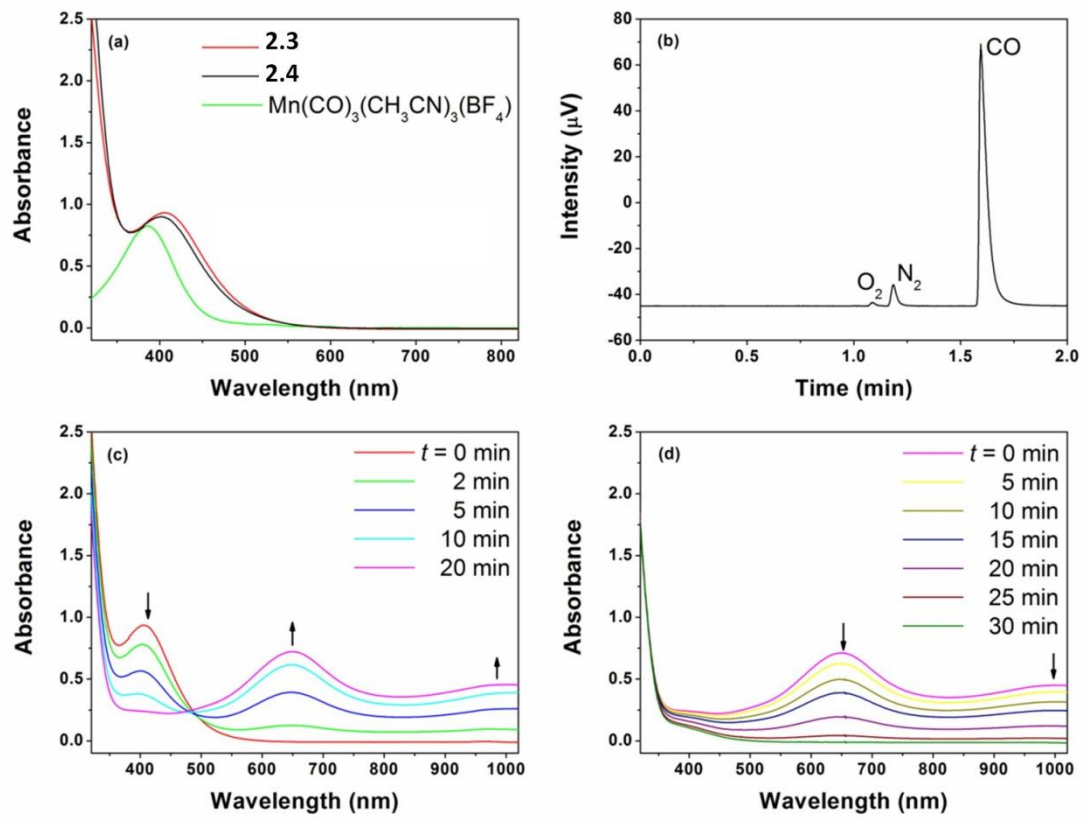

Figure 2-7 (a) Normalized UV-vis spectra of aqueous **2.3**, **2.4** and $[Mn(CO)_3]^+$ (2 equivalents); (b) GC signals for a gas sample from the head space of a quartz cell containing **2.3** after photolysis (deaerated by argon); (c) Time-dependent UV-vis spectra of **2.3** in a sealed and deaerated quartz cell exposed to a LED-lamp light (455 nm wavelength, 17mW); (d) Time-dependent UV-vis spectra of the post-photolysis solution of **2.3** in the quartz cell exposed to air. Arrows in (c) and (d) indicate the directions of amplitude changes.

Table 2-3 DFT-optimized Cartesian coordinates (in Å) of all atoms of polyanion **2.1** at its ground singlet (S_0) ground electronic state.

C	2.42284000	5.58109800	-1.45224200
C	-2.42196300	-5.59046900	1.43418200
C	2.39144500	5.65237100	1.22514200
C	-2.37606900	-5.64058700	-1.24264700
C	4.68158500	5.17240800	-0.07628500
C	-4.67671500	-5.17639200	0.05284700

O	2.10514100	6.31020500	-2.31671500
O	-2.10570200	-6.32563900	2.29403300
O	2.04573300	6.42214400	2.04233000
O	-2.01895200	-6.40051400	-2.06407300
O	5.73467300	5.68896100	-0.07419200
O	-5.72892400	-5.69463100	0.04286000
O	2.97843100	-1.98591500	2.92525800
O	-2.97990200	1.99706700	-2.92093700
O	5.13901700	-2.58732500	1.55036200
O	-5.14150300	2.59175100	-1.54508500
O	3.70214300	-4.71024800	2.82526800
O	-3.70631900	4.72102100	-2.81042800
O	1.51253700	-3.75320200	1.39516000
O	-1.51548600	3.75853600	-1.38608700
O	3.79119900	-4.30532100	0.05479100
O	-3.79391500	4.30611600	-0.04203000
O	6.58812900	0.78481900	2.15581500
O	-6.58728300	-0.78147400	-2.15738400
O	7.70131800	-1.79910100	2.46134000
O	-7.70335900	1.80156800	-2.45566300
O	5.28810800	-0.97145100	3.61286100
O	-5.28941800	0.97977600	-3.60995900
O	4.34150100	1.52332600	3.54585600
O	-4.33886100	-1.51252200	-3.55033100
O	6.67090900	-0.93050800	0.01107900

O	-6.67124800	0.92984100	-0.00783800
O	4.25975500	0.07697900	1.40982500
O	-4.26004100	-0.07144200	-1.41026500
O	3.11764900	-0.32269200	5.26116400
O	-3.11700000	0.34072600	-5.25987900
O	1.89907800	0.43240300	2.78211500
O	-1.90042200	-0.42357300	-2.78060800
O	5.99573300	3.52616100	2.47091800
O	-5.98773000	-3.52111100	-2.48375800
O	3.52415600	2.82255600	1.31051200
O	-3.52124800	-2.81568200	-1.31399200
O	5.74856600	2.18422600	-0.01249500
O	-5.74886500	-2.18582000	0.00501100
O	5.98400400	3.46379000	-2.52445800
O	-5.99050700	-3.47114100	2.51156400
O	6.58480400	0.72434300	-2.16666800
O	-6.58615800	-0.73050200	2.16494900
O	4.34377800	1.43177400	-3.57105800
O	-4.34570200	-1.44332000	3.56682800
O	3.12732600	-0.44042000	-5.25805000
O	-3.12836600	0.42275400	5.25933200
O	5.29999400	-1.06890700	-3.58863900
O	-5.29978700	1.05904500	3.59199900
O	7.70905800	-1.86986100	-2.41189400
O	-7.70935200	1.86341300	2.41812200

O	5.15443400	-2.64718900	-1.47854200
O	-5.15453900	2.64148200	1.48509100
O	3.01196600	-2.07202500	-2.88859100
O	-3.01193500	2.06142400	2.89269900
O	2.66959400	-1.90970700	0.02625300
O	-2.67091300	1.91057200	-0.02272500
O	-1.50987800	3.77243000	1.30435400
O	1.50837200	-3.77483500	-1.29628100
O	0.99945200	3.41648200	-0.05218900
O	-0.99950900	-3.41319200	0.05402000
O	-0.20483200	1.49901000	4.18178100
O	0.19793900	-1.50007200	-4.17978300
O	-0.27244400	1.34555300	1.33540700
O	0.27145800	-1.34440000	-1.33428000
O	-0.28093000	1.33111000	-1.41975400
O	0.28211500	-1.32678400	1.42098500
O	1.89646500	0.31535300	-2.79593700
O	-1.89571100	-0.32280500	2.79625800
O	3.68462700	-4.79267300	-2.70003600
O	-3.68519300	4.78174600	2.71563100
O	0.19145500	-1.18848800	4.31062100
O	-0.18652700	1.18971500	-4.31028900
O	4.26480200	0.02315500	-1.40801800
O	-4.26575600	-0.02941600	1.40775800
O	3.51357100	2.73477000	-1.36035400

O	-3.51588500	-2.74375000	1.35711000
Re	2.95321300	4.38458800	-0.07451700
Re	-2.94983900	-4.38492800	0.06345200
Sb	2.82117600	0.11376900	-0.00569900
Sb	-2.82171100	-0.11236800	0.00536500
W	3.31850600	-3.42594600	1.71438400
W	-3.32297500	3.43393700	-1.70277000
W	6.22888700	-1.08096400	1.86832500
W	-6.23025400	1.08382600	-1.86380100
W	6.22405700	-1.15079900	-1.85232600
W	-6.22445600	1.14489100	1.85750100
W	3.52628800	-0.22406100	3.57626700
W	-3.52559500	0.23934900	-3.57512100
W	5.13693900	2.14423100	1.84627400
W	-5.13225900	-2.13861200	-1.85632300
W	5.15865800	2.08535600	-1.84911600
W	-5.16208000	-2.09299600	1.83892200
W	3.53581500	-0.28984500	-3.57546900
W	-3.53684100	0.27499700	3.57643300
W	3.30564300	-3.46394600	-1.64035800
W	-3.30547500	3.45660300	1.65155500
W	0.00154900	0.10436200	3.15263600
W	-0.00215000	-0.10361500	-3.15183400
W	-0.51911500	2.46826500	-0.05181500
W	0.51913400	-2.46535800	0.05415500

Table 2-4 The band origin S_0-S_1, and bright S_0-S_n transitions (f > 0.001 a.u.) in water

State	E/eV	λ/nm	osc. str. (a.u.)
S1	2.5172	492.54	f=0.0003
S2	2.6124	474.59	f=0.0015
S9	2.6252	472.29	f=0.0017
S11	2.6357	470.41	f=0.0011
S16	2.8045	442.09	f=0.0038
S17	2.8058	441.88	f=0.0015
S18	2.8078	441.57	f=0.0042
S24	2.8912	428.83	f=0.0114
S28	2.9173	424.99	f=0.0039
S32	2.9524	419.95	f=0.0022
S33	2.9696	417.51	f=0.0013
S35	2.9975	413.62	f=0.0016
S36	3.0012	413.12	f=0.0059
S37	3.002	413.01	f=0.0066
S38	3.0108	411.8	f=0.0026
S40	3.0208	410.43	f=0.0013
S41	3.0256	409.79	f=0.0126
S42	3.0358	408.41	f=0.0004
S43	3.0989	400.09	f=0.0080
S52	3.1852	389.26	f=0.0026
S63	3.2426	382.36	f=0.0022
S69	3.2605	380.26	f=0.0025

2.4 Conclusions

Four polytungstate-supported tricarbonyl metal derivatives have been synthesized through a facile approach and characterized by X-ray crystallography andspectroscopic methods. These compounds contain very similar geometrical structures: $[XW_9O_{33}(WO_2)\{M(CO)_3\}]_2^{12-}$ (X = Sb, Bi and M = Re, Mn). Notably, **2.1** and **2.2** show broad absorptions in the visible region. Unlike **2.1** and **2.2**, **2.3** and **2.4** are unstable upon irradiation. The charge transfer transitions from the Mn centers to the POMs result in decomposition of the starting compounds.

The preparation of these four compounds is performed in aqueous solutions under mild conditions. This synthetic approach is more convenient than reported preparations of similar compounds where organic solvents or one-pot hydrothermal methods are used. This stepwise synthesis indicates that the multi-dentate multi-defect POMs, $[X_2W_{22}O_{74}(OH)_2]^{12-}$ (X = Sb or Bi), are versatile starting materials for construction of functionalized POMs of this type. Together with the previously reported structures by Krebs, the examples in this report suggest that these POM precursors can be further used to coordinate topologically equivalent units, $[LMR_3]^{n+}$ (L = tridentate ligand; M = transition metal; R = weak ligands, such as H_2O, CH_3CN, etc.) that might display chromophoric or catalytic properties of interest.

References

(1) Kulkarni, A.; Lobo-Lapidus, R. J.; Gates, B. C. *Chem. Commun.* **2010**, *46*, 5997.

(2) Gouzerh, P.; Proust, A. *Chem. Rev.* **1998**, *98*, 77.

(3) Besecker, C. J.; Klemperer, W. G. *J. Am. Chem. Soc.* **1980**, *25*, 7598.

(4) Day, V. W.; Fredrich, M. F.; Thompson, M. R.; Klemperer, W. G.; Liu, R. S.; Shum, W. *J. Am. Chem. Soc.* **1981**, *103*, 3597.

(5) Besecker, C. J.; Day, V. W.; Klemperer, W. G.; Thompson, M. R. *Inorg. Chem.* **1985**, *24*, 44.

(6) Klemperer, W. G.; Main, D. J. *Inorg. Chem.* **1990**, *29*, 2355.

(7) Klemperer, W. G.; Zhong, B. X. *Inorg. Chem.* **1993**, *32*, 5821.

(8) Siedle, A. R.; Lyon, P. A.; Hodgson, K. O.; Roe, A. L. *Inorg. Chem.* **1987**, *26*, 219.

(9) Nagata, T.; Pohl, B. M.; Weiner, H.; Finke, R. G. *Inorg. Chem.* **1997**, *36*, 1366.

(10) Besserguenev, A. V.; Dickman, M. H.; Pope, M. T. *Inorg. Chem.* **2001**, *40*, 2582.

(11) Villanneau, R.; Delmont, R.; Proust, A.; Gouzerh, P. *Chem. Eur. J.* **2000**, *6*, 1184.

(12) Villanneau, R.; Proust, A.; Robert, F.; Gouzerh, P. *Chem. Eur. J.* **2003**, *9*, 1982.

(13) Sadakane, M.; Iimuro, Y.; Tsukuma, D.; Bassil, B. S.; Dickman, M. H.; Kortz, U.; Zhang, Y.; Ye, S.; Ueda, W. *Dalton Trans.* **2008**, 6692.

(14) Niu, J.; Yang, L.; Zhao, J.; Ma, P.; Wang, J. *Dalton Trans.* **2011**, *40*, 8298.

(15) Zhao, J.; Wang, J.; Zhao, J.; Ma, P.; Wang, J.; Niu, J. *Dalton Trans.* **2012**, *41*, 5832.

(16) Zhao, J.; Zhao, J.; Ma, P.; Wang, J.; Niu, J.; Wang, J. *J. Mol. Struct.* **2012**, *1019*, 61.

(17) Long, D.-L.; Tsunashima, R.; Cronin, L. *Angew. Chem. Int. Ed.* **2010**, *49*, 1736.

(18) Long, D.-L.; Burkholder, E.; Cronin, L. *Chem. Soc. Rev.* **2007**, *36*, 105.

(19) Kikukawa, Y.; Yamaguchi, K.; Mizuno, N. *Inorg. Chem.* **2010**, *49*, 8194.

(20) Zhu, G.; Geletii, Y. V.; Zhao, C.; Musaev, D. G.; Song, J.; Hill, C. L. *Dalton Trans.* **2012**, *41*, 9908.

(21) Proust, A.; Matt, B.; Villanneau, R.; Guillemot, G.; Gouzerh, P.; Izzet, G. *Chem. Soc. Rev.* **2012**, *41*, 7605.

(22) Bosing, M.; Loose, I.; Pohlmann, H.; Krebs, B. *Chem. Eur. J.* **1997**, *3*, 1232.

(23) Loose, I.; Droste, E.; Boesing, M.; Pohlmann, H.; Dickman, M. H.; Rosu, C.; Pope, M. T.; Krebs, B. *Inorg. Chem.* **1999**, *38*, 2688.

(24) Bi, L.-H.; Al-Kadamany, G.; Chubarova, E. V.; Dickman, M. H.; Chen, L.; Gopala, D. S.; Richards, R. M.; Keita, B.; Nadjo, L.; Jaensch, H.; Mathys, G.; Kortz, U. *Inorg. Chem.* **2009**, *48*, 10068.

(25) Sheldrick, G. M. *Acta Crystallogr., Sect. A* **1990**, *46*, 467.

(26) Sheldrick, G. M. *SHELXL-97, Program for the Refinement of Crystal Structures*; University of Göttingen: Germany, 1997.

(27) Sanchez, C.; Livage, J.; Launay, J. P.; Fournier, M.; Jeannin, Y. *J. Am. Chem. Soc.* **1982**, *104*, 3194.

(28) Sanchez, C.; Livage, J.; Launay, J. P.; Fournier, M. *J. Am. Chem. Soc.* **1983**, *105*, 6817.

(29) Buckley, R. I.; Clark, R. J. H. *Coord. Chem. Rev.* **1985**, *65*, 167.

(30) Kozik, M.; Hammer, C. F.; Baker, L. C. W. *J. Am. Chem. Soc.* **1986**, *108*, 7627.

(31) Papaconstantinou, E. *Chem. Soc. Rev.* **1989**, *18*, 1.

(32) Chiang, M.-H.; Soderholm, L.; Antonio, M. R. *Eur. J. Inorg. Chem.* **2003**, *2003*, 2929.

Chapter 3

Mono-lacunary Polytungstate-supported Metal Carbonyl Complexes

(Published partially in *J. Am. Chem. Soc.* **2011**, *133 (50)*, 20134–20137.)

With Zhuangqun Huang, William Rodríguez-Córdoba, Choon Sung Kambara, Kevin P. O'Halloran, Ken I. Hardcastle, Djamaladdin G. Musaev, Tianquan Lian and Craig L. Hill

3.1 Introduction

POM-based organometallic derivatives have been widely investigated for designing new materials with distinct structures and multi-functionalities.[1-3] These inorganic-organic hybrid compounds can integrate the advantages of POMs (i.e. oxidative, hydrolytic and thermal stability, multi-electronic redox activities, photochemical properties and so on), and organometallic complexes (i.e. chirality, magnetism, catalysis and visible-light activity). Sometimes synergistic properties also appear in the hybrid systems. Up to date most of these compounds are POM-based organo- tin/germanium/ruthenium complexes usually with phenyl or alkyl ligands.[4-24] POM-supported metal carbonyl complexes (PSMCs) are relatively less studied. Initially, PSMCs were used to mimic the metal carbonyl derivatives deposited onto the surfaces of solid oxides. The latter are stable and efficient heterogeneous catalysts for industrial reactions such as hydrogenation and hydrocarbonation.[25-27] The fine structures, especially short-range orders and local compositions of these modified solid-oxide surfaces were less studied, although limited information could be revealed somehow by various techniques, i.e. EXAFS. Single crystal X-ray diffraction is limited because of their heterogeneous nature. POMs are metal-oxide molecular analogues and thus modeling the interaction between metal carbonyl and solid-oxide supports at an atomic level.

In this section we investigated PSMCs based on the mono-lacunary POM ligands [α-$PW_{11}O_{39}]^{7-}$ and [α_2-$P_2W_{17}O_{61}]^{10-}$. We expanded the research concerning the "twisted-sandwich" tungstophosphates, which have extended the family of Krebs-type "slipped-sandwich" tungstoantimonates and tungstobismuthates as mentioned in **Chapter 2**. In this work, several novel PSMCs have been successfully isolated and fully characterized:

$K_6Na_4P_2W_{23}O_{80}\{Re(CO)_3\}_2 \cdot 23H_2O$ (**3.1**), $(C_3H_{10}N)_8Na_2P_2W_{23}O_{80}\{Re(CO)_3\}_2 \cdot 12H_2O$ (**3.1a**), $(C_3H_{10}N)_6Na_4P_2W_{23}O_{80}\{Mn(CO)_3\}_2 \cdot 18H_2O$ (**3.2**) and $K_{15}NaP_4W_{35}O_{124}\{Re(CO)_3\}_2 \cdot 37H_2O$ (**3.3**) $K_{15}NaP_4W_{35}O_{124}\{Mn(CO)_3\}_2 \cdot 32H_2O$ (**3.4**). Synthetic methodology, crystal structures, spectroscopy and electrochemical properties have been thoroughly investigated.

3.2 Experimental

3.2.1. Materials and Instrumentation

Chemicals were reagent grade and used as supplied. The Keggin and Dawson polyoxometalate precursors $Na_7[\alpha\text{-}PW_{11}O_{39}]$ and $K_{10}[\alpha_2\text{-}P_2W_{17}O_{61}]$ were prepared according to the literature.[28,29] The low-valence complexes $M(CO)_3(CH_3CN)_3(BF_4)$ (M = Re, Mn) were made following known methods with only $AgClO_4$ replaced by $AgBF_4$.[30] The purities of these compounds were analyzed by ^1H NMR, ^{31}P NMR and FT-IR spectroscopy.

The FT-IR spectra were acquired on a Thermo Nicolet 6700 spectrometer with KBr pellets (2%). UV-vis spectra were collected using an Agilent 8453 spectrophotometer equipped with a diode-array detector and an Agilent 89090A cell temperature controller unit. ^{31}P NMR spectra (162.13 MHz) in D_2O were measured on a Varian INOVA 400 spectrometer with respect to an external standard of 85% H_3PO_4 (0 ppm). Elemental analyses were performed by Galbraith Lab Inc., Knoxville, TN (K, Na, P, Re, W) and Atlantic Microlab Inc., Norcross, GA (C, H, N). Thermogravimetric analysis was acquired on a Perkin Elmer STA 6000 analyzer.

3.2.2. Synthesis

$K_6Na_4P_2W_{23}O_{80}\{Re(CO)_3\}_2\cdot 23H_2O$ (3.1). $Na_7PW_{11}O_{39}$ (0.1 mmol, 286 mg) and $Re(CO)_3(CH_3CN)_3BF_4$ (0.1 mmol, 48 mg) were dissolved in 15 mL of hot water. The mixtures were heated at ~70^o C for 0.5 h, during which the solution color slowly became orange-red. The solution was then cooled to room temperature and the pH was adjusted to ~2.5 by 1.0 M HCl. The solution became dark-red in color and was filtered. KCl (200 mg) was added to the above solution in small portions. Single crystals in plate shapes and suitable for X-ray diffraction were collected after slow evaporation in about 3 weeks. Yield: 45 mg (13% based on P). FTIR (2500 – 400 cm^{-1}): 2013 (s), 1900 (s), 1879 (s), 1099 (s), 1046 (s), 956 (s), 903 (m), 838 (s), 785 (w), 743 (w), 708 (w), 653 (w), 598 (w), 513 (w). Electronic spectral data (350 – 700 nm, in H_2O): ε_{400} ~ 1.1×10^4 $M^{-1}\cdot cm^{-1}$. ^{31}P NMR: -12.7 ppm. Anal. Calcd. for $C_6H_{46}O_{109}K_6Na_4P_2Re_2W_{23}$: K, 3.4; Na, 1.3; P, 0.90; Re, 5.4; W, 61.7. Found: K, 3.8; Na, 1.1; P, 0.83; Re, 5.1; W, 59.5. Thermogravimetric analysis (TGA): weight loss, 8.5%.

$(C_3H_{10}N)_8Na_2P_2W_{23}O_{80}\{Re(CO)_3\}_2\cdot 12H_2O$ (3.1a). The preparation was similar to that for **3.1** but with trimethylammonium bromide (~100 mg) substituted for KCl. Large block-shape crystals suitable for X-ray diffraction measurement were obtained overnight. Yield: 240 mg (70% based on P). FTIR (2500 – 400 cm^{-1}): 2006 (s), 1900 (s), 1876 (s), 1099 (s), 1103 (s), 1047 (s), 954 (s), 895 (m), 835 (s), 817 (s), 781 (w), 703 (s), 654 (w), 595 (w), 513 (w). Electronic spectral data (350 – 700 nm, in H_2O): ε_{400} ~ 1.1×10^4 $M^{-1}\cdot cm^{-1}$. ^{31}P NMR: -12.7 ppm. Anal. Calcd. for $C_{30}H_{104}N_8O_{98}Na_2P_2Re_2W_{23}$: C, 5.26; H, 1.53; N, 1.63; Na, 0.67. Found: C, 5.26; H, 1.46; N, 1.65; Na, 0.71. TGA: weight loss, 12.6%.

$(C_3H_{10}N)_6Na_4P_2W_{23}O_{80}\{Mn(CO)_3\}_2\cdot 18H_2O$ (3.2). $Mn(CO)_5Br$ (0.1 mmol, 27 mg) and $AgNO_3$ (0.1 mmol, 17 mg) were dissolved in 1 mL methanol. The mixtures were stirred in the dark at room temperature for ~2 hrs and then filtered. The filtrate containing the *in situ* formed $[Mn(CO)_3]^+$ precursors was then added to an aqueous solution (15 mL) of $Na_7PW_{11}O_{39}$ (0.1 mmol, 286 mg). The mixtures were stirred in the dark at ~50° C for another ~2 hrs and then filtered. 1 M HCl was added dropwise until the final pH was ~2.5. Trimethylammonium bromide (~20 mg) was then added and the solution was filtered again. The solution was kept in the dark for slow evaporation. Black-red crystals in large block shapes were collected after ~2 weeks. Yield: 150 mg (45% based on P). FTIR (2500 – 400 cm^{-1}): 2031 (s), 1930 (s), 1921 (s), 1099 (s), 1049 (s), 955 (s), 895 (m), 841 (m), 823 (w), 767 (w), 750 (w), 714 (s), 677 (w), 598 (w), 582 (w), 509 (m). Electronic spectral data (350 – 700 nm, in H_2O): $\varepsilon_{400} \sim 9.7\times10^3$ $M^{-1}\cdot cm^{-1}$. ^{31}P NMR: -12.6 ppm. Anal. Calcd. for $C_{24}H_{96}N_6O_{104}Na_4Mn_2P_2W_{23}$: C, 4.35; H, 1.46; N, 1.27; Na, 1.4; Mn, 1.6; P, 0.93; W, 63.8. Found: C, 4.41; H, 1.39; N, 1.26; Na, 1.2; Mn, 1.5; P, 0.83; W, 61.3. TGA: weight loss, 12.9%.

$K_{15}NaP_4W_{35}O_{124}\{Re(CO)_3\}_2\cdot 37H_2O$ (3.3). $K_{10}[\alpha_2\text{-}P_2W_{17}O_{61}]\cdot 20H_2O$ (0.1 mmol, 487 mg) and $Re(CO)_3(CH_3CN)_3(BF_4)$ (0.1 mmol, 48 mg) were dissolved in 20 ml H_2O at pH 2.5 adjusted by 1 M HCl. The mixture was heated at ~70 ℃ for 1 h and the color finally changed to dark red. KCl (200 mg) was added to the solution and then the solution was filtered through a fine filter paper. Dark-red and plate-shaped crystals were obtained by slow evaporation over the course of several days. Yield: 320 mg (30% based on P). Analytical data: ^{31}P NMR (D_2O): -8.5 and -13.5 ppm. FTIR (2% KBr pellet, 2500 - 400 cm^{-1}): 2006 (m), 1901(m), 1880 (m), 1654 (m), 1081 (m), 943 (s), 806 (s), 769(s), 704

(s), 527 (m). Electronic spectral data (300 - 800 nm, in H_2O, 0.2 cm cell pathlength): λ_{400} ~ 6200 $M^{-1}\cdot cm^{-1}$. Elemental analysis found Na in the sample, which is attributed to $Na_2WO_4\cdot 2H_2O$ used during the preparation of $K_{10}[\alpha_2\text{-}P_2W_{17}O_{61}]\cdot 20H_2O$. Anal. Calcd. for $C_6H_{76}O_{168}K_{15}NaP_4Re_2W_{35}$: K, 5.6; Na, 0.22; P, 1.2; Re, 3.6; W, 62.1. Found: K, 5.5; Na, 0.21; P, 1.1; Re, 3.4; W, 62.7. Thermogravimetric analysis (TGA): weight loss, 8.07%.

$K_{15}NaP_4W_{35}O_{124}\{Mn(CO)_3\}_2\cdot 32H_2O$ (3.4). $K_{10}P_2W_{17}O_{61}$ (0.1 mmol, 480 mg) was dissolved in 10 mL of H_2O at ~ 70° C. Pre-synthesized $Mn(CO)_3(CH_3CN)_3BF_4$ (0.1 mmol, 35 mg) was added and the mixtures were stirred in the dark for 1 hr. HCl (1.0 M) was added slowly to the above solution until the pH was ~2.2. The solution turned a dark-red color and was stirred for another 15 mins. KCl (400 mg) was then added and the mixtures were filtered. The filtrate was kept in the dark and red crystals were obtained within several hours. The remaining solution became greenish. Yield: 80 mg (16% based on P). FTIR (2500 – 400 cm^{-1}): 2034 (s), 1948 (s), 1936 (s), 1085 (s), 1056 (m), 1017 (m), 945 (s), 913 (m), 798 (s), 738 (s), 600 (w), 566 (w), 523 (m). Electronic spectral data (350 – 700 nm, in H_2O): ε_{400} ~ 4.8×10^3 $M^{-1}\cdot cm^{-1}$. ^{31}P NMR: -7.6 and -13.2 ppm. $C_6H_{64}O_{162}K_{15}NaP_4Mn_2W_{35}$: elemental analysis need to be done. TGA: weight loss, 7.5%.

3.2.3. Crystallography

X-ray analysis was performed on a Bruker D8 SMART APEXII CCD sealed tube diffractometer. Diffraction intensities were measured using graphite monochromated Mo Kα radiation (λ = 0.71073 Å) at 173(2) K. Data collection, indexing, and initial cell refinements were carried out using APEX2 v2011.2-4 (Bruker, 2011). Data reduction and cell refinements were carried out using SAINT v7.68A (Bruker, 2009). A multi-scan absorption correction that included face-indexing was done using the program

SADABS.[31-33] The molecular structures were determined by Direct Methods and Fourier techniques and refined by full-matrix least squares. Structure solution, refinement, graphics were generated with and generation of publication materials were accomplished using SHELXTL-97 software.[34,35] The largest residual electron density for each structure was located close to the W atoms and was most likely due to imperfect absorption corrections frequently encountered in heavy-metal atom structures. Crystal data collection and refinement parameters are given in Table 3-3.

3.2.4. Electrochemistry

Cyclic voltammograms (CVs) of **3.1**, **3.2** and **3.4** were obtained at room temperature using a BAS CV-50W potentiostat using the standard three-electrode configuration. A glassy-carbon electrode was used as the working electrode. The reference electrode was Ag/AgCl (3 M NaCl) (BASi) and a platinum wire was used as the counter electrode. All reported reduction potentials are relative to this reference electrode. CVs were performed in 20 mM sodium acetate buffer (pH = 4) with 0.2 M $LiClO_4$ as supporting electrolyte.

3.3 Experimental

3.3.1 Synthesis and Crystal Structures

Table 3-1 summarizes all PSMCs up to this point.[5,36-53] The majority of these compounds include the Lindqvist-type derivatives (Entry #2,3,6,7,8,10). Keggin and Dawson (especially the defect) based PSMCs are relatively rare. Furthermore, most compounds are made by one-pot hydrothermal methods and frequently in organic solvents, which are comparatively less convenient. As mentioned in **Chapter 2**, we successfully immobilized the $[M(CO)_3]^+$ (M = Re, Mn) groups onto the vacant sites of Krebs-type "slipped-

sandwich" POMs $[X_2W_{20}O_{70}]^{14-}$ (X = Sb, Bi) through a facile method (Entry #13).[15,54-59] With respect to the phosphor-centered analogues, however, $[P_2W_{20}O_{72}]^{14-}$ was rarely observed (Scheme 3-1), although other dimeric species such as $[P_2W_{19}O_{69}(OH_2)]^{14-}$, $[P_2W_{20}O_{70}(OH_2)_2]^{10-}$ and $[P_2W_{21}O_{71}(OH_2)_3]^{6-}$ were seen previously.[60-64] The $[PW_9O_{34}]^{9-}$ ligands usually capture transition-metal ions to become the well-known eclipsed sandwich structures with tri-/tetra- nuclear cores.[65-76] Earlier Hill *et al.* reported an Ir(III)-substituted POM, $[(IrCl_4)KP_2W_{20}O_{72}]^{14-}$, a pre-catalyst for water oxidation.[77] In this structure, the $[IrCl_4]^-$ group locates in the external position of $[P_2W_{20}O_{72}]^{14-}$, a similar "slipped-sandwich" geometry to the Krebs-type complexes. An interesting discovery by Kirschhock *et al.* shows a one-step transformation from $[PW_{12}O_{40}]^{3-}$ to $[P_2W_{20}O_{72}]^{14-}$ mediated by chromate.[78]. It should be pointed out that $[\alpha_2\text{-}P_2W_{17}O_{61}]^{10-}$ and $[\alpha\text{-}PW_{11}O_{39}]^{7-}$ are mono-lacunary, based on which the transition-metal substituted complexes usually appear as 1) the typical 1:1 monomeric Keggin/Dawson-type of $[PW_{11}O_{39}M(H_2O)]^{3-/4-}$ and $[P_2W_{17}O_{61}M(H_2O)]^{6-/7-/8-}$ (M = Mn^{II}, Fe^{III}, Co^{II}, Ni^{II}, Cu^{II}, Ru^{III}, Ti^{IV}, Zr^{IV}, etc.);[79-87] 2) the achiral 2:2 dimeric forms of $[\{PW_{11}O_{39}M(\mu\text{-}OH)\}_2]^{8-/10-}$ and $[\{P_2W_{17}O_{61}M(\mu\text{-}OH)(H_2O)\}_2]^{14-/16-}$ (M = Ru^{III}, Hf^{IV}, Zr^{IV}, etc.);[88-95] 3) the chiral 2:1 dimers $[(PW_{11}O_{39})_2M(H_2O)]^{10-/11-}$ and $[(P_2W_{17}O_{61})_2M]^{16-/17-}$ (M = Ce^{III}, Zr^{IV}, Hf^{IV}, Ti^{IV}, etc.).[96-105] On the other side, the organometallic derivatives (especially the organo-ruthenium substituted) derived from monovacant POM ligands were studied intensively.[16,17,63,106-125] These discoveries have inspired us to investigate more intensively in the coordination chemistry between mono-lacunary POMs and metal carbonyl groups.

Table 3-1 Summary of PSMCs

No.	Formulas	Conditions	Comments	Refs
1	$[\{CpFe(CO)_2Sn\}SiW_{11}O_{39}]^{5-}$ $[Co(CO)_3(SnSiW_{11}O_{39})_2]^{11-}$ $[\{CpFe(CO)_2Sn\}_2PW_{10}O_{38}]^{5-}$ and related compounds	Trichlorostannanes or trichlorogermanes (e.g. $CpFe(CO)_2SnCl_3$) were reacted with the mono-lacunary POMs or Na_2WO_4/NaH_2PO_4 in one-pot; precipitates were isolated upon adding K^+ or TBA/TMA	Early examples of PSMCs; no crystal structures reported; characterized by FTIR, ^{31}P and ^{183}W NMR spectroscopy	5,36
2	$[(OC)_3M(Nb_2W_4O_{19})]^{3-}$ (M = Re and Mn) $[\{(CO)_2Rh\}_5(Nb_2W_4O_{19})_2]^{3-}$ $[\{(CO)_2Rh\}_3(Nb_2W_4O_{19})_2]^{5-}$ $[\{(CO)_2Ir\}_2H(Nb_2W_4O_{19})_2]^{5-}$	$[M(CO)_3(CH_3CN)_3](PF_6)$ (M = Re, Mn) or $[Rh(CO)_2Cl]_2$ were refluxed with $TBA_4(Nb_2W_4O_{19})$; bubbled CO into $TBA_5[\{(C_8H_{12})Ir\}_2H(Nb_2W_4O_{19})_2]$ in CH_3CN	Crystal structures were determined for the Re/Mn compounds but disordered; no X-ray structures for the Rh/Ir complexes; ^{17}O and ^{183}W NMR were also studied	37-39
3	$[\{CpTi(Mo_5O_{18})\}Mn(CO)_3]^{2-}$ $[(CpTiW_5O_{18})_2Ru_2(CO)_4]^{4-}$	$[Mn(CO)_3(CH_3CN)_3](PF_6)$ reacted with $[CpTi(Mo_5O_{18})(MoO_2Cl)]$ in CH_3CN; $[(CH_3CN)_6Ru_2(CO)_4](PF_6)_2$ reacted with $TBA_3[CpTiW_5O_{18}]$ in CH_2Cl_2	Bifunctional POM-supported organometallic compounds; no crystal structures; ^{17}O NMR and FTIR spectroscopy provided some structural information	40,41
4	$[(Ph_3P)_2Rh(CO)(CH_3CN)]_n[XM_{12}O_{40}]$ (X = Si, P; M = W, Mo; *n* = 3,4)	Mixed hydrated $H_4SiW_{12}O_{40}$ and $[(Ph_3P)_3Rh(CO)]^+[HC(SO_2CF_3)_2]^-$ in EtOH/MeCN solution and collected the precipitates	Ion pairs; no structures were determined but EXAFS was studied; heterogeneous catalysts for hydroformylation of olefins	42
5	$[Re(CO)_3P_2W_{15}Nb_3O_{62}]^{8-}$ $[Ir(CO)_2P_2W_{15}Nb_3O_{62}]^{8-}$ $[Rh(CO)_2P_2W_{15}Nb_3O_{62}]^{8-}$	$[Re(CO)_3(CH_3CN)_3](BF_4)$ reacted with $TBA_9P_2W_{15}Nb_3O_{62}$ in CH_3CN; bubbled CO into a solution of $[M(1,5\text{-}COD)\text{-}P_2W_{15}Nb_3O_{62}]^{8-}$ (M = Ir and Rh)	PSMCs with Dawson POMs, but no crystal structures were determined; ^{31}P and ^{183}W NMR, FTIR were studied	43
6	$[M_6O_{19}\{M'(CO)_3\}_n]^{(8-n)-}$ (M = Nb, Ta; M' = Mn, Re; *n* = 1, 2)	$[Mn(CO)_3]^+$ and $[Re(CO)_3]^+$ reacted with POMs $K_7HNb_6O_{19}$ and $K_8Ta_6O_{19}$ in water by hydrothermal methods in autoclave	X-ray structures determined; ^{17}O NMR and FTIR were also studied	44
7	$[Mo_2O_5(OMe)_5\{M(CO)_3\}_2]^-$ (M = Re and Mn) $[Mo_2O_4(OMe)_6\{Mn(CO)_3\}_2]$ $[Mo_2O_6(OMe)_4\{Re(CO)_3\}_2]^{2-}$ $[Mo_2O_4\{RC(CH_2O)_3\}_2\{Mn(CO)_3\}_2]$ (R = Me and CH_2OH) and the related	The solvated precursors $[Mn(CO)_3]^+$ and $[Re(CO)_3]^+$ were reacted with $TBA_2Mo_2O_7$ in MeOH; *w/o* the presence of $RC(CH_2OH)_3$ (R = Me, CH_2OH)	Crystal structures determined; electronic connection study revealed the isolobal analogy between d^0-*fac*-$\{MoO_2X\}$ (X = O, OR, Cl) and d^6-*fac*-$\{M(CO)_3\}$ (M = Mn, Re)	45
8	$[M(CO)_3(H_2O)\{Mo_5O_{13}\text{-}(OMe)_4(NO)\}]^{2-}$ (M = Re, Mn), $[Na\{Mo_5O_{13}(OMe)_4(NO)\}_2\{Mn(CO)_3\}_2]^{3-}$ and the other similar compounds	The solvated $[Mn(CO)_3]^+$ and $[Re(CO)_3]^+$ precursors reacted with $TBA_2[Na(MeOH)\text{-}\{Mo_5O_{13}(OMe)_4(NO)\}]$ in MeOH	Structures determined; $[Mo_5O_{13}(OMe)_4(NO)]^{3-}$ ion is a multifunctional ligand	46

9	$[SiW_{11}O_{39}Ru(CO)]^{6-}$	$Ru(acac)_3$ and $[\alpha\text{-}SiW_{11}O_{39}]^{8-}$ were reacted under hydrothermal conditions in autoclave.	No crystal structure; structure was characterized by XRD, ^{13}C NMR and FTIR; photo-induced redox chemistry was studied	47
10	$[(H_2W_8O_{30})\{M(CO)_3\}_2]^{8-}$ $[(H_2Mo_8O_{30})\{M(CO)_3\}_2]^{8-}$ (M = Re, Mn)	One-pot synthesis of $[Mn(CO)_3]^+$ and $[Re(CO)_3]^+$ with Na_2WO_4 ,or with $[Mo_7O_{24}]^{6-}$ in H_2O/AcOH	Structures obtained; Lindqvist isopolyoxotungstate supported metal carbonyl derivatives	49,53
11	$[Mn(CO)_3(A\text{-}\alpha\text{-}H_2XW_9O_{34})]^{8-}$ (X = Si, Ge)	Mixed solvated $[Mn(CO)_3]^+$ and $[\gamma\text{-}XW_{10}O_{36}]^{8-}$ (X = Si, Ge) in H_2O/CH_3CN solution at neutral pH	Structures determined; crystal formation due to the degradation $[\gamma\text{-}XW_{10}O_{36}]^{8-}$ (X = Si, Ge)	51
12	$[Mn(CO)_3(CH_3CN)_3]_3[XM_{12}O_{40}]$, $[Mn(CO)_3(CH_3CN)_3]_3[X_2M_{18}O_{40}]$ (X = P, As, Si, Ge; M = W, Mo)	Mixed solvated $[Mn(CO)_3]^+$ and $[Re(CO)_3]^+$ groups with plenary Dawson/Keggin POMs in H_2O/CH_3CN	Structures were determined; Ion pairs	50
13	$[X_2W_{20}O_{70}\{M(CO)_3\}_2]^{12-}$ (X = Sb, Bi; M = Re, Mn)	Mixed $[Mn(CO)_3]^+$ and $[Re(CO)_3]^+$ with the Krebs-type $[X_2W_{22}O_{74}(OH)_2]^{12-}$ (X = Sb, Bi) in water	Structures obtained; also shown topologically equivalent units between *fac*-$[M(CO)_3]^+$ and *fac*-$[TM(H_2O)_3]^{2+/3+}$ (TM = Co, Cu, Zn, Fe)	52
14	$[P_4W_{35}O_{124}\{M(CO)_3\}_2]^{16-}$ $[P_2W_{23}O_{80}\{M(CO)_3\}_2]^{10-}$ (M = Re, Mn)	Solvated $[M(CO)_3]^+$ (M = Re, Mn) precursors reacted with $[\alpha_2\text{-}P_2W_{17}O_{61}]^{10-}$ or $[\alpha\text{-}PW_{11}O_{39}]^{7-}$ in water at pH 2 ~ 2.5	Defect Dawson or Keggin PSMCs with sigle-crystal structures; visible-light active MPCT was studied	48 and herein

Cp = cyclopentadieny; TBA = tetrabutylammonium; TMA = tetramethylammonium; COD = 1,5-cyclooctadiene;

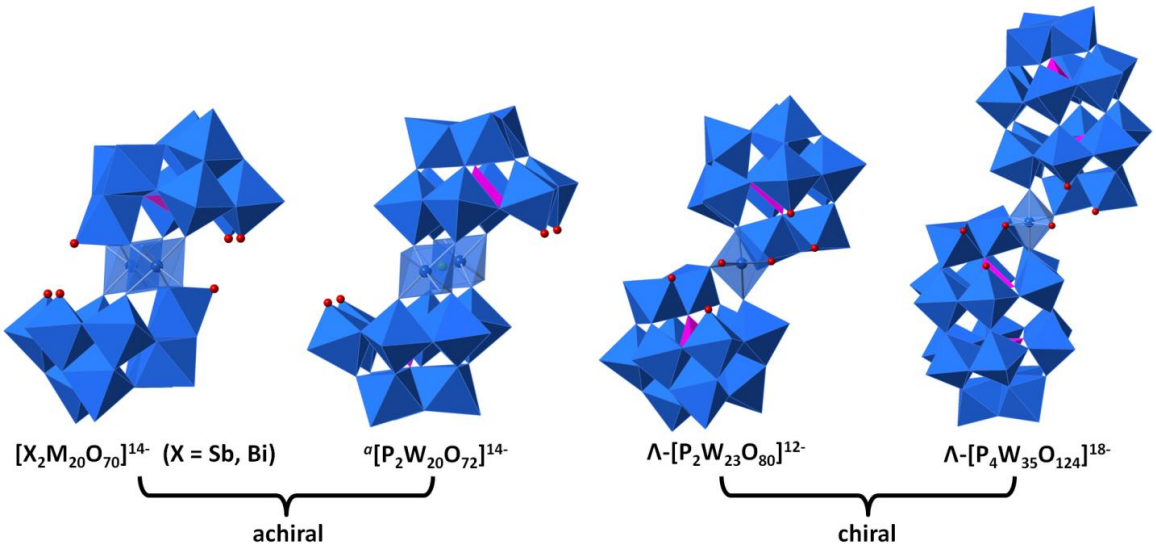

Scheme 3-1 Representative "slipped" and "twisted" sandwich polytungsten ligands. WO_6: blue octahedra; XO_4 (X = Sb, Bi, P): purple tetrahedra. Oxygen atoms in red-ball notation represent the coordinating sites, otherwise are omitted for clarity. [a] One K^+ ion locates in the inversion center.

The experimental results proved that the methods we established are versatile: mixing the POM precursors, $[\alpha_2\text{-}P_2W_{17}O_{61}]^{10-}$ or $[\alpha\text{-}PW_{11}O_{39}]^{7-}$, with the solvated $[Re(CO)_3]^+$ (generated from pre-synthesized $Re(CO)_3(CH_3CN)_3BF_4$) or $[Mn(CO)_3]^+$ (from $Mn(CO)_3(CH_3CN)_3BF_4$ or prepared *in situ* by $Mn(CO)_5Br$ and $AgNO_3$), at a certain acidic pH (<4), we can readily obtain the novel "twisted-sandwich"-type PSMCs: $[P_4W_{35}O_{124}\{M(CO)_3\}_2]^{16-}$ and $[P_2W_{23}O_{80}\{M(CO)_3\}_2]^{10-}$ (M = Re, Mn). Initially, $[\alpha_2\text{-}P_2W_{17}O_{61}]^{10-}$ and $[\alpha\text{-}PW_{11}O_{39}]^{7-}$ are tetra-oxygen donors and the four oxygen atoms are almost planar with a diagonal distance of ~ 4.20 Å (Figure 3-1). $[M(CO)_3]^+$ cannot bind to the above four terminal oxygens through three covalent M-O-W bonds directly; an additional vacant site is required. We also found that an acidic pH value is crucial for dimerization; these compounds do not form at higher pH (>5). Comparing the resulting dimeric structures with Krebs-type POMs, we find that the terminal oxygen atoms in the

latter order trigonally with distances between 2.70 to 2.88 Å in $[X_2W_{20}O_{70}]^{14-}$ (X = Sb or Bi).[54,55] Thus, they match well with the tri-vacant sites of $[M(CO)_3]^+$ (M = Re, Mn).[52]

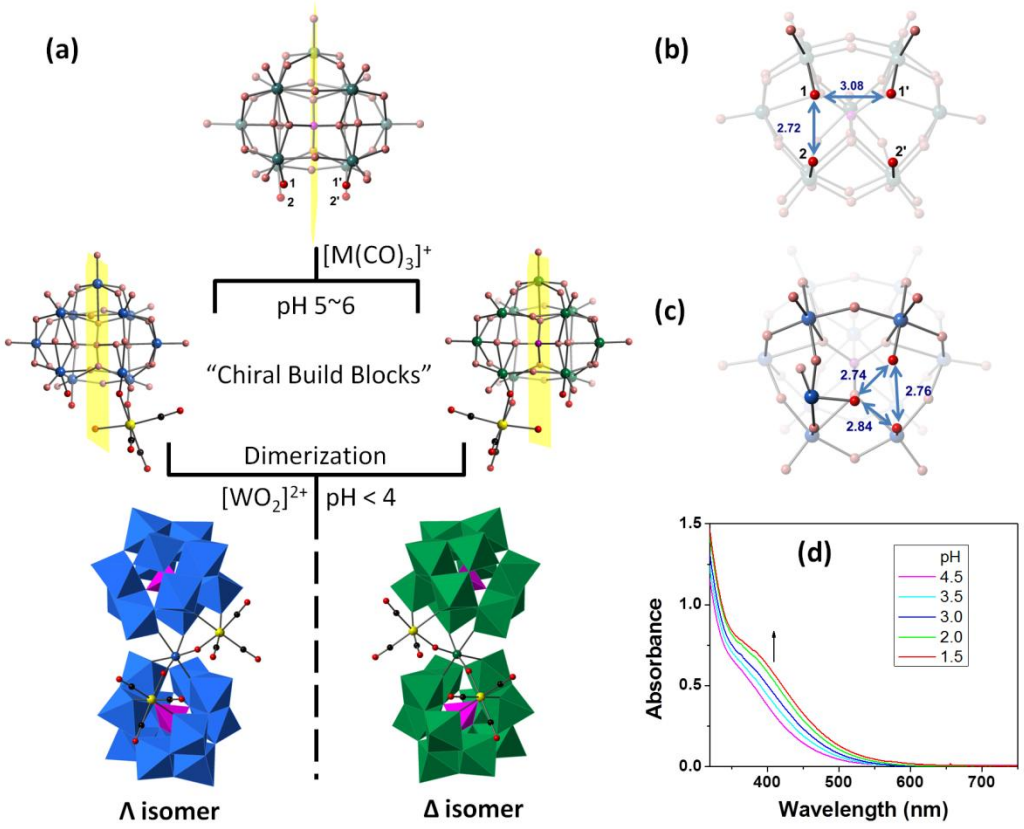

Figure 3-1 (a) Scheme of the proposed synthetic pathways of **3.1** and **3.2**. Color codes: O, red; C, black; P and PO_4, violet; Re or Mn, yellow; W and WO_6, blue or green. The yellow rectangles represent the mirror planes in $[\alpha\text{-}PW_{11}O_{39}]^{7-}$. Compound **3.3** and **3.4** follow the similar mechanism only with $[\alpha_2\text{-}P_2W_{17}O_{61}]^{10-}$ replacing $[\alpha\text{-}PW_{11}O_{39}]^{7-}$. (b) Representative distances (unit: Å) of the tetra-oxygen donors in $[\alpha\text{-}PW_{11}O_{39}]^{7-}$. (c) The trigonal coordination sites (unit: Å) appeared in the chiral structure (only half moiety is shown). (d) UV-vis absorption spectra in the course of preparing **3.1** at different pH. $[\alpha\text{-}PW_{11}O_{39}]^{7-}$ was firstly reacted with $[Re(CO)_3]^+$ (ratio 1:1) in water at 70 ^oC for 0.5 h. The spectra were record thereafter while changing pH by adding 1.0 M HCl.

Thus, we propose the self-assembly pathways as follows: at first, the solutions containing equivalent POMs and $[M(CO)_3]^+$ (M = Re, Mn) become reddish in color upon heating, a characteristic feature of MPCT transition, indicating the formation of W-O-M

bonds. As shown in Figure 3-1, $[M(CO)_3]^+$ tends to bind to the coordination sites, O(1) and O(2) (or the mirroring O(1') and O(2')), because the distances between them are 2.72 and 2.78 Å respectively, while the distances of O(1)-O(1') and O(2)-O(2') are 3.08 and 3.22 Å. The resulting bi-coordinated intermediates, denoted as [POM-*1,2*-$M(CO)_3]^{\neq}$ and [POM-*1',2'*-$M(CO)_3]^{\neq}$, are chirality-predefined building blocks. These intermediates lead to the chirality of each polyanion and the racemic configurations of solid states upon dimerization. The extra $[WO_2]^{2+}$ unit is derived from degraded POMs or additional tungstate salts added complementarily. While decreasing pH (<4), solution colors become darker and the visible absorption becomes more intensely, indicating the ongoing dimerization processes. In our trials, the four crystals were prepared at pH ~2-2.5.

The structure of **3.1** shows an ideal C_2 symmetry with only one peak appeared in ^{31}P NMR (Figure 3-2). The bond distances of Re-O and C-O are in the range of 1.87 to 1.91 Å and 1.16 to 1.20 Å respectively, which are similar to those of PSMCs reported previously.[5,36-52] Specifically, the structure can be regarded as dimerization of two [α-$PW_{11}O_{39}]^{7-}$ polyanion with an extra $[WO_2]^{2+}$ unit as the rotating center. The resulting "twisted sandwich" provides trigonally ordered terminal coordination sites, constructed from two oxygens from [α-$PW_{11}O_{39}]^{7-}$ and one oxygen from $[WO_2]^{2+}$ with O-O distances of 2.72 – 2.78 Å (Figure 3-1). This feature is similar to some organo-ruthenium substituted POMs,[109,116] but different from the Krebs-type Sb/Bi-centered POMs. The supported $[Re(CO)_3]^+$ moieties are in the "out-of-pocket" positions (Figure 3-1).[126,127] The central W atom locates in a distorted octahedral cage, and the four neighboring metal centers (Re, the central W and the other two adjacent W) are almost in the same plane (±1º; see the green planes in Figure 3-3). The chirality derives from two [α-$PW_{11}O_{39}]^{7-}$

units staggered relative to one another around the central W atom, i.e. a torsion angle of ±48.5º between the two green planes in **Figure 3-1**. However, unlike $[Hf(PW_{11}O_{39})_2]^{11-}$ which crystallizes in a chiral space group,[103,128-130] **3.1** crystallizes in a centrosymmetric space group $P\bar{1}$. Thus, **3.1** is racemic (Λ- and Δ- forms of two enantiomers co-exist with 1:1 ratio) in the solid state. Since **3.1** has a low yield probably due to high solubility, trimethylammonium (TMA) was added to facilitate crystallization (70% yield). Interestingly, the resulting **3.1a** crystallizes in the orthorhombic space group *Pbca*. The crystal quality is not as good as **3.1**, which is probably due to the shorter crystallization time, highly disordered TMA cations, the high symmetry space group and a very large unit cell volume. **Figure 3-4** shows the ordered atomic positions of the Λ- and Δ- forms assembled in the unit cell.

Table 3-2 Selective bond lengths (Å) and bond angles (°)

	3.1	**3.1a**[c]	**3.2**	**3.3**	**3.4**
P-O[a]	1.52-1.56	1.50-1.59	1.50-1.55	1.51-1.60	1.52-1.58
M-O[a]	2.07-2.15	1.99-2.20	1.97-2.03	2.10-2.13	1.96-2.03
M-C[b]	1.88-1.91	1.71-1.90	1.80-1.83	1.85-1.93	1.78-1.85
C-O[b]	1.16-1.20	1.20-1.23	1.13-1.16	1.12-1.22	1.08-1.15
M-C-O[b]	176-180	172-179	174-179	170-177	173-180
C-O stretching	2013, 1900, 1879	2005, 1897, 1877	2031, 1930, 1921	2006, 1901, 1880	2034, 1948, 1936

[a] Oxygen from the POM frameworks (X = Sb or Bi; M = Re or Mn). [b] Carbon from the carbonyl groups. [c] Oxygen from the carbonyl groups.

A similar racemic structure is also observed in **3.2** while changing $[Re(CO)_3]^+$ to $[Mn(CO)_3]^+$. Mn-C and C-O bond distances are in the range of 1.80 to 1.83 Å and 1.12 to 1.16 Å, respectively. The twist angle is ±44.1º. Interestingly, the TMA directed crystallization results in a monoclinic, *C*2/c space group (**Figure 3-4**). Compound **3.3** and

3.4 also shows the "twisted-sandwich" structure (±44.1º) similar to **3.1** and **3.2** but with a larger Dawson ligand (**Figure 3-3**). The structural chirality of each polyanion is similar to the one in $[Ce_2(H_2O)_8(P_2W_{17}O_{61})_2]^{14-}$,[97] but both compounds crystallize in a centrosymmetric space group, triclinic $P\bar{1}$ (**Figure 3-4**).

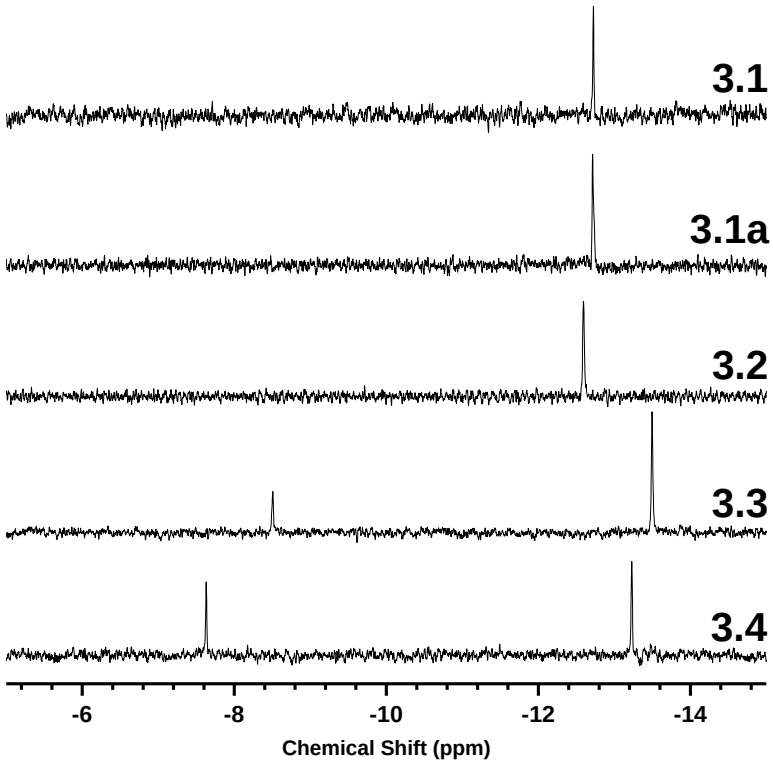

Figure 3-2 ^{31}P NMR of **3.1** (D_2O), **3.1a** (D_2O with LiCl), **3.2** (D_2O with LiCl), **3.3** (in D_2O) and **3.4** (in D_2O) with respect to 85% H_3PO_4 (0 ppm).

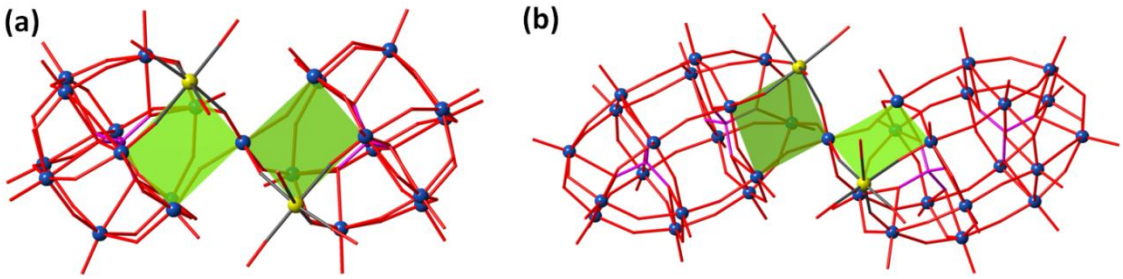

Figure 3-3 X-ray structures of Λ-**3.1** (a) and Λ-**3.4** (b) in ball-and-stick modes. Color codes: C, gray; O, red; Re/Mn, yellow; W, blue. The green planes illustrate the relatively twisted positions of the two POM ligands and the torsion angles.

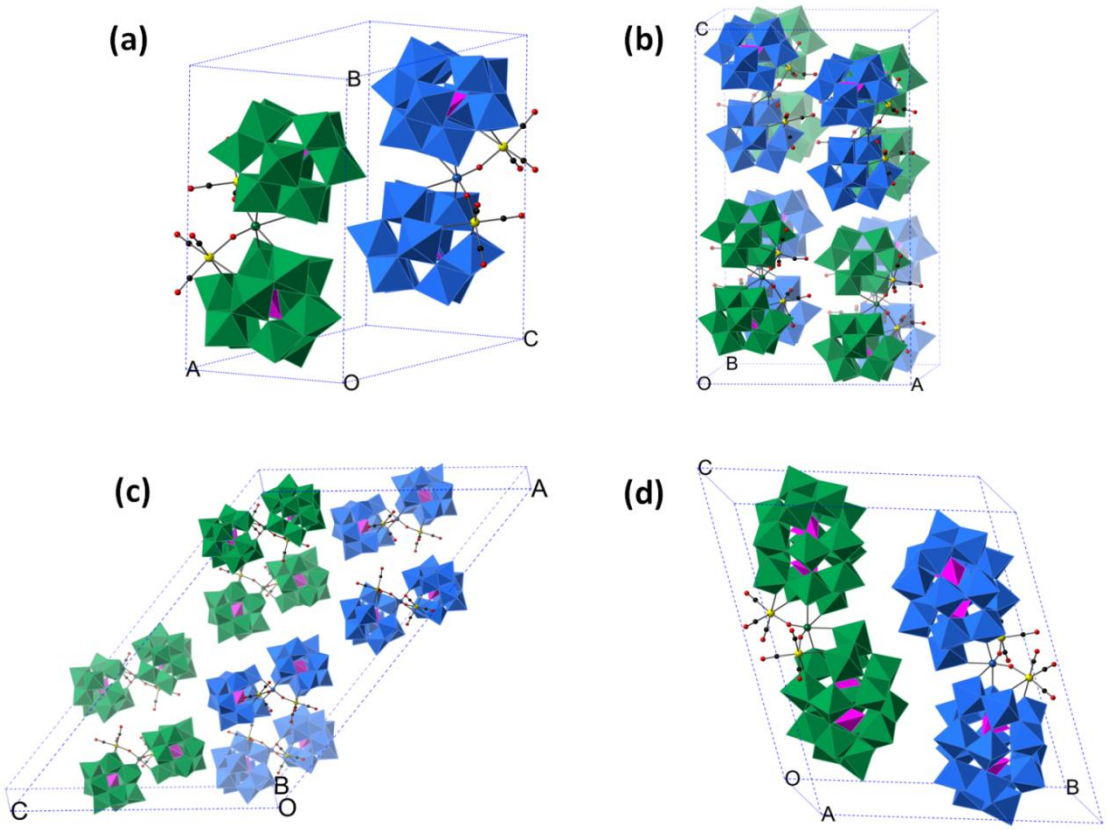

Figure 3-4 The packing arrangements of Λ- (blue) and Δ- (green) isomers in the single unit cells of crystal structures of (a) **3.1**, (b) **3.1a**, (c) **3.2** and (d) **3.4**. Color codes: O, red; C, black; PO_4, violet; Re or Mn, yellow; WO_6, blue or green.

Because these complexes show C_2 symmetry and each $\{M(CO)_3\}^+$ unit has local C_{3v} symmetry, two symmetric and one anti-symmetric IR-active C-O stretching modes, appear in the FTIR spectra (**Figure 3-5**). Compounds **3.1** and **3.3** (the Re derivatives) have lower C-O frequencies relative to those in **3.2** and **3.4** (the Mn derivatives) respectively, which is consistent with the stronger M-to-CO dπ-π* back bonding as Re(I) is more electron donating than Mn(I).

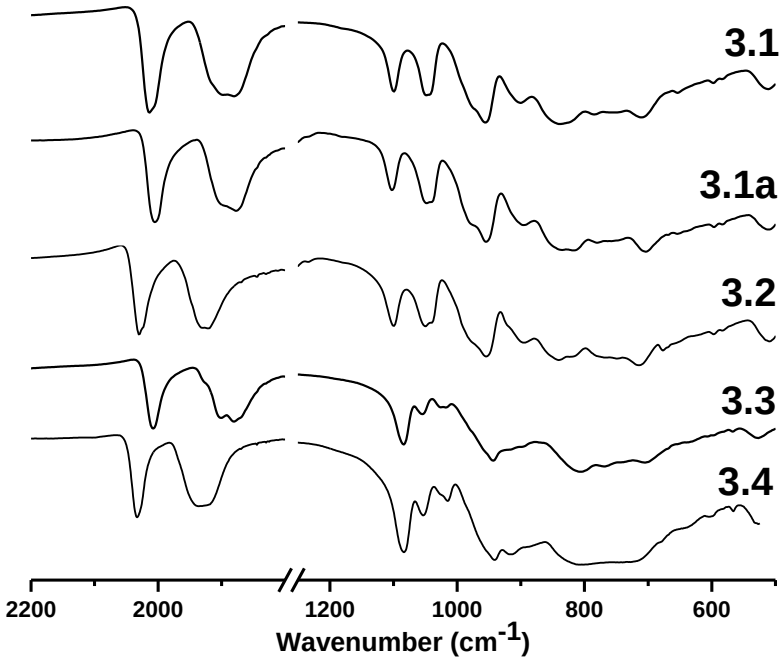

Figure 3-5 FTIR spectra (KBr pellets).

Table 3-3 Crystal structure data for compounds **3.1**, **3.1a**, **3.2**, **3.3** and **3.4**

	3.1	**3.1a**	**3.2**	**3.3**	**3.4**
Empirical formula	$C_6H_{46}O_{109}K_6Na_4P_2Re_2W_{23}$	$C_{30}H_{104}N_8O_{98}Na_2P_2Re_2W_{23}$	$C_{24}H_{96}N_6O_{104}Na_4Mn_2P_2W_{23}$	$C_6H_{76}O_{168}K_{15}NaP_4Re_2W_{35}$	$C_6H_{64}O_{162}K_{15}NaP_4Mn_2W_{35}$
T [K]	173(2)	173(2)	173(2)	173(2)	173(2)
M_r [g mol^{-1}]	6851.59	6853.80	6625.10	10377.09	10006.11
Crystal system	Triclinic	Orthorhombic	Monoclinic	Triclinic	Triclinic
Space group	$P\bar{1}$	*P*bca	*C*2/c	$P\bar{1}$	$P\bar{1}$
a [Å]	13.0794(4)	23.0635(18)	57.054(8)	12.819(3)	12.7431(17)
b [Å]	19.8716(6)	26.1690(19)	13.2708(18)	22.511(6)	25.174(3)
c [Å]	21.3258(6)	38.199(3)	36.998(5)	25.188(6)	26.124(4)
α [°]	76.506(2)	90	90	100.326(4)	106.744(2)
β [°]	84.428(2)	90	127.936(2)	97.652(4)	103.886(2)
γ [°]	82.631(2)	90	90	92.667(4)	100.912(2)
V [Å^3]	5332.3(3)	23055(3)	22094(5)	7068(3)	7483.4(17)
Z	2	8	8	2	2
ρ_{calcd} [g cm^{-3}]	4.224	3.715	3.863	4.753	4.281
μ [mm^{-1}]	27.349	25.062	24.213	30.669	27.364
Reflection collected	179537	111668	105508	119590	125138
Independent reflections (R_{int})	24038 (0.0761)	21084 (0.2267)	26339 (0.0594)	33843 (0.1886)	35575 (0.1146)
Goodness-of-fit	1.064	1.025	1.011	1.002	1.022
R_1 [I>2σ(I)]	0.0416	0.1086	0.0438	0.0729	0.0686
wR_2	0.1045	0.2668	0.1117	0.1355	0.1603
R_1 (all data)	0.0578	0.2098	0.0572	0.1750	0.1295
wR_2	0.1165	0.3060	0.1194	0.1721	0.1955
Largest diff. peak and hole [e Å^3]	6.237, -4.372	3.608, -4.796	5.587, -1.939	4.337, 3.794	8.122, -9.123

$R_1 = \Sigma\ ||F_0|-|F_c||/\Sigma|F_0|$; $wR_2 = \{\Sigma[w(F_0^2-F_c^2)^2/\Sigma w(F_0^2)^2]\}^{1/2}$

3.3.2 Electrochemistry

All CV diagrams are reproducible from run to run except the first cycle. As shown in Figure 3-6, in the negative potential region **3.1** shows two separated reversible peaks with $E_{1/2}$ at -0.64 and -0.84 V respectively. These voltammetric patterns, similar to those of [α-$PW_{11}O_{39}$]$^{7-}$ derivatives, i.e. [$M(PW_{11}O_{39})_2$]$^{11-}$ (M = lanthanide and actinide elements), can be assigned to W(VI/V) reduction.[96,105] The anodic peak currents, $i_{p,a}$, are proportional to the square root of the scan rate, $v^{1/2}$ (R^2 = 0.996), indicating that the redox processes of **3.1** are diffusion-controlled. As seen in Figure 3-6, **3.2** in the positive potential region shows a quasi-reversible (E_{pc} = 0.71 and E_{pa} = 0.82 V) peak assigned to the oxidation of Mn centers. In the negative region, reduction of W centers follows a similar pattern as in **3.1**, however the waves are poorly separated and can be better resolved at slower scan rate. Furthermore, two reversible peaks which appear with $E_{1/2}$ at ~ 0 and -0.28 V respectively, can be also assigned to oxidation of Mn centers in the [$Mn(CO)_3$]$^+$ fragments. These peaks are seen in other POM-supported [$Mn(CO)_3$]$^+$ structures as well.[51] The redox processes are diffusion controlled but with a lower linear dependence between $i_{p,a}$ and $v^{1/2}$ (R^2 = 0.966), which is likely due to hydrolytic instability of [$Mn(CO)_3$]$^+$ fragments. In **3.4**, similar to [$M(P_2W_{17}O_{61})_2$]$^{16-/17-}$ (M = lanthanide and actinide elements),[100,101] the CV consists of three cathodic peaks at -0.37, -0.59 and -0.92 V, and three anodic peaks at -0.31, -0.51 and -0.81 V, respectively. These correspond to three steps of redox processes involving the W(VI/V) centers. Similar to **3.2**, **3.4** shows one quasi-reversible (E_{pc} = 0.71 and E_{pa} = 0.82 V) and two reversible peaks ($E_{1/2}$ = 0.02 and -0.17 V), which can be attributed to the redox processes in Mn centers. As with the

earlier compounds, $i_{p,a}$ is proportional to $v^{1/2}$ (R^2 = 0.999), indicating that the redox processes of **3.4** are also diffusion-controlled.

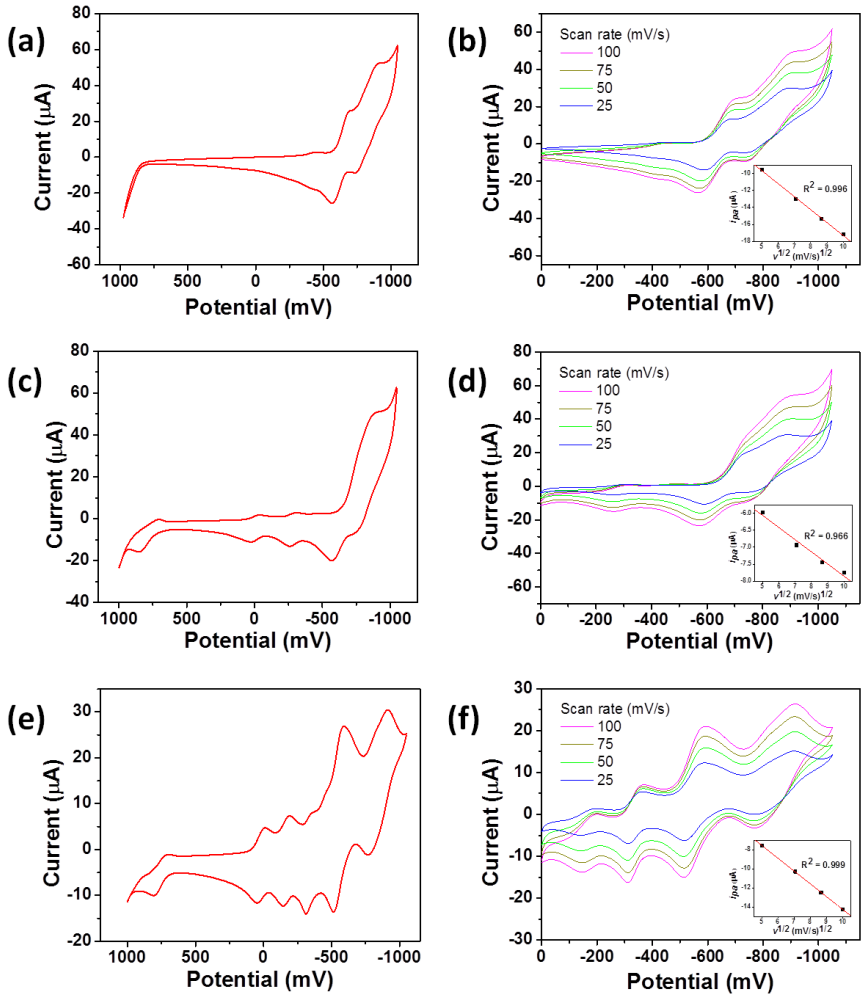

Figure 3-6 Cyclic voltammograms of (a) **3.1**, (c) **3.2** and (e) **3.4** at scan rate of 100 mV s^{-1} and in the range of +1.1 to -1.1 V. Also shown the cyclic voltammograms of (b) **3.1**, (d) **3.2** and (f) **3.4** at scan rates of 25, 50, 75 and 100 mV s^{-1} in the range of 0 to -1.1 V. The insets illustrate the correlation between the selected anodic peak currents and the root-square of scan rates.

3.4 Conclusions

In this section, we thoroughly investigated the coordination chemistry between metal tricarbonyl precursors and mono-lacunary Keggin/Dawson POMs, $[\alpha\text{-}PW_{11}O_{39}]^{7-}$ and $[\alpha_2$-

$P_2W_{17}O_{61}]^{10-}$, and successfully isolated three PSMCs with comprehensive structural and spectroscopic characterization. We also briefly reviewed all PSMCs published up to date. This study shows that our work contains a more convenient synthetic methodology and a novel POM scaffold, named "twisted-sandwich" in PSMCs. These new PSMCs are chiral in each single polyanion, but the crystals are racemic. Given the potentially catalytic properties of PSMCs, it would be very interesting if the enantiopure crystallites can be isolated. The genuine PSMC enantiomers would be valued in POM-based chiral catalysts.

References

(1) Gouzerh, P.; Proust, A. *Chem. Rev.* 1998, *98*, 77.

(2) Proust, A.; Thouvenot, R.; Gouzerh, P. *Chem. Commun.* 2008, 1837.

(3) Proust, A.; Matt, B.; Villanneau, R.; Guillemot, G.; Gouzerh, P.; Izzet, G. *Chem. Soc. Rev.* 2012, *41*, 7605.

(4) Knoth, W. H. *J. Am. Chem. Soc.* 1979, *101*, 759.

(5) Knoth, W. H. *J. Am. Chem. Soc.* 1979, *101*, 2211.

(6) Zonnevijlle, F.; Pope, M. T. *J. Am. Chem. Soc.* 1979, *101*, 2731.

(7) Besecker, C. J.; Day, V. W.; Klemperer, W. G.; Thompson, M. R. *J. Am. Chem. Soc.* 1984, *106*, 4125.

(8) Knoth, W. H.; Domaille, P. J.; Farlee, R. D. *Organometallics* 1985, *4*, 62.

(9) Chorghade, G. S.; Pope, M. T. *J. Am. Chem. Soc.* 1987, *109*, 5134.

(10) Weeks, M. S.; Hill, C. L.; Schinazi, R. F. *J. Med. Chem.* 1992, *35*, 1216.

(11) Randall, W. J.; Weakley, T. J. R.; Finke, R. G. *Inorg. Chem.* 1993, *32*, 1068.

(12) Xin, F.; Pope, M. T. *Organometallics* 1994, *13*, 4881.

(13) Xin, F.; Pope, M. T.; Long, G. J.; Russo, U. *Inorg. Chem.* 1996, *35*, 1207.

(14) Xin, F.; Pope, M. T. *Inorg. Chem.* 1996, *35*, 5693.

(15) Sazani, G.; Dickman, M. H.; Pope, M. T. *Inorg. Chem.* 2000, *39*, 939.

(16) Artero, V.; Proust, A.; Herson, P.; Villain, F.; Moulin, C. C. d.; Gouzerh, P. *J. Am. Chem. Soc.* 2003, *125*, 11156.

(17) Bareyt, S.; Piligkos, S.; Hasenknopf, B.; Gouzerh, P.; Lacôte, E.; Thorimbert, S.; Malacria, M. *J. Am. Chem. Soc.* 2005, *127*, 6788.

(18) Kortz, U.; Hussain, F.; Reicke, M. *Angew. Chem. Int. Ed.* 2005, *44*, 3773.

(19) Mal, S. S.; Nsouli, N. H.; Dickman, M. H.; Kortz, U. *Dalton Trans.* 2007, 2627.

(20) Besson, C.; Musaev, D. G.; Lahootun, V.; Cao, R.; Chamoreau, L.-M.; Villanneau, R.; Villain, F.; Thouvenot, R.; Geletii, Y. V.; Hill, C. L.; Proust, A. *Chem. Eur. J.* 2009, *15*, 10233.

(21) Sazani, G.; Dickman, M. H.; Pope, M. T. *Inorg. Chem.* 2000, *39*, 939.

(22) Bi, L.-H.; Chubarova, E. V.; Nsouli, N. H.; Dickman, M. H.; Kortz, U.; Keita, B.; Nadjo, L. *Inorg. Chem.* 2006, *45*, 8575.

(23) Bi, L.-H.; Hou, G.-F.; Li, B.; Wu, L.-X.; Kortz, U. *Dalton Trans.* 2009, 6345.

(24) Joo, N.; Renaudineau, S.; Delapierre, G.; Bidan, G.; Chamoreau, L.-M.; Thouvenot, R.; Gouzerh, P.; Proust, A. *Chem. Eur. J.* 2010, *16*, 5043.

(25) Gates, B. C. *Chem. Rev.* 1995, *95*, 511.

(26) Fierro-Gonzalez, J. C.; Kuba, S.; Hao, Y. L.; Gates, B. C. *J. Phys. Chem. B* 2006, *110*, 13326.

(27) Kulkarni, A.; Lobo-Lapidus, R. J.; Gates, B. C. *Chem. Commun.* 2010, *46*, 5997.

(28) Brevard, C.; Schimpf, R.; Tournié, G.; Tournié, C. M. *J. Am. Chem. Soc.* 1983, *105*, 7059.

(29) Randall, W. J.; Droege, M. W.; Mizuno, N.; Nomiya, K.; Weakley, T. J. R.; Finke, R. G. In *Inorg. Synth.*; Cowley, A. H., Ed.; John Wiley & Sons, Inc.: New York, 1997; Vol. 31, p 167.

(30) Edwards, D. A.; Marshalsea, J. *J. Organomet. Chem.* 1977, *131*, 73.

(31) Bruker AXS, I.; Analytical X-ray Sysems: Madison, WI, 2003.

(32) Bruker AXS, I.; Analytical X-ray Systems: Madison, WI, 2003.

(33) Sheldrick, G. In *SADABS*; ver. 2.10 ed. 2003.

(34) Bruker AXS, I. Madison, WI, 2003.

(35) Sheldrick, G. M. *Acta Crystallogr., Sect. A* 1990, *46*, 467.

(36) Knoth, W. H.; Domaille, P. J. *Inorg. Chem.* 1983, *22*, 818.

(37) Besecker, C. J.; Klemperer, W. G. *J. Am. Chem. Soc.* 1980, *25*, 7598.

(38) Besecker, C. J.; Day, V. W.; Klemperer, W. G.; Thompson, M. R. *Inorg. Chem.* 1985, *24*, 44.

(39) Klemperer, W. G.; Main, D. J. *Inorg. Chem.* 1990, *29*, 2355.

(40) Day, V. W.; Fredrich, M. F.; Thompson, M. R.; Klemperer, W. G.; Liu, R. S.; Shum, W. *J. Am. Chem. Soc.* 1981, *103*, 3597.

(41) Klemperer, W. G.; Zhong, B. X. *Inorg. Chem.* 1993, *32*, 5821.

(42) Siedle, A. R.; Lyon, P. A.; Hodgson, K. O.; Roe, A. L. *Inorg. Chem.* 1987, *26*, 219.

(43) Nagata, T.; Pohl, B. M.; Weiner, H.; Finke, R. G. *Inorg. Chem.* 1997, *36*, 1366.

(44) Besserguenev, A. V.; Dickman, M. H.; Pope, M. T. *Inorg. Chem.* 2001, *40*, 2582.

(45) Villanneau, R.; Delmont, R.; Proust, A.; Gouzerh, P. *Chem. Eur. J.* 2000, *6*, 1184.

(46) Villanneau, R.; Proust, A.; Robert, F.; Gouzerh, P. *Chem. Eur. J.* 2003, *9*, 1982.

(47) Sadakane, M.; Iimuro, Y.; Tsukuma, D.; Bassil, B. S.; Dickman, M. H.; Kortz, U.; Zhang, Y.; Ye, S.; Ueda, W. *Dalton Trans.* 2008, 6692.

(48) Zhao, C.; Huang, Z.; Rodr ǵuez-Córdoba, W.; Kambara, C. S.; O'Halloran, K. P.; Hardcastle, K. I.; Musaev, D. G.; Lian, T.; Hill, C. L. *J. Am. Chem. Soc.* 2011, *133*, 20134.

(49) Niu, J.; Yang, L.; Zhao, J.; Ma, P.; Wang, J. *Dalton Trans.* 2011, *40*, 8298.

(50) Zhao, J.; Zhao, J.; Ma, P.; Wang, J.; Niu, J.; Wang, J. *J. Mol. Struct.* 2012, *1019*, 61.

(51) Zhao, J.; Wang, J.; Zhao, J.; Ma, P.; Wang, J.; Niu, J. *Dalton Trans.* 2012, *41*, 5832.

(52) Zhao, C.; Kambara, C. S.; Yang, Y.; Kaledin, A. L.; Musaev, D. G.; Lian, T.; Hill, C. L. *Inorg. Chem.* 2013, *52*, 671.

(53) Zhang, D.; Zhao, J.; Zhang, Y.; Hu, X.; Li, L.; Ma, P.; Wang, J.; Niu, J. *Dalton Trans.* 2013, *42*, 2696.

(54) Bosing, M.; Loose, I.; Pohlmann, H.; Krebs, B. *Chem. Eur. J.* 1997, *3*, 1232.

(55) Loose, I.; Droste, E.; Boesing, M.; Pohlmann, H.; Dickman, M. H.; Rosu, C.; Pope, M. T.; Krebs, B. *Inorg. Chem.* 1999, *38*, 2688.

(56) Piepenbrink, M.; Limanski, E. M.; Krebs, B. *Z. Anorg. Allg. Chem.* 2002, *628*, 1187.

(57) Laurencin, D.; Villanneau, R.; Herson, P.; Thouvenot, R.; Jeannin, Y.; Proust, A. *Chem. Commun.* 2005, *0*, 5524.

(58) Bi, L.-H.; Li, B.; Bi, S.; Wu, L.-X. *J. Solid State Chem.* 2009, *182*, 1401.

(59) Bi, L.-H.; Al-Kadamany, G.; Chubarova, E. V.; Dickman, M. H.; Chen, L.; Gopala, D. S.; Richards, R. M.; Keita, B.; Nadjo, L.; Jaensch, H.; Mathys, G.; Kortz, U. *Inorg. Chem.* 2009, *48*, 10068.

(60) Tourné, C. M.; Tourné, G. F.; Weakley, T. J. R. *J. Chem. Soc., Dalton Trans.* 1986, 2237.

(61) Tourné, C. M.; Tourné, G. F. *J. Chem. Soc., Dalton Trans.* 1988, 2411.

(62) Contant, R. *Can. J. Chem.* 1987, *65*, 568.

(63) Cao, R.; O'Halloran, K. P.; Hillesheim, D. A.; Hardcastle, K. I.; Hill, C. L. *CrystEngComm* 2010, *12*, 1518.

(64) Cao, R.; O'Halloran, K. P.; Hillesheim, D. A.; Lense, S.; Hardcastle, K. I.; Hill, C. L. *CrystEngComm* 2011, *13*, 738.

(65) Finke, R. G.; Droege, M.; Hutchinson, J. R.; Gansow, O. *J. Am. Chem. Soc.* 1981, *103*, 1587.

(66) Gómez-García, C. J.; Coronado, E.; Borrasalmenar, J. J. *Inorg. Chem.* 1992, *31*, 1667.

(67) Zhang, X.; Chen, Q.; Duncan, D. C.; Lachicotte, R. J.; Hill, C. L. *Inorg. Chem.* 1997, *36*, 4381.

(68) Clemente-Juan, J. M.; Coronado, E.; Galán-Mascarós, J., J. R. ; Gómez-García, C. J. *Inorg. Chem.* 1999, *38*, 55.

(69) Kim, K. C.; Pope, M. T. *J. Am. Chem. Soc.* 1999, *121*, 8512.

(70) Nomiya, K.; Takahashi, M.; Ohsawa, K.; Widegren, J. A. *J. Chem. Soc., Dalton Trans.* 2001, 2872.

(71) Kortz, U.; Mbomekalle, I. M.; Keita, B.; Nadjo, L.; Berthet, P. *Inorg. Chem.* 2002, *41*, 6412.

(72) Okun, N. M.; Anderson, T. M.; Hill, C. L. *J. Am. Chem. Soc.* 2003, *125*, 3194.

(73) Long, D.-L.; Tsunashima, R.; Cronin, L. *Angew. Chem. Int. Ed.* 2010, *49*, 1736.

(74) Yin, Q.; Tan, J. M.; Besson, C.; Geletii, Y. V.; Musaev, D. G.; Kuznetsov, A. E.; Luo, Z.; Hardcastle, K. I.; Hill, C. L. *Science* 2010, *328*, 342.

(75) Lv, H.; Geletii, Y. V.; Zhao, C.; Vickers, J. W.; Zhu, G.; Luo, Z.; Song, J.; Lian, T.; Musaev, D. G.; Hill, C. L. *Chem. Soc. Rev.* 2012, *41*, 7572.

(76) Zhu, G.; Geletii, Y. V.; Kögerler, P.; Schilder, H.; Song, J.; Lense, S.; Zhao, C.; Hardcastle, K. I.; Musaev, D. G.; Hill, C. L. *Dalton Trans.* 2012, *41*, 2084.

(77) Cao, R.; Ma, H.; Geletii, Y. V.; Hardcastle, K. I.; Hill, C. L. *Inorg. Chem.* 2009, *48*, 5596.

(78) Bajpe, S. R.; Breynaert, E.; Robeyns, K.; Houthoofd, K.; Absillis, G.; Mustafa, D.; Parac-Vogt, T. N.; Maes, A.; Martens, J. A.; Kirschhock, C. E. A. *Eur. J. Inorg. Chem.* 2012, 3852.

(79) Cavani, F.; Comuzzi, C.; Dolcetti, G.; Etienne, E.; Finke, R.; Selleri, G.; Trifiro, F.; Trovarelli, A. *J. Catal.* 1996, *160*, 317.

(80) Szczepankiewicz, S. H.; Ippolito, C. M.; Santora, B. P.; Ven, T. J. V. d.; Ippolito, G. A.; Fronckowiak, L.; Wiatrowski, F.; Power, T.; Kozik, M. *Inorg. Chem.* 1998, *37*, 4344.

(81) Keita, B.; Girard, F.; Nadjo, L.; Contant, R.; Canny, J.; Richet, M. *J. Electroanal. Chem.* 1999, *478*, 76.

(82) Keita, B.; Lu, Y. W.; Nadjo, L.; Contant, R. *Eur. J. Inorg. Chem.* 2000, *2000*, 2463.

(83) Kharat, A. N.; Pendleton, P.; Badalyan, A.; Abedini, M.; Amini, M. M. *J. Mol. Catal. A: Chem.* 2001, *175*, 277.

(84) Nomiya, K.; Torii, H.; Nomura, K.; Sato, Y. *J. Chem. Soc., Dalton Trans.* 2001, 1506.

(85) Mialane, P.; Dolbecq, A.; Rivière, E.; Marrot, J.; Sécheresse, F. *Angew. Chem. Int. Ed.* 2004, *43*, 2274.

(86) Zhang, C.; Howell, R. C.; Luo, Q.-H.; Fieselmann, H. L.; Todaro, L. J.; Francesconi, L. C. *Inorg. Chem.* 2005, *44*, 3569.

(87) Khenkin, A. M.; Kumar, D.; Shaik, S.; Neumann, R. *J. Am. Chem. Soc.* 2006, *128*, 15451.

(88) Luo, Q.-H.; Howell, R. C.; Dankova, M.; Bartis, J.; Williams, C. W.; William DeW. Horrocks, J.; Victor G. Young, J.; Rheingold, A. L.; Francesconi, L. C.; Antonio, M. R. *Inorg. Chem.* 2001, *40*, 1894.

(89) Sadakane, M.; Ostuni, A.; Pope, M. T. *J. Chem. Soc., Dalton Trans.* 2002, 63.

(90) Zhang, C.; Howell, R. C.; Scotland, K. B.; Perez, F. G.; Todaro, L.; Francesconi, L. C. *Inorg. Chem.* 2004, *43*, 7691.

(91) Kato, C. N.; Shinohara, A.; Hayashi, K.; Nomiya, K. *Inorg. Chem.* 2006, *45*, 8108.

(92) Kato, C. N.; Hara, K.; Hatano, A.; Goto, K.; Kuribayashi, T.; Hayashi, K.; Shinohara, A.; Kataoka, Y.; Mori, W.; Nomiya, K. *Eur. J. Inorg. Chem.* 2008, 3134.

(93) Kato, C. N.; Hayashi, K.; Negishi, S.; Nomiya, K. *J. Mol. Catal. A: Chem. Special Issue* 2007, *262*, 25.

(94) Kholdeeva, O. A.; Maksimov, G. M.; Maksimovskaya, R. I.; Vanina, M. P.; Trubitsina, T. A.; Naumov, D. Y.; Kolesov, B. A.; Antonova, N. S.; Carbó, J. J.; Poblet, J. M. *Inorg. Chem.* 2006, *45*, 7224.

(95) Chen, S.-W.; Villanneau, R.; Li, Y.; Chamoreau, L.-M.; Boubekeur, K.; Thouvenot, R.; Gouzerh, P.; Proust, A. *Eur. J. Inorg. Chem.* 2008, *2008*, 2137.

(96) Haraguchi, N.; Okaue, Y.; Isobe, T.; Matsuda, Y. *Inorg. Chem.* 1994, *33*, 1015.

(97) Sadakane, M.; Dickman, M. H.; Pope, M. T. *Inorg. Chem.* 2001, *40*, 2715.

(98) Luo, Q.; Howell, R. C.; Bartis, J.; Dankova, M.; DeW. Horrocks, J., William; Rheingold, A. L.; Francesconi, L. C. *Inorg. Chem.* 2002, *41*, 6112.

(99) Chiang, M.-H.; Williams, C. W.; Soderholm, L.; Antonio, M. R. *Eur. J. Inorg. Chem.* 2003, *2003*, 2663.

(100) Chiang, M.-H.; Soderholm, L.; Antonio, M. R. *Eur. J. Inorg. Chem.* 2003, *2003*, 2929.

(101) Gao, G.; Xu, L.; Wang, W.; An, W.; Qiu, Y. *J. Mater. Chem.* 2004, *14*, 2024.

(102) Zhang, C.; Bensaid, L.; McGregor, D.; Fang, X.; Howell, R. C.; Burton-Pye, B.; Luo, Q.; Todaro, L.; Francesconi, L. C. *J. Cluster Sci.* 2006, *17*, 389.

(103) Hou, Y.; Fang, X.; Hill, C. L. *Chem. Eur. J.* 2007, *13*, 9442.

(104) Fan, L.; Xu, L.; Gao, G.; Li, F.; Li, Z.; Qiu, Y. *Inorg. Chem. Commun.* 2006, *9*, 1308.

(105) Fan, L.-H.; Xu, L.; Zhang, C.-H.; Li, F.-Y.; Li, Z.-K.; Liu, X.-Z. *Struct. Chem.* 2007, *18*, 917.

(106) Rong, C.; Pope, M. T. *J. Am. Chem. Soc.* 1992, *114*, 2932.

(107) Bagno, A.; Bonchio, M.; Sartorel, A.; Scorrano, G. *Eur. J. Inorg. Chem.* 2000, *2000*, 17.

(108) Bi, L.-H.; Kortz, U.; Keita, B.; Nadjo, L. *Dalton Trans.* 2004, 3184.

(109) Artero, V.; Laurencin, D.; Villanneau, R.; Thouvenot, R.; Herson, P.; Gouzerh, P.; Proust, A. *Inorg. Chem.* 2005, *44*, 2826.

(110) Belai, N.; Pope, M. T. *Polyhedron* 2006, *25*, 2015.

(111) Dablemont, C.; Hamaker, C. G.; Thouvenot, R.; Sojka, Z.; Che, M.; Maatta, E. A.; Proust, A. *Chem. Eur. J.* 2006, *12*, 9150.

(112) Laurencin, D.; Villanneau, R.; Gérard, H.; Proust, A. *J. Phys. Chem. A* 2006, *110*, 6345.

(113) Kato, C. N.; Kasahara, Y.; Hayashi, K.; Yamaguchi, A.; Hasegawa, T.; Nomiya, K. *Eur. J. Chem.* 2006, 4834.

(114) Kato, C. N.; Shinohara, A.; Moriya, N.; Nomiya, K. *Catal. Commun.* 2006, *7*, 413.

(115) Sakai, Y.; Shinohara, A.; Hayashi, K.; Nomiya, K. *Eur. J. Inorg. Chem.* 2006, *2006*, 163.

(116) Nomiya, K.; Hayashi, K.; Kasahara, Y.; Iida, T.; Nagaoka, Y.; Yamamoto, H.; Ueno, T.; Sakai, Y. *Bull. Chem. Soc. Jpn.* 2007, *80*, 724.

(117) Lahootun, V.; Besson, C.; Villanneau, R.; Villain, F.; Chamoreau, L.-M.; Boubekeur, K.; Blanchard, S.; Thouvenot, R.; Proust, A. *J. Am. Chem. Soc.* 2007, *129*, 7127.

(118) Micoine, K.; Hasenknopf, B.; Thorimbert, S.; Lacôte, E.; Malacria, M. *Org. Lett.* 2007, *9*, 3981.

(119) Hasegawa, T.; Murakami, H.; Shimizu, K.; Kasahara, Y.; Yoshida, S.; Kurashina, T.; Seki, H.; Nomiya, K. *Inorg. Chim. Acta* 2008, *361*, 1385.

(120) Liu, H.; Gómez-García, C. J.; Peng, J.; Sha, J.; Lia, Y.; Yana, Y. *Dalton Trans.* 2008, 6211.

(121) Besson, C.; Geletii, Y. V.; Villain, F.; Villanneau, R.; Hill, C. L.; Proust, A. *Inorg. Chem.* 2009, *48*, 9436.

(122) Liu, H.-S.; Peng, J.; Wang, L.-X. *Z. Anorg. Allg. Chem.* 2009, *635*, 2688.

(123) Sadakane, M.; Rinn, N.; Moroi, S.; Kitatomi, H.; Ozeki, T.; Kurasawa, M.; Itakura, M.; Hayakawa, S.; Kato, K.; Miyamoto, M.; Ogo, S.; Ide, Y.; Sano, T. *Z. Anorg. Allg. Chem.* 2011, *637*, 1467.

(124) Sadakane, M.; Tsukuma, D.; Dickman, M. H.; Bassil, B.; Kortz, U.; Higashijima, M.; Ueda, W. *Dalton Trans.* 2006, *0*, 4271.

(125) Nomiya, K.; Togashi, Y.; Kasahara, Y.; Aoki, S.; Seki, H.; Noguchi, M.; Yoshida, S. *Inorg. Chem.* 2011, *50*, 9606.

(126) Quiñonero, D.; Wang, Y.; Morokuma, K.; Khavrutskii, L. A.; Botar, B.; Geletii, Y. V.; Hill, C. L.; Musaev, D. G. *J. Phys. Chem.* 2006, *110*, 170.

(127) Quiñonero, D.; Morokuma, K.; Geletii, Y. V.; Hill, C. L.; Musaev, D. G. *J. Mol. Catal. A: Chem.* 2007, *262*, 227.

(128) Hasenknopf, B.; Micoine, K.; Lacôte, E.; Thorimbert, S.; Malacria, M.; Thouvenot, R. *Eur. J. Inorg. Chem.* 2008, 5001.

(129) Du, D.-Y.; Yan, L.-K.; Su, Z.-M.; Li, S.-L.; Lan, Y.-Q.; Wang, E.-B. *Coord. Chem. Rev.* 2013, *257*, 702.

(130) Zhang, J.; Hao, J.; Wei, Y.; Xiao, F.; Yin, P.; Wang, L. *J. Am. Chem. Soc.* 2009, *132*, 14.

Chapter 4

Spectroscopic and Computational Studies of a Metal-to-Polyoxometalate Charge Transfer Molecular Chromophore

(Published partially in *J. Am. Chem. Soc.* **2011**, *133 (50)*, 20134–20137.)

With Zhuangqun Huang, William Rodríguez-Córdoba, Choon Sung Kambara, Kevin P. O'Halloran, Ken I. Hardcastle, Djamaladdin G. Musaev, Tianquan Lian and Craig L. Hill

4.1 Introduction

In **Chapter 1**, we introduce the general properties of POMs and the novel applications of POMs in artificial photosynthesis. In a typical photo-driven reaction, both WOCs and $[Ru(bpy)_3]Cl_2$, the photosensitizer, are required. The Ru^{II} oligopyridine complexes have been widely chosen as light-harvesting chromophores over decades, and their photochemical, photophysical and electrochemical properties were well-studied. Particularly, their high coefficient in the visible and long lifetime in the excited states make them act as ideal light-capture antenna. These complexes exhibit intense ligand-centered absorption bands in the UV region extended to metal-to-ligand charge-transfer (MLCT) in the visible region; they also show a relatively long-lived luminescence in the red spectral region, originating from the lowest ^{3}MLCT level. During a water-oxidation reaction, it should be noted that the oxidizing species is not the excited state of $[Ru(bpy)_3]^{2+}$ (denoted: $*[Ru(bpy)_2]^{2+}$) but actually is $[Ru(bpy)_3]^{3+}$. The latter, generated by quenching $*[Ru(bpy)_2]^{2+}$ with a sacrificial electron acceptor, shows a high potential ($[Ru(bpy)_3]^{3+}/[Ru(bpy)_3]^{2+}$ = + 1.26 V relative to NHE), which makes it strong enough for water oxidation.[1,2]

In addition to the Ru^{II} complexes, other chromophores such as porphyrins, organic polyphenylene and some host-guest systems were intensively studied. For example, $(bpy)Re(CO)_3Cl$ and its analogues have been widely used as chromophores and CO_2 reduction catalysts.[3-5] The ground-state and excited-state properties of these complexes during a CO_2 reduction cycle have been systematically characterized. However, all of these molecular chromophores contain the less-stable organic ligands. It would be very

interesting if we can replace the organic groups with water-compatible and stable POM ligands.

Recently, chromophores containing hetero-binuclear groups linked by an oxo bridge (M–O–M'; M = Zr^{IV}, Ti^{IV}; M' = Cu^{I}, Ce^{III}, Sn^{II}, etc.) and supported on mesoporous substrates have been shown to be promising in conjunction with photocatalytic solar fuel production.[6-18] These heterogeneous heterobinuclear units possess enhanced visible absorptivity and all-inorganic structures for oxidative stability. Their visible absorption properties originate from the photo-induced formation of long-lived metal-to-metal charge transfer (MMCT) excited states that can be effectively coupled with multi-electron-transfer catalysts.[19-23] In spite of the reported successes from these heterobinuclear chromophores, molecular/homogeneous counterparts are sought because their geometrical and electronic structures as well as their chemical properties (e.g. interfacing with catalysts) can be more extensively altered and all their properties can be studied and optimized more readily than for heterogeneous analogues. Inspired by the heterogeneous bimetallic assemblies on mesoporous silica and the well-known metal-to-(organic) ligand charge transfer (MLCT) complex, (bpy)$Re^{I}(CO)_3Cl$ (bpy = 2,2'–bipyridyl),[24-26] we have been seeking a new general type of charge transfer chromophore in which a polyoxometalate (POM) unit as a whole (delocalized orbitals involving many tungsten atoms) replaces the single metal center or bpy as the electron acceptor. POMs would be logical candidates for such an application because they are oxidatively, hydrolytically (over varying pH ranges) and thermally stable, can accommodate multiple metals with varying potentials, but they have not yet been systematically explored as tunable electron-accepting chromophores.[27,28]

In the previous sections, we report several POM-supported metal carbonyl complexes (PSMCs). They are examples of a potentially general transition that we will refer to as metal-to-POM charge transfer (MPCT). We chose one of these complexes here, $K_{15}Na[P_4W_{35}O_{124}\{Re(CO)_3\}_2]\cdot 37H_2O$ (**3.3**), for computational and multiple time-resolved spectroscopic studies.

4.2 Experimental

4.2.1. Synthesis

$[(C_4H_9)_4N]_{15}HP_4W_{35}O_{124}\{Re(CO)_3\}_2\cdot 0.3CH_2Cl_2$ (4.1). The organic-solvent-soluble tetrabutylammonium (TBA) salt of **3.3** was prepared by a modification of the procedure reported by Katsoulis and Pope.[29] Thus, an aqueous solution of **3.3** (0.01 mmol, 104 mg) in 10 ml H_2O was shaken with an equal volume of a solution of tetrabutylammonium bromide (0.2 mmol, 65 mg) in CH_2Cl_2. The red-colored organic layer in the bottom was separated and washed by H_2O (10 mL x 5 times). A small amount of liquid was directly taken from this organic layer for time-resolved spectroscopic studies. The organic layer was then dried in vacuo. Yield: 60 mg (50% based on P). Elemental analysis revealed a formula consistent with $[(C_4H_9)_4N]_{15}HP_4W_{35}O_{124}\{Re(CO)_3\}_2\cdot 0.3CH_2Cl_2$ (**4.1**). Anal. Calcd. For $C_{246.3}H_{541.6}N_{15}Cl_{0.6}O_{130}P_4Re_2W_{35}$: C, 23.2; H, 4.3; N, 1.6; Cl, 0.17. Found: C, 23.2; H, 4.4; N, 1.5; Cl, 0.18. (K, Na < 100 ppm; Br < 300 ppm). Molecular weight: 12746.6 g mol^{-1}). Electronic spectral data (300 - 800 nm, in CH_2Cl_2, 0.2 cm cell pathlength): $\lambda_{400} \sim 4500\ M^{-1}\cdot cm^{-1}$.

4.2.2. Transient Spectroscopic Studies

(a) Ultrafast Visible Transient Absorption Measurements. Our femtosecond transient absorption spectrometer is based on a regeneratively amplified Ti:sapphire laser system (coherent Legend, 800 nm, 150 fs, 3 mJ/pulse and 1 kHz repetition rate) and the Helios spectrometer (Ultrafast Systems LLC). The excitation pulse at 400 nm was generated by doubling the frequency of the fundamental 800 nm pulse in a β-barium borate (BBO) type I crystal. The energy of the 400 nm pump pulse was controlled to be ~250 nJ/pulse with a neutral density filter. The pump beam diameter at the sample was ~400 μm, corresponding to an excitation density of ~2 μJ/cm^2 per pulse. A white light continuum (WLC) (450~720 nm), used as a probe, was generated by attenuating and focusing 10 μJ of the fundamental 800 nm pulse into a sapphire window. This WLC was split in two parts used as a probe and reference beams. The probe beam was focused with an aluminum parabolic reflector into the sample with a beam diameter of ~150 μm. The reference and probe beams were focused into a fiber-coupled multichannel spectrometer with CMOS sensors and detected at a frequency of 1 kHz. To minimize low-frequency laser fluctuations every other pump pulse was blocked with a synchronized chopper (New Focus Model 3501) at 500 Hz, and the absorbance change was calculated with two adjacent probe pulses (pump-blocked and pump-unblocked). The delay between the pump and probe pulses was controlled by a motorized translational stage. Samples were kept in a 1 mm quartz cuvette (NSG Precision Cells) and constantly stirred by a magnetically-coupled stirring system (SYS 114, SPECTROCELL). In all transient absorption spectra, the chirp and time zero correction were performed with Surface Explorer software (v.1.1.5, Ultrafast Systems LCC) using a dispersion correction curve

obtained by fitting the representative kinetics of the transient absorption experiments of the solvent. The typical instrument response of our spectrometer is well represented by a Gaussian function with a full width at half-maximum (FWHM) of 180 ± 10 fs.

(b) Ultrafast Visible Pump/IR Probe and IR Pump/IR Probe Transient Absorption Measurements. Our tunable femtosecond infrared spectrometer is based on a Clark IR optical parametric amplifier (OPA) which generates two tunable near-IR pulses in the 1.1 to 2.5 μm spectral range (signal and idler, respectively). The broad mid-IR pulses centered at 2000, 1900 and 1870 cm^{-1} were generated by difference frequency generation (DFG) combining the corresponding signal and idler in a 1-mm-thick type II $AgGaS_2$ crystal. The frequency tuning of the mid-IR pulses was achieved by changing the signal and idler frequencies at the OPA and optimizing the timing between the pulses and the phase matching angles of the BBO (OPA crystal) and the $AgGaS_2$ crystal. After the difference frequency generation, the mid-IR pulse was collimated and split in two parts with a 90% beamsplitter. The 90% reflected part was used as a pump in the IR Pump-IR Probe experiments, while the 10% transmitted part was used as a probe in both the Visible-IR and IR-IR transient absorption measurements**.** To prevent cumulative heating in the sample and to avoid the saturation of the detector, the intensity of the probe mid-IR pulse was attenuated using neutral density filters to approximately 40 μJ, before it was focused into a 0.4 μm CaF_2 path-length cell containing the sample. At the focal point, the probe was spatially overlapped with the temporally delayed 400 nm or mid-IR excitation pulse with pump energy of about 2 or 0.7 μJ/pulse, respectively. To avoid rotational diffusion effects, the polarization angle of the excitation beams were controlled with a

half-wave plate and set to the magic angle (54.7°) relative to the probe beam. The diameter of the pump and probe beams were 400 and 200 μm, respectively.

In both experimental setups, the mid-infrared probe pulse was spectrally dispersed with an imaging spectrograph (CVI, Digikrom 240) and imaged onto a 32-element infrared HgCdTe (MCT) array detector. The difference absorption spectra were calculated by subtracting the absorption spectrum of the excited sample from the absorption spectrum of the sample in the ground state by blocking every other pump pulse with a phase-locked optical chopper (New Focus) at 500 Hz. The instrument response function of our spectrometer was well represented by a Gaussian function with a 230 ± 10 and 270 ± 10 fs full width at half-maximum (FWHM) for the VIS-IR and the IR-IR setup, respectively.

4.3 Results and Discussion

4.3.1. Steady-state Specstrocopy

In contrast to its colorless components, $K_{10}[\alpha_2\text{-}P_2W_{17}O_{61}]\cdot 20H_2O$ and $Re(CO)_3(CH_3CN)_3(BF_4)$, solid **3.3** is dark red in color. The UV-vis spectrum of **4.1** in CH_2Cl_2 (Figure 4-1) and **3.3** in H_2O (Figure 4-2) shows intense broad absorption (up to 700 nm) covering the entire UV and visible regions. The synthetic precursor, $[\alpha_2\text{-}P_2W_{17}O_{61}]^{10-}$, has O*2p* → W*5d* transitions that absorb only below 300 nm and the ligand-to-metal-charge-transfer band in the $[Re(CO)_3(CH_3CN)_3]^+$ precursor absorbs only below 380 nm (Figure 4-2). In addition, **4.1** has unexpectedly high visible absorptivity (ε_{400nm} ~ 4,500 $M^{-1}\cdot cm^{-1}$ in CH_2Cl_2). Importantly, the wide spectral range and the high extinction coefficients of **4.1** are comparable to those of many ruthenium polybipyridyl

photosensitzers,[30,31] but **4.1** is free of the oxidatively and hydrolytically unstable polypyridyl ligands.

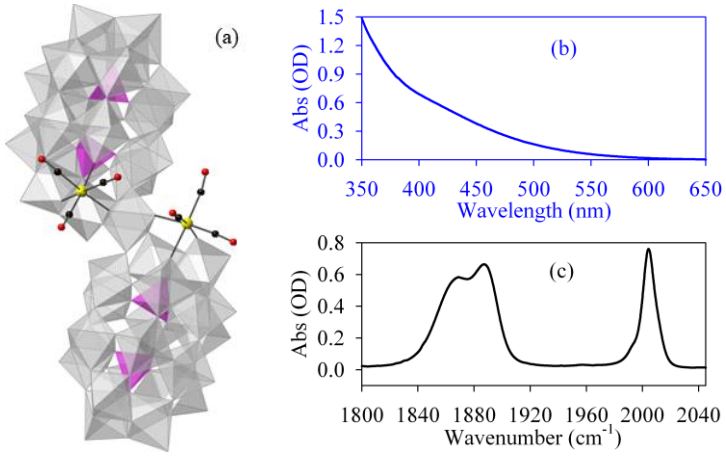

Figure 4-1 (a) X-ray structure of $[P_4W_{35}O_{124}\{Re(CO)_3\}_2]^{16-}$ (**4.1**) in combined polyhedral and ball-and-stick notation. Re: yellow; O: red; C: black; WO_6 octahedra: gray; PO_4 tetrahedra: purple. (b) UV–Vis and (c) FTIR spectra of **4.1** in CH_2Cl_2.

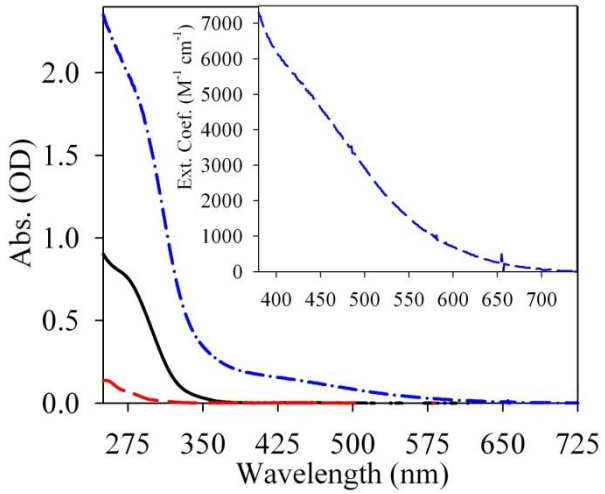

Figure 4-2 UV-Vis absorption spectra of $K_{10}[\alpha_2\text{-}P_2W_{17}O_{61}]\cdot 20H_2O$ (black line), $Re(CO)_3(CH_3CN)_3(BF_4)$ (red dashed) and **3.3** (blue dash-dot) in H_2O. The inset shows the extinction coefficients of **3.3** in H_2O.

4.3.2. Computational Studies

All calculations were performed using the Gaussian_09 quantum chemical program package.[32] The geometries of all species under investigation were optimized without symmetry constraints at the B3LYP level of theory[33-35] in conjunction with lanl2dz basis sets and the corresponding Hay-Wadt effective core potentials (ECPs) for Re-centers and 6-31G(d) split-valence basis sets for other atoms.[36-38]

Complex $[P_4W_{35}O_{124}\{Re(CO)_3\}_2]^{16-}$ (**4.1**) is a dimer of $[P_2W_{17}O_{57}\{Re(CO)_3\}]^{8-}$ (**1_mono**) which linked by WO_6-unit. It is too large to be studied computationally with reasonable accuracy. Therefore, for our computational studies, we used the model **M1** that includes **1_mono** and the associated WO_6-linkage (Figure 4-3). Based on the available experimental data (geometry) for **4.1** we model the associated WO_6-linkage in **M1** as $(H_2O)(OH)WO_4$. In fact, as seen in Figure 4-4, the B3LYP/lanl2dz approach used throughout this paper in conjunction with model **M1** describes the important geometry parameters of **4.1** with reasonable accuracy.

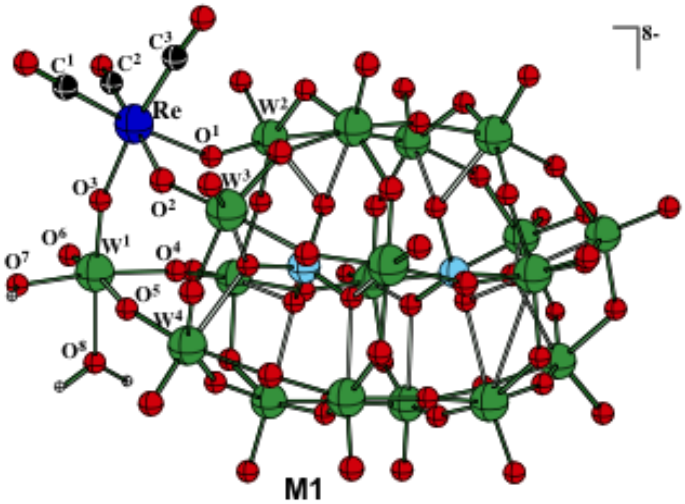

Figure 4-3 Model systems **M1** used in the presented computational studies

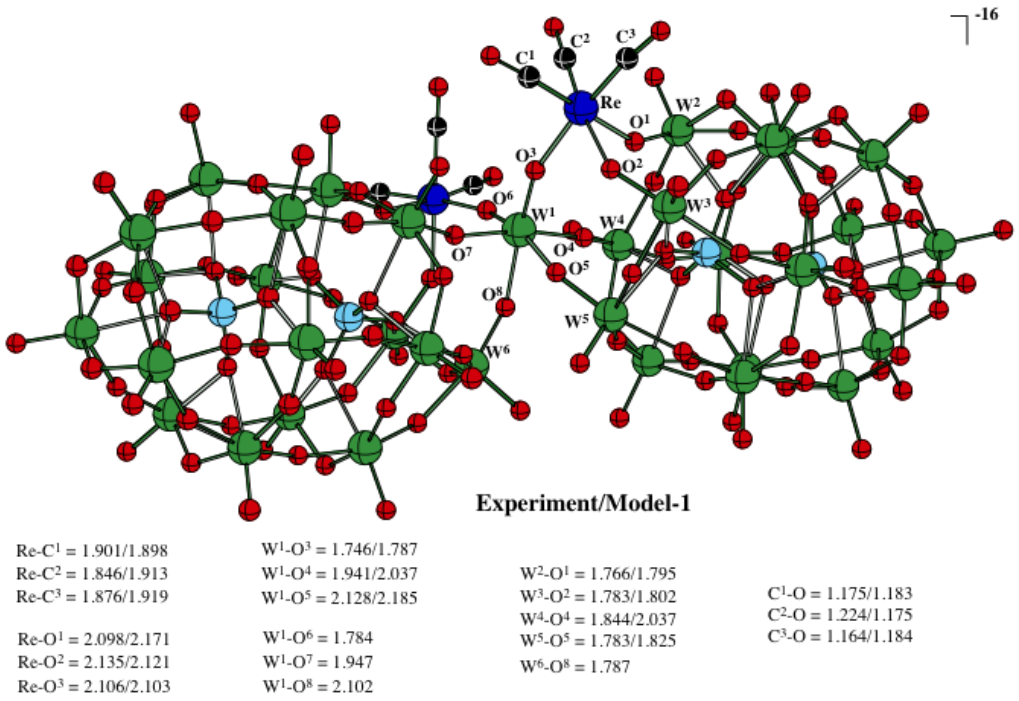

Figure 4-4 The calculated (using model **M1**) and experimental bond distances (in Å) of $[P_4W_{35}O_{124}\{Re(CO)_3\}_2]^{16-}$ (**4.1**).

We have investigated the origin of high visible absorptivity of **4.1** by computational modeling. As shown in Figure 4-5, the HOMO and LUMO of **M1** (which is a computational model of **4.1)** are very clearly the $Re(CO)_3$- and POM-based orbitals, respectively. The lowest excited state of **M1** is a triplet at 56.3 kcal/mol (or 2.45 ev, or 506 nm) higher in energy than the ground singlet state. In this triplet state, almost one unpaired spin is located on the W and O atoms of POM ligand indicating a transfer of the electron density from the $Re(CO)_3$-based HOMO to the POM-based LUMO. Another unpaired spin (~1.02e) is located on the $-O_b$-$Re(CO)_3$ fragment, where O_b is the bridging oxygen atom between the $Re(CO)_3$ unit and the POM. Thus, the visible absorption of **4.1**, shown in Figure 4-1, can be attributed to the Re-to-POM ligand charge transfer transition. Similar to previously reported MMCT chromophores, the charge transfer interaction is

enhanced by the formation of W-O-Re covalent bonds and occurs mostly among the metal centers. However, the electron in the charge transfer excited state in **4.1** is delocalized among many W and O centers, a characteristic that resembles the MLCT states in Re and Ru bipyridyl complexes.

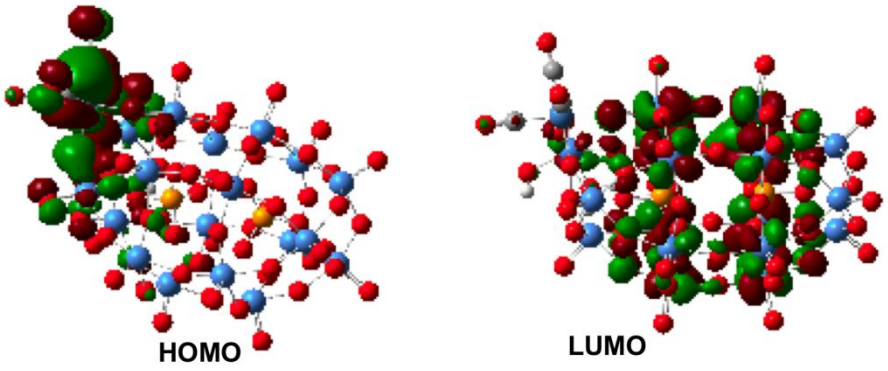

Figure 4-5 The calculated HOMO and LUMO of the model complex $[\{P_2W_{18}O_{63}[Re(CO)_3]\}(H_2O)(OH)]^{8-}$, **M1**.

4.3.3. Transient Spectral and Kinetic Analysis

The charge transfer dynamics were investigated by femtosecond visible pump-probe spectroscopy. The transient visible absorption spectra (Figure 4-6) of **4.1** show a new broad absorbing species with maximum at ~640 nm. This absorption feature can be attributed to the W(V) d-d transitions and W(V)-W(VI) intervalence charge transfer (IVCT) transitions in the reduced Wells-Dawson anionic ligand, generally known as "heteropoly blues". In addition, for a Wells-Dawson POM anion, the polar and equatorial sites have different electron affinities and the reduction preferentially occurs in the equatorial sites.[39-43] This is also the case for **4.1**, in which the electron density in the LUMO is distributed among the 12 equatorial WO_6 octahedrons, as shown in Figure 4-5. The kinetics of the formation and decay of this photo-induced absorption feature can be monitored at 640 nm. As shown in Figure 4-7 and Table 4-1, the best fit yields a

formation time of ~35 ± 15 fs, which can be considered as instantaneous within the time resolution of this measurement (~150 fs), consistent with the nature of the metal-to-POM charge transfer transition. However, this CT excited state is short lived, decaying with an average lifetime of 1.4 ps.

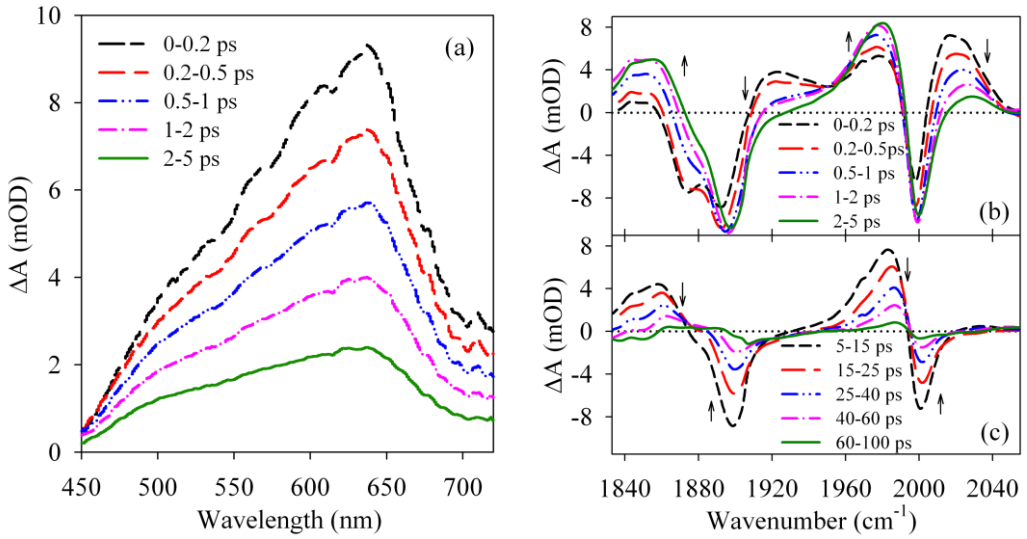

Figure 4-6 Average transient visible (a), and mid-IR (b, 0~5 ps; c, 5~100 ps) absorption spectra of **4.1** in CH_2Cl_2 at indicated delay time windows after 400 nm excitation. Arrows in (b) and (c) indicate the directions of amplitude changes.

In addition to the formation of the reduced POM ligands discussed above, the MPCT excited state of **4.1** should also generate oxidized Re(II) centers. The latter can be most unambiguously probed by monitoring the CO stretching bands, the frequencies of which are sensitive to the charge density on the Re center because of the Re-to-CO dπ-π* back bonding.[44] For this reason, the dynamics of CO stretching modes of **4.1** were investigated using femtosecond visible pump and IR probe spectroscopy. Following 400 nm excitation, bleaches of the CO stretching bands in the ground electronic state (~1860, 1890 and ~2000 cm^{-1}) and two new absorption bands at~1925 and 2020 cm^{-1}, blue-shifted from the ground state positions, were formed instantaneously. This is consistent

with the formation of the MPCT excited state, in which the electron density at the Re center is reduced, shifting the CO stretching to higher frequencies.[44] Because of the spectral overlaps, only one broad feature at ~1925 cm^{-1} (instead of two peaks) is observed. The transient kinetics of excited state CO stretching bands are compared in Figure 4-7, which show the same decay kinetics as the transient visible feature assigned to the reduced POM ligand. This agreement further confirms the assignment of the Re-to-POM CT transition in **4.1**.

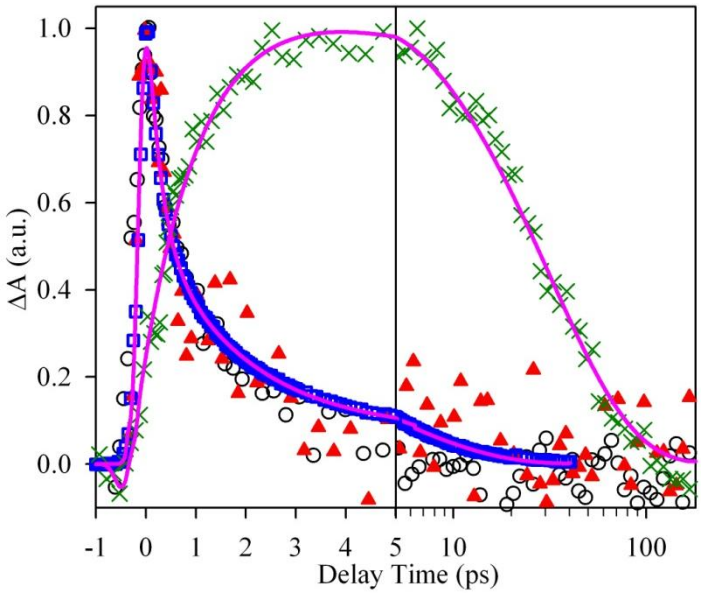

Figure 4-7 Transient kinetics of **4.1** in CH_2Cl_2 at 640 nm (blue squares), 1927 cm^{-1} (red triangles), 1982 cm^{-1} (green crosses) and 2020 cm^{-1} (circles) after 400 nm excitation. Also shown are fits (pink lines) to the kinetics at 640 nm and 1982 cm^{-1} by multiple exponential functions. The delay time is in linear scale in the left panel (-1 to 5 ps) and in logarithmic scale in the right panel (5 – 200 ps).

The decay of the MPCT excited state leads to the formation of two positive absorption bands at ~1850, and 1980 cm^{-1}, red-shifted from the ground state bleaches, as shown in Figure 4-6. This can also be clearly seen in Figure 4-7 and Figure 4-9, which

shows that the formation kinetics of these features agrees well with the decay of the MPCT excited state bands (in the visible and mid-IR). We attribute these features to the formation of "hot" ground state molecules, in which the energy of the excitation is converted into the vibrational energy of the complex in the ground electronic state. The broadened and red-shifted CO bands undergo a continuous blue shift and narrowing with a time constant of 32 ps (Table 4-1), consistent with a vibrational cooling process of related molecules.[45-50] The red-shifted CO stretching bands can result from the vibration excitation of the CO stretching modes as well as anharmonically coupled low frequency modes. To further clarify the nature of the hot ground state, we conducted transient IR pump/IR probe experiments where only the CO stretching mode at the electronic ground state is excited. In this case (Figure 4-8), a red-shifted CO band assignable to the 1-2 transition is also observed and it decays with a similar time constant. However, this feature does not undergo continuous blue shift and narrowing. This comparison suggests that the hot ground state (shown in Figure 4-6) contains both the excitation of the CO stretching mode (to $v = 1$ state) and anharmonically coupled low frequency modes.

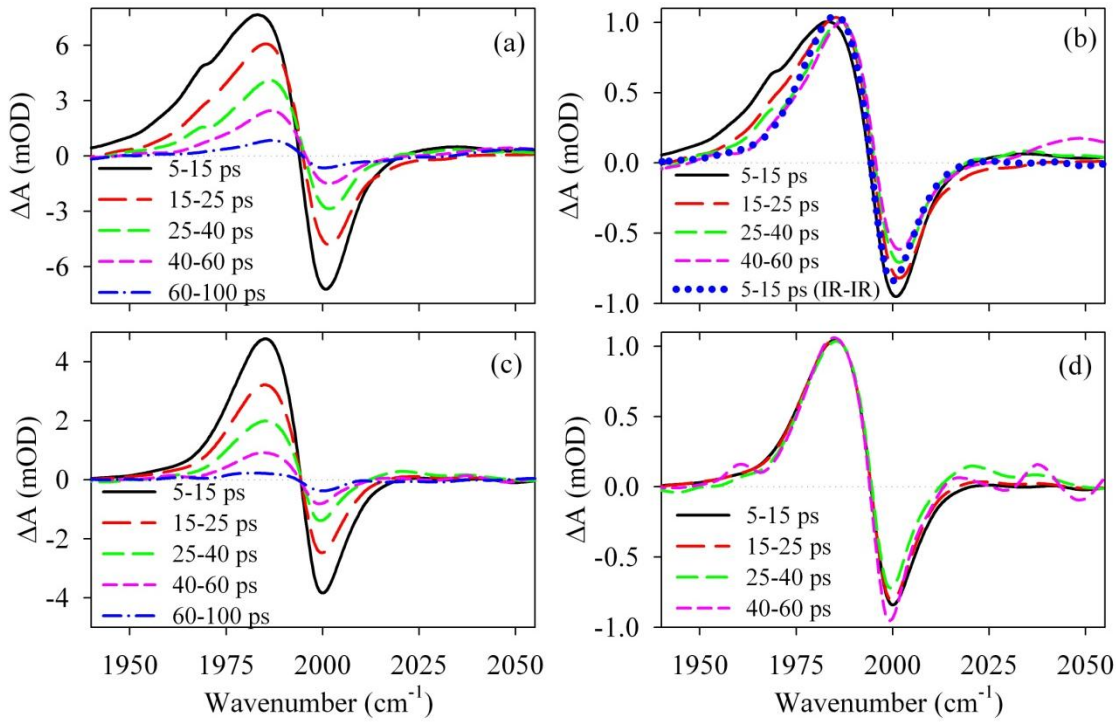

Figure 4-8 Average transient IR spectra at indicated delay time windows after 400 nm (a and b) and 2000 cm^{-1} (c and d) excitation. (b) and (d) are the normalized spectra of (a) and (c), respectively. In (b), the normalized spectrum from panel (d) (at 5~15 ps after 2000 cm^{-1} excitation) is also shown for comparison.

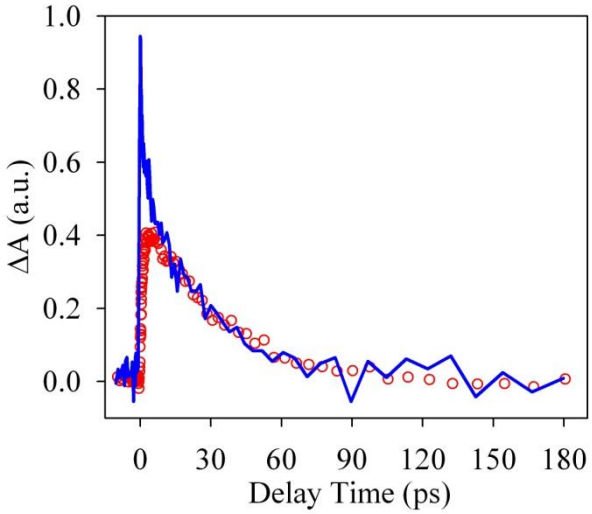

Figure 4-9 Comparison of transient kinetics monitored at 1982 cm^{-1} after 400 nm (red circles) and 2000 cm^{-1} (blue line) excitation. These kinetics show the same decay after ~ 5 ps. The initial component in the kinetics resulted from IR (2000 cm^{-1}) excitation can be attributed to a fast energy transfer among the CO stretching modes.

Table 4-1 Fitting parameters for kinetic traces after 400 nm excitation. The kinetic traces were modeled as multi-exponential decays analytically convoluted with the instrument response function. τ_{ave} is the amplitude weighted average time constant, $\Sigma(a_i \times \tau_i) / \Sigma a_i$.

	Rise time, fs	τ_1, ps (a_1, %)	τ_2, ps (a_2, %)	τ_3, ps (a_3, %)	τ_{ave}, ps
640 nm	35 ± 15	0.25 ± 0.07 (60)	1.4 ± 0.2 (29)	7.3 ± 0.5 (11)	1.4 ± 0.2
2020 cm^{-1}	35 ± 15	0.24 ± 0.05 (50)	1.6 ± 0.2 (50)	--	0.92 ± 0.13
1982 cm^{-1}	1200 ± 180	32 ± 0.3 (100)	--	--	32 ± 0.3

4.4 Conclusions

In conclusion, we have synthesized a molecular metal-to-polyoxometalate CT (MPCT) chromophore through a facile approach. Comprehensive computational and spectroscopic studies show that the high visible absorption in this complex can be attributed to a MPCT transition involving charge transfer from the Re(I) center to the POM. The orbitals and transition addressed in this study are distinct from those in the well-documented heterobimetallic systems because the acceptor orbitals are delocalized and multi-metal. In constrast, the heterobimetallic systems exhibit fairly localized orbitals that reside primarily on a single acceptor metal.[6-18] Photoactivities of this charge transfer complex in some solar-conversion devices are under investigation. In addition, structural modifications to introduce electron trapping centers in this MPCT chromophore for lengthening the lifetime of the charge transfer excited states are ongoing.

References

(1) Balzani, V.; Credi, A.; Venturi, M. *ChemSusChem* 2008, *1*, 26.

(2) Fujita, E.; Muckerman, J. T.; Domen, K. *ChemSusChem* 2011, *4*, 155157.

(3) Hawecker, J.; Lehn, J. M.; Ziessel, R. *Nouv. J. Chim.* 1983, *7*, 271.

(4) Hawecker, J.; Lehn, J.-M.; Ziessel, R. *Helv. Chim. Acta* 1986, *69*, 1990.

(5) Fujita, E. *Coord. Chem. Rev.* 1999, *185-186*, 373.

(6) Lin, W.; Frei, H. *J. Am. Chem. Soc.* 2005, *127*, 1610.

(7) Nakamura, R.; Frei, H. *J. Am. Chem. Soc.* 2006, *128*, 10668.

(8) Han, H.; Frei, H. *Microporous Mesoporous Mater.* 2007, *103*, 265.

(9) Nakamura, R.; Okamoto, A.; Osawa, H.; Irie, H.; Hashimoto, K. *J. Am. Chem. Soc.* 2007, *129*, 9596.

(10) Han, H.; Frei, H. *J. Phys. Chem. C* 2008, *112*, 8391.

(11) Han, H.; Frei, H. *J. Phys. Chem. C* 2008, *112*, 16156.

(12) Wu, X.; Weare, W. W.; Frei, H. *Dalton Trans.* 2009, 10114.

(13) Somorjai, G. A.; Frei, H.; Park, J. Y. *J. Am. Chem. Soc.* 2009, *131*, 16589.

(14) Takashima, T.; Nakamura, R.; Hashimoto, K. *J. Phys. Chem. C* 2009, *113*, 17247.

(15) Cuk, T.; Weare, W. W.; Frei, H. *J. Phys. Chem. C* 2010, *114*, 9167.

(16) Yu, H.; Irie, H.; Shimodaira, Y.; Hosogi, Y.; Kuroda, Y.; Miyauchi, M.; Hashimoto, K. *J. Phys. Chem. C* 2010, *114*, 16481.

(17) Irie, H.; Shibanuma, T.; Kamiya, K.; Miura, S.; Yokoyama, T.; Hashimoto, K. *Appl. Catal., B* 2010, *96*, 142.

(18) Sivasankar, N.; Weare, W. W.; Frei, H. *J. Am. Chem. Soc.* 2011, *133*, 12976.

(19) Hou, Y.; Abrams, B. L.; Vesborg, P. C. K.; Björketun, M. E.; Herbst, K.; Bech, L.; Setti, A. M.; Damsgaard, C. D.; Pedersen, T.; Hansen, O.; Rossmeisl, J.; Dahl, S.; Nørskov, J. K.; Chorkendorff, I. *Nature Mater.* 2011, *10*, 434.

(20) Duan, L. L.; Tong, L. P.; Xu, Y. H.; Sun, L. C. *Energy Environ. Sci.* 2011, *4*, 3296.

(21) Yin, Q.; Tan, J. M.; Besson, C.; Geletii, Y. V.; Musaev, D. G.; Kuznetsov, A. E.; Luo, Z.; Hardcastle, K. I.; Hill, C. L. *Science* 2010, *328*, 342.

(22) Sala, X.; Romero, I.; Rodríguez, M.; Escriche, L.; Llobet, A. *Angew. Chem. Int. Ed.* 2009, *48*, 2842.

(23) Wang, M.; Sun, L. *ChemSusChem* 2010, *3*, 551.

(24) Kalyanasundaram, K. *J. Chem. Soc., Faraday Trans. 2* 1986, *82*, 2401.

(25) Worl, L. A.; Duesing, R.; Chen, P.; Ciana, L. D.; Meyer, T. J. *J. Chem. Soc., Dalton Trans.* 1991, 849.

(26) Ziessel, R.; Juris, A.; Venturi, M. *Inorg. Chem.* 1998, *37*, 5061.

(27) *Special Thematic Issue on Polyoxometalates*; Hill, C. L., Ed., 1998; Vol. 98, No. 1.

(28) Borrás-Almenar, J. J.; Coronado, E.; Müller, A.; Pope, M. T. *Polyoxometalate Molecular Science. Proceedings of the NATO Advanced Study Institute, Tenerife, Spain from 25 August to 4 September 2001*; Kluwer Academic Publishers: Dordrecht, 2003; Vol. 98.

(29) Katsoulis, D. E.; Pope, M. T. *J. Am. Chem. Soc.* 1984, *106*, 2737.

(30) Kalyanasundaram, K. *Coord. Chem. Rev.* 1982, *46*, 159.

(31) Kalyanasundaram, K.; Grätzel, M. *Coord. Chem. Rev.* 1998, *77*, 347.

(32) Frisch, M. J.; Trucks, G. W.; Schlegel, H. B.; Scuseria, G. E.; Robb, M. A.; Cheeseman, J. R.; Montgomery, J., J. A.; Vreven, T.; Kudin, K. N.; Burant, J. C.; Millam, J. M.; Iyengar, S. S.; Tomasi, J.; Barone, V.; Mennucci, B.; Cossi, M.; Scalmani, G.; Rega, N.; Petersson, G. A.; Nakatsuji, H.; Hada, M.; Ehara, M.; Toyota, K.; Fukuda, R.; Hasegawa, J.; Ishida, M.; Nakajima, T.; Honda, Y.; Kitao, O.; Nakai, H.; Klene, M.; Li, X.; Knox, J. E.; Hratchian, H. P.; Cross, J. B.; Adamo, C.; Jaramillo, J.; Gomperts, R.; Stratmann, R. E.; Yazyev, O.; Austin, A. J.; Cammi, R.; Pomelli, C.; Ochterski, J. W.; Ayala, P. Y.; Morokuma, K.; Voth, G. A.; Salvador, P.; Dannenberg, J. J.; Zakrzewski, V. G.; Dapprich, S.; Daniels, A. D.; Strain, M. C.; Farkas, O.; Malick, D. K.; Rabuck, A. D.; Raghavachari, K.; Foresman, J. B.; Ortiz, J. V.; Cui, Q.; Baboul, A. G.; Clifford, S.; Cioslowski, J.; Stefanov, B. B.; Liu, G.; Liashenko, A.; Piskorz, P.; Komaromi, I.; Martin, R. L.; Fox, D. J.; Keith, T.; Al-Laham, M. A.; Peng, C. Y.; Nanayakkara, A.; Challacombe, M.; Gill, P. M. W.; Johnson, B.; Chen, W.; Wong, M. W.; Gonzalez, C.; Pople, J. A.; 03 Rev. C1 ed.; Gaussian, Inc.: Pittsburgh, 2003.

(33) Becke, A. D. *Phys. Rev. A* 1988, *38*, 3098.

(34) Lee, C.; Yang, W.; Parr, R. G. *Phys. Rev. B* 1988, *37*, 785.

(35) Becke, A. D. *J. Chem. Soc.* 1993, *98*, 1372.

(36) Hay, P. J.; Wadt, W. R. *J. Chem. Phys.* 1985, *82*, 270.

(37) Hay, P. J.; Wadt, W. R. *J. Chem. Phys.* 1985, *82*, 299.

(38) Wadt, W. R.; Hay, P. J. *J. Chem. Phys.* 1985, *82*, 284.

(39) Prados, R. A.; Pope, M. T. *Inorg. Chem.* 1976, *15*, 2547.

(40) Sanchez, C.; Livage, J.; Launay, J. P.; Fournier, M. *J. Am. Chem. Soc.* 1983, *105*, 6817.

(41) Buckley, R. I.; Clark, R. J. H. *Coord. Chem. Rev.* 1985, *65*, 167.

(42) Kozik, M.; Hammer, C. F.; Baker, L. C. W. *J. Am. Chem. Soc.* 1986, *108*, 7627.

(43) Keita, B.; Jean, Y.; Levy, B.; Nadjo, L.; Contant, R. *New J. Chem.* 2002, *26*, 1314.

(44) Wang, Y.; Asbury, J. B.; Lian, T. *J. Phys. Chem. A* 2000, 4291.

(45) Lian, T.; Bromberg, S. E.; Asplund, M. C.; Yang, H.; Harris, C. B. *J. Phys. Chem.* 1996, *100*, 11994.

(46) Doorn, S. K.; Dyer, R. B.; Stoutland, P. O.; Woodruff, W. H. *J. Am. Chem. Soc.* 1993, *115*, 6398.

(47) Li, G.; Parimal, K.; Vyas, S.; Hadad, C. M.; Flood, A. H.; Glusac, K. D. *J. Am. Chem. Soc.* 2009, *131*, 11656.

(48) Gabrielsson, A.; Hartl, F.; Zhang, H.; Smith, J. R. L.; Towrie, M.; Anton ń Vlček, J.; Perutz, R. N. *J. Am. Chem. Soc.* 2006, *128*, 4253.

(49) Wang, C.; Mohney, B. K.; Williams, R. D.; Petrov, V.; Hupp, J. T.; Walker, G. C. *J. Am. Chem. Soc.* 1998, *120*, 5848.

(50) Dougherty, T. P.; Heilweil, E. J. *Chem. Phys. Lett.* 1994, *227*, 19.

Chapter 5

An Inorganic Chromophore Based on a Molecular Oxide Supported Metal Carbonyl Cluster: $[P_2W_{17}O_{61}\{Re(CO)_3\}_3\{ORb(H_2O)\}(\mu_3\text{-}OH)]^{9-}$

(Published partially in *Inorg. Chem.* **2013**, DOI: 10.1021/ic4018823)

With William Rodríguez-Córdoba, Alexey L. Kaledin, Ye Yang, Yurii V. Geletii, Tianquan Lian, Djamaladdin G. Musaev, Craig L. Hill

5.1 Introduction

Dyadic systems comprising an metal-to-ligand charge-transfer (MLCT) chromphore $[Ru(bpy)_3]^{2+}$ (and its derivatives), and semiconductor metal oxide acceptor, most frequently TiO_2, form the basis of dye-sensitized solar cell (DSSC) technology.[1-3] Since the original Grätzel $[Ru(bpy)_3]^{2+}$-TiO_2 dyadic structures, there has been and continue to be major efforts to study and optimize the photodynamic, stability and optical properties of these promising systems. More recently, these systems have been coupled with water oxidation catalysts to function as triadic photoanodes for water oxidation.[4-9] However, these systems show limited stability under water oxidizing conditions, primarily because the organic ligands (usually *bpy*) get oxidized. As a consequence, there have been major recent efforts to prepare metal-to-metal charge-transfer (MMCT) chromphores containing no organic ligands, including extensive work on bimetallic assemblies supported on mesporous silica reported by Frei and coworkers.[10-13] However, all the above mentioned dyadic configurations are heterogeneous in nature making it very difficult to acquire a precise atomistic level understanding of their physicochemical properties. In this paper we report a homogenous dyadic structure in the form of a multi-metal electron donor unit attached to the outside of a polyoxometalate (POM) electron acceptor unit, $[P_2W_{17}O_{61}\{Re(CO)_3\}_3\{ORb(H_2O)\}(\mu_3\text{-}OH)]^{9-}$ (**5.1**). Like TiO_2 and most other semiconductor metal oxides of interest in solar energy conversion,[14-18] the POM ligand in **5.1** is readily reducible at low energy (modest reduction potentials in solution of -0.4 to -0.8 V versus NHE).[19-25] Compound **5.1** is a new kind of chromophore with little or no oxidizable organic structure for possible use in solar fuel production assemblies. This investigation includes a comprehensive characterization of the geometrical and electronic

structure of **5.1** using several spectroscopic methods, X-ray crystallography, time-resolved methods and computational studies.

5.2 Experimental

5.2.1. Synthesis

Materials. All chemicals were reagent grade and used as supplied. The precursor compound, $K_{16}[P_4W_{35}O_{124}\{Re(CO)_3\}_2]$, was synthesized according to **Chapter 3**. The low-valent complex $Re(CO)_3(CH_3CN)_3(BF_4)$ was made following the known procedures with only the $AgClO_4$ replaced by $AgBF_4$.[26] The purities of these compounds were checked with FTIR spectroscopy and NMR (^1H and ^{31}P).

Instrumentation. UV-vis spectra were acquired using an Agilent 8453 spectrophotometer equipped with a diode-array detector and an Agilent 89090A cell temperature controller unit. The solid-state FT-IR spectra were measured on a Thermo Nicolet 6700 spectrometer with KBr pellets (2%). ^{31}P NMR spectra (162.13 MHz) in D_2O were measured on a Varian INOVA 400 spectrometer with respect to an external standard of 85% H_3PO_4 (0 ppm). Elemental analyses (C, P, K, Rb, Re, W) were performed by Galbraith Lab Inc., Knoxville, TN, 37921. Thermogravimetric analysis was acquired on a Perkin Elmer STA 6000 analyzer.

Synthesis of 5.1: 0.1 mmol (48 mg) of pre-synthesized $Re(CO)_3(CH_3CN)_3(BF_4)$ was dissolved in 10 mL of hot water (~70 ^oC), and then 0.01 mmol (~108 mg) $K_{16}[P_4W_{35}O_{124}\{Re(CO)_3\}_2]$ was added to the hot solution slowly. The mixture was heated at ~70 ^oC for 1h, during which time the pH value was kept between 5 to 5.5 by 0.1 M KOH solution. The color of the solution gradually changed from dark red to orange-

brown. RbCl (1.0 mL of 1.0 M solution) was added to the solution dropwise. The solution was then filtered through a fine filter paper. Colorless crystals of un-reacted [α_2-$P_2W_{17}O_{61}$]$^{10-}$ salts formed first in the next 3 days and were subsequently removed by filtration. The filtrate was collected for further slow evaporation and after a week brown needle-like crystals for **5.1** were collected (a small amount of [α_2-$P_2W_{17}O_{61}$]$^{10-}$ salt impurities were separated manually). Yield: 35 mg (27%, based on P). Experimental trials proved that direct synthesis of **5.1** from $Re(CO)_3(CH_3CN)_3(BF_4)$ and [α_2-$P_2W_{17}O_{61}$]$^{10-}$ was unsuccessful: thus only $K_{16}[P_4W_{35}O_{124}\{Re(CO)_3\}_2]$ is a viable synthetic precursor for the synthesis of **5.1**. ^{31}P NMR (D_2O): -7.9 and -13.8 ppm with respect to 85% H_3PO_4 (0 ppm). FT-IR (2% KBr pellet, 1100 - 400 cm^{-1}): 1088 (m), 1051 (m), 1020 (sh), 944 (s), 916 (m), 799 (s), 747 (sh), 701 (sh). Electronic absorption spectral data (300 - 800 nm, in H_2O): $\varepsilon_{400nm} \sim 3500$ M^{-1}·cm^{-1}. Elemental analysis (%) calcd for $C_9H_{91}O_{117}P_2K_{0.9}Rb_{9.1}Re_3W_{17}$: C, 1.6; P, 0.93; K, 0.53; Rb, 11.7; W, 47.1; Re, 8.4. Found: C, 1.6; P, 0.92; K, 0.56; Rb, 12.2; W, 46.4; Re, 8.2.

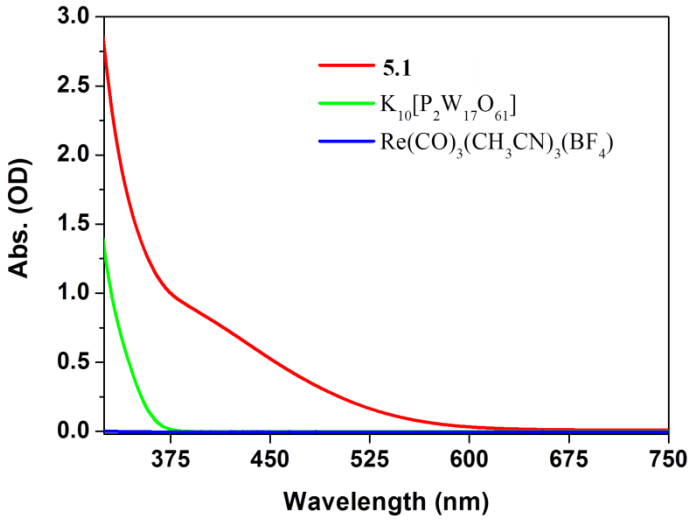

Figure 5-1 UV-vis spectra of **5.1** and the precursors in aqueous solution

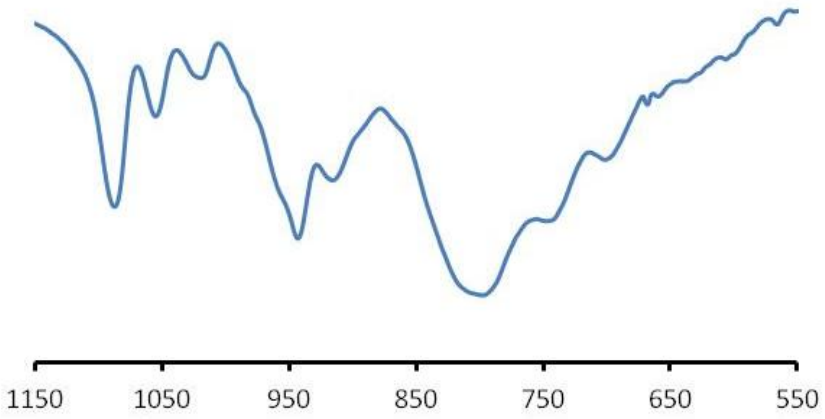

Figure 5-2 FTIR spectra of **5.1** in the POM region (KBr pellets; 1100 - 500 cm^{-1})

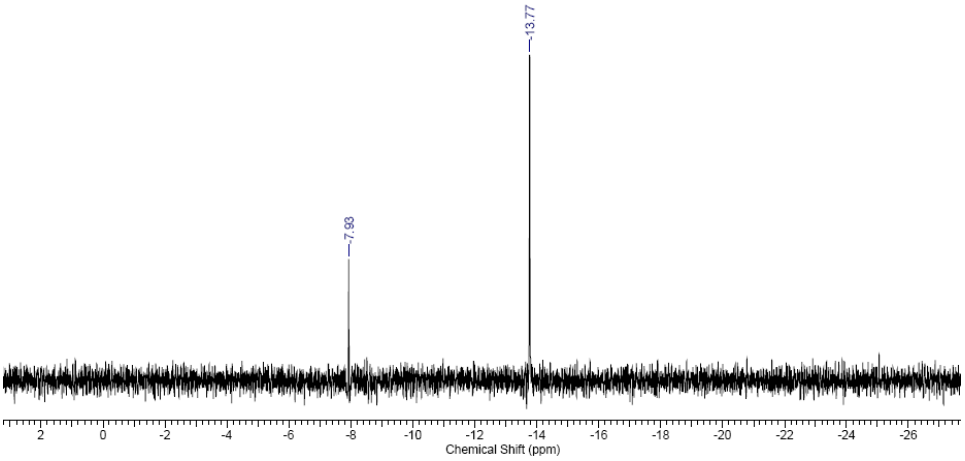

Figure 5-3 ^{31}P NMR of **5.1** in D_2O (0 ppm, 85% H_3PO_4)

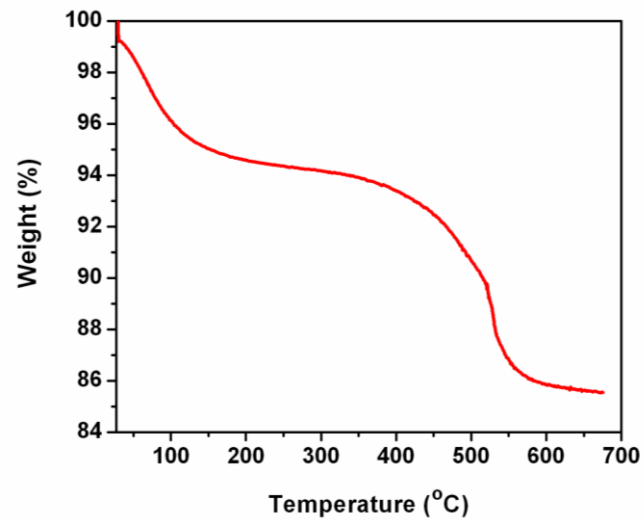

Figure 5-4 Thermogravimetric analysis (TGA) of **5.1**

5.2.2 Crystallography

A single crystal of **5.1** suitable for X-ray analysis was measured on a Bruker D8 SMART APEX CCD sealed tube diffractometer. Diffraction intensities were measured using graphite monochromated Mo Kα radiation (λ = 0.71073 Å) at 173(2) K. Data collection, indexing, and initial cell refinements were carried out using SMART;[27] frame integration and final cell refinements were done using SAINT.[28] A multiple absorption correction including face-indexing was done by SADABS.[29] The molecular structure of **5.1** was determined by Direct Methods and Fourier techniques and refined by full-matrix least squares. Heavy atoms of P, Rb, K, Re and W and most oxygen atoms on the POM framework were refined anisotropically. The largest residual electron density for each structure was located close to the Rb and W atoms, most likely due to imperfect absorption corrections frequently encountered in heavy-metal atom structures. Structure solution, refinement, graphic and generation of publication materials were performed by using SHELXTL-97 software.[30] CCDC-913443 contains the supplementary crystallographic data. These data can be obtained free of charge from The Cambridge Crystallographic Data Center via www.ccdc.cam.ac.uk/data_request/cif.

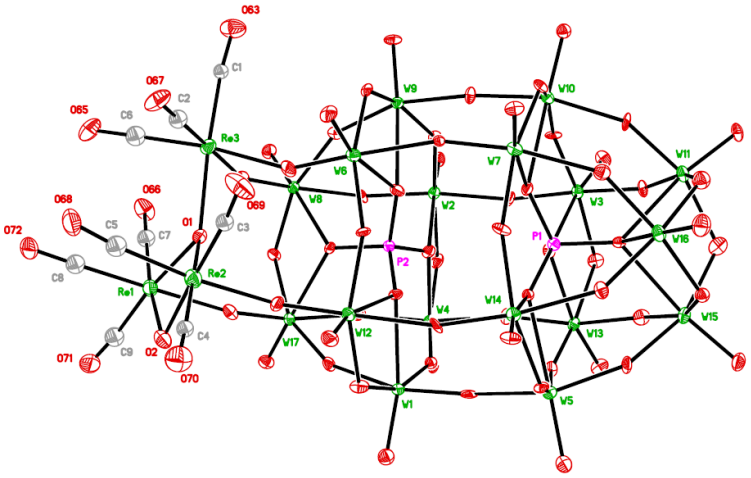

Figure 5-5 Thermal ellipsoid plot (30% probability) and numbering scheme for **5.1** ($[Rb(H_2O)]^+$ is omitted for clarity)

Table 5-1 Crystal data collection and refinement parameters for compound **5.1**

Empirical formula	$C_9H_{91}O_{117}P_2K_{0.9}Rb_{9.1}Re_3W_{17}$	
Formula weight	6629.35	
Temperature	293(2) K	
Wavelength	0.71073 Å	
Crystal system	Triclinic	
Space group	$P\bar{1}$	
Unit cell dimensions	a = 13.1263(10) Å	α = 79.7220(10) °
	b = 14.3600(10) Å	β = 83.8730(10) °
	c = 22.6164(16) Å	γ = 77.6240(10) °
Volume	4086.8(5) $Å^3$	
Z	2	
Density (calculated)	4.894 Mg/m^3	
Absorption coefficient	33.774 mm^{-1}	
F(000)	5198	
Crystal size	0.23 x 0.07 x 0.05 mm^3	
Theta range for data collection	1.47 to 27.10 °.	
Index ranges	-16<=h<=16, -18<=k<=18, -28<=l<=28	
Reflections collected	68532	
Independent reflections	17984 [*R*(int) = 0.0712]	
Completeness to theta = 27.10 °	99.8 %	
Absorption correction	Numerical	

Max. and min. transmission	0.2830 and 0.0477
Refinement method	Full-matrix least-squares on F^2
Data / restraints / parameters	17984 / 0 / 996
Goodness-of-fit on F^2	1.020
Final R indices [I>2sigma(I)]	R_1 = 0.0598, wR_2 = 0.1444
R indices (all data)	R_1 = 0.0901, wR_2 = 0.1595
Largest diff. peak and hole	5.065 and -6.081 e.Å^{-3}

$R_1 = \Sigma \, ||F_0|-|F_c||/\Sigma|F_0|$; w$R_2 = \{\Sigma[w(F_0^2-F_c^2)^2/\Sigma w(F_0^2)^2]\}^{1/2}$

5.2.3 Spectroelectrochemistry

Cyclic voltammograms (CVs) were obtained at room temperature using a BAS CV-50W electrochemical analyzer equipped with a Pt-wire auxiliary electrode, a Ag/AgCl (3 M NaCl) BAS reference electrode, and a glassy-carbon (GC) or a FTO coated glass slide working electrode respectively. All reduction potentials are measured relative to this reference electrode. The prepared solution contained 1.0 mM **5.1** in 20 mM sodium acetate buffer (pH = 4.7) with 0.2 M $LiClO_4$ as supporting electrolyte. The CVs are similar using these two different working electrodes: both show two reduction peaks.

The above solutions were then used for spectroelectrochemical studies. Visible-light spectroelectrochemical experiments were performed with a BASi CV-50W potentiostat, in an ALS SEC-2F spectroelectrochemical flow cell equipped with an Ocean Optics USB2000+ spectrometer and a LS-1 tungsten lamp. The pathlength of the cell is 0.5 mm. The working electrode was an FTO coated glass slide, the reference electrode was Ag/AgCl in 3M NaCl (BASi) and the auxiliary electrode was a stainless steel tube. Ocean Optics Spectrasuite software was used to record visible spectra and collect absorbance *vs.* time measurements at different applied potentials. Typically, a new broad band (~600 – 1000 nm) grows during electrochemical reduction. Upon finishing each

experiment under a certain potential, the cell was washed and filled with fresh solution (an external syringe was used to pump into the starting solution). The spectra of the newly filled solutions are the same as the beginning, which means compound **5.1** was stable during this electrochemistry study. No deposited film was observed on the FTO working electrode after all the experiments were finished and the equipments were dissembled.

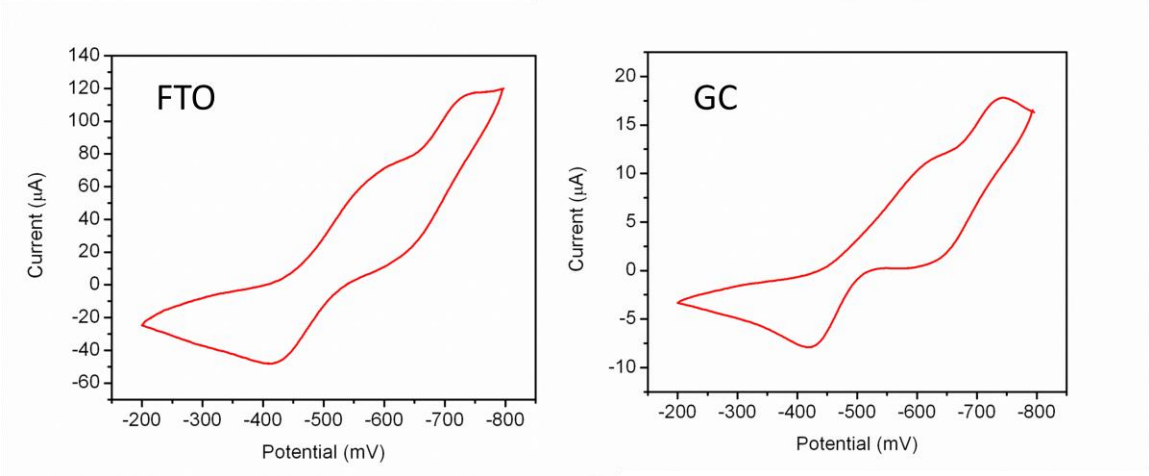

Figure 5-6 CVs of **5.1**. Scan rate 25 mV s^{-1}, at ambient temperature

5.2.4. Transient Spectral and Kinetic Analysis

Our femtosecond transient absorption spectrometer is based on a regeneratively amplified Ti:sapphire laser system (coherent Legend, 800 nm, 150 fs, 3 mJ/pulse and 1 kHz repetition rate) and the Helios spectrometer (Ultrafast Systems LLC). The tunable femtosecond infrared spectrometer is based on a Clark IR optical parametric amplifier (OPA) which generates two tunable near-IR pulses in the 1.1 to 2.5 μm spectral range (signal and idler, respectively). All details about the instrumental setup can be found in **Chapter 4**.

The organic-solvent-soluble salt of **5.1** for femtosecond measurements was prepared according to **Chapter 4**. **5.1** (0.01 mmol, 65 mg) was dissolved in 5 mL of water. An equal volume of a CH_2Cl_2 solution of tetrabutylammonium bromide (0.1 mmol, 33 mg) was added to the above solution under vigorous stirring. The orange-colored organic layer was separated and washed with water using a separatory funnel. The CH_2Cl_2 solution of **5.1** was concentrated by blowing with a N_2 flow and then used for femtosecond transient measurements.

5.2.5. Computational Procedures and Modeling

Models used. As mentioned in experimental section the $[P_2W_{17}O_{61}\{Re(CO)_3\}_3\{\mu_2\text{-}O^2\}(\mu_3\text{-}O^1)]^{11-}$ contains eleven counter cations, one of which (Rb^+) forms an ion-pair with the polyanion unit with a Rb-O^2 bond distance of 2.801Å involving the bridging oxygen of $Re^1\text{-}(\mu_2\text{-}O^2)\text{-}Re^2$ fragment. In order to capture this ion-pairing feature of the **5.1** in computational modeling (which does not include counter cations) we did protonate the bridging μ_2-O^2 and used the $[P_2W_{17}O_{61}\{Re(CO)_3\}_3(\mu_2\text{-}O^2H)(\mu_3\text{-}O^1)]^{10-}$ model system, referred to below as structure **m1**. Furthermore, to validate the protonation state of the μ_3-O^1-center in **5.1**, we also performed calculations of the $[P_2W_{17}O_{61}\{Re(CO)_3\}_3(\mu_2\text{-}O^2H)(\mu_3\text{-}O^1H)]^{9-}$ model system, referred to below as structure **m2**. The calculated important geometry parameters of these two model systems are given in **Table 5-2** along with their experimental values. **Figure 5-9** shows the notations used for the important atoms.

Computational methods used. Geometries of the **m1** and **m2** compounds were optimized, both in gas phase with no geometry constraints, in their ground singlet ($\mathbf{S_0}$)

and the first excited triplet ($\mathbf{T_1}$) states. Vibrational normal mode analyses were performed to ensure that all converged structures are true minima. In these calculations we used the DFT method (B3LYP functional)[31,32] in conjunction with the split-valence 6-31G(d,p) basis sets for H, C, O, P and LanL2DZ basis sets and associated ECPs[33-35] for the W and Re atoms, which are referred to below as B3LYP/[lanl2dz + (6-31G(d,p)]. The solvent effects were approximated, at the gas-phase optimized geometries, by the polarizable continuum model (PCM)[36,37] employing the UFF[38] radii for all atoms. Electronic spectra and electric dipole transition moments for $\mathbf{S_0}$-$\mathbf{S_n}$ transitions of **m2** were calculated at the optimized geometries of $\mathbf{S_0}$ for the corresponding compound using the time-dependent (TD)[39] DFT [i.e. TD-B3LYP/[lanl2dz + (6-31G(d,p)] approach. The above calculations were carried out with Gaussian 09 software package.[40]

5.3 Results and Discussion

5.3.1. Structral studies

Compound **5.1** is prepared in aqueous solution (see Experimental section). The crystal structure of **5.1** (**Figure 5-7**) reveals an "out-of-pocket" motif [41,42] with a tri-rhenium carbonyl "cap" grafted on the defect site of $[\alpha_2\text{-}P_2W_{17}O_{61}]^{10-}$ (the "support"). The Re-C bond lengths range from 1.87 to 1.92 Å, while the C-O bonds range from 1.15 to 1.21 Å. It should be noted that POM-supported metal carbonyl complexes constitute molecular models for metal-oxide-supported metal-carbonyl catalysts.[43-45] Several have been prepared previously but all these complexes contain only a mononuclear $\{M(CO)_x\}^+$ unit (or separated mononuclear units).[46-58] Compound **5.1** is the first with an oxo-centered multi-metal electron donor sub-structure. Interestingly, the three Re(I) centers reside in different coordination environments (**Figure 5-7**). Re^1 and Re^2 are similar and bonded by

O^1 and O^2 forming one Re-O-W bond to $[\alpha_2\text{-}P_2W_{17}O_{61}]^{10-}$. In contrast, Re^3 is bonded to O^1 and forms two Re-O-W bonds to the POM moiety. An aqua alkali metal moiety $[Rb(H_2O)]^+$ (bonded to disordered O11w and O12w with an occupancy of 0.5 for each) is also strongly (2.80 Å bond distance) bonded to O^2. The Rb^+ cation further coordinates to the bridging/terminal oxo ligands in the adjacent POMs with distances ranging from 2.84 to 3.14 Å, defining a quasi-1D chain.

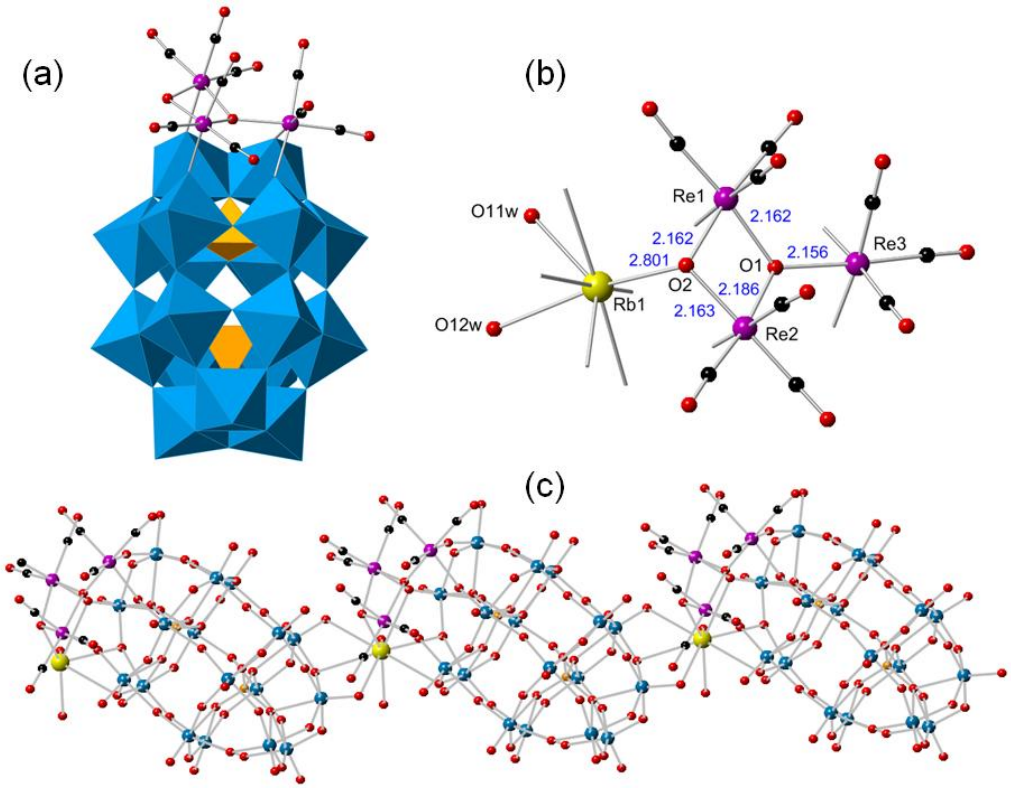

Figure 5-7 (a) X-ray structure of **5.1** in combined ball-and-stick and polyhedral representations ($[Rb(H_2O)]^+$ is omitted for clarity). Re, purple; O, red; C, black; WO_6 octahedra: blue; PO_4 tetrahedra: gold. (b) Top view of the tri-rhenium "cap" (including the $[Rb(H_2O)^+]$ unit) with representative bond distances (Å). The bridging oxygens to the POM are omitted. (c) Ball-and-stick representation of the quasi-1D chain of **5.1** along the *b*-axis.

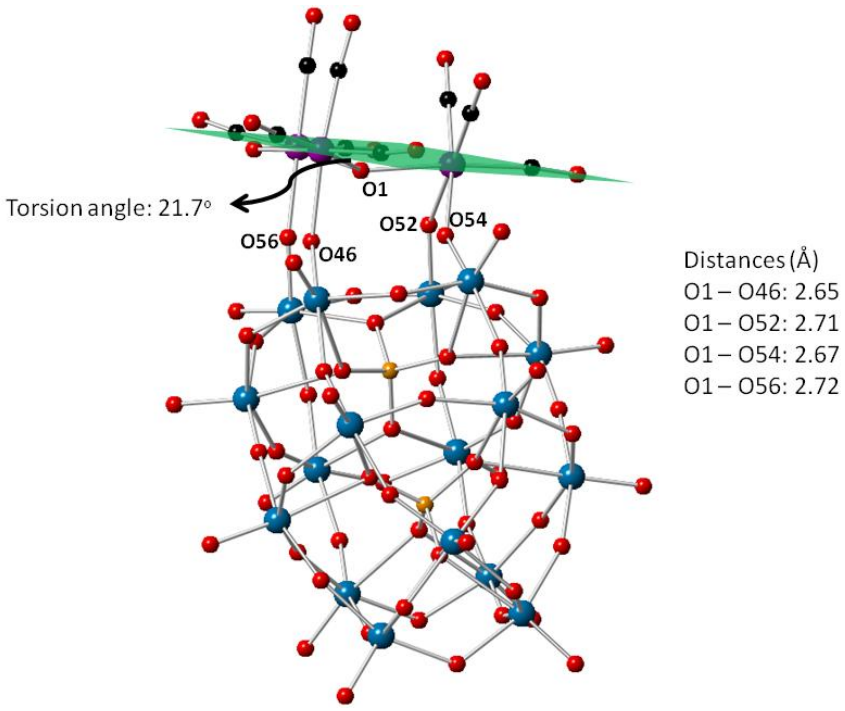

Figure 5-8 X-ray structure showing the torsion angle of O^1 relative to the tri-rhenium plane and representative distances between O^1 and bridging oxygen atoms from the POM ligand.

Computational (DFT) studies of two model systems, namely $[P_2W_{17}O_{61}\{Re(CO)_3\}_3(\mu_2\text{-}O^2H)(\mu_3\text{-}O^1)]^{10-}$ (**m1**) and $[P_2W_{17}O_{61}\{Re(CO)_3\}_3(\mu_2\text{-}O^2H)(\mu_3\text{-}O^1H)]^{9-}$ (**m2**), model the Rb^+--O^2 ion-pairing feature of **5.1** by replacing Rb^+ by a proton. The difference between **m1** and **m2** is the protonation state of the central μ_3-O^1-unit in **5.1**. A comparison of the calculated and experimental geometry parameters provide strong support for the structural assignment of **5.1**. As expected the calculated geometries of **m1** and **m2** are very close to each other and, in general, are in reasonable agreement with their experimental values, except the Re^n-O^1 (n = 1-3) bond distances and improper torsion angle (Re^2,Re^1,Re^3,O^1; see **Table 5-2** and **Figure 5-9**). In **m2**, the calculated Re^n-O^1 (n = 1-3) bond distances are only 0.08-0.10 Å longer and the torsion angle is only 4.9° smaller than the experimental values. Although in **m1** the discrepancy of the calculated and experimental values of Re^n-O^1 (n = 1-3) bond distances is relatively small (calculated

values are shorter by 0.02-0.04 Å), the improper torsion angle (Re^2,Re^1,Re^3,O^1) (of 3.4°) is almost 6.4 times smaller than its experimental value. These findings strongly support the assignment of a central μ_3-O^1H unit in **5.1**.

Table 5-2 The calculated important geometry parameters of model systems **m1** and **m2**, and comparison with their experimental results

Parameters	**m1**	**m2**	Expt.
Re^1-O^2	2.168	2.168	2.162
Re^2-O^2	2.168	2.166	2.163
Re^1-O^1	2.129	2.278	2.162
Re^2-O^1	2.125	2.269	2.186
Re^3-O^1	2.137	2.256	2.156
Re^1-O^4	2.118	2.055	2.109
Re^2-O^3	2.185	2.105	2.152
Re^3-O^5	2.144	2.101	2.105
Re^3-O^6	2.191	2.126	2.091
Re^1-C^1	1.924	1.930	1.886
Re^1-C^2	1.903	1.917	1.923
Re^1-C^3	1.913	1.886	1.882
Re^2-C^4	1.927	1.932	1.912
Re^2-C^5	1.918	1.892	1.871
Re^2-C^6	1.890	1.907	1.899
Re^3-C^7	1.906	1.917	1.903
Re^3-C^8	1.891	1.905	1.866
Re^3-C^9	1.931	1.905	1.902
(Re^2,Re^1,Re^3,O^1)	3.4	16.8	21.7

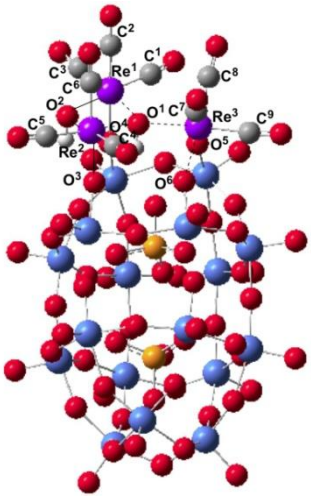

Figure 5-9 The notations used for important atoms

The central atom, O^1, can be assigned as hydroxide, i.e μ_3-OH, based on several arguments: 1) the "cap" $[\{Re(CO)_3\}_3\{ORb(H_2O)\}(\mu_3\text{-}OH)]^+$ is positively charged which makes it more likely stabilized by the anionic POM ligand; 2) the μ_3-OH assignment is consistent with the elemental analysis results and charge balance (counter ions: Rb^+ and K^+); 3) the experimental and computational torsional angles compare well as mentioned above; 4) the bond distances (Re^1-O^1: 2.162; Re^2-O^1: 2.186; Re^3-O^1: 2.156 Å) are similar to those in $[Re_3(CO)_9(\mu_3\text{-}OH)(\mu\text{-}OH)_3]^-$ (mean values: Re-O 2.167 Å), but longer than the ones in $[Re_3(CO)_9(\mu_3\text{-}O)(GlycH_{-3})]^{2-}$ (Glyc = glycerol; mean values: Re-O 2.122 Å);[59-62] 5) intramolecular hydrogen bonds are likely present between O^1 and the bridging oxygen atoms in $[\alpha_2\text{-}P_2W_{17}O_{61}]^{10-}$ which can further stabilize the structure (**Figure 5-8**);

5.3.2. Steady-state spectroscopy

The charge-transfer studies in the CO_2 reduction catalyst (2,2'-bipyridyl)Re(CO),[63-65] and in some POM-supported mono-metal carbonyl complexes,[55] as well as in other POM–photosensitizer dyads,[66-69] inspired us to investigate the photochemical properties of **5.1**. As seen in **Figure 5-1** and **Figure 5-12**, the UV-vis spectrum of **5.1** shows an intense broad absorption covering the entire UV and visible region extending to ~700 nm with a high absorptivity (ε_{400nm} ~3,500 $M^{-1}\cdot cm^{-1}$ in water) comparable with many rhenium (I) polybipyridyl photosensitizers (e.g. ε_{370nm} ~2500 $M^{-1}\cdot cm^{-1}$ for $(bpy)Re(CO)_3Cl$ in MeCN).[65] The precursors $[\alpha_2\text{-}P_2W_{17}O_{61}]^{10-}$ and $[Re(CO)_3]^+$ only have the ligand-to-metal charge-transfer (LMCT) transitions below ~350 nm, so this visible absorption of **5.1** is likely due to metal-to-polyoxometalate charge-transfer (MPCT) transition from the Re

centers to the POM ligands.[55] The stability of **5.1** has also been evaluated: the UV-visible spectrum of **5.1** stored in solution for several days exhibits no obvious change.

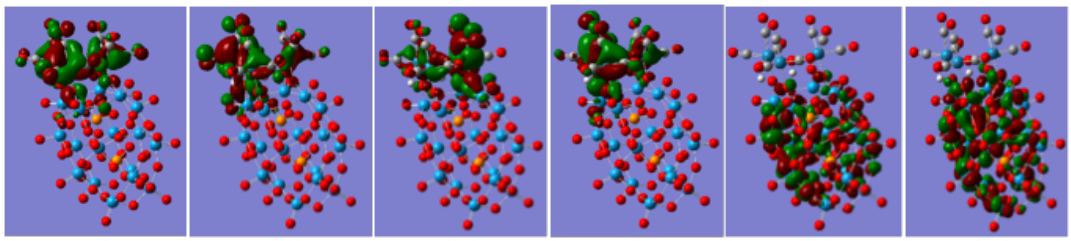

Figure 5-10 Several highest occupied (HOMO, or H) and lowest unoccupied (LUMO, or L) orbitals and their orbital energies (in Hartree) of the model complex **m2**.

The calculated frontier orbitals (**Figure 5-10**) and UV spectra (see **Figure 5-11**, **Table 5-3** and **Table 5-4**) of **m2** support the experimental conclusions given above and reveal important details. As seen in **Figure 5-10**, the HOMO orbital is entirely localized on the $[\{Re(CO)_3\}(\mu_2\text{-}O^2H)(\mu_3\text{-}O^1H)]$ fragment of $[P_2W_{17}O_{61}\{Re(CO)_3\}_3(\mu_2\text{-}O^2H)(\mu_3\text{-}O^1H)]^{9-}$, **m2**. Contributions from the Re^1 and Re^2 atoms to the HOMO are dominant. Close examination of this orbital reveals a noticeable overlap between the orbitals of Re^2 and O^3 (see **Figure 5-9**). In contrast, the LUMO of **m2** is a purely POM-based orbital consisting predominantly of W-O anti-bonding π* orbitals.

As in **Figure 5-11**, the UV spectrum of **m2** has a relatively narrow double feature on the 350-550 nm range. All bright transitions that make up this feature are excitations from doubly occupied Re d orbitals to the virtual POM orbitals (**Table 5-3**). No excitations originating on a Re orbital and ending on a virtual Re orbital are found among the 50 calculated states (**Table 5-4**). Such transitions can be expected to occur at wavelengths shorter than 350 nm.

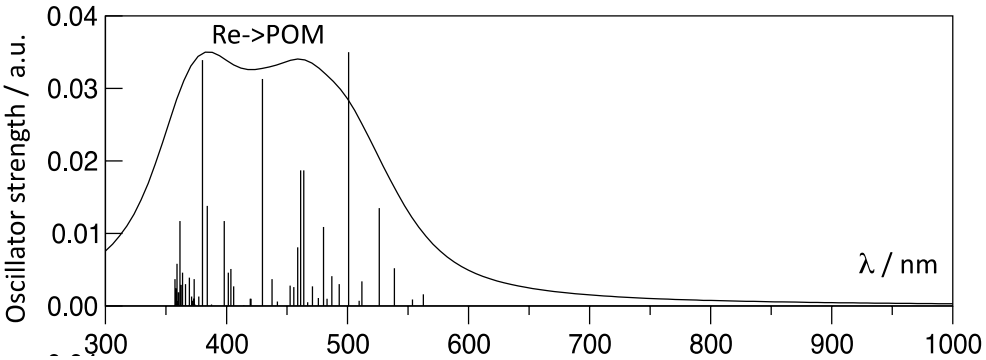

Figure 5-11 UV spectra of S_0 state of model complex **m2**

Table 5-3 Low energy singlet and triplet excited states of complex **m2**

	E/eV	**λ/nm**	**Osc. str.**	**Char.**
T_1	2.152	576		$H \rightarrow L$
S_1	2.203	562	0.0016	$H \rightarrow L$
T_2	2.203	562		$H_{-1} \rightarrow L$
S_2	2.239	553	0.0009	$H_{-1} \rightarrow L$
T_3	2.263	547		$H_{-3} \rightarrow L$; $H \rightarrow L$
S_3	2.301	538	0.0052	$H_{-2} \rightarrow L$
T_4	2.287	542		$H_{-2} \rightarrow L$
S_4	2.356	526	0.0135	$H_{-3} \rightarrow L$

Table 5-4 Singlet excited states of m2 computed with TD-DFT

Sn	**E/eV**	**λ/nm**	**f/a.u.**
S_1	2.2035	562.68	0.0016
S_2	2.2397	553.56	0.0009
S_3	2.3017	538.65	0.0052
S_4	2.3565	526.13	0.0135
S_5	2.3944	517.82	0.0000
S_6	2.4224	511.83	0.0034
S_7	2.4332	509.56	0.0007
S_8	2.4757	500.81	0.0350
S_9	2.5139	493.19	0.0030
S_{10}	2.5458	487.02	0.0041
S_{11}	2.5672	482.96	0.0010
S_{12}	2.5822	480.16	0.0109
S_{13}	2.6051	475.92	0.0011
S_{14}	2.6325	470.97	0.0027
S_{15}	2.6550	466.98	0.0005
S_{16}	2.6732	463.81	0.0187
S_{17}	2.6881	461.23	0.0187
S_{18}	2.7022	458.82	0.0081

S_{19}	2.7211	455.64	0.0026
S_{20}	2.7396	452.57	0.0028
S_{21}	2.8054	441.95	0.0006
S_{22}	2.8334	437.59	0.0037
S_{23}	2.8857	429.66	0.0313
S_{24}	2.9507	420.18	0.0010
S_{25}	2.9545	419.64	0.0010
S_{26}	2.9930	414.25	0.0001
S_{27}	3.0543	405.93	0.0027
S_{28}	3.0723	403.55	0.0051
S_{29}	3.0881	401.50	0.0046
S_{30}	3.1143	398.12	0.0117
S_{31}	3.1981	387.68	0.0002
S_{32}	3.2275	384.15	0.0138
S_{33}	3.2615	380.14	0.0339
S_{34}	3.2847	377.46	0.0000
S_{35}	3.2884	377.04	0.0013
S_{36}	3.3164	373.85	0.0002
S_{37}	3.3222	373.20	0.0037
S_{38}	3.3254	372.84	0.0010
S_{39}	3.3349	371.78	0.0007
S_{40}	3.3408	371.12	0.0013
S_{41}	3.3569	369.34	0.0039
S_{42}	3.3864	366.12	0.0030
S_{43}	3.4100	363.59	0.0046
S_{44}	3.4211	362.41	0.0029
S_{45}	3.4292	361.56	0.0117
S_{46}	3.4409	360.32	0.0019
S_{47}	3.4447	359.93	0.0006
S_{48}	3.4534	359.02	0.0058
S_{49}	3.4614	358.19	0.0024
S_{50}	3.4685	357.46	0.0037

5.3.3. Transient spectroscopy

Femtosecond visible pump-probe spectroscopy was used to study the charge-transfer dynamics. As shown in **Figure 5-12**, the transient absorption spectra of **5.1** show a new broad absorption species with a maximum at ~620 nm. Upon electrochemical reduction of **5.1** at multiple potentials, broad absorption bands (~600 – 1000 nm) in different shapes appear with maxima around 600 to 700 nm (**Figure 5-12**, **Figure 5-13**, **Figure 5-14**), which are consistent with other compounds containing a reduced $[\alpha_2\text{-}P_2W_{17}O_{61}]^{10-}$ unit.[70-72] All these new absorption bands can be attributed to the well-documented W(V) d-d and

W(V)-W(VI) inter-valence charge-transfer (IVCT) transitions in the reduced Wells-Dawson POMs, known as "heteropoly blues".[73-79] Note that the electrochemical spectra also show some absorption in the near-IR region (~800 – 1000 nm). We probed the transient spectra in this region and found an enhanced absorption feature, consistent with a "heteropoly blue" species,[80,81] containing a maximum at ~920 nm (**Figure 5-12**). The kinetics of this photo-induced absorption feature were monitored at 620 nm and 920 nm and fitted by a multi-exponential function. The two traces show identical kinetics (**Figure 5-15** and **Figure 5-16**). The best fit yields an instantaneous formation of the excited state within the time resolution of measurement (~150 fs) and its bi-exponential decay (~0.4 and 4.8 ps) to form a "hot" ground state (**Table 5-5**; see more details below).

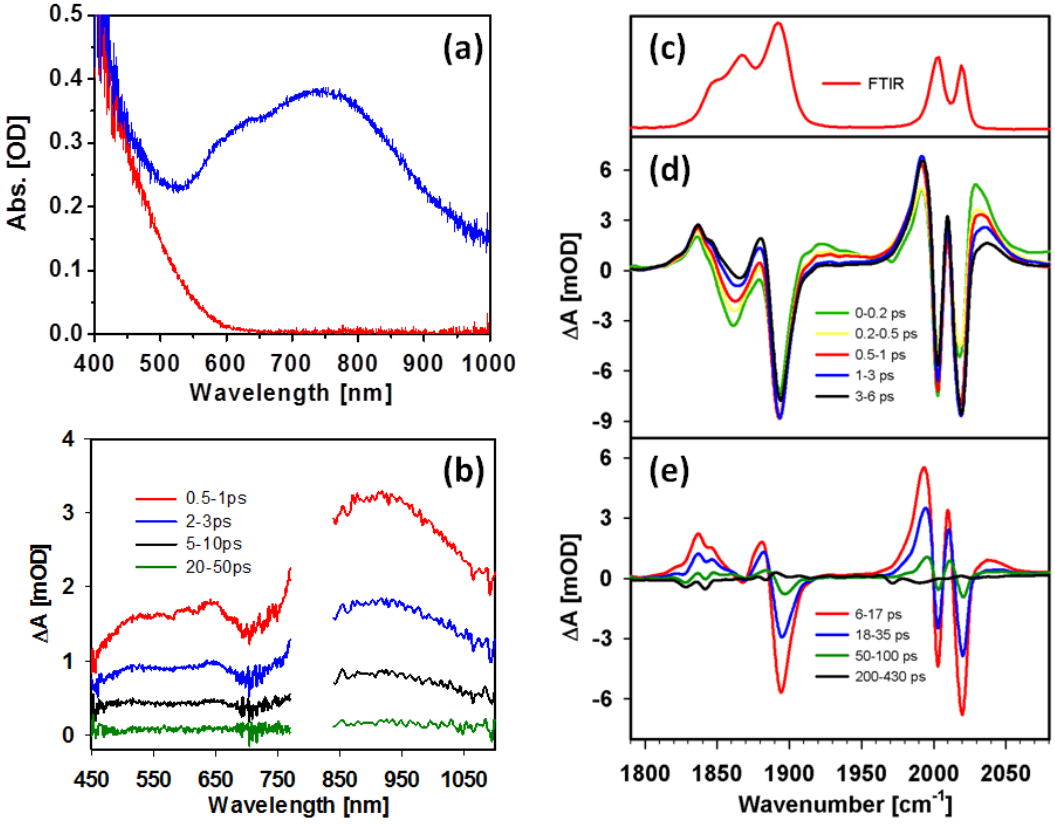

Figure 5-12 (a) Ground state UV-vis absorption spectra of **5.1** (red) and electrochemically reduced **5.1** (blue) generated at an applied potential of -0.65 V vs. Ag/AgCl in sodium acetate

buffer recorded in an electrochemical cell. (b) Average visible-to-near IR transient absorption spectra of **5.1** in CH_2Cl_2 at indicated delay time windows after 400 nm excitation. (c) Ground state FTIR spectrum of **5.1** in CH_2Cl_2. (d,e) Vis-pump/IR-probe transient spectra of **5.1** in CH_2Cl_2 at indicated delay times (d, 0 – 6 ps; e, 6 – 430 ps) windows after 400 nm excitation.

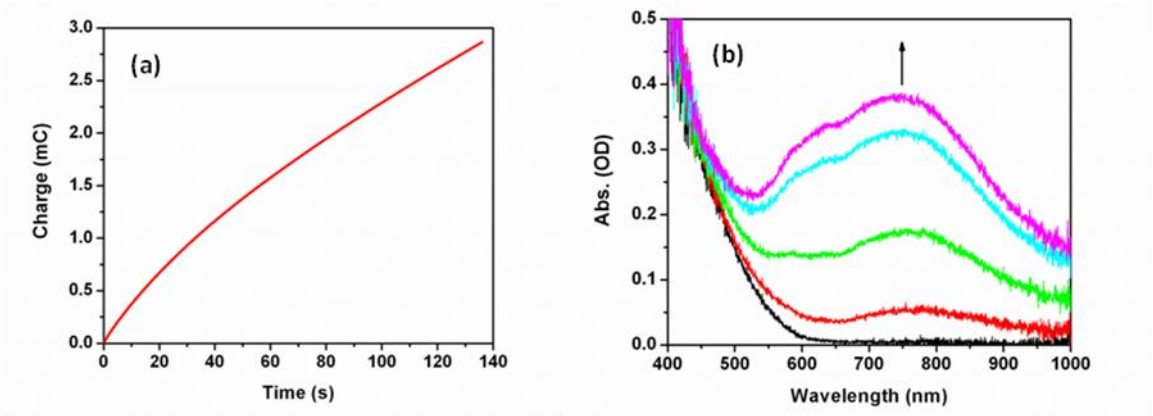

Figure 5-13 (a) Bulk electrolysis of **5.1** at a FTO slide working electrode in the sodium acetate buffer. (b) Electronic absorption spectra recorded during the electrochemical reduction of **5.1** at -0.65 V *vs.* Ag/AgCl.

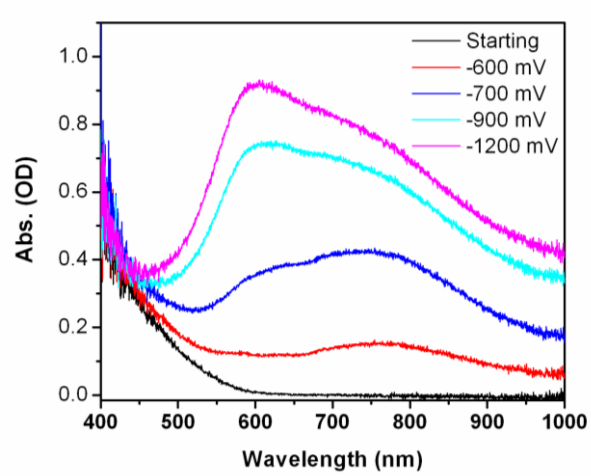

Figure 5-14 Electronic absorption spectra recorded during the electrochemical reduction of **5.1** with different applied potentials *vs.* Ag/AgCl. Each spectrum was recorded well after no further changes were apparent.

Time-resolved infrared spectroscopy provides detailed information on the excited states of rhenium carbonyl complexes owing to their high sensitivity to electron-density distribution. Since the entire molecule has low symmetry (C_1), the three Re(I) centers are

asymmetrically bridged, and each $[Re(CO)_3]^+$ moiety has local C_{3v} symmetry, the triple sets of three IR-active C-O stretching modes, two symmetric and one anti-symmetric, are coupled and overlapped. As shown in **Figure 5-12**, the ground-state FTIR spectra are complicated which show approximately 3:2 stretching bands in the lower and higher wavelength regions respectively (1847, 1868, 1892 cm^{-1}; 2002, 2019 cm^{-1}).

Figure 5-12 shows the transient absorption spectra in the short and long time scales. Excitation into the MPCT band at 400 nm results in the depletion of the ν(CO) ground state bands at approximately 1865, 1894, 2003 and 2020 cm^{-1} and instantaneous formation of two new blue-shifted absorption bands at ~1924 and 2031 cm^{-1}, relative to the ground-state positions. Dynamic shifts to higher energies of the excited-state bands are due to relaxation processes and are consistent with the formation of the MPCT excited state. The dynamic of the excited state absorption bands at 1924 and 2031 cm^{-1} can be fit to a tri-exponential function with $\tau_1 = 60 \pm 20$ fs (formation time), $\tau_2 = 0.50 \pm 0.4$ ps and $\tau_3 = 5 \pm 2$ ps and $\tau_1 = 60 \pm 20$ fs (formation time), $\tau_2 = 0.87 \pm 0.3$ ps and $\tau_3 = 4.7 \pm 2$ ps, respectively. The decay components (τ_2, τ_3) are assigned to the formation of "hot" ground state molecules and agree very well with the formation time of two new positive absorption bands at 1837 and 1992 cm^{-1}. These hot ground state absorption bands are red-shifted relative to the parent bands (**Figure 5-15**, **Figure 5-17** and **Table 5-6**). These hot ground state (HGA) formation times also agree well with the decay of the excited state absorption at 920 and 620 nm (**Figure 5-12**). Once the "hot" ground state molecules are totally formed with a time constant of ~10 ps (**Figure 5-12**), both the recovery of the GSB and the decay of the HGA happen on a similar time scales of

approximately 27 ps. The similar kinetics therefore suggest that the slow decays are due to vibrational cooling.

To completely understand the vibrational dynamics of ν(CO) in **5.1** and the nature of the hot ground state, we performed transient IR-pump/IR-probe experiments monitoring the vibrational relaxation following IR excitation at ~1870 cm^{-1} and 2007 cm^{-1}, respectively. As shown in **Figure 5-18**, at early delay times the transient IR-pump/IR-probe spectra consist of instantaneous bleaches of the ground state CO stretches (υ=0 to υ=1 transition) and the corresponding excited state absorptions (υ=1 to υ=2 transition) at ~1884, 1876, 1996 and 2013 cm^{-1}. Spectra at longer delay times show that all the GSB and HGA bands recover and decay on very similar time scales. These results are consistent with the relaxation of the molecules back to the ground vibrational state. The results and fitting parameters are given in **Figure 5-19** and **Table 5-7**. Both the GSB and HGA are characterized by ultrafast response times in the sub-picosecond time scale following by a bi-exponential decay of the υ = 1 population with time constants of approximately τ_2 = 0.3 ps and τ_3 = 26 ps. All traces show nearly identical kinetics with values within the experimental error, implying that their relaxation pathways are the same. We attribute the ultrafast decay component to the coupling between the different carbonyl stretching modes, and the slower decay component to the total vibrational population relaxation time. Our results are in agreement with previous studies on the vibrational relaxation dynamics of several metal carbonyl complexes.[82-85] Both the spectra and kinetics of the hot ground state generated by IR excitation of the CO stretching modes **Figure 5-18** and **Figure 5-19**) agree well with the hot ground state generated by 400 nm excitation of the MPCT state (**Figure 5-12**), suggesting that HGA

features in the latter are due to the formation of υ = 1 states of the CO stretching modes upon relaxation from the excited state. Finally, a general energy-level diagram displaying the MPCT process in this novel inorganic donor (tri-rhenium) – acceptor (POM) system is shown in **Figure 5-15**.

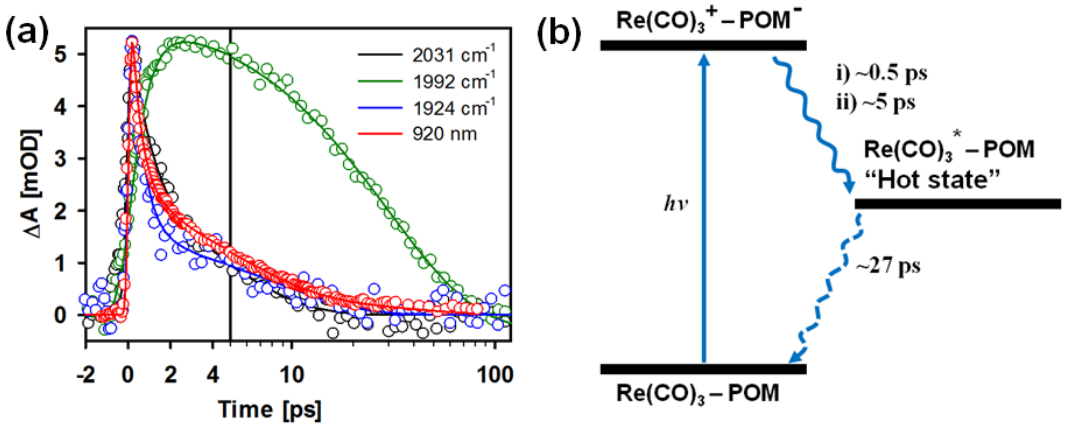

Figure 5-15 (a) Transient kinetics of **5.1** in CH_2Cl_2 at 920 nm (red), 1924 cm^{-1} (blue), 1992 cm^{-1} (green) and 2031 cm^{-1} (black) after 400 nm excitation. Solid lines show the multiple-exponential fits. The delay time is on a linear scale in the left panel (-2 to 5 ps) and a logarithmic scale in the right panel (5 – 120 ps). (b) Energy-level diagram of the electron-transfer steps involved in the charge-separation processes in **5.1**.

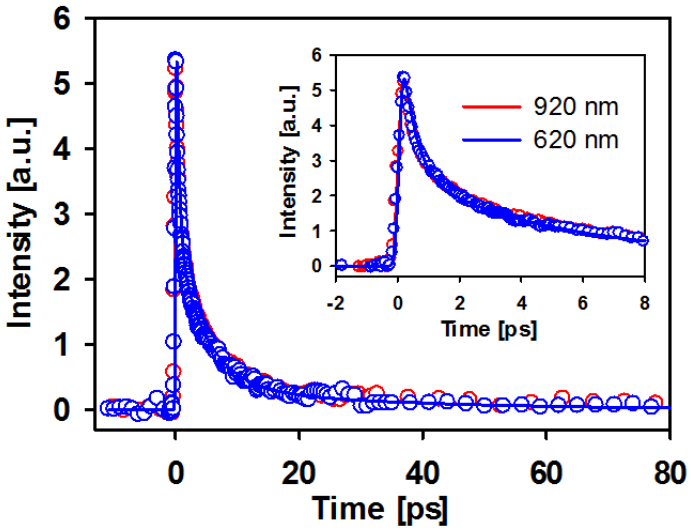

Figure 5-16 Transient kinetics of **5.1** in CH_2Cl_2 after 400 nm excitation. Also shown are multiple-exponential fits to the kinetics (solid line). The insets show the transient kinetics in the first ten picoseconds.

Table 5-5 Fitting parameters for kinetic traces after 400 nm excitation. The kinetic traces were modeled as multi-exponential decays analytically convoluted with the instrument response function.

Wavelength	α_1	τ_1 [ps]	α_2	τ_2 [ps]	α_3	τ_3 [ps]	α_4	τ_4 [ps]
920	-1	0.059 ± 0.03	0.61	0.42 ± 0.4	0.34	4.8 ± 3	0.05	31.5
620	-1	0.059 ± 0.03	0.62	0.43 ± 0.4	0.33	4.6 ± 3	0.05	31.7

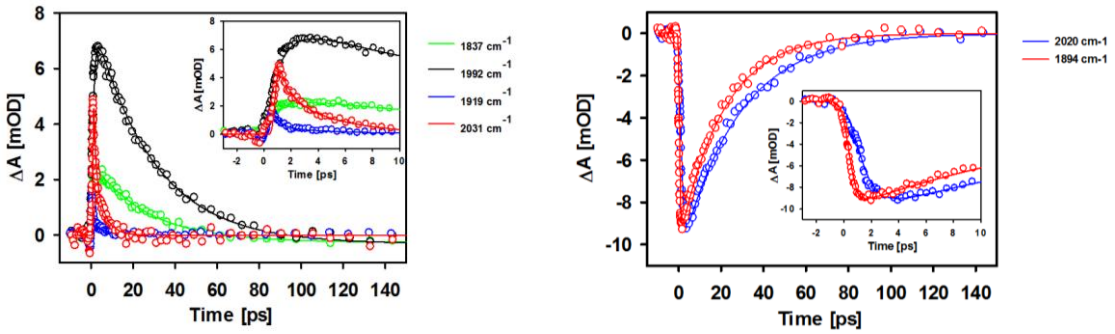

Figure 5-17 Vis-pump/IR-probe transient kinetics of different traces of **5.1** in CH_2Cl_2 after 400 nm excitation. Solid lines are convoluted multi-exponential fits to the data. The insets show the transient kinetics in the first ten picoseconds.

Table 5-6 Fitting parameters for the GSB and EA kinetics for the **5.1** in in CH_2Cl_2 after 400 nm excitation. The kinetic traces were modeled as multi-exponential decays analytically convoluted with the instrument response function.

Wavelength	α_1	τ_1 [fs]	α_2	τ_2 [ps]	α_3	τ_3 [ps]
1865	1	60 ± 20	-0.71	0.43 ± 0.4	-0.29	3.8 ± 2
1924	-1	60 ± 20	0.77	0.50 ± 0.4	0.23	5.0 ± 2
2031	-1	60 ± 20	0.66	0.87 ± 0.3	0.34	4.7 ± 2
1837	-0.84	60 ± 20	-0.16	0.80 ± 0.2	1	27 ± 2
1992	-0.83	60 ± 20	-0.17	0.76 ± 0.2	1	29 ± 2
2020	0.88	60 ± 20	0.12	0.79 ± 0.2	-1	28 ± 2
2003	1	60 ± 20	-0.14	0.69 ± 0.3	-0.86	26 ± 2
1894	0.90	60 ± 20	0.10	0.81 ± 0.1	-1	22 ± 3

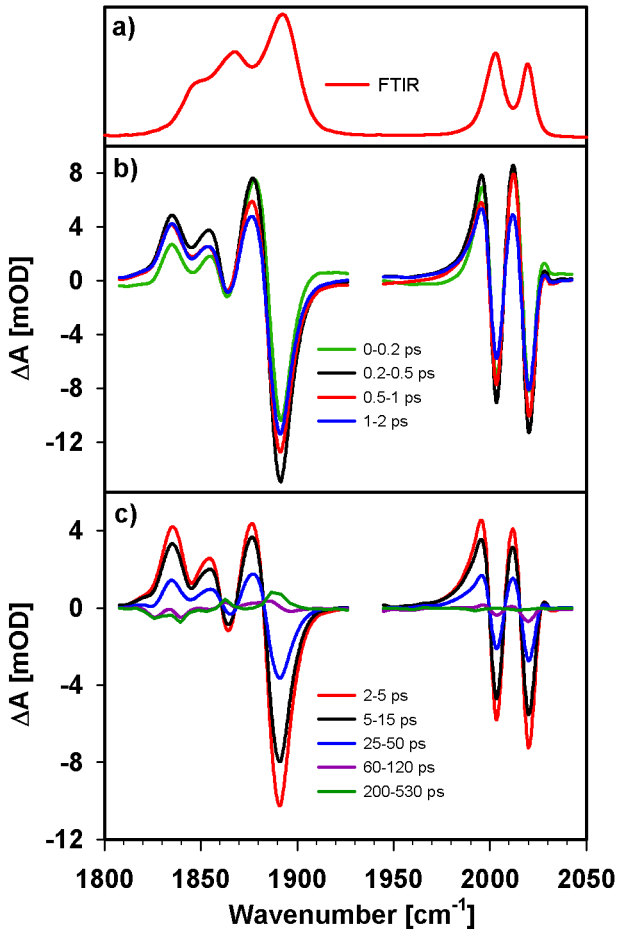

Figure 5-18 IR-pump/IR-Probe transient spectra of **5.1** in CH_2Cl_2 at indicated delay time windows averaged. Ground state FTIR spectrum a) and transient absorption spectra in the short b) and long c) time scale.

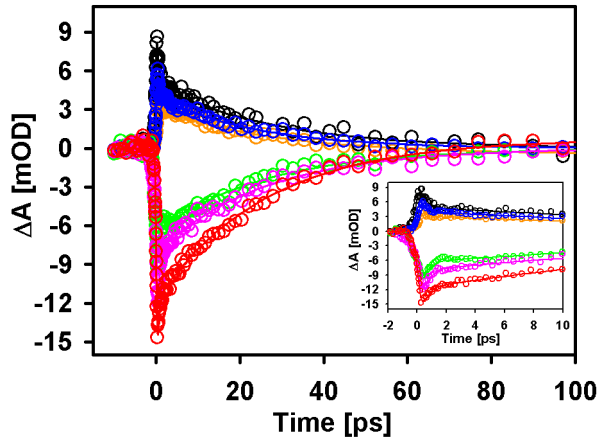

Figure 5-19 IR-pump/IR-Probe transient kinetics of **5.1** in CH_2Cl_2 at 1830 cm^{-1} (orange), 1876 cm^{-1} (black), 1891 cm^{-1} (red), 1992 cm^{-1} (blue), 2003 cm^{-1} (green), 2019 cm^{-1} (pink). Solid lines are convoluted multiexponential fits to the data. The insets show the transient kinetics in the first ten picoseconds time scale.

Table 5-7 Fitting parameters for the GSB and EA kinetics for **5.1** in CH_2Cl_2 after mid-IR excitation. The kinetic traces were modeled as multi-exponential decays analytically convoluted with the instrument response function.

Wavelength	α_1	τ_1 [ps]	α_2	τ_2 [ps]	α_3	τ_3 [ps]
1830	-1	0.057 ± 0.02	0.22	0.28 ± 0.2	0.78	29 ± 2
1876	-1	0.050 ± 0.02	0.49	0.30 ± 0.3	0.51	28 ± 2
1891	1	0.058 ± 0.02	-0.16	0.31 ± 0.2	-0.84	26 ± 2
1992	-1	0.061 ± 0.02	0.25	0.38 ± 0.2	0.75	24 ± 3
2003	1	0.057 ± 0.02	-0.29	0.35 ± 0.2	-0.71	26 ± 2
2019	1	0.059 ± 0.02	-0.30	0.29 ± 0.2	-0.70	26 ± 3

5.3.4. Computational modeling of CO streching

To further complement the details of reported IR and transient absorption spectra of compound **5.1**, we again turned to computation. Inspection of the S_0 IR spectrum shows that the CO portions of the spectrum appear in two manifolds, a broad, structured triplet in the 1850-1960 cm^{-1} range and a narrower doublet in the 2020-2080 cm^{-1} range (**Figure**

5-20 and **Table 5-8**), which is consistent with the experiments. Individual features of each manifold are assigned based on the Re center involvement, i.e., the first peak involves Re^1 and Re^2 centers, with very little Re^3, and the second peak is mainly Re^3 with smaller mixture of Re^1 and Re^2. The assignments reveal that the triplet manifold consists of six distinct out-of-phase super-positions of anti-symmetric local CO stretches. In all six peaks, up to five CO bond stretches are strongly involved. The doublet manifold is comprised of three peaks, which are out-of-phase (the first two) and in-phase (the third) super-positions of symmetric local CO stretches.

Table 5-8 Vibrational frequencies (**ω**; cm^{-1}) and IR intensities (km/mol) of the carbonyl groups of **m2**. The combinations of Re centers are in the order of decreasing magnitude according to contributions.

ω(S_0)	**IR(S_0)**	**ω(T_1)**	**IR(T_1)**	**Character**
1868	601	1868	680	$Re^2 + Re^1$
1889	671	1890	590	$Re^3 + Re^2 + Re^1$
1899	1140	1906	1076	$Re^2 + Re^1 + Re^3$
1925	35	1923	78	$Re^1 + Re^3$
1932	2361	1931	1861	$Re^3 + Re^1$
1947	1185	1961	1657	Re^2
2031	580	2028	687	$Re^3 + Re^1$
2039	1302	2037	1443	$Re^1 + Re^2 + Re^3$
2057	906	2062	1239	Re^2

The $\mathbf{T_1}$ state of **m2** is characterized by the HOMO-LUMO excitation, which removes an electron mainly from Re^1 and Re^2 centers and to a lesser degree from the Re^3 center. Electronic spin density shows that there is ~0.8 of unpaired spin on the Re^2-O^3 bond. The IR CO spectrum reflects the change experienced by the electron density. The deviations of the $\mathbf{T_1}$ lineshape from that of $\mathbf{S_0}$ occur at frequencies with the most activity from the Re^2 group of CO's. At 1900 cm^{-1}, the 2-1-3 peak shifts to the blue by about 10 cm^{-1}. There is an even larger blue shift at ~1950 cm^{-1} where there is strong CO activity on the Re^2 center. Another shift can be seen at ~2060 cm^{-1} where another dominant CO mode on

Re^2 is located. Although the agreement of the computed and measured IR spectra is not quantitative, the observed blue shift of the CO stretching bands upon excitation of the complex is well reproduced in the computed spectrum, consistent with the nature of an MPCT transition.

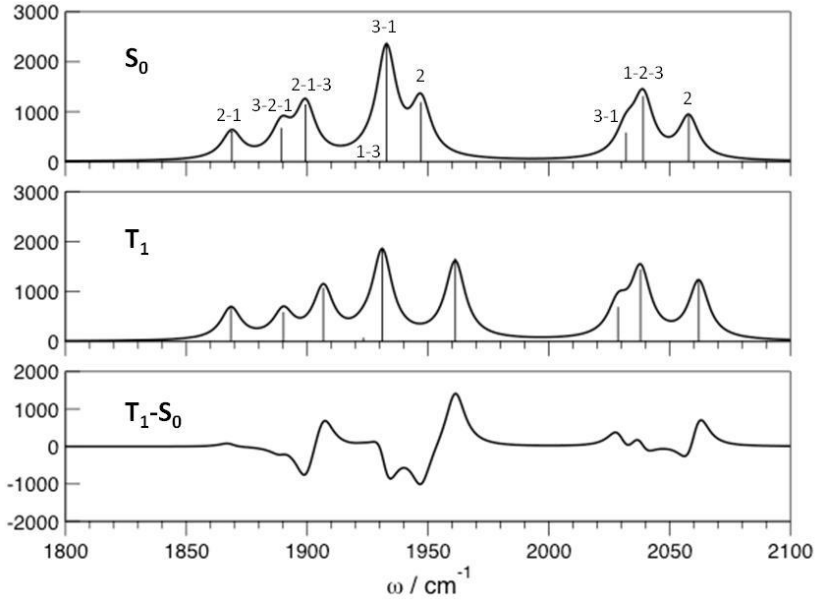

Figure 5-20 IR spectra of the model complex **m2** in the CO range of S_0 (top), T_1 (middle) and difference spectra (bottom). Peak labels show Re^I-Re^J-Re^K center involvement in the order of decreasing magnitude, where any I, J, K index can be 1, 2 or 3.

5.4 Conclusion

In conclusion, we report for the first time a molecular representation of the much studied TiO_2-$Ru(bpy)_3$ Grätzel diad systems in the form of an inorganic dye donor covalently bonded to a redox active metal oxide-like POM acceptor, $[P_2W_{17}O_{61}\{Re(CO)_3\}_3\{ORb(H_2O)\}(\mu_3\text{-}OH)]^{9-}$, **5.1**. Comprehensive investigation of the photophysical properties of **5.1** using computational and two different time-resolved spectroscopic methods clearly reveal the presence of a metal-to-polyoxometalate charge

transfer (MPCT) transition. The stepwise mechanism of charge-separation and charge-recombination process has been established.

References

(1) Serpone, N.; E.Pelizzetti; Gratzel, M. *Coord. Chem. Rev.* **1985**, *64*, 225.

(2) Grätzel, M. *Nature* **2001**, *414*, 338.

(3) Ardo, S.; Meyer, G. J. *Chem. Soc. Rev.* **2009**, *38*, 115.

(4) Youngblood, W. J.; Lee, S.-H. A.; Kobayashi, Y.; Hernandez-Pagan, E. A.; Hoertz, P. G.; Moore, T. A.; Moore, A. L.; Gust, D.; Mallouk, T. E. *J. Am. Chem. Soc.* **2009**, *131*, 926.

(5) Brimblecombe, R.; Koo, A.; Dismukes, G. C.; Swiegers, G. F.; Spiccia, L. *J. Am. Chem. Soc.* **2010**, *132*, 2892.

(6) Li, L.; Duan, L.; Xu, Y.; Gorlov, M.; Hagfeldt, A.; Sun, L. *Chem. Commun.* **2010**, *46*, 7307.

(7) Moore, G. F.; Blakemore, J. D.; Milot, R. L.; Hull, J. F.; Song, H.-e.; Cai, L.; Schmuttenmaer, C. A.; Crabtree, R. H.; Brudvig, G. W. *Energy Environ. Sci.* **2011**, *4*, 2389.

(8) Song, W.; Brennaman, M. K.; Concepcion, J. J.; Jurss, J. W.; Hoertz, P. G.; Luo, H.; Chen, C.; Hanson, K.; Meyer, T. J. *J. Phys. Chem. C* **2011**, *115*, 7081.

(9) Li, G.; Sproviero, E. M.; McNamara, W. R.; III, R. C. S.; Crabtree, R. H.; Brudvig, G. W.; Batista, V. S. *J. Phys. Chem. B* **2010**, *114*, 14214.

(10) Lin, W.; Frei, H. *J. Am. Chem. Soc.* **2005**, *127*, 1610.

(11) Han, H.; Frei, H. *J. Phys. Chem. C* **2008**, *112*, 16156.

(12) Nakamura, R.; Okamoto, A.; Osawa, H.; Irie, H.; Hashimoto, K. *J. Am. Chem. Soc.* **2007**, *129*, 9596.

(13) Takashima, T.; Yamaguchi, A.; Hashimoto, K.; Nakamura, R. *Chem. Commun.* **2012**, *48*, 2964.

(14) Nozik, A. J. *Ann. Rev. Phys. Chem.* **1978**, *29*, 189.

(15) Tan, M. X.; Laibinis, P. E.; Nguyen, S. T.; Kesselman, J. M.; Stanton, C. E.; Lewis, N. S. In *Prog. Inorg. Chem.*; Karlin, K. D., Ed.; Wiley & Sons: 1994; Vol. 41, p 21.

(16) Prezhdo, O. V. *Acc. Chem. Res.* **2009**, *42*, 2005.

(17) Hoffmann, M. R.; Martin, S. T.; Choi, W.; Bahnemann, D. W. *Chem. Rev.* **1995**, *95*, 69.

(18) Nozik, A. J.; Beard, M. C.; Luther, J. M.; Law, M.; Ellingson, R. J.; Johnson, J. C. *Chem. Rev.* **2010**, *110*, 6873.

(19) Pope, M. T.; Müller, A. *Angew. Chem. Int. Ed.* **1991**, *30*, 34.

(20) *Special Thematic Issue on Polyoxometalates*; Hill, C. L., Ed., 1998; Vol. 98, No. 1.

(21) Hill, C. L.; Prosser-McCartha, C. M. *Coord. Chem. Rev.* **1995**, *143*, 407.

(22) Okuhara, T.; Mizuno, N.; Misono, M. *Advances in Catalysis* **1996**, *41*, 113.

(23) Neumann, R. *Prog. Inorg. Chem.* **1998**, *47*, 317.

(24) Long, D.-L.; Tsunashima, R.; Cronin, L. *Angew. Chem. Int. Ed.* **2010**, *49*, 1736.

(25) Miras, H. N.; Yan, J.; Long, D.-L.; Cronin, L. *Chem. Soc. Rev.* **2012**, *41*, 7403.

(26) Edwards, D. A.; Marshalsea, J. *J. Organomet. Chem.* **1977**, *131*, 73.

(27) Bruker AXS, I.; Analytical X-ray Sysems: Madison, WI, 2003.

(28) Bruker AXS, I.; Analytical X-ray Systems: Madison, WI, 2003.

(29) Sheldrick, G.; 4th edition ed. 2007.

(30) Sheldrick, G. M. *SHELXL-97, Program for the Refinement of Crystal Structures*; University of Göttingen: Germany, 1997.

(31) Becke, A. D. *J. Chem. Phys.* **1993**, *98*, 5648.

(32) Lee, C.; Yang, W.; Parr, R. G. *Phys. Rev. B* **1988**, *37*, 785.

(33) Hay, P. J.; Wadt, W. R. *J. Chem. Phys.* **1985**, *82*, 270.

(34) Hay, P. J.; Wadt, W. R. *J. Chem. Phys.* **1985**, *82*, 299.

(35) Wadt, W. R.; Hay, P. J. *J. Chem. Phys.* **1985**, *82*, 284.

(36) Tomasi, J.; Persico, M. *Chem. Rev.* **1994**, 2027.

(37) Cammi, R.; Tomasi, J. *J. Comput. Chem.* **1995**, *16*, 1449.

(38) Rappe, A. K.; Casewit, C. J.; Colwell, K. S.; Goddard, W. A.; Skiff, W. M. *J. Am. Chem. Soc.* **1992**, *114*, 10024.

(39) Ahlrichs, R.; Bär, M.; Baron, H.-P.; Bauernschmitt, R.; Böcker, S.; Crawford, N.; Deglmann, P.; Ehrig, M.; Eichkorn, K.; Elliott, S.; Furche, F.; Haase, F.; Häser, M.; Hättig, C.;

Hellweg, A.; Horn, H.; Huber, C.; Huniar, U.; Kattannek, M.; Köhn, A.; Kölmel, C.; Kollwitz, M.; May, K.; Nava, P.; Ochsenfeld, C.; Öhm, H.; Patzelt, H.; Rappoport, D.; Rubner, O.; Schäfer, A.; Schneider, U.; Sierka, M.; Treutler, O.; Unterreiner, B.; Arnim, M. v.; Weigend, F.; Weis, P.; Weiss, H.; Universität Karlsruhe, Institüt fur Physikalische Chemie und Elektrochemie, Lehrstuhl für Theoretische Chemie: 2008.

(40) Frisch, M. J.; Trucks, G. W.; Schlegel, H. B.; Scuseria, G. E.; Robb, M. A.; Cheeseman, J. R.; Scalmani, G.; Barone, V.; Mennucci, B.; Petersson, G. A.; Nakatsuji, H.; Caricato, M.; Li, X.; Hratchian, H. P.; Izmaylov, A. F.; Bloino, J.; Zheng, G.; Sonnenberg, J. L.; Hada, M.; Ehara, M.; Toyota, K.; Fukuda, R.; Hasegawa, J.; Ishida, M.; Nakajima, T.; Honda, Y.; Kitao, O.; Nakai, H.; Vreven, T.; J. A. Montgomery, J.; Peralta, J. E.; Ogliaro, F.; Bearpark, M.; Heyd, J. J.; Brothers, E.; Kudin, K. N.; Staroverov, V. N.; Kobayashi, R.; Normand, J.; Raghavachari, K.; Rendell, A.; Burant, J. C.; Iyengar, S. S.; Tomasi, J.; Cossi, M.; N. Rega, J. M. M.; Klene, M.; Knox, J. E.; Cross, J. B.; Bakken, V.; Adamo, C.; Jaramillo, J.; Gomperts, R.; Stratmann, R. E.; Yazyev, O.; Austin, A. J.; Cammi, R.; Pomelli, C.; Ochterski, J. W.; Martin, R. L.; K. Morokuma, V. G. Z.; Voth, G. A.; Salvador, P.; Dannenberg, J. J.; Dapprich, S.; Daniels, A. D.; Ö. Farkas, J. B. F.; Ortiz, J. V.; Cioslowski, J.; Fox, D. J.; Revision A.1 ed.; Gaussian, I., Ed. Wallingford CT., 2009.

(41) Quiñonero, D.; Wang, Y.; Morokuma, K.; Khavrutskii, L. A.; Botar, B.; Geletii, Y. V.; Hill, C. L.; Musaev, D. G. *J. Phys. Chem.* **2006**, *110*, 170.

(42) Wang, Y.; Zheng, G.; Morokuma, K.; Geletii, Y. V.; Hill, C. L.; Musaev, D. G. *J. Phys. Chem: B* **2006**, *110*, 5230.

(43) Kulkarni, A.; Lobo-Lapidus, R. J.; Gates, B. C. *Chem. Commun.* **2010**, *46*, 5997.

(44) Hu, A. G.; Neyman, K. M.; Staufer, M.; Belling, T.; Gates, B. C.; Rosch, N. *J. Am. Chem. Soc.* **1999**, *121*, 4522.

(45) Fierro-Gonzalez, J. C.; Kuba, S.; Hao, Y. L.; Gates, B. C. *J. Phys. Chem. B* **2006**, *110*, 13326.

(46) Knoth, W. H. *J. Am. Chem. Soc.* **1979**, *101*, 2211.

(47) Besecker, C. J.; Klemperer, W. G. *J. Am. Chem. Soc.* **1980**, *25*, 7598.

(48) Klemperer, W. G.; Main, D. J. *Inorg. Chem.* **1990**, *29*, 2355.

(49) Siedle, A. R.; Lyon, P. A.; Hodgson, K. O.; Roe, A. L. *Inorg. Chem.* **1987**, *26*, 219.

(50) Nagata, T.; Pohl, B. M.; Weiner, H.; Finke, R. G. *Inorg. Chem.* **1997**, *36*, 1366.

(51) Besserguenev, A. V.; Dickman, M. H.; Pope, M. T. *Inorg. Chem.* **2001**, *40*, 2582.

(52) Villanneau, R.; Delmont, R.; Proust, A.; Gouzerh, P. *Chem. Eur. J.* **2000**, *6*, 1184.

(53) Villanneau, R.; Proust, A.; Robert, F.; Gouzerh, P. *Chem. Eur. J.* **2003**, *9*, 1982.

(54) Sadakane, M.; Iimuro, Y.; Tsukuma, D.; Bassil, B. S.; Dickman, M. H.; Kortz, U.; Zhang, Y.; Ye, S.; Ueda, W. *Dalton Trans.* **2008**, 6692.

(55) Zhao, C.; Huang, Z.; Rodríguez-Córdoba, W.; Kambara, C. S.; O'Halloran, K. P.; Hardcastle, K. I.; Musaev, D. G.; Lian, T.; Hill, C. L. *J. Am. Chem. Soc.* **2011**, *133*, 20134.

(56) Niu, J.; Yang, L.; Zhao, J.; Ma, P.; Wang, J. *Dalton Trans.* **2011**, *40*, 8298.

(57) Zhao, J.; Zhao, J.; Ma, P.; Wang, J.; Niu, J.; Wang, J. *J. Mol. Struct.* **2012**, *1019*, 61.

(58) Zhao, C.; Kambara, C. S.; Yang, Y.; Kaledin, A. L.; Musaev, D. G.; Lian, T.; Hill, C. L. *Inorg. Chem.* **2013**, *52*, 671.

(59) Alberto, R.; Egli, A.; Abram, U.; Hegetschweiler, K.; Gramlich, V.; Schubiger, P. A. *J. Chem. Soc., Dalton Trans.* **1994**, 2815.

(60) Egli, A.; Hegetschweiler, K.; Alberto, R.; Abram, U.; Schibli, R.; Hedinger, R.; Gramlich, V.; Kissner, R.; Schubiger, P. A. *Organometallics* **1997**, *16*, 1833.

(61) Herrmann, W. A.; Egli, A.; Herdtweck, E.; Alberto, R.; Baumgärtner, F. *Angew. Chem. Int. Ed.* **1996**, *35*, 432.

(62) Hinrichs, M.; Hofbauer, F. R.; Klufers, P. *Chem. Eur. J.* **2006**, *12*, 4675.

(63) Hawecker, J.; Lehn, J.-M.; Ziessel, R. *J. Chem. Soc., Chem. Commun.* **1983**, 536.

(64) Kalyanasundaram, K. *J. Chem. Soc., Faraday Trans. 2* **1986**, *82*, 2401.

(65) Ziessel, R.; Juris, A.; Venturi, M. *Inorg. Chem.* **1998**, *37*, 5061.

(66) Matt, B.; Xiang, X.; Kaledin, A. L.; Han, N.; Moussa, J.; Amouri, H.; Alves, S.; Hill, C. L.; Lian, T.; Musaev, D. G.; Izzet, G.; Proust, A. *Chem. Sci.* **2013**, *4*, 1737.

(67) Odobel, F.; Séverac, M.; Pellegrin, Y.; Blart, E.; Fosse, C.; Cannizzo, C.; Mayer, C. R.; Elliott, K. J.; Harriman, A. *Chem. Eur. J.* **2009**, *15*, 3130.

(68) Harriman, A.; Elliott, K. J.; Alamiry, M. A. H.; Pleux, L. L.; Séverac, M.; Pellegrin, Y.; Blart, E.; Fosse, C.; Cannizzo, C.; Mayer, C. R.; Odobel, F. *J. Phys. Chem. C* **2009**, *113*, 5834.

(69) Allain, C.; Favette, S.; Chamoreau, L.-M.; Vaissermann, J.; Ruhlmann, L.; Hasenknopf, B. *Eur. J. Inorg. Chem.* **2008**, 3433.

(70) Haraguchi, N.; Okaue, Y.; Isobe, T.; Matsuda, Y. *Inorg. Chem.* **1994**, *33*, 1015.

(71) Sun, W.; Yang, F.; Liu, H.; Kong, J.; Jin, S.; Xie, G.; Deng, J. *J. Electroanal. Chem.* **1998**, *451*, 49.

(72) Gao, G.; Xu, L.; Wang, W.; An, W.; Qiu, Y. *J. Mater. Chem.* **2004**, *14*, 2024.

(73) Sanchez, C.; Livage, J.; Launay, J. P.; Fournier, M.; Jeannin, Y. *J. Am. Chem. Soc.* **1982**, *104*, 3194.

(74) Kozik, M.; Hammer, C. F.; Baker, L. C. W. *J. Am. Chem. Soc.* **1986**, *108*, 7627.

(75) Kozik, M.; Casañ-Pastor, N.; Hammer, C. F.; Baker, L. C. W. *J. Am. Chem. Soc.* **1988**, *110*, 7697.

(76) Papaconstantinou, E. *Chem. Soc. Rev.* **1989**, *18*, 1.

(77) Yamase, T. *Chem. Rev.* **1998**, *98*, 307.

(78) Renneke, R. F.; Kadkhodayan, M.; Pasquali, M.; Hill, C. L. *J. Am. Chem. Soc.* **1991**, *113*, 8357.

(79) Hill, C. L.; Kozik, M.; Winkler, J.; Hou, Y.; Prosser-McCartha, C. M. *Adv. Chem. Ser.* **1993**, *238*, 243.

(80) Yamase, T.; Usami, T. *J. Chem. Soc., Dalton Trans.* **1988**, 183.

(81) Duncan, D. C.; Netzel; L., T.; Hill, C. L. *Inorg. Chem.* **1995**, *34*, 4640.

(82) Beckerle, J. D.; Casassa, M. P.; Cavanagh, R. R.; Heilweil, E. J.; Stephenson, J. C. *Chem. Phys.* **1992**, *160*, 487.

(83) Tokmakoff, A.; Sauter, B.; Kwok, A. S.; Fayer, M. D. *Chem. Phys. Lett.* **1994**, *221*, 412.

(84) Lian, T.; Bromberg, S. E.; Yang, H.; Proulx, G.; Bergman, R. G.; Harris, C. B. *J. Am. Chem. Soc.* **1996**, *118*, 3769.

(85) Gabrielsson, A.; Hartl, F.; Zhang, H.; Smith, J. R. L.; Towrie, M.; Antonín Vlček, J.; Perutz, R. N. *J. Am. Chem. Soc.* **2006**, *128*, 4253.

Chapter 6

Cobalt(II) and Tin(II) Complexes Based-on Trivacant Polyoxoanion Ligands: Synthesis, Structures, Physicochemistry and Catalytic Water Oxidation Activity

6.1 Introduction

In **Chapter 1**, we briefly discussed the general properties of POMs, and their emergent applications in the generation of solar fuels and construction of porous materials. Previously a large effort was devoted to studying the catalytic activities of POMs.[1,2] Recently POMs as all-inorganic and stable catalysts have garnered much attention for water oxidation.[3-9] Water-oxidation is a key step in photosynthesis. The development of stable and efficient water-oxidation catalysts (WOCs) is crucial for artificial photosynthesis.[10,11] One new method to make tunable WOCs is by replacing the less-stable organic ligands with all-inorganic and water-compatible POM ligands. Recently, the Hill group and the Bonchio group simultaneously reported the synthesis and structure of $[Ru^{IV}_4O_4(OH)_2(OH_2)_4(\gamma\text{-}SiW_{10}O_{36})_2]^{12-}$ (**Ru4**), and its catalytic water oxidation activity.[4,12] Subsequently, the Hill group reported two Ru/Ir- substituted POMs, $[(\gamma\text{-}PW_{10}O_{36})_2Ru^{IV}_4O_6(OH_2)_4]^{10-}$ and $[(IrCl_4)KP_2W_{20}O_{72}]^{14-}$, as WOCs.[13,14] A more significant POM WOC is $[Co_4(H_2O)_2(PW_9O_{34})_2]^{10-}$ (**Co4**), which is composed of only earth abundant elements while being very stable and efficient.[6] To date many groups have worked in this area. A list of all the POM-based WOCs can be found in a recent review.[15]

At the same time, POM chemistry has interfaced with metal-organic framework (MOF) chemistry. MOF, as noted in **Chapter 1**, are a large class of porous compounds with controllable composites and internal cavities. MOFs have potentially attractive applications in catalysis, magnetism, gas absorption and separation, drug delivery and photochromism.[16-18] Recently, nanoparticles were introduced into MOFs to realize synergistic catalytic structures.[19-22] In a similar manner, POMs have recently been

incorporated into the pores of MOFs. The resulting POM-modified MOFs or metal-organic cages exhibit promise for use in aerobic decontamination and artificial photosynthesis.[23-28]

Lacunary POMs with multi-vacant sites can accommodate several metal ions. Multi-transition-metal-substituted POMs display tunable catalytic and photochemical activities,[15,29-31] as well as some unusual architectures, i.e. giant POM-based "molecular wheels".[32-34] Instead of using organic linkages, POMs are ideal components to construct all-inorganic metal-oxo frameworks. Given the thermal stability of POMs and the diversity of transition metals, POM frameworks should be as robust as zeolites and mesporous silica,[35] yet also exhibit catalytic or photochemical activities (depending on the incorporated transition metal(s)). Nonetheless, these purely inorganic frameworks are little studied; only a limited number of examples derived from conventional plenary POMs have been reported.[36-40] The porous architectures involving transition-metal-substituted POMs were rarely observed. Cronin and co-workers recently discovered a giant porous structure, a Mn(II)-linked $[P_8W_{48}O_{184}]^{40-}$ POM framework, which has very large cavities and electronically controlled cation-exchange activities.[41]

We are interested in using the trivacant POM ligands such as $[\alpha\text{-}SiW_9O_{34}]^{10-}$, $[\alpha\text{-}GeW_9O_{34}]^{10-}$ and $[B\text{-}SbW_9O_{33}]^{9-}$ as precursors. In addition to the classical sandwich structures with tri-/tetra- nuclear metallic cores,[42-46] nanosized giant clusters with high nuclearity have gained recent attention in particular.[47-52] It is worthwhile noting that Krebs and co-authors have done systematic work on the dimerization of $[B\text{-}SbW_9O_{33}]^{9-}$. The resulting $[Sb_2W_{22}O_{74}(OH)]^{12-}$ was consequently used as versatile building-block to construct a large family of POMs, $[Sb_2W_{20}M_2O_{70}(H_2O)_6]^{(14-2n)-}$ (M = Fe^{3+}, Co^{2+}, Mn^{2+},

Ni^{2+}).[53] In **Chapter 2**, we also developed several inorganic-organic hybrid POM analogies with the metal carbonyl components.

Thus, three cobalt(II)-substituted POMs, $Na_{12}[\{Co(H_2O)\}_3(SbW_9O_{33})_2]\cdot 34H_2O$ (**6.1**), $Na_{13}H[\{Co(H_2O)\}\{CoCl\}_2(SbW_9O_{33})_2]\cdot 35H_2O$ (**6.2**) and $Na_{10}[\{Co(H_2O)_3\}_2\{WO_2\}_2(SbW_9O_{33})_2]\cdot 28H_2O$ (**6.3**), are reported in this section. We discovered that **6.1** and **6.2** are hydrolytically unstable and slowly convert to **6.3**. We evaluated the catalytic water-oxidation activity of **6.3**. We also attempted to build metal-oxide frameworks based on polynuclear Sn(II) POMs. Hexa- and nona-nuclear tin(II) POMs were prepared by reactions of $SnCl_2$ and tri-vacant POMs, $[B\text{-}SbW_9O_{33}]^{9-}$ and $[\alpha\text{-}XW_9O_{34}]^{10-}$ (X = Si or Ge). The nonanuclear derivatives, $[Na_7Si_2W_{18}Sn_9Cl_5O_{68}\cdot(H_2O)_{35}]_n$ (**6.4**) and $[Na_7Ge_2W_{18}Sn_9Cl_5O_{68}\cdot(H_2O)_{41}]_n$ (**6.5**), display all-inorganic, chloride-bridged, three-dimensional (3D) porous architectures with large, water-filled channels. The hexanuclear complex, $Na_6[\{Na(\mu\text{-}OH_2)(OH_2)_2\}_6\{Sn_6(B\text{-}SbW_9O_{33})_2\}_2]\cdot 50H_2O$ (**6.6**), exhibits as a "double-sandwich" through a polymeric aqua-Na^+ cation ring. These complexes show high absorption in the visible region. A comprehensive study including synthesis, structure and spectroscopy has been performed to characterize these unusual high nuclear compounds.

6.2 Experimental

6.2.1. Materials and Instrumentation

All chemicals were reagent grade and used as supplied. The tri-vacant polyoxometalate precursors $Na_{10}[\alpha\text{-}SiW_9O_{34}]\cdot nH_2O$, $Na_{10}[\alpha\text{-}GeW_9O_{34}]\cdot nH_2O$ and $Na_9[B\text{-}SbW_9O_{33}]\cdot nH_2O$, were prepared according to reported methods in the literatures.[54-56] Their purities were

determined through FT-IR spectroscopy. UV-vis spectra were acquired using an Agilent 8453 spectrophotometer equipped with a diode-array detector and an Agilent 89090A cell temperature controller unit. The FT-IR spectra were measured on a Thermo Nicolet 6700 spectrometer with KBr pellets (2%). Elemental analyses were performed by Galbraith Lab Inc., Knoxville, TN, 37921. Thermogravimetric analysis was acquired on a Perkin Elmer STA 6000 analyzer.

6.2.1. Syntheses

$Na_{12}[\{Co(H_2O)\}_3(SbW_9O_{33})_2]\cdot 34H_2O$ (**6.1**). $Co(NO_3)\cdot 6H_2O$ (0.29g, 1 mmol) and $Na_9SbW_9O_{33}\cdot 19.5H_2O$ (2.86g, 1 mmol) were dissolved in 0.5 M $NaNO_3$ aqueous solution. The mixture was heated at ~70 ^oC for 1 hr with constant stirring. The solution was then cooled to room temperature and filtered. The solution was left undisturbed and greenish block-shape crystals were obtained by slow evaporation after several days. Yield: 350 mg (60% based on Co^{2+}). Anal. Calcd. for $H_{74}Co_3Na_{12}Sb_2W_{18}O_{103}$: Na, 4.8; Co, 3.1; Sb, 4.3; W, 57.8. Found: Na, 5.0; Co, 3.3; Sb, 4.2; W, 60.2. FTIR (2% KBr pellet, 1100 – 400 cm^{-1}): 947 (s), 898 (m), 877 (s), 778 (m), 730 (m), 625(w). TGA: weight loss, 11.0% (30 – 500 ºC).

$Na_{13}H[\{Co(H_2O)\}\{CoCl\}_2(SbW_9O_{33})_2]\cdot 35H_2O$ (**6.2**). Compound **6.2** was synthesized by a similar procedure as **6.1**, but using $CoCl_2\cdot 6H_2O$ and NaCl solution during the reaction. Yield: 330 mg (55% based on Co^{2+}). Anal. Calcd. for $H_{73}Cl_2Co_3Na_{13}Sb_2W_{18}O_{102}$: Na, 5.1; Cl, 1.2; Co, 3.1; Sb, 4.2; W, 57.0. Found: Na, 4.9; Cl, 1.1; Co, 3.2; Sb, 4.1; W, 61.0. FTIR (2% KBr pellet, 1100 – 400 cm^{-1}): 940 (s), 895 (m), 875 (s), 780 (m), 730 (m), 630(w). TGA: weight loss, 11.7% (30 – 500 ºC).

$Na_{10}[\{Co(H_2O)_3\}_2\{WO_2\}_2(SbW_9O_{33})_2]\cdot 28H_2O$ (**6.3**). $Co(NO_3)\cdot 6H_2O$ (0.58g, 2 mmol) and $Na_9SbW_9O_{33}\cdot 19.5H_2O$ (5.72g, 2 mmol) were dissolved in 20 mL 1.0 M sodium acetate buffer (pH = 4.7). The solution was turning to purple-red color upon heating to ~70 ^oC for ~2 hours. Pink needle-like crystals were obtained after a week. The crystals were collected and then re-crystallized in 0.5 M NaCl aqueous solution (pH = 6.5). Purple-pink needle-shape crystals were obtained overnight. Yield: 420 mg (35% based on Co^{2+}). Anal. Calcd. for $H_{68}Co_2Na_{10}Sb_2W_{20}O_{104}$: Na, 3.8; Co, 2.0; Sb, 4.0; W, 61.3. Found: Na, 3.8; Co. 1.8; Sb. 3.8; W, 58.2. FTIR (2% KBr pellet, 1100 – 400 cm^{-1}): 950 (s), 886 (m), 845 (s), 804 (s), 758 (m), 700 (m), 666(m). TGA: weight loss, 9.7% (30 – 500 ºC).

$[Na_7Si_2W_{18}Sn_9Cl_5O_{68}\cdot(H_2O)_{35}]_n$ (**6.4**). The pre-synthesized $Na_{10}[\alpha\text{-}SiW_9O_{34}]\cdot nH_2O$ (1.6 g, 0.6 mmol) was dissolved in 20 mL H_2O, followed by addition of 1.0 M HCl until the pH was ~6.7. The white solids gradually dissolve. $SnCl_2\cdot 2H_2O$ (285 mg, 1.25 mmol) was added to the above solution quickly. The solution color became orange immediately and simultaneously some white precipitate forms. The pH became ~2.0. NaCl (400 mg) was then added. The mixtures were heated to 70 ºC for 0.5 h and then cooled to room temperature and filtered. Orange needle-shape crystals were obtained from the filtrate after slow evaporation within a week. Yield: 430 mg (47% based on Sn). FTIR (1100 – 500 cm^{-1}; 2% KBr pellets): 996 (m), 948 (m), 890 (s), 786 (m), 687 (s), 646 (m), 532 (w). Electronic spectra data (350 – 700 nm, in DMF/H_2O = 10/1 mixed solution): $\varepsilon_{400\ nm}$ ~1800 $M^{-1}\cdot cm^{-1}$. Anal. Calcd. for $H_{70}O_{103}Cl_5Na_7Si_2Sn_9W_{18}$: Cl, 2.7; Na, 2.5; Si, 0.86; Sn, 16.5; W, 51.0. Found: Cl, 2.5; Na, 2.4; Si, 0.84; Sn, 15.5; W, 49.6. TGA: weight loss, 9.7% (30 – 500 ºC; "$35H_2O$") and 2.7% (500 – 700 ºC; "5Cl").

$[Na_7Ge_2W_{18}Sn_9Cl_5O_{68}\cdot(H_2O)_{41}]_n$ (**6.5**). A similar procedure was used as above except using $Na_{10}[\alpha\text{-}GeW_9O_{34}]\cdot nH_2O$ (1.7 g, 0.6 mmol). Yield: 370 mg (40% based on Sn). FTIR (1100 – 500 cm^{-1}; 2% KBr pellets): 945 (m), 880 (s), 797 (s), 683 (s), 639 (m), 526 (w). Electronic spectra data (350 – 700 nm, in DMF/H_2O = 10/1): $\varepsilon_{400\ nm}$ ~1800 $M^{-1}\cdot cm^{-1}$. Anal. Calcd. for $H_{82}O_{109}Cl_5Na_7Ge_2Sn_9W_{18}$: Cl, 2.7; Na, 2.4; Ge, 2.2; Sn, 16.0; W, 49.5. Found: Cl, 2.3; Na, 2.2; Ge, 1.9; Sn, 15.1; W, 47.1. TGA: weight loss, 11.0% (30 – 500 ºC; "41H_2O") and 2.7% (500 – 700 ºC; "5Cl").

$Na_6[\{Na(\mu\text{-}OH_2)(OH_2)_2\}_6\{Sn_6(B\text{-}SbW_9O_{33})_2\}_2]\cdot 50H_2O$ (**6.6**). $Na_9[B\text{-}SbW_9O_{33}]\cdot nH_2O$ (1.6 g, 0.6 mmol) was dissolved in 0.5 M NaCl solution. Then pH was adjusted to ~6.5 by adding 1.0 M HCl. $SnCl_2\cdot 2H_2O$ (285 mg, 1.25 mmol) was added and the mixtures were heated for 15 min. The solution then was filtered for slow evaporation and red crystals were obtained within two days. Yield: 370 mg (40% based on Sn). FTIR (1100 – 500 cm^{-1}; 2% KBr pellets): 943 (s), 905 (m), 857 (m), 789 (s), 718 (s), 667 (s). Electronic spectra data (350 – 700 nm, in DMF/H_2O = 10/1): $\varepsilon_{400\ nm}$ ~1.05×10^4 $M^{-1}\cdot cm^{-1}$. Anal. Calcd. for $H_{136}O_{200}Na_{12}Sb_4Sn_{12}W_{36}$: Na, 2.3; Sb, 4.0; Sn, 11.7; W, 54.5. Found: Na, 2.2; Sb, 3.7; Sn, 11.2; W, 55.0. TGA: weight loss, 7.3% (30 – 500 ºC; "50H_2O").

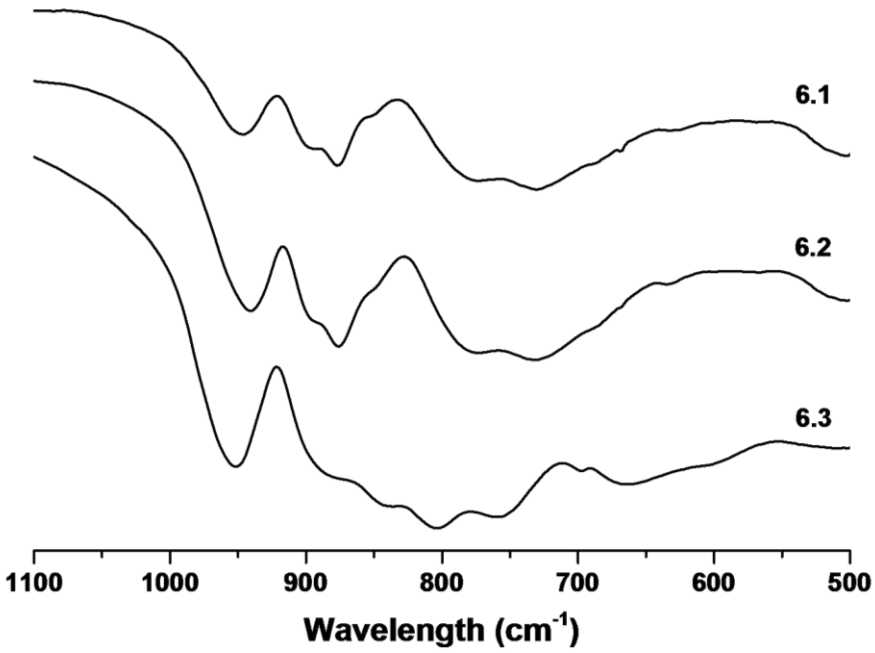

Figure 6-1 FTIR spectra for **6.1**, **6.2** and **6.3** in the range of 1100 to 500 cm^{-1} (2% KBr pellet)

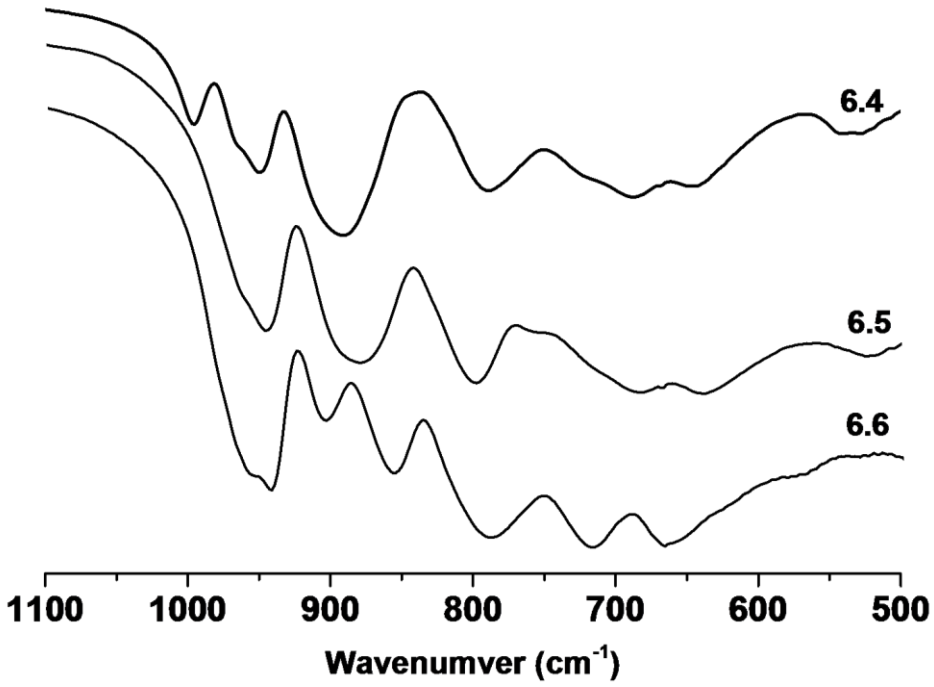

Figure 6-2 FTIR spectra for **6.4**, **6.5** and **6.6** in the range of 1100 to 500 cm^{-1} (2% KBr pellet)

6.2.2. X-Ray crystallography

Single crystals suitable for X-ray structure analysis were each coated with Paratone-N oil, suspended on a small fiber loop and placed in a cooled nitrogen gas stream at 173 K on a Bruker D8 APEX II CCD sealed tube diffractometer with graphite-monochromated Mo Kα (λ = 0.71073 Å) radiation. Data collection, indexing and initial cell refinements were all carried out using SMART.[57] Frame integration and final cell refinements were done using SAINT.[58] The molecular structure of each complex was determined using direct methods and Fourier techniques, and refined by the standard full-matrix least-squares procedure. A multiple absorption correction, including face indexing, was applied using the program SADABS.[59] The largest residual electron density for each structure was located close to (less than 1.0 Å from) the W atoms and was most likely due to imperfect absorption corrections frequently encountered in heavy-metal atom structures. Structure solution, refinement, graphic and generation of publication materials were performed by using SHELXTL, v 6.14 software.[60] The crystal data and structure refinement parameters are summarized in **Table 6-1**.

Table 6-1 Crystal data and structural refinement for the X-ray structure analyses of **6.1**, **6.2**, **6.3**, **6.4**, **6.5** and **6.6**.

	6.1	**6.2**	**6.3**
Molecular formula	$H_{74}O_{103}Co_3Na_{12}Sb_2W_{18}$	$H_{73}O_{102}Cl_2Co_3Na_{13}Sb_2W_{18}$	$H_{68}O_{104}Co_2Na_{10}Sb_2W_{20}$
Formula wt. / g mol^{-1}	5727.84	5804.73	6000.56
Temperature / K	173(2)	173(2)	173(2)
Crystal system	Monoclinic	Triclinic	Monoclinic
Space group	*C*2/c	*P*-1	*P*2(1)/n
a / Å	14.157(7)	13.1847(12)	12.830(4)
b / Å	23.069(12)	17.9900(17)	25.017(8)
c / Å	32.352(19)	21.013(2)	15.820(5)
α / °	90.00	79.2970(10)	90.00
β / °	99.133(8)	86.0660(10)	93.765(5)
γ / °	90.00	69.4620(10)	90.00
V / Å^3	10432(10)	4586.0(7)	5067(3)

Z	4	2	2
ρ_{calcd} / g cm^{-3}	3.722	4.151	3.962
μ / mm^{-1}	20.905	23.822	23.605
Reflections collected	88037	78761	84975
Independent refl. (R_{int})	12452 (0.0575)	21827 (0.1472)	12061 (0.0879)
Goodness-of-fit on F^2	1.098	1.013	1.032
Final R indices [$R > 2\sigma(I)$]	R_1[a] = 0.0330, wR_2[b] = 0.0865	R_1[a] = 0.0454, wR_2[b] = 0.1149	R_1[a] = 0.0510, wR_2[b] = 0.1735
	6.4	**6.5**	**6.6**
Molecular formula	$H_{70}O_{103}Cl_5Na_7Si_2Sn_9W_{18}$	$H_{82}O_{109}Cl_5Na_7Ge_2Sn_9W_{18}$	$H_{136}O_{200}Na_{12}Sb_4Sn_{12}W_{36}$
Formula wt. / g mol^{-1}	6490.37	6687.51	12142.64
Temperature / K	173(2)	173(2)	173(2)
Crystal system	Tetragonal	Tetragonal	Rhombohedral
Space group	$P4_2/ncm$	$P4_2/ncm$	R-3
a / Å	21.438(4)	21.416(3)	17.778(5)
b / Å	21.438(4)	21.416(3)	17.778(5)
c / Å	23.126(4)	23.133(3)	45.221(13)
α / °	90	90	90
β / °	90	90	90
γ / °	90	90	120
V / Å^3	10629(3)	10610(2)	12378(6)
Z	4	4	6
ρ_{calcd} / g cm^{-3}	3.696	3.758	4.506
μ / mm^{-1}	21.697	22.268	27.514
Reflections collected	93868	58692	13110
Independent refl. (R_{int})	5454 (0.1042)	5861 (0.0895)	6271 (0.0674)
Goodness-of-fit on F^2	1.151	1.177	1.031
Final R indices [$R > 2\sigma(I)$]	R_1[a] = 0.0685, wR_2[b] = 0.1948	R_1[a] = 0.0666, wR_2[b] = 0.1747	R_1[a] = 0.0773, wR_2[b] = 0.2633

$R_1 = \Sigma\ ||F_0|-|F_c||/\Sigma|F_0|$; $wR_2 = \{\Sigma[w(F_0^2-F_c^2)^2/\Sigma w(F_0^2)^2]\}^{1/2}$

6.3 Results and Discussion

6.3.1 Characterization of Cobalt(II) POMs

Complex **6.1** was synthesized in a chlorine-free environment. A similar structure was reported by Niu previously.[61] As shown in Figure 6-3, the conventional sandwich structure contains three Co^{2+} in the belt position and two $[SbW_9O_{33}]^{9-}$ ligands. Unlike Niu's compound, which shows a nearly hexagonal $\{Co_3Na_2K\}$ distribution in the belt

region, **6.1** contains a bimetallic hexagonal arrangement $\{Co_3Na_3\}$. Thus, **6.1** resides in an idealized D_{3h} point symmetry rather than $C_{2h.}$

Compound **6.2** was prepared under a similar conditions but with an excess amount of Cl^-. Its structure is analogous to **6.1**, but two terminal water molecules on Co^{2+} are replaced by Cl^-. Each Co^{2+} ion is located in a square pyramidal coordination geometry with Co-O distances from 1.983 Å to 2.051 Å on the basal plane. The axial position is occupied by a terminal water molecule, with a Co-O distance of 2.062 Å, or by a terminal Cl^- ion with a Co-Cl distance of 2.380 and 2.349 Å, respectively. The Co-O(H_2O) distance is similar to the ones in **6.1**. The longer Co-Cl bonds make the $\{CoO_4Cl\}$ moiety an elongated pyramid. The presence of Cl^- ion reduces the point group symmetry in **6.2** to an idealized C_{2h}.

Compound **6.3** has a similar structure to the one reported by Krebs previously.[53] The difference arises from the cations, which are Na^+ instead of NH_4^+. The selective bond lengths can be found in Table 6-2.

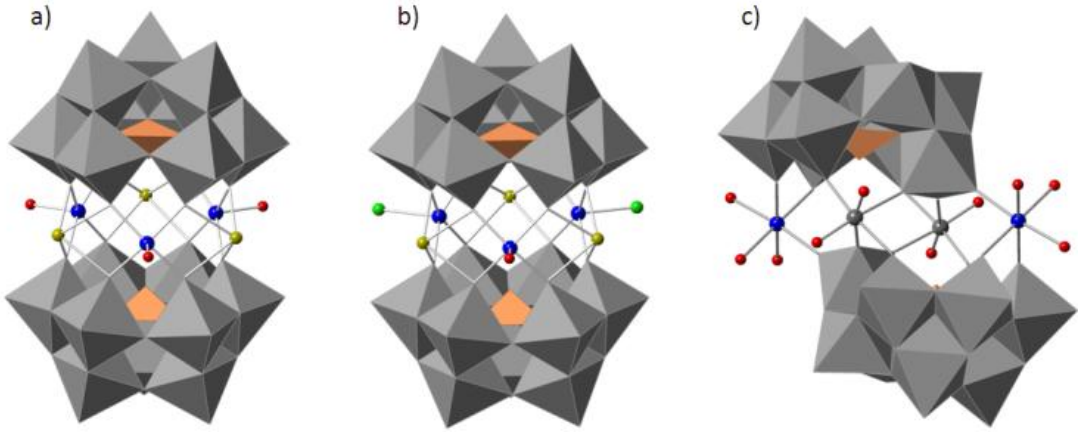

Figure 6-3 The X-ray structures of **6.1** (a), **6.2** (b) and **6.3** (c) in combined polyhedral and ball-and-stick notation (Some of the Na^+ and H_2O are omitted). Co: blue; O: red; Cl: green; WO_6 octahedra: gray; SbO_4 tetrahedra: brown.

Table 6-2 Selective bond lengths (Å)

	6.1	**6.2**	**6.3**
Sb-O	2.01-2.02	1.97-2.00	1.97-1.98
Co-O (bridged)	2.00-2.02	1.98-2.05	2.06-2.06
Co-O (terminal)	2.04-2.07	2.06	2.13-2.16
Co-Cl	-	2.35-2.38	-

Compound **6.1** and **6.2** are not stable in aqueous solution. We used UV-vis absorption spectroscopy to monitor the transformation of **6.1** and **6.2** and their subsequent conversion to **6.3**. A freshly-prepared aqueous solution of **6.1** shows a high absorption band at ~650 nm, which is consistent with the blue color of the starting solution. This low-energy absorption feature is due to the five-coordinate Co(II) centers. This absorption band decreases rapidly and finally disappears, while a new absorption feature at ~540 nm is forming, which is consistent with the apparent pink-color in the final solution. This absorption is due to the octahedral six-coordinate Co(II) center. Similar patterns are also observed in the UV-vis absorption spectrum of **6.2**. The final spectra are similar to that of **6.3**, which means that both **6.1** and **6.2** have been converted to **6.3**, the thermodynamically more stable species. Furthermore, crystals of **6.3** can be isolated from the above solutions of **6.1** and **6.2** after a few days. The stability of **6.3** was evaluated by back-and-forward titrations, as shown in Figure 6-5, the UV-vis spectra of **6.3** are highly reversible in the pH range of 3.8-6.6 and show an isosbestic point at ~525 nm.

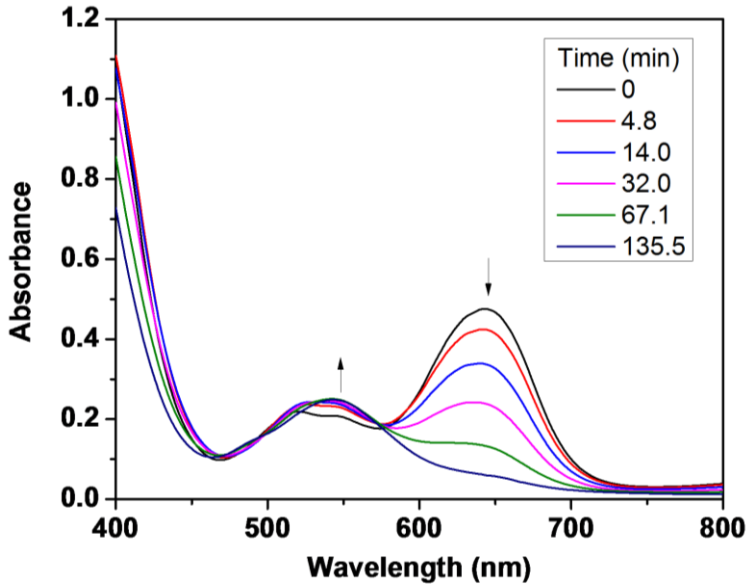

Figure 6-4 Time-dependent UV-vis absorption spectra of **6.1** in an aqueous solution

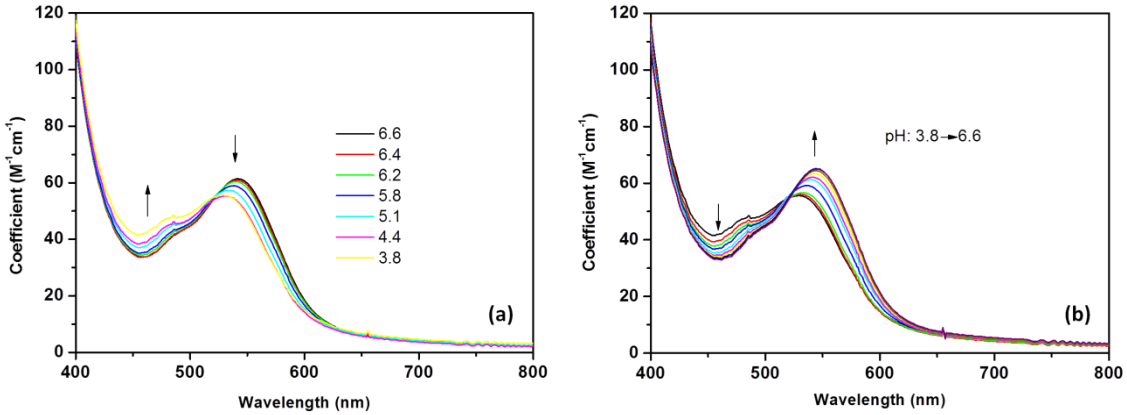

Figure 6-5 pH-dependent UV-vis absorption spectra of **6.3** in back-and-forward titration processes. Arrows indicate the changing directions.

6.3.2 Water-oxidation Activity of $Na_{10}[\{Co(H_2O)_3\}_2\{WO_2\}_2(SbW_9O_{33})_2]$

The catalytic water-oxidation activity of **6.3** was studied in a sodium borate buffer (pH 8.4). $[Ru(bpy)_3]^{2+}$ was used as the photosensitizer and $S_2O_8^{2-}$ as the sacrificial electron acceptor, which are well known to react as in eq 1.

$$2\ [Ru(bpy)_3]^{2+} + S_2O_8^{2-} + h\nu \rightarrow 2[Ru(bpy)_3]^{3+} + 2\ SO_4^{2-} \quad (1)$$

The light-driven mechanism has been well-studied.(ftnts) The excited state, $[Ru(bpy)_3]^{2+*}$, is quenched by $S_2O_8^{2-}$ resulting in $[Ru(bpy)_3]^{3+}$ and $SO_4^{\cdot-}$. The $SO_4^{\cdot-}$ consequently produces a second molecule of $[Ru(bpy)_3]^{3+}$. Finally four equivalents of $[Ru(bpy)_3]^{3+}$ oxidize two equivalents of water to produce O_2 and four protons (eq 2):

$$2\ S_2O_8^{2-} + 2\ H_2O + 2\ h\nu \rightarrow 4\ SO_4^{2-} + O_2 + 4\ H^+ \quad (2)$$

The O_2 yield in pH 8.5 buffer is shown in Figure 6-6. During ~15 mins reaction time, the reaction is complete because of depletion of all $S_2O_8^{2-}$ agents. The turnover number (TON) is approaching ~300 and the chemical yield is 0.42. The O_2 yield is related to the catalyst concentrations, which indicates that TON increases along with a higher catalyst concentration, but eventually it reaches a plateau.

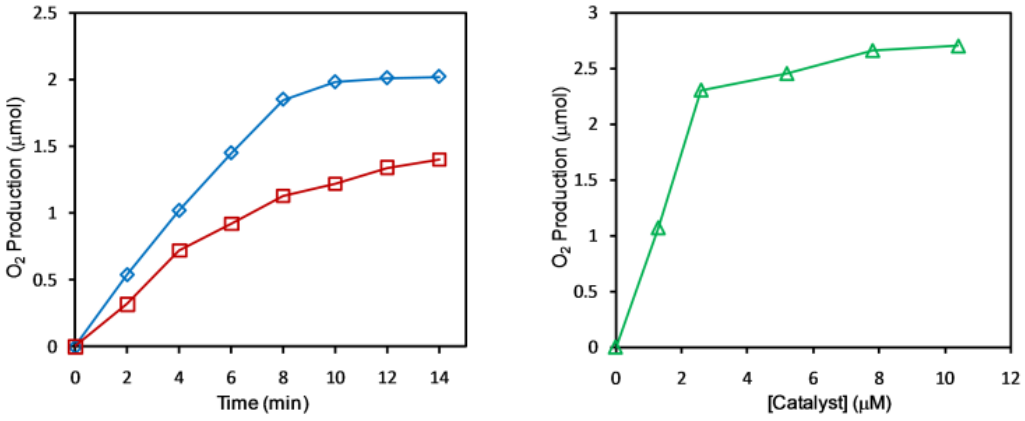

Figure 6-6 Kinetics of catalytic light-driven O_2 evolution from water. Conditions: LED, 455 nm, 17 mW light beam with a diameter of ~0.5 cm focused on the reaction solution, 1.0 mM $[Ru(bpy)_3]^{2+}$, 5.0 mM $Na_2S_2O_8$, 40 mM sodium borate buffer in a total reaction volume of 2.0 mL, vigorous agitation. Left: 1.8 µM catalyst in pH 8.4 (red squares) and pH 8.9 (blue diamond). Right: various catalyst concentrations in pH 8.4 (green triangle) after 15 minutes' reaction time.

6.3.3 Characterization of Tin(II) POMs

Although the organo-tin(IV)-substituted POMs have a rich chemistry,[45,62-64] very few tin(II)-containing POMs are known. The latter are $[Sn(SiW_{11}O_{39})]^{6-}$, $[Sn_3(\alpha$-

SiW9O34)$_2$]$^{14-}$, [Sn$_3$(α-PW$_9$O$_{34}$)$_2$]$^{12-}$, [Sn$_6$(SnW$_9$O$_{33}$)$_2$]$^{8-}$, [Sn$_3$(α-AsW$_9$O$_{34}$)$_2$]$^{12-}$ and [H$_3$SnW$_{18}$O$_{60}$]$^{7-}$,[65-71] and so on. Complexes **6.4** and **6.5** were prepared from the reaction of excess [α-XW$_9$O$_{34}$]$^{10-}$ and SnCl$_2$·2H$_2$O in an acidic aqueous solution (pH ~2.0). The extra POM ligand present stabilizes the Sn(II) ions with respect to aerobic oxidation to Sn(IV). Previously, the trinuclear POM [Sn$_3$(SiW$_9$O$_{34}$)$_2$]$^{14-}$ was made at pH 8 while the tetranuclear compound [Sn$_4$(SiW$_9$O$_{34}$)$_2$]$^{12-}$ was made at pH 4.[66,72] The SnCl$_2$ in these two preparations are in excess. Complexes **6.4** and **6.5** are iso-structural so we focus on **6.4** here. As seen in **Figure 6-7**, the structure of **6.4** consists of two [α-SiW$_9$O$_{34}$]$^{10-}$ anions linked by nine Sn(II) centers into an assembly of idealized D_{3h} symmetry. Bond valence sum (BVS) calculations of all nine tin centers range from 1.75 to 1.98, consistent with all being in the Sn(II) oxidation state. These two complexes contain the highest nuclearity of Sn centers in known POMs to our knowledge. The structure can be also viewed as a typical sandwich motif {Sn$_3$(XW$_9$)$_2$} (X = P or Si) surrounded by a 12-membered ring. {Sn$_6$Cl$_6$}. in the belt position (**Figure 6-7**). Compared to [Sn$_3$(SiW$_9$O$_{34}$)$_2$]$^{14-}$ and [Sn$_4$(SiW$_9$O$_{34}$)$_2$]$^{12-}$, in which each of the three internal Sn(II) centers is located in a pseudo-trigonal-bipyramidal SnO$_3$ geometry with Sn-O distances of 2.12 – 2.29 Å and Sn-O-Sn bond angles of 78.9º – 94.1º, in **6.4** the inner Sn(II) ions displays a SnO$_4$ seesaw molecular geometry. The Sn-O distances are from 2.25 to 2.29 Å; the O-Sn-O angles range from 114.5º – 115.9º (O$_{ax}$-Sn-O$_{ax}$, O$_{eq}$-Sn-O$_{eq}$) and 69.6º – 77.4º (O$_{ax}$-Sn-O$_{eq}$), respectively. The lone-pair of electrons on Sn(II) occupy the third equatorial position and point towards the C_3 axis of the anion.

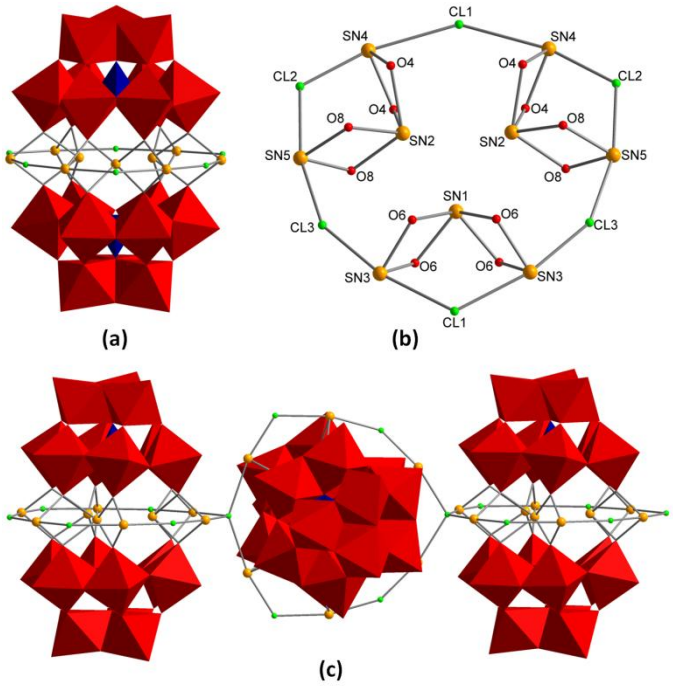

Figure 6-7 (a) X-ray structure of a single unit of **6.4** in combined bond-and-stick and polyhedral notation. (b) Representation of the central nine Sn(II) ions. Atoms with the same labels are symmetry equivalent. (c) 1D chain structure of **6.4** through μ_4-Cl bridges. Code: Cl, green; Sn, orange; SiO_4, blue; WO_6, red.

The $\{Sn_6Cl_6\}$ ring encircles the sandwich $[Sn_3(SiW_9O_{34})_2]^{14-}$ through oxo-bridged Sn-O-Sn bonds. The Sn-O-Sn bond angles are 106.2º – 107.3º. Each external Sn(II) ion resides in a seesaw-geometry SnO_2Cl_2 unit with two chlorides in the axial position and two oxygens in the equatorial position. The lone-pair of electrons face away from the central C_3 axis. The Cl-Sn-Cl bond angles are 165.5º – 166.5º while the O-Sn-O angles are 74.6º – 75.3º. The Sn-O bond distances are 2.12 – 2.15 Å, while Sn-Cl bonds are far longer (2.68 to 3.18 Å). The relatively shorter bond length is in the Sn-(μ_2-Cl)-Sn unit, while the longer length (2.94 and 3.18 Å) is in the Sn-(μ_4-Cl)-Sn unit. In the latter unit, the Cl ion is four-coordinate (inducing a consequently longer Sn-Cl bond) and bridges the adjacent $\{Sn_6Cl_6\}$ rings.[73-77]

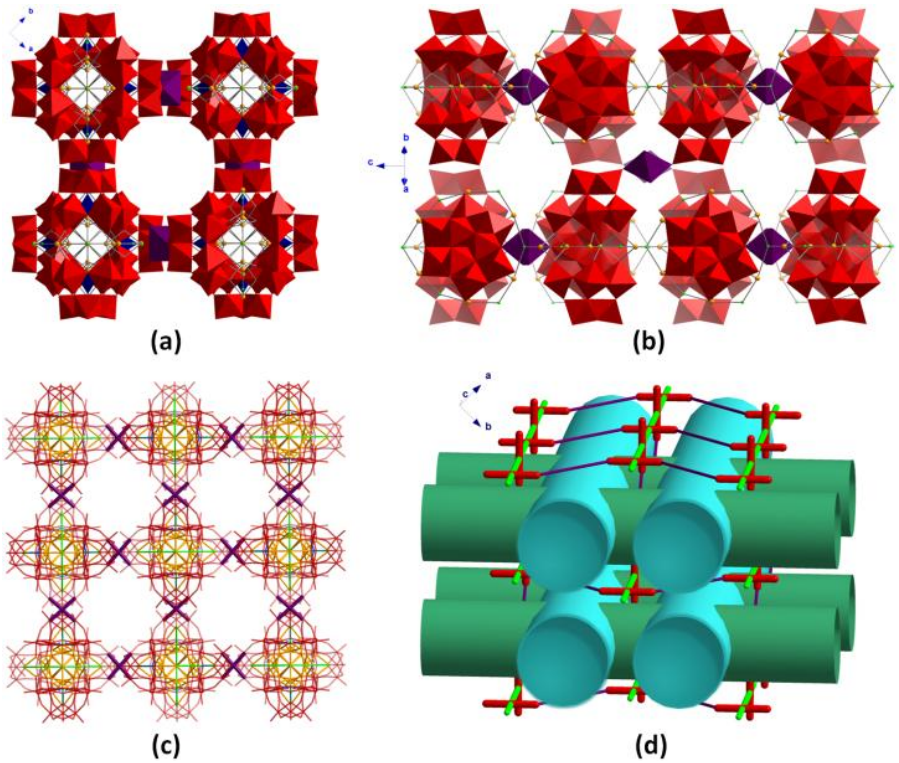

Figure 6-8 (a) Porous channels along the *c*-axis in **6.4** confined by four 1D chains assembled around the *four*-fold axis. (b) The secondary channels along [110] direction. Code: Na, purple. (c) The 3D open framework of **6.4** shown in stick notation. (d) A topological representation of **6.4**. The channels inside which are shown in blue/green tubes. The red sticks represent each single unit of **6.4** and the green sticks stand for the chloride bridges.

As shown in **Figure 6-7**, the structure of **6.4** displays as an infinite one-dimensional (1D) chain due to the chloride-bridged linkages. The μ_4-Cl is located in a tetrahedral coordination environment, Sn_4Cl, with Sn-Cl-Sn angles of 99.7º – 142.6º. Each single-POM unit of **6.4** is perpendicular to the adjacent POM unit. To our knowledge, a Cl-bridged 1D chain of transition-metal-substituted POMs has not been reported previously. Furthermore, each 1D chain is bonded to the neighboring chain through hydrated sodium ions, $[Na(H_2O)_4]^+$. Because the structure resides in the *P*42/ncm space group, the resulting symmetry equivalent 1D chains surround the central *4*-fold axis generating an internal 1D porous channel along *c*-axis. The channel diameter is about 9.2 Å estimated

from the bordering oxygen separations (**Figure 6-8**). Along direction [110], another kind of 1D channels are also present. Half of these are partially filled with $[Na(H_2O)_4]^+$ ions and the other half are empty with a diameter of 6.1 Å from the edge chloride to edge chloride (**Figure 6-8**).

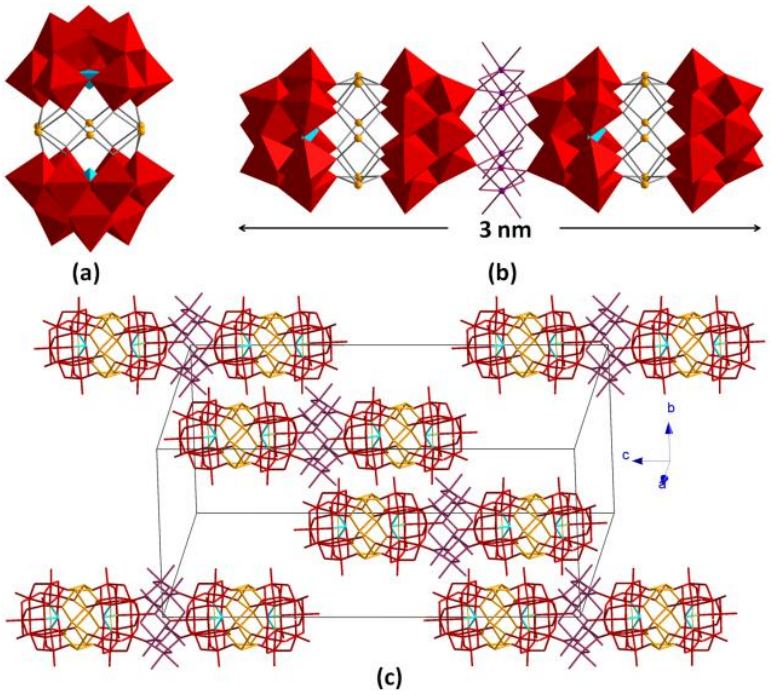

Figure 6-9 (a) X-ray structure of $[Sn_6(B\text{-}SbW_9O_{33})_2]^{6-}$ in combined bond-and-stick and polyhedral notations. Code: Sb, cyan. (b) A "double-sandwich" structure of **6.6** involving a hexanuclear aqua-Na^+ cation. (c) The arrangement of **6.6** in a unit cell shown in stick notation.

The anionic "double-sandwich" structure of $Na_6[\{Na(\mu\text{-}OH_2)(OH_2)_2\}_6\{Sn_6(B\text{-}SbW_9O_{33})_2\}_2]\cdot 50H_2O$ (**6.6**) is a tetramer constructed from two hexanuclear Sn(II) POM dimers, $[Sn_6(B\text{-}SbW_9O_{33})_2]^{6-}$, linked to each other through a polymeric hydrated Na^+ cation, $[Na_6(\mu\text{-}OH_2)_6(OH_2)_{12}]^{6+}$. Each sandwich comprises two $[B\text{-}SbW_9O_{33}]^{9-}$ ligands joined together by six Sn(II) centers. This geometry is similar to the one in $[Sn_8W_{18}O_{66}]^{8-}$. Unlike the symmetry in **6.4**, a similar structure to $[Sn_6(SnW_9O_{33})_2]^{8-}$, the dimer $[Sn_6(B\text{-}SbW_9O_{33})_2]^{6-}$ and the resulting **6.6** exhibit D_{3d} symmetry instead of D_{3h}. Complexes

$[Sn_3(SiW_9O_{34})_2]^{14-}$ and $[Sn_3(PW_9O_{34})_2]^{12-}$ show virtual D_3 symmetry because one of the POM ligands is twisted by a small angle round the C_3 axis. In **6.6** one $[B\text{-}SbW_9O_{33}]^{9-}$ unit is rotated by 60º relatively to the other. This compound crystallizes in the *R*-3 space group. The central hexanuclear Sn(II) "belt" is linked to the POM units through Sn-O bonds with distances ranging from 2.25 to 2.29 Å, which are longer than those in $[Sn_6(SnW_9O_{33})_2]^{8-}$. Each Sn(II) ion in **6.6** is four-coordinated and in +2 oxidation state as revealed by BVS calculation. The Sn-O-Sn bond angles are 107.8º – 109.5º, while the O-Sn-O angles are in the range of 118.1º – 118.7º (O_{ax}-Sn-O_{ax}, O_{eq}-Sn-O_{eq}) and 70.4º – 79.7º (O_{ax}-Sn-O_{eq}), respectively. In the central cation, $[Na_6(\mu\text{-}OH_2)_6(OH_2)_{12}]^{6+}$, each Na^+ ion is located in an octahedral environment. The bond Na-O distances are 2.24 – 2.26 Å (terminal) and 2.43 – 2.49 Å (bridged), respectively. This nano-scale cluster has a diameter of approximate 3 nm.

6.3.4 Spectroscopic Study of Tin(II) POMs

The solubility of the above complexes was evaluated. Their solubility in water is low but increases considerably upon addition of DMF. This is different from conventional POMs, because alkali salts of POMs are usually far more soluble in aqueous solution than in organic solvents. The reason for this unusual solubility is not clear but may involve solvation of the lone-pair electrons on the belt-position Sn(II) centers. The chemical reactivity of Sn(II) lone pairs was previously studied by Pope and co-workers, who demonstrated that Sn(II)-POM derivatives are susceptible toward electrophilic attack and oxidation. The UV-vis spectra in **Figure 6-10** were collected in a DMF/H_2O = 9:1 solution. Three complexes exhibit an orange (**6.4** and **6.5**) or red (**6.6**) color in the solid state, and the spectra of all three in solution show a broad absorption covering the UV-

visible region extending to about 650 nm ($\varepsilon_{400\ nm}$: **6.4** and **6.5**, 1800 $M^{-1}\cdot cm^{-1}$; **6.6**, 1.05×10^4 $M^{-1}\cdot cm^{-1}$). Given that the precursors, $SnCl_2$ and $[\alpha\text{-}SiW_9O_{34}]^{10-}$, are both colorless (absorb exclusively in the UV region), this new visible-light absorption feature is likely due to the charge transfer between Sn(II) centers and POM ligands. These features parallel the metal-to-POM charge-transfer (MPCT) transitions in the rhenium(I) POM chromophore described earlier in the thesis (**Chapter 4**).[30,31]

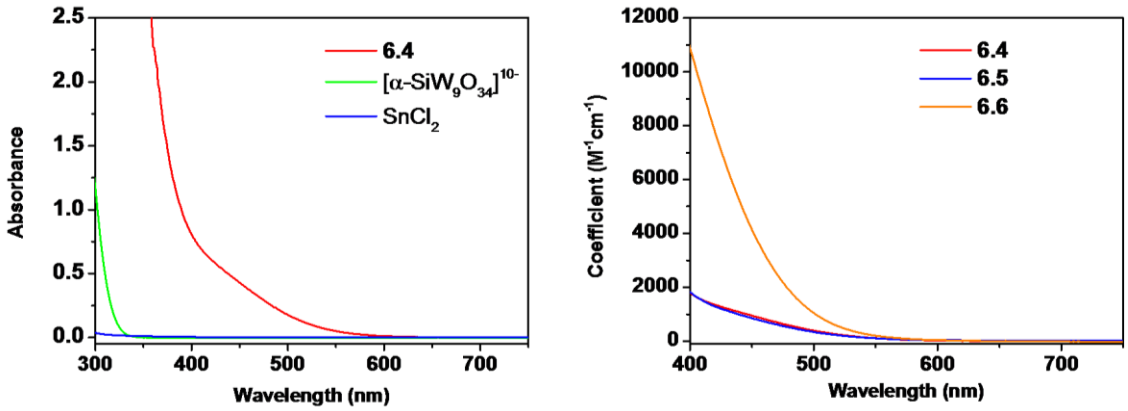

Figure 6-10 (Left) Normalized UV-vis spectra of **6.4** (in 90% DMF), 2 equivalent $[\alpha\text{-}SiW_9O_{34}]^{10-}$ (in H_2O) and 9 equivalent $SnCl_2$ (in H_2O). (Right) UV-vis absorption spectra of **6.4**, **6.5** and **6.6** in 90% DMF.

The stability of these complexes in solution was then studied. Sn(II) ions are unstable with respect to air-based oxidation, and these complexes undergo a slow oxidative degradation on exposure to the ambient environment. As shown in **Figure 6-11**, the absorbance of the stock solution of **6.6** decreases by 38% in buffer and 43% in DMF, respectively over a period of 20 hours. In DMF solution, the degradation shows faster kinetics at early times. The stock solution becomes colorless within a week indicating a complete decomposition. Similarly, **6.4** and **6.5** decompose over several days.

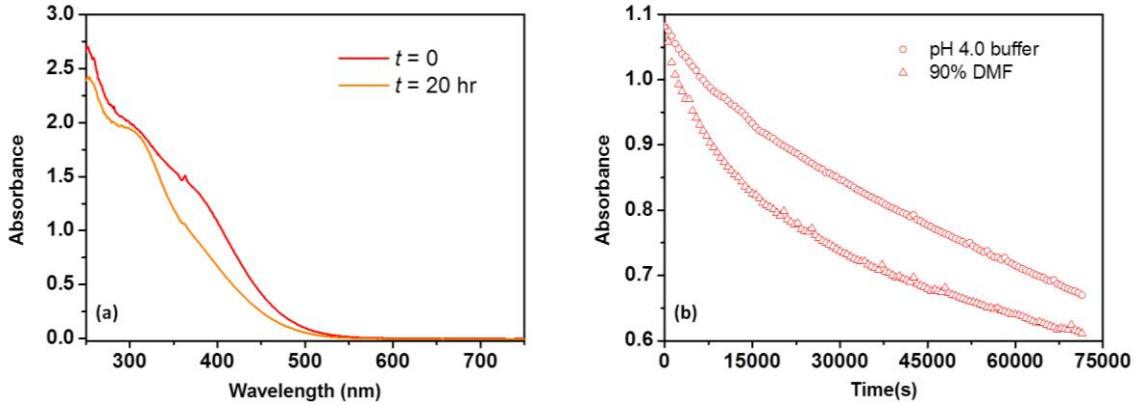

Figure 6-11 (a) UV-vis spectra for **6.6** in a pH 4.0 buffer solution, initially, and after 20 hours. (b) Normalized time trace of absorption record at a wavelength of 400 nm for **6.6** in a buffer and a DMF solution respectively over a 20-hour period.

The redox properties of **6.6** were studied by cyclic voltammetry (CV). As shown in Figure 6-12, in the negative potential domain the CV is quasi-reversible with two poorly resolved peaks in a 1:1 current ratio which is consistent with two one-electron transfer processes. These patterns are similar to those in the POM $[B\text{-}SbW_9O_{33}]^{9-}$ derivatives.[78,79] The wide and low-current CV peaks are consistent with slow electron transfer processes, which are likely due to high reorganization energies in **6.6**. The peaks at negative domain are assigned to the W(VI)-to-W(V) reduction. The anodic peak currents, $i_{p,a}$, are proportional to the square root of the scan rate, indicating that the redox processes associated with **6.6** are diffusion-controlled. There are no CV-detectable peaks for the Sn-centered redox processes. Since **6.4** and **6.5** have poor solubility in the acetate buffer, they were not investigated by CV.

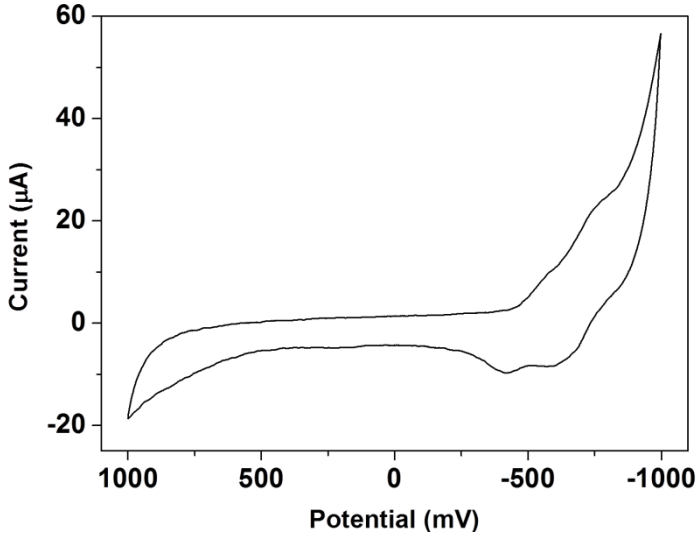

Figure 6-12 Cyclic voltammograms of **6.6** at a scan rate of 100 mV s^{-1} in the range of +1.0 to -1.0 V vs. Ag/AgCl.

6.4 Conclusions

Three cobalt(II) polytungstates based on the sub-valent antimony(III)-centered ligand, [*B*-$SbW_9O_{33}]^{9-}$, have been prepared and characterized. The results show that the ligand [*B*-$SbW_9O_{33}]^{9-}$ tends to form two types of architecture: the eclipsed and the slipped sandwich structures. The eclipsed structure is hydrolytically unstable while the slipped-sandwich structure assembly is kinetically stable. Complex **6.3**, the stable species, is an efficient water oxidation catalyst.

Three tin(II) polytungstates have also been prepared from trivacant lacunary POM ligands. These high-nuclearity Sn(II) POMs display infinite framework-like structures which are comparable with MOFs, but they are all-inorganic. Complexes **6.4** and **6.5** are the highest nuclearity Sn(II) POMs known to date, and they are the first examples of one-dimensional POM chains connected by chloride bridges. These complexes have high absorption in the visible region, which suggests potential applications as inorganic chromophores.

References

(1) Maayan, G.; Neumann, R. *Chem. Commun.* **2005**, 4595.

(2) Ettedgui, J.; Diskin-Posner, Y.; Weiner, L.; Neumann, R. *J. Am. Chem. Soc.* **2011**, *133*, 188.

(3) Howells, A. R.; Sankarraj, A.; Shannon, C. *J. Am. Chem. Soc.* **2004**, *126*, 12258.

(4) Geletii, Y. V.; Botar, B.; Kögerler, P.; Hillesheim, D. A.; Musaev, D. G.; Hill, C. L. *Angew. Chem. Int. Ed.* **2008**, *47*, 3896.

(5) Sartorel, A.; Carraro, M.; Scorrano, G.; Zorzi, R. D.; Geremia, S.; McDaniel, N. D.; Bernhard, S.; Bonchio, M. *J. Am. Chem. Soc.* **2008**, *130*, 5006.

(6) Yin, Q.; Tan, J. M.; Besson, C.; Geletii, Y. V.; Musaev, D. G.; Kuznetsov, A. E.; Luo, Z.; Hardcastle, K. I.; Hill, C. L. *Science* **2010**, *328*, 342.

(7) Huang, Z.; Luo, Z.; Geletii, Y. V.; Vickers, J.; Yin, Q.; Wu, D.; Hou, Y.; Ding, Y.; Song, J.; Musaev, D. G.; Hill, C. L.; Lian, T. *J. Am. Chem. Soc.* **2011**, *133*, 2068.

(8) Sartorel, A.; Miro, P.; Salvadori, E.; Romain, S.; Carraro, M.; Scorrano, G.; Valentin, M. D.; Llobet, A.; Bo, C.; Bonchio, M. *J. Am. Chem. Soc.* **2009**, *131*, 16051.

(9) Toma, F. M.; Sartorel, A.; Iurlo, M.; Carraro, M.; Parisse, P.; Maccato, C.; Rapino, S.; Gonzalez, B. R.; Amenitsch, H.; Ros, T. D.; Casalis, L.; Goldoni, A.; Marcaccio, M.; Scorrano, G.; Scoles, G.; Paolucci, F.; Prato, M.; Bonchio, M. *Nature Chem.* **2010**, *2*, 826.

(10) Lewis, N. S.; Nocera, D. G. *Proc. Natl. Acad. Sci.* **2006**, *103(43)*, 15729.

(11) Cook, T. R.; Dogutan, D. K.; Reece, S. Y.; Surendranath, Y.; Teets, T. S.; Nocera, D. G. *Chem. Rev.* **2010**, *110*, 6474.

(12) Bonchio, M.; Sartorel, A.; Carraro, M.; Scorrano, G.; De Zorzi, R.; Geremia, S.; McDaniel, N. D.; Bernhard, S. In *Abstracts of Papers, 237th ACS National Meeting, Salt Lake City, UT, United States, March 22-26, INOR-256* 2009.

(13) Besson, C.; Huang, Z.; Geletii, Y. V.; Lense, S.; Hardcastle, K. I.; Musaev, D. G.; Lian, T.; Proust, A.; Hill, C. L. *Chem. Commun.* **2010**, 2784.

(14) Cao, R.; Ma, H.; Geletii, Y. V.; Hardcastle, K. I.; Hill, C. L. *Inorg. Chem.* **2009**, *48*, 5596.

(15) Lv, H.; Geletii, Y. V.; Zhao, C.; Vickers, J. W.; Zhu, G.; Luo, Z.; Song, J.; Lian, T.; Musaev, D. G.; Hill, C. L. *Chem. Soc. Rev.* **2012**, *41*, 7572.

(16) Eddaoudi, M.; Kim, J.; Rosi, N.; Vodak, D.; Wachter, J.; O'Keeffe, M.; Yaghi, O. M. *Science* **2002**, *295*, 469.

(17) Mueller, U.; Schubert, M. M.; Yaghi, O. M. In *Handbook of Heterogeneous Catalysis (2nd Edition)* 2008; Vol. 1, p 247.

(18) Long, J. R.; Yaghi, O. M. *Chem. Soc. Rev.* **2009**, *38*, 1213.

(19) Wang, C.; Xie, Z.; deKrafft, K. E.; Lin, W. *J. Am. Chem. Soc.* **2011**, *133*, 13445.

(20) Wang, C.; deKrafft, K. E.; Lin, W. *J. Am. Chem. Soc.* **2012**, *134*, 7211.

(21) Lee, J. Y.; Farha, O. K.; Roberts, J.; Scheidt, K. A.; Nguyen, S. B. T.; Hupp, J. T. *Chem. Soc. Rev.* **2009**, *38*, 1450.

(22) Lu, G.; Li, S.; Guo, Z.; Farha, O. K.; Hauser, B. G.; Qi, X.; Wang, Y.; Wang, X.; Han, S.; Liu, X.; DuChene, J. S.; Zhang, H.; Zhang, Q.; Chen, X.; Ma, J.; Loo, S. C. J.; Wei, W. D.; Yang, Y.; Hupp, J. T.; Huo, F. *Nat. Chem.* **2012**, *4*, 310.

(23) Rodriguez-Albelo, L. M.; Ruiz-Salvador, A. R.; Sampieri, A.; Lewis, D. W.; Gómez, A.; Nohra, B.; Mialane, P.; Marrot, J.; Sécheresse, F.; Mellot-Draznieks, C.; Biboum, R. N.; Keita, B.; Nadjo, L.; Dolbecq, A. *J. Am. Chem. Soc.* **2009**, *131*, 16078.

(24) Nohra, B.; El Moll, H.; Rodriguez-Albelo, L. M.; Mialane, P.; Marrot, J. é; Mellot-Draznieks, C.; O'Keeffe, M.; Ngo Biboum, R.; Lemaire, J.; Keita, B.; Nadjo, L.; Dolbecq, A. *J. Am. Chem. Soc.* **2011**, *133*, 13363.

(25) Song, J.; Luo, Z.; Britt, D.; Furukawa, H.; Yaghi, O. M.; Hardcastle, K. I.; Hill, C. L. *J. Am. Chem. Soc.* **2011**, *133*, 16839.

(26) Zheng, S.-T.; Zhang, J.; Yang, G.-Y. *Angew. Chem. Int. Ed.* **2008**, *47*, 3909.

(27) Ma, F.-J.; Liu, S.-X.; Sun, C.-Y.; Liang, D.-D.; Ren, G.-J.; Wei, F.; Chen, Y.-G.; Su, Z.-M. *J. Am. Chem. Soc.* **2011**, *133*, 4178.

(28) Zheng, S.-T.; Zhang, J.; Li, X.-X.; Fang, W.-H.; Yang, G.-Y. *J. Am. Chem. Soc.* **2010**, *132*, 15102.

(29) Long, D.-L.; Tsunashima, R.; Cronin, L. *Angew. Chem. Int. Ed.* **2010**, *49*, 1736.

(30) Zhao, C.; Kambara, C. S.; Yang, Y.; Kaledin, A. L.; Musaev, D. G.; Lian, T.; Hill, C. L. *Inorg. Chem.* **2013**, *52*, 671.

(31) Zhao, C.; Huang, Z.; Rodríguez-Córdoba, W.; Kambara, C. S.; O'Halloran, K. P.; Hardcastle, K. I.; Musaev, D. G.; Lian, T.; Hill, C. L. *J. Am. Chem. Soc.* **2011**, *133*, 20134.

(32) Müller, A.; Shah, S. Q. N.; Bogge, H.; Schmidtmann, M. *Nature* **1999**, *397*, 48.

(33) Mal, S. S.; Kortz, U. *Angew. Chem. Int. Ed.* **2005**, *44*, 3777.

(34) Bassil, B. S.; Dickman, M. H.; Römer, I.; von der Kammer, B.; Kortz, U. *Angew. Chem. Int. Ed.* **2007**, *46*, 6192.

(35) Csicsery, S. M. *Pure Appl. Chem.* **1986**, *58*, 841.

(36) Bonfim, R. d. P. F.; Moura, L. C. d.; Pizzala, H.; Caldarelli, S.; Paul, S.; Eon, J. G.; Mentré, O.; Capron, M.; Delevoye, L.; Payen, E. *Inorg. Chem.* **2007**, *46*, 7371.

(37) Han, X.-B.; Zhang, Z.-M.; Wang, Z.-S.; Zhang, H.; Duan, H.; Wang, E.-B. *Inorg. Chem. Commun.* **2012**, *18*, 47.

(38) Pang, H.; Zhang, C.; Shi, D.; Chen, Y. *Cryst. Growth Des.* **2008**, *8*, 4476.

(39) Gao, S.; Cao, R.; Bi, W.; Li, X.; Lin, Z. *Microporous Mesoporous Mater.* **2005**, *80*, 139.

(40) Mothé-Esteves, P.; Pereira, M. M.; Arichi, J.; Louis, B. *Cryst. Growth Des.* **2009**, *10*, 371.

(41) Mitchell, S. G.; Streb, C.; Miras, H. N.; Boyd, T.; Long, D.-L.; Cronin, L. *Nature Chem.* **2010**, *2*, 308.

(42) Drewes, D.; Piepenbrink, M.; Krebs, B. *J. Cluster Sci.* **2006**, *17*, 361.

(43) Sazani, G.; Dickman, M. H.; Pope, M. T. *Inorg. Chem.* **2000**, *39*, 939.

(44) Keita, B.; Mialane, P.; Sécheresse, F.; Oliveira, P. d.; Nadjo, L. *Electrochem. Commun.* **2007**, *9*, 164.

(45) Sazani, G.; Dickman, M. H.; Pope, M. T. *Inorg. Chem.* **2000**, *39*, 939.

(46) Zhu, G.; Geletii, Y. V.; Kögerler, P.; Schilder, H.; Song, J.; Lense, S.; Zhao, C.; Hardcastle, K. I.; Musaev, D. G.; Hill, C. L. *Dalton Trans.* **2012**, *41*, 2084.

(47) Zhu, G.; Geletii, Y. V.; Zhao, C.; Musaev, D. G.; Song, J.; Hill, C. L. *Dalton Trans.* **2012**, *41*, 9908.

(48) Goberna-Ferrón, S.; Vigara, L.; Soriano-López, J.; Galán-Mascarós, J. R. *Inorg. Chem.* **2012**, *51*, 11707.

(49) Mitchell, S. G.; Khanra, S.; Sanchez, P. M.; Miras, H. N.; Long, D.-L.; Cronin, L. *Angew. Chem.* **2011**, in preparation for submission.

(50) Lisnard, L.; Mialane, P.; Dolbecq, A.; Marrot, J.; Clemente-Juan, J. M.; Coronado, E.; Keita, B.; de Oliveira, P.; Nadjo, L.; Sécheresse, F. *Chem. Eur. J.* **2007**, *13*, 3525.

(51) Mialane, P.; Dolbecq, A.; Marrot, J.; Rivière, E.; Sécheresse, F. *Angew. Chem. Int. Ed.* **2003**, *42*, 3523.

(52) Yamase, T.; Fukaya, K.; Nojiri, H.; Ohshima, Y. *Inorg. Chem.* **2006**, *45*, 7698.

(53) Piepenbrink, M.; Limanski, E. M.; Krebs, B. *Z. Anorg. Allg. Chem.* **2002**, *628*, 1187.

(54) Tézé, A.; Hervé, G. *J. Inorg. Nucl. Chem.* **1977**, *39*, 2151.

(55) Tézé, A.; Hervé, G. *J. Inorg. Nucl. Chem.* **1977**, *39*, 999.

(56) Bosing, M.; Loose, I.; Pohlmann, H.; Krebs, B. *Chem. Eur. J.* **1997**, *3*, 1232.

(57) Bruker AXS, I.; Analytical X-ray Sysems: Madison, WI, 2003.

(58) Bruker AXS, I.; Analytical X-ray Systems: Madison, WI, 2003.

(59) Sheldrick, G. In *SADABS*; ver. 2.10 ed. 2003.

(60) Bruker AXS, I. Madison, WI, 2003.

(61) Wang, J.-P.; Ma, P.-T.; Li, J.; Niu, H.-Y.; Niu, J.-Y. *Chem. Asian J.* **2008**, *3*, 822.

(62) Hussain, F.; Kortz, U.; Clark, R. J. *Inorg. Chem.* **2004**, *43*, 3237.

(63) Reinoso, S.; Dickman, M. H.; Praetorius, A.; Piedra-Garza, L. F.; Kortz, U. *Inorg. Chem.* **2008**, *47*, 8798.

(64) Kortz, U.; Hussain, F.; Reicke, M. *Angew. Chem. Int. Ed.* **2005**, *44*, 3773.

(65) Chorghade, G. S.; Pope, M. T. *J. Am. Chem. Soc.* **1987**, *109*, 5134.

(66) Xin, F.; Pope, M. T. *J. Amer. Chem. Soc.* **1996**, *118*, 7731.

(67) Botar, A.; Botar, B.; Gili, P.; Müller, A.; Meyer, J.; Bögge, H.; Schmidtmann, M. *Z. Anorg. Allg. Chem.* **1996**, *622*, 1435.

(68) Sokolov, M. N.; Izarova, N. V.; Virovets, A. V.; Fedin, V. P.; Starikova, Z. A.; Antipin, M. Y. *Dalton Trans.* **2003**, 4389.

(69) Khoshnavazi, R.; Bahrami, L. *J. Coord. Chem.* **2009**, *62*, 2067.

(70) Krebs, B.; Droste, E.; Piepenbrink, M.; Vollmer, G. *C.R. Acad. Sci., Ser. IIc: Chim.* **2000**, *3*, 205.

(71) Sokolov, M. N.; Kalinina, I. V.; Peresypkina, E. V.; Moroz, N. K.; Naumov, D. Y.; Fedin, V. P. *Eur. J. Inorg. Chem.* **2013**, *2013*, 1772.

(72) Zhang, Z.; Lin, Q.; Zheng, S.-T.; Bu, X.; Feng, P. *Chem. Commun.* **2011**, *47*, 3918.

(73) Veith, M.; Wolfanger, H.; Huch, V. *Z. Naturforsch., B: Chem. Sci.* **1995**, *50*, 1130.

(74) Schulte, M.; Schurmann, M.; Jurkschat, K.; Dakternieks, D. *Chem. Commun.* **1999**, 1291.

(75) Mehring, M.; Paulus, I.; Zobel, B.; Schürmann, M.; Jurkschat, K.; Duthie, A.; Dakternieks, D. *Eur. J. Inorg. Chem.* **2001**, *2001*, 153.

(76) Alcock, N. W.; Pennington, M.; Willey, G. R. *J. Chem. Soc., Dalton Trans.* **1985**, 2683.

(77) Boyle, T. J.; Segall, J. M.; Alam, T. M.; Rodriguez, M. A.; Santana, J. M. *J. Amer. Chem. Soc.* **2002**, *124*, 6904.

(78) Kortz, U.; Savelieff, M. G.; Bassil, B. S.; Keita, B.; Nadjo, L. *Inorg. Chem.* **2002**, *41*, 783.

(79) Bi, L.-H.; Li, B.; Bi, S.; Wu, L.-X. *J. Solid State Chem.* **2009**, *182*, 1401.